Characterisation and Disruption of Extracellular Polymeric Substances in Clinically Relevant Biofilms

Abdullah Ali Albarrak

A thesis submitted for the degree of Doctor of Philosophy

Cardiff University

September 2025

Acknowledgement

I would like to express my deepest gratitude to all those who have supported me throughout the course of my PhD journey, especially my supervisors Professor David Williams, Dr Melanie Wilson and Professor Ian Fallis.

My heartfelt thanks go to Professor Williams, whose mentorship has been a defining part of this journey. His guidance, patience, and encouragement have made me a better student, a better researcher, and a better person. I hope one day to make him as proud of me as I am to have worked under his supervision.

I am also grateful to Dr Wilson, for generously giving her time to read my work, provide valuable feedback, and offer kind words of guidance and support along the way. I would also like to thank Professor Ian Fallis for his kindness and guidance.

I would like to acknowledge the incredible technical team, Fiona, Alan, Wendy, Martin, Sarah, and Maria, for their assistance and expertise in the laboratory. My sincere thanks also go to Dr Anthony Hayes, Claire, and Marc for their support during the long hours working in the Bioimaging Hub. A special thanks to Professor Paola Borri, Professor Wolfgang Langbein and Dr Iestyn Pope for giving me the opportunity and support to work on Raman microscopy, which became such a valuable part of this thesis.

A special thank you goes to Emma, who shared the office with me when I first started. At a time when everything was new and unfamiliar, her daily conversations and kindness made the experience truly enjoyable and helped me feel at home. I would also like to thank all my colleagues and office mates over the years for their company, collaboration, and for creating such a friendly and supportive work environment.

I am thankful to my sponsors, Saudi Arabian Cultural Bureau and Ministry of Education, for facilitating this journey and providing the support and resources that made this work possible.

Finally, I am forever grateful to my family for their love and encouragement. To my wife Shatha, thank you for your patience, understanding, and belief in me. Sharing this journey with you has made the challenges lighter and the achievements more meaningful.

Contents

List of tables

List of figures

Abstract

Antimicrobial resistance and biofilms contribute to treatment failure and pose a global burden on healthcare systems. Biofilms are microbial communities attached to surfaces with the cells encased within self-produced extracellular polymeric substance (EPS) matrix. The EPS is involved in the biofilm's structural stability, nutrient retention, and protection against external stresses including the presence of antimicrobial agents. Persistence of biofilm infections and their increased tolerance have made them a major focus of current microbiological and clinical research. In this PhD, the overarching research aim was to assess the role of EPS in promoting tolerance of *in vitro* biofilms to antimicrobials.

Initial studies sought to determine suitable *in vitro* conditions to grow biofilms using selected bacterial species as well as *Candida albicans*. Assessment of biofilm quantity was done by culture and confocal laser scanning microscopy (CLSM) with live/dead staining. It was determined that polycarbonate was a suitable substrate to support biofilm growth in full strength medium under continuous flow in a CDC biofilm reactor. There were minor exceptions depending on the combinations of microorganisms used.

Having established biofilm growth parameters, CLSM coupled with appropriate fluorescent probes was used to detect and quantify specific EPS components of clinically relevant biofilm-forming microorganisms including *S. sanguinis, S. gordonii, S. salivarius, C. albicans* and *N. gonorrhoeae*, providing details on their spatial distribution. The most frequently detected EPS components were carbohydrates, followed by proteins. Extracellular DNA was not detected in *in vitro* biofilms. It was however found that *N. gonorrhoea* biofilms produced by mutants lacking Lig E (and considered unable to generate eDNA) were less pathogenic in a reconstituted vaginal epithelium model. Typically, in unsupplemented media, biofilms had limited EPS and when present it was closely associated with cells. However, research found that when *Streptococcus mutans* was present in biofilms, both biofilm and EPS production increased when the culture medium was supplemented with 1% (w/v) sucrose and dextran (1 µM).

Using CSLM, Raman microscopy and carbohydrate quantification it was shown that dextranase (0.25%) degraded the EPS of *S. mutans* biofilms. For antimicrobial testing, biofilms exhibited higher tolerance to chlorhexidine (CHX) compared to planktonic growth, with EPS rich biofilms being less susceptible compared to biofilms with limited EPS. Furthermore, EPS degradation during biofilm formation using 0.25% dextranase, reduced tolerance of 1% sucrose and 1 µM dextran supplemented biofilm to levels comparable to biofilm with limited EPS. Biofilms treated with dextranase post formation for 1 h, followed by CHX exposure, resulted in increased numbers of dead cells compared to biofilms with intact EPS.

In conclusion, results of this research highlighted the role of EPS in antimicrobial tolerance and showed the potential of enzymatic degradation in rendering biofilms more susceptible to CHX. This suggests that EPS targeting may not only inhibit the establishment of complex biofilms but may facilitate their eradication when coupled with conventional antimicrobial treatments.

Chapter 1

Introduction and Literature Review

1.1 Microorganisms and human diseases

The discovery of microorganisms marked a pivotal moment in scientific history, fundamentally altering the understanding of the natural world. This breakthrough was possible by observing samples using microscopes. In the 17th century, after visualising mould under a microscope, Robert Hooke described his observation with illustrations of the microscopic fungus, making him the first person to report the presence of microorganisms. Several years later, Antonie Van Leeuwenhoek started to share observations of various samples using his own developed microscope. In one of his reports, he mentions the microscopic observation of scrapings of the white film on his teeth and mixed it with clean water, revealing 'animalcules' a term he used to describe what we now call bacteria (Gest 2004).

Centuries later, scientists found that these microorganisms have critical roles in a range of biological and ecological processes, both beneficial and harmful (D'Abramo and Neumeyer 2020). For example, microorganisms are involved in fermentation, a natural metabolic process in the production of essential food and drink including bread and yoghurt (Bourdichon et al. 2012). In plants, microorganisms contribute to the nitrogen cycle by fixing atmospheric nitrogen into forms that are beneficial to growth and productivity (Compant et al. 2019). In the human body, the presence of microorganisms can, in many cases, be beneficial and are involved in metabolism and development of immunity (Valencia et al. 2025). In the gut, microorganisms are involved in the synthesis of vitamins and lipids, food digestion, control of fat storage and in the generation of energy (Xiao and Kang 2020; Corbin et al. 2023). Moreover, microorganisms in the gut (Ma et al. 2022) and mouth (Şenel 2021) aid in maintenance of the barrier function of the skin and mucosa. Furthermore, from an immunology point of view, these harmless microorganisms can protect the host by producing antimicrobial substances and inhibiting the colonisation of pathogens (Kilian et al. 2016; Hou et al. 2022).

In contrast, microorganisms can be harmful, causing infections in humans, animals, and plants. Pathogenic bacteria, fungi and viruses are responsible for a wide range of infectious diseases, from common illnesses such as respiratory infections to severe life-threatening conditions such as tuberculosis and malaria (Daily 2017; Litvinjenko et al. 2023). In the 19th century, Louis Pasteur and Robert Koch led the scientific community to establish the 'germ theory' that demonstrated that many infections were caused by specific microorganisms (Opal 2010).

Pasteur's work on fermentation and spoilage showed that microbial growth was responsible for biochemical changes in organic matter, by demonstrating that microorganisms arose from pre-existing microbes rather than from non-living material (Mostowy 2022).

Koch provided experimental proof of microbial causation of disease through systematic isolation, cultivation, and reinfection studies, most notably with *Bacillus anthracis*, establishing what became known as Koch's postulates (Singh et al. 2016), which state that:

A microorganisms must be consistently associated with diseased host and absent in healthy individuals. Then the microorganism is isolated and grown in pure culture and should cause the disease when it is introduced to a healthy individual. Finally, the microorganism must be reisolated from infected host and shown to be identical to original isolate.

This led to advances in microbiology research in different fields, especially in medicine, by linking diseases to causative agents and in the discovery and development of antibiotics (Durand et al. 2019). Historically, microorganisms have been studied in liquid culture medium, in a free-living state referred to as planktonic growth. However, in the 1970s it became evident that the majority of microorganisms primarily existed attached to a surface in a growth form referred to as a biofilm (Donlan 2002).

1.2 Biofilm

A biofilm is defined as a heterogeneous community of microorganisms that are often attached to a surface and characterised by the aggregation of the constituent microorganisms (Figure 1.1). Biofilms are ubiquitous and found in natural, industrial, and clinical environments. In the case of the latter, biofilms have been linked to a wide range of infections.

A key feature of biofilms is the presence of extracellular polymeric substances (EPS) which can constitute the majority of a biofilm's biomass (Donlan 2002; Flemming and Wingender 2010). Importantly, microbial cells in biofilms typically have high antimicrobial tolerance compared to their planktonic (free-living) counterparts (Uruén et al. 2020; Thöming and Häussler 2022). Unsurprisingly, biofilm infections are widespread, hard to treat and attract the attention of clinicians and researchers in many fields.

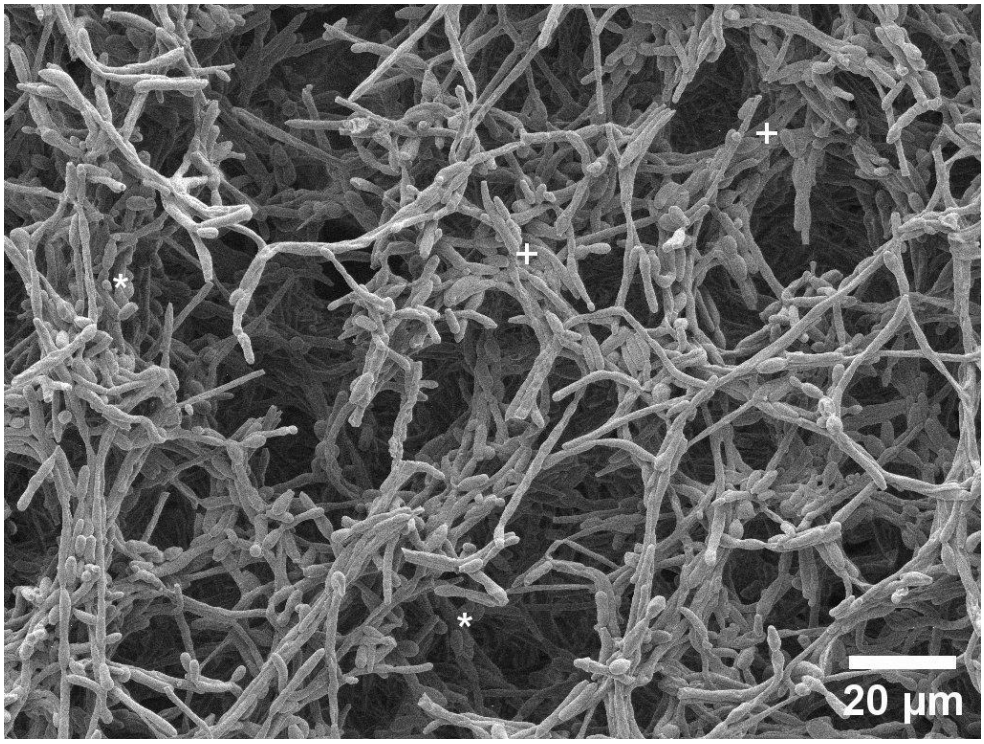

Figure 1.1 A scanning electron micrograph showing an *in vitro Candida albicans* biofilm.

A mixture of yeast (*) and hyphal (+) morphologies are evident within this biofilm (1,500× magnification; generated from research during this PhD).

Infections are a major cause of morbidity and mortality around the world (Scheld 2012), and many are associated with biofilm formation. Examples include urinary tract infections (Flores-Mireles et al. 2015), cystic fibrosis (LiPuma 2010), chronic wounds (Ding et al. 2022), and oral infections (Marsh 2006; Mirzaei et al. 2020; Meyer et al. 2021).

Oral biofilms are directly associated with dental caries and periodontal diseases, and their presence on dental implants and dentures is associated with peri-implantitis and denture stomatitis (Marsh 2006). Biofilms occur on other medical device surfaces including those of catheters, prosthetic joints, and endotracheal tubes where they can be difficult to remove and responsible for chronic infection (Davies 2003; Djeribi et al. 2012).

1.3 Extracellular polymeric substances (EPS)

EPS serves as a structural support for biofilms, facilitating cell attachment to both the surface and other microbial cells, thereby contributing to the architecture of biofilm and formation of microcolonies (Yang et al. 2011).

Extensive research has been conducted on the significance of EPS in biofilms, and this requires clarification of its structure, arrangement, similarities, and heterogeneity across different biofilms. (Pinto et al. 2020). EPS plays a crucial role in promoting microbial cell retention, intercellular signalling and communication through the closely-knit microbial community (Sharma et al. 2023b). EPS presents a physical and chemical barrier to antimicrobial agents and also aids surface attachment to withstand external shear forces (Davies 2003).

1.3.1 The composition and function of EPS

EPS contains a variety of molecules that provide a wide range of functions (Table 1.1). EPS is primarily synthesised by microorganisms and envelops the producing cells. However, EPS components may also originate from dead cells or environmental molecules (Costa et al. 2018;

Oliva et al. 2025). Polysaccharides are widely acknowledged as primary EPS constituents of many biofilms although often exhibit significant heterogeneity between biofilms (Bales et al. 2013). Proteins identified in EPS, include amongst others, enzymes responsible for the modification of the EPS structure and for facilitating microbial cell dispersion (Pinto et al. 2020). The various EPS components perform distinct roles that contribute to the functions of biofilms.

Table 1.1 Common extracellular polymeric substance (EPS) components identified with biofilms of specific microorganisms and their associated functions

Microorganism	EPS component	Function of EPS component	Reference
Pseudomonas aeruginosa	Alginate	Enhances antibiotic tolerance, immune evasion and maintains biofilm hydration and structure	(Jacobs et al. 2022; Rowe III et al. 2023)
	Pel	Cell aggregation, structural integrity and tolerance to antibiotics and stress.	(Jennings et al. 2015; Kasetty et al. 2021)
	Psl	Mediates early biofilm attachment, motility, immune evasion, antibiotic tolerance, interspecies protection, and biofilm matrix stability.	(Pestrak et al. 2019; Kasetty et al. 2021)
	rhamnolipid	Biofilm formation and structural maintenance	(Davey et al. 2003)
	eDNA	Structural and mechanical integrity	(Ferguson et al. 2023)
Staphylococcus aureus	Adhesins	Adhesion to host matrix proteins	(Bhattacharya and Horswill 2024)
	eDNA	Attachment and structural integrity	(Bowden et al. 2024)
	Poly-N-acetylglucosamine	Promotes cell aggregation, immune evasion, antibiotic tolerance and resistance to mechanical stressors	(Tan et al. 2024)
Escherichia coli	Curli	Adhesion and structural integrity	(Jeffries et al. 2021)
	Cellulose	Retention, structural support and cohesion	
Bacillus subtilis	Amyloid protein TasA	Adhesion, structural integrity and retention	(Berlanga-Clavero et al. 2022)

Table 1.1 (Continued) common extracellular polymeric substance components identified with biofilms of specific microorganisms and their associated functions in biofilms

Microorganism	EPS component	Function of EPS component	Reference
Vibrio cholerae	*Vibrio* polysaccharide	Structural integrity	(Teschler et al. 2022)
	Matrix proteins (RbmA, RbmC and Bap1)	Attachment and aggregation	
	eDNA	Stability and horizontal gene transfer	
Candida albicans	Polysaccharides (Mannan and Glucan)	Structural integrity and antifungal resistance	(Zarnowski et al. 2014)
	Metabolic proteins and enzymes	Remodelling and digestion	
	eDNA	Structural integrity	
	Lipids	Signalling and antifungal tolerance	
Streptococcus mutans	Glucan	Attachment, aggregation and structural integrity	(Duque et al. 2011)
	Fructan	Extracellular storage molecule	(Burne et al. 1996)
	Glucosyltransferases	Breakdown of sucrose and production of glucan	(Bowen and Koo 2011)
	eDNA	Aggregation and structural integrity	(Liao et al. 2014)

The initial attachment of primary colonising microorganisms to a surface, as well as their aggregation to each other, is promoted by polysaccharides, proteins, and DNA in the EPS (Zhao et al. 2023). Polysaccharides are also responsible for water retention in biofilms and alongside proteins can be protective against harmful agents, including antimicrobials and host defence mechanisms (Balducci et al. 2023). The process of horizontal gene transfer (HGT) between microbial cells is thought to be enhanced in biofilms and can involve extracellular DNA (eDNA) (Liu et al. 2024). The electronegativity of extracellular DNA (eDNA) also promotes microbial aggregation and sequestration of cationic molecules (Lewenza 2013). EPS provides additional functions, such as being a source of nutrition, and in this regard enzymes in the EPS are key to the digestion of nutrients and the alteration of EPS structure (Sutherland 2001; Luppens et al. 2002; Flemming and Wingender 2010; Karygianni et al. 2020b; Sauer et al. 2022).

1.4 Biofilm formation

1.4.1 Contact and initial attachment of microorganisms to surfaces

The transition of microorganisms from a planktonic state to a surface-attached, fully developed biofilm is typically divided into distinct stages, each characterised by specific microbial behaviours and interactions (Funari and Shen 2022). The initial stage of biofilm development is the adhesion of microbial cells to a surface. It has been suggested that the act of cells encountering a surface, in conjunction with the presence of the surrounding milieu, triggers distinct metabolic pathways that facilitate advancement of biofilm formation (Chang 2018). This initial attachment is influenced by molecular interactions and the surface structure of microbial cells. In the context of dental plaque formation on a tooth surface, the tooth is initially covered by an acquired pellicle (AP). The AP consists of various proteins, including glycoproteins and mucins, and these promote the attachment of primary colonisers such as certain *Streptococcus* species. In this context, the genes responsible for EPS are upregulated

in initial stages of biofilm development (McDougald et al. 2012). Microorganisms involved in this stage are referred to as primary colonisers, and these microorganisms attach directly to the surface and bind to other microorganisms (O'Toole et al. 2000). The loose attachment of microorganisms in this stage means that it is largely a reversible process (Armbruster and Parsek 2018).

1.4.2 Further attachment and secondary colonisation in biofilm formation

Following initial attachment, additional microorganisms referred to as secondary colonisers, may be recruited to the biofilm. Even if they are unable to bind directly to the surface, they can undergo coaggregation with primary colonisers through specific cell-cell interactions (Soleimani et al. 2023). Following this, there is an attachment of additional secondary colonisers, which in oral biofilms include species of *Actinomycetes* and *Fusobacterium,* and some of these microorganisms act as 'bridges' between primary and secondary colonisers (O'Toole et al. 2000; Simões et al. 2008). For example, *Fusobacterium nucleatum* is a Gram-negative bacterial species found in the mouth and other parts of the human body. The species is an opportunistic pathogen involved in periodontal diseases as well as other infections. *Fusobacterium nucleatum,* is considered one of the main 'bridging microorganisms,' and this property is enabled by the presence of surface proteins that bind to a wide range of receptors on both Gram-positive and Gram-negative bacteria (Chen et al. 2022).

1.4.3 Biofilm maturation

Biofilm maturation is recognised as a stage in biofilm development where the biofilm transitions from a thin layer of attached cells to a thick structured multilayered community of cells. The biofilm at this stage is complex due to the presence of several microenvironments that vary in oxygen levels, pH, nutrition, and exposure to external forces. These variable

factors are responsible for biofilm complexity leading to different physiological states of constituent cells, including cells with reduced metabolic activity (dormant cells) (Niu et al. 2024).

EPS genes continue to be expressed during maturation, and resultant EPS is embedded around constituent cells increasing the strength of attachment to the surface and between the cells. Moreover, EPS provides protection to the biofilm cells from the action of antimicrobial agents and host defence molecules (Sutherland 2001; Li et al. 2020). The EPS matrix exhibits voids and water channels that facilitate transportation and interchange of nutrients, waste products, and gases (Quan et al. 2022). During biofilm maturation, the biofilm is rich with a diverse array of microbial species in an environment that permits easier cell to cell communication and HGT (Madsen et al. 2012).

1.4.4 Biofilm dispersion

The process of biofilm dispersal or cell detachment is important for dissemination of microorganisms, allowing them to colonise new sites, form new biofilms, and potentially continue cycles of infection (McDougald et al. 2012). Dispersed cells frequently have higher potential for virulence compared to their planktonic counterparts (Chua et al. 2014; Uppuluri et al. 2018) and may lead to invasion and infection of other organs or sites within the body. An example of this is infective endocarditis, where heart valves become colonised by oral streptococci originating from dental plaque biofilms (Barraud et al. 2015; Jamal et al. 2018).

1.5 Biofilm involvement in health and disease (symbiosis and dysbiosis)

Microorganisms in their natural environment reside and occupy diverse ecological niches in the human body, forming intricate communities of microbiota (Cho and Blaser 2012). The presence of microbial biofilms in different parts of the body does not necessarily imply the

occurrence of infection. Indeed, a vast number of biofilms exist and promote health in individuals including in the mouth, gut or on the skin (Sasidharan Pillai et al. 2024). The organisms in these biofilms are generally considered commensal microorganisms (Malard et al. 2021).

In health, the microbiota exists in harmony with its surrounding environment and host responses. A symbiotic relationship can arise when the relationship is mutually beneficial to both the host and its microbiota. Microorganisms benefit from a rich environment which ensures their survival, whilst they simultaneously act as 'gatekeepers' inhibiting colonisation by pathogens and contributing to community metabolic processes (Li et al. 2025). For example, certain gut microbiota constituents, such as *Bacteroides thetaiotaomicron,* have been linked with carbohydrate breakdown, contributing to glucose metabolism and improved insulin sensitivity (Laudes et al. 2021; Mora-Flores et al. 2023). However, this equilibrium is susceptible to disruption or alteration, leading to what is referred to as dysbiosis, which is an imbalance in the abundance or impact of microorganisms and is typically associated with disease (Kozak and Pawlik 2023). Biofilm involvement in disease represents a substantial clinical and economic burden. It has been estimated that biofilms contribute to more than 80% of microbial infections in the human body (Penesyan et al. 2021). In a multidisciplinary assessment of the global impact of biofilms, Cámara *et al.* (2022) quantified their burden across healthcare, industry, and the environment, estimating a total global economic impact of approximately 3,967 billion dollars per year, with around 387 billion attributable to medical and human health sectors alone (Cámara et al. 2022). These findings highlight that biofilm-associated dysbiosis is a major contributor to disease burden and healthcare costs.

Dysbiosis can occur due to varying factors, for instance changes in diet, antibiotic use, stress, and smoking (Huang et al. 2023). An example is in the case of *Streptococcus mutans* colonisation. This species is known for its role in dental caries, where it metabolises sugars and produces acids (Marsh and Zaura 2017). The lactic acid produced from fermentation of carbohydrates is implicated in caries development and at the same time, creates a selective environment (Bedoya-Correa et al. 2021). Microorganisms sensitive to the lactic acid will be disadvantaged, while acidogenic (acid producing) and aciduric (acid tolerant) microorganisms will be favoured in such an environment (Radaic and Kapila 2021). A significant shift towards dysbiosis occurs by reducing competition from microorganisms unable to thrive. It is this imbalance in the microbial community that is critical to the development of dental caries (Liu et al. 2025). Similarly, in periodontal diseases, where various factors *e.g.*, plaque accumulation, impaired immune response (Lertpimonchai et al. 2017) and smoking (Tamashiro et al. 2023) cause a shift in the composition of the microbial community allowing microorganisms, such as *Porphyromonas gingivalis*, with known association to periodontal diseases to flourish (Abusleme et al. 2013). Table 1.2 lists common biofilm-forming microorganisms that are reported to be involved in diseases. In both symbiotic and dysbiotic environments, microbial cells respond to changes in the environment to promote their own survival (Nguyen et al. 2021). One of the ways is through coordinated action, facilitated by quorum sensing (QS).

QS is a communication network between microbial cells, characterised by the production and sensing of small extracellular molecules called autoinducers (Wu and Luo 2021). The concentration of these QS molecules is representative of the cell density and QS molecules coordinate the biofilm community's behaviour by regulating gene expression and biofilm formation, leading to both individual and population level responses (Moreno-Gámez et al.

2023). Autoinducers vary in chemical composition for different species (Rued et al. 2021). QS can be species-specific or interspecies, for example, Autoinducer-2, a common QS molecule amongst streptococci, and produced by *Streptococcus gordonii,* enhances hyphal formation of *C. albicans* in co-culture (Bamford et al. 2009).

Table 1.2 Examples of biofilm-forming microorganisms and associated diseases

Microorganism	Associated Disease(s)	Reference
Pseudomonas aeruginosa	Chronic lung infections in cystic fibrosis	(Harrington et al. 2020)
Staphylococcus aureus	Medical device-associated infections and chronic wound infections	(Tran et al. 2023)
*Candida albicans**	Medical device-associated infections	(Pereira et al. 2021b)
Escherichia coli	Urinary tract infections	(Ballén et al. 2022)
*Streptococcus mutans**	Dental caries	(Gao et al. 2024)
Enterococcus faecalis	Dental periapical infection	(Elashiry et al. 2023)
Klebsiella pneumoniae	Pneumonia	(Guerra et al. 2022)
Streptococcus pneumoniae	Otitis media	(Narciso et al. 2025)
*Neisseria gonorrhoeae**	Gonorrhoeae	(Ayala et al. 2024)

*These microorganisms are included in this research and addressed in the following section

1.6 *Candida albicans*

Candida albicans is a polymorphic fungus that frequently is present as a commensal microorganism on soft tissue surfaces of humans (Shao et al. 2022). Under certain conditions, *C. albicans* can transition from a commensal microorganism to a pathogen and is therefore considered an opportunistic pathogen of humans (Lionakis et al. 2023). Of the many candidal species, *C. albicans i*s most frequently associated with disease and is estimated to be responsible for 60% and 40% of mucosal candidosis and cases of candidemia, respectively (Kamali and Sarvtin 2023).

Candida albicans is polymorphic and can grow as spherical yeast, as well as pseudohyphal and true hyphal forms (Mukaremera et al. 2017). Such morphological transformation is key to the species adaptability to changing environments such as temperature, pH, CO_2 levels, and nutrient availability, allowing it to thrive in diverse host niches (Prasad and Tippana 2023). The yeast form facilitates adhesion to host tissues, bloodstream dissemination, and immune evasion, while the hyphal form enables tissue invasion, resistance to phagocytosis, and the expression of virulence factors like adhesins, proteases, and cytolytic toxins (Chow et al. 2021). In addition, *C. albicans* is adept at forming biofilms on mucosal and medical device surfaces (Pohl 2022). The species can also develop resistance to commonly used antifungal agents (Board-Davies et al. 2023)

The ability to form hyphae is an important factor in *C. albicans* pathogenicity, with strains lacking this property reportedly being less pathogenic (Sharma et al. 2023a). Other virulence factors expressed by *C. albicans* include various proteins that enhance adherence and invasion, phenotypic diversity, and the production of enzymes that target host cell components (Talapko et al. 2021), Table 1.3 summarises virulence factors of *C. albicans*.

Among these, hyphae specific mechanism play a critical role in pathogenesis as researchers recently identified a novel virulence factor of *C. albicans*, a cytolytic peptide toxin called candidalysin (Moyes et al. 2016). By screening of factors inducing epithelial damage, authors found that mutants lacking extent of cell elongation 1 (*ECE1*) gene, which is highly expressed in hyphae form during epithelial infection, did not cause damage to epithelial cells or induce a proinflammatory response. The *ECE1* gene encodes a polyprotein precursor, which is processed by Kex2p to produce candidalysin. Canddialysin is a 31 amino acid α helical peptide with amphipathic properties that facilitate integration into the cell membrane of host cells (Richardson et al. 2022). This happens as positively charged C terminal of candidalysin interacts with the negatively charged membrane resulting in pore formation and membrane disruption. This process ultimately leads to cell lysis as demonstrated by LDH measurement assays. In addition to cell lysis, upon candidalysin insertion to host membrane it induces calcium ion influx, disrupting haemostasis and initiating signalling cascades (Moyes et al. 2016), activating the matrix metalloproteinases and induces epidermal growth factor receptor signalling, which further triggers mitogen activated protein kinase (MAPK) pathways, including extracellular signal-regulated kinase 1/2 and p38 activation. Which results in c-Fos activation, which regulates the epithelial immune response by stimulating the release of cytokines and chemokines (Naglik et al. 2019). Furthermore, candidalysin secretion can be directed towards a specific part of infection site, allowing for increased accumulation of candidalysin to ensure high concentration maximising cell damage (Mogavero et al. 2021). Candidalysins have since been identified in other *Candida* species, including *C. dubliniensis* and *C. tropicalis*, which caused epithelial cell damage to a lesser extent compared to *C. albicans* (Richardson et al. 2022).

Table 1.3 Putative virulence factors of *Candida albicans*

Virulence factor	Effect	Reference
Hyphal development	Reduces phagocytosis, aiding evasion of host immune defences	(Calderone and Fonzi 2001)
Hydrolytic enzyme production	Facilitates host cell and extracellular matrix damage, promoting tissue invasion	
Phenotypic switching	Modifies antigenic properties to evade host defences	(Mayer et al. 2013; Talapko et al. 2021)
Secreted aspartyl proteinase production	Destroys secretory IgA to undermine mucosal immunity	(Bras et al. 2024)
Biofilm development and maturation	Enhances antifungal resistance and immune evasion by forming protective biofilm structures	(Atriwal et al. 2021)
Candidalysin (hyphal toxin)	Damages epithelial cells, facilitating tissue invasion and systemic infection	(Ho et al. 2019)
Cell surface hydrophobicity	Enhances adhesion to oral surfaces, promoting non-specific retention in the mouth	(Singleton et al. 2005)
Expression of cell surface adhesins	Facilitates specific adherence to oral surfaces, aiding colonisation	(Rosiana et al. 2021)
Hyphal development	Promotes invasion of oral epithelium and facilitates tissue penetration	(Desai 2018)
Complement evasion (*e.g.*, binding factor H)	Reduces complement activation, preventing immune detection and destruction	(Harpf et al. 2020)

Growth conditions favourable to *C. albicans* include warm and moist areas, and unsurprisingly mucocutaneous surfaces such as those of the oral cavity, gastrointestinal tract, and genitalia serve as preferred habitats (Kennedy 1988). Its pathogenicity across the different parts of the body is attributed to its ability to attach to various surfaces, including soft and hard tissues

and dentures, as well as its invasion of epithelial layers, while avoiding the host's immune response (Contaldo et al. 2023). *Candida albicans* is involved in several infections including topical candidosis typically presenting as white lesions on oral and vaginal mucosa (Alves et al. 2014; Pereira et al. 2021a). In severe cases, *C. albicans* can cause systemic candidosis, which has a high mortality rate. In candidemia, where the infection has spread into the bloodstream, high morbidity and mortality occurs and is particularly evident in immunocompromised individuals (Tsui et al. 2016).

In the oral cavity, *C. albicans* is the *Candida* species most often isolated from candidosis (Talapko et al. 2021). Oral candidosis can present as white lesions, redness, and soreness (Lewis and Williams 2017). Predisposing factors include a weakened immune system, use of broad-spectrum antibiotics, constant wearing of dentures with poor denture cleaning, and the presence of certain medical conditions, for example, diabetes (Perić et al. 2024).

There are several distinct types of oral candidosis including pseudomembranous candidosis, also known as oral thrush, which appears as superficial white plaques that can be wiped off easily and are underlined by an erythematous mucosal surface. Commonly affecting infants and the elderly, pseudomembranous candidosis can present as an acute infection but may be chronic in those with long term predisposing factors (Williams and Lewis 2011). Secondly, acute erythematous candidosis is a red flat lesion of mucosa and is particularly prevalent on the tongue and palate. This type of oral candidosis is often related to the prolonged use of antibiotics and is also common in poorly managed patients with AIDS and HIV (Contaldo et al. 2023). Thirdly, chronic hyperplastic candidosis occurs as asymptomatic white plaques on the oral mucosa which are not easily removed. The diagnosis of this infection is important because of the potential malignant transformation of lesions (Lorenzo-Pouso et al. 2022). Finally,

Candida-associated denture stomatitis is a common condition in denture wearers, characterised by the inflammation of the mucosa bearing denture surface although it is often asymptomatic (McReynolds et al. 2023). The aetiology of this form of candidosis is multifactorial, with *Candida* being considered the primary cause, and other factors such as poor oral and denture hygiene, prolonged wearing of dentures, and reduced salivary flow also being of relevance (Perić et al. 2024; Tamai and Kiyoura 2025). Nevertheless, denture wearing is the primary etiological factor in the development of denture stomatitis, as it creates an environment favourable to the growth of *Candida* (Perić et al. 2024). Clearly, appropriate management of identified predisposing factors, is key in the treatment of the different forms of oral candidosis (Williams and Lewis 2011). Importantly, oral and denture hygiene and lifestyle modification are fundamental, especially in denture wearers where effective care reduces the severity of denture-associated stomatitis and decreases the population of *C. albicans,* other microbes and biofilms (Williams and Lewis 2011; Ribeiro et al. 2022)

1.6.1 Antifungal treatment of *Candida albicans* infections

In some cases, addressing the issue of a predisposing factor might not be feasible, such as the use of immunosuppressive drugs for organ transplant, in such instances, antifungals may be used in the management of oral candidosis (Lewis and Williams 2017). The choice of topical or systemic administration is guided by the severity and extent of the infection. Topical antifungals are applied directly to the infected site and there is minimal systemic absorption, and potentially fewer side effects. In the case of chronic infections, systemic antifungals are often used (Appleton 2000; Hellstein and Marek 2019; Ribeiro et al. 2022).

1.7 *Streptococcus mutans*

Streptococcus is a genus of Gram-positive bacteria, with many species being members of the human microbiota, where they play active roles in both health and disease. The species are characterised by their spherical shape and the formation of chains of cells (Krzyściak et al. 2013). *Streptococcus* species can be classified into subgroups based on their haemolytic properties, antigenic profiles, genetic composition, and growth characteristics (Pattnaik et al. 2020). Streptococci are amongst the early colonisers of the oral cavity, especially on the tooth surface and are a major member of dental plaque (Baty et al. 2022). Dental plaque is an oral biofilm that is present both supragingivally on the enamel surfaces of teeth as well as subgingivally. Dental plaque biofilm is comprised of a complex microbial population and their associated EPS along with additional molecules from the environment such as salivary components (Oba et al. 2021).

Plaque development follows a dynamic sequential process that commences when salivary proteins and glycoproteins are adsorbed onto the surface. Thereafter, specific microorganisms, including streptococci, that possess the necessary adhesins to bind to receptor molecules establish the early attachment phase, followed by biofilm formation. Plaque formation is evident in both health and disease. The latter includes dental caries and periodontal diseases, in which altered growth or dysbiosis of the constituent microbiota predisposes to a pathogenic state (Davey 2008; Valm 2019).

Among the constituents of plaque, *S. mutans* has gained particular attention due to its role in dental caries (Khan et al. 2023). *Streptococcus mutans* is highly efficient in metabolising fermentable carbohydrates, especially sucrose, and producing lactic acid (Marsh and Zaura 2017). This process is known as acidogenicity and is key in the pathophysiology of dental caries

(Bedoya-Correa et al. 2021). *Streptococcus mutans* uses different pathways to metabolise carbohydrates, although it is mainly through the glycolytic pathway (Jurakova et al. 2023). Enzymes such as glucosyltransferases (Gtfs) and fructosyltransferases are produced extracellularly and breakdown sucrose, resulting in lactic acid and glucan matrix formation (Costa Oliveira et al. 2021). Lactic acid contributes to a lowering of the pH of the local environment leading to initiation of carious lesions by dissolution of tooth minerals (Guo et al. 2013). The glucan matrix facilitates retention of lactic acid within the environment, as well as providing the previous mentioned functions of EPS (Guo et al. 2015). *Streptococcus mutans* and certain other microorganisms, including *Lactobacillus*, *Actinomyces*, *Bifidobacterium*, and *Scardovia* species, can survive these acidic environments, a trait referred to as being aciduric, which ensures persistence in the biofilm and reduces competition from other species (Zhang et al. 2022a; Spatafora et al. 2024). In dental caries, continuous acidity followed by the destruction of the tooth surface reaches an irreversible stage with an imbalance in demineralisation and remineralisation, which if untreated eventually progresses through the dentine of the tooth to the pulp tissue, causing pulpal necrosis, abscess formation and frequently the spread of infection beyond the of the root apex of tooth (Warreth 2023). *Streptococcus mutans* is considered one of the major inhabitants of dental plaque in an environment abundant with carbohydrates (Metwalli et al. 2013). Glucan is the most prevalent EPS component in oral biofilms and *S. mutans* is the predominant producer, making it a prime pathogen in caries (Bowen et al. 2018).

In these complex environments, both the host and microbial cells react to the changes within their surroundings. For instance, the role of saliva in the oral cavity is of importance in the formation of the acquired pellicle (Enax et al. 2023). In doing so it facilitates attachment of microorganisms. Saliva also has a buffering role in protecting the tooth surface from acidic

effects and abrasion. Furthermore, saliva is a lubricant of the oral cavity's tissues, in addition to roles in mineral haemostasis and remineralisation (Chawhuaveang et al. 2021).

1.8 *Neisseria gonorrhoeae*

Neisseria gonorrhoeae is a Gram-negative bacterium that is responsible for causing gonorrhoea in humans (Unemo et al. 2019). Gonorrhoea is a sexually transmitted disease that has significant health implications especially when left untreated, as this can lead to pelvic inflammatory disease, potentially resulting in infertility and ectopic pregnancies (Reekie et al. 2019). *Neisseria gonorrhoea* has a remarkable ability to develop resistance to antimicrobial agents, due to its capacity for rapid genetic mutation and horizontal gene transfer (Manoharan-Basil et al. 2021). *Neisseria gonorrhoea* cells can rapidly adhere to the host's epithelial cells using pili and other outer membrane proteins (Kim et al. 2019). It is also capable of invading epithelial cells and avoiding host response by altering proteins to evade phagocytosis (Alcott et al. 2022). Within *N. gonorrhoea* biofilms, eDNA has been documented as a major EPS component with a critical role in the formation and structural integrity of its biofilms (Falsetta et al. 2011). eDNA is produced via various mechanisms, which include autolytic release following cell destruction which leads to the release of cellular contents to the outer environment, or active secretion via the type IV system, a system used by bacteria to transfer DNA across the cell wall (Ibáñez de Aldecoa et al. 2017). This system is dependent on channels that allow for substrate transportation from the cytoplasm to extracellular space or adjacent cells. The presence of eDNA within the biofilm because of either mechanism would serve to facilitate horizontal gene transfer by spreading resistance genes (Zweig et al. 2014).

1.9 Management of biofilms

Biofilms pose significant challenges not only in the medical context, but also in industrial fields. Biofilms cause biofouling, affecting water treatment systems, food processing, pipelines, and marine vessels, resulting in economic impact alongside health risks (Highmore et al. 2022). Biofilm formation in water systems alters water quality and may cause turbidity or malodour. Also, biofilms may cause damage to system parts by increasing the corrosion rate of certain materials (Alhoshy et al. 2025). Similarly, in ships and marine vessels, biofilms attach to vessel surfaces followed by further colonisation by micro and macro-organisms (Georgiades et al. 2021). This may lead to issues such as reduced hydrodynamics and increased fuel consumption (Georgiades et al. 2021; Shineh et al. 2023). In dental practice, biofilms form within the dental unit waterline, posing a risk of cross-infection through water output (Bayani et al. 2023). Despite the diverse contexts in which biofilms exist, there is a notable convergence in the management approaches. Preventive measures to inhibit biofilm formation, are described in the following sections alongside the targeting of established biofilms.

1.9.1 Surface modification to inhibit biofilms

A common approach to biofilm management is surface modification to limit microbial adhesion by altering surface properties such as its hydrophobicity and smoothness. Gayani *et al*. (2021) found that creating superhydrophobic surfaces in urinary catheters led to biofilm inhibition which was attributed to the materials enhanced ability to 'wash out' molecules that aided biofilm formation (Gayani et al. 2021). Additionally, the development of surfaces coated materials with antimicrobial properties has been researched. For example, the use of farnesol

to prevent *C. albicans* biofilm formation on denture materials, has been documented to limit both attachment of cells and hyphal formation (Petrovic et al. 2022).

1.9.2 Mechanical removal of biofilms

Another common approach in biofilm management is the mechanical removal of potential nutrient sources and microbial colonisation. Such approaches are possible where biofilms are accessible to routine cleaning and maintenance procedures. In surgical instruments where organic material and biofilm formation is evident, manual or automatic mechanical cleaning is required to remove attached biofilm prior to sterilisation (Rosário et al. 2022). In chronic wounds, biofilms can be a cause of acute infection or delayed wound healing and is a major global health and economical issue. The first line management for biofilms in chronic wounds is debridement, which is the physical disruption and removal of biofilm and dead tissues at the wound site. This mechanical removal reduces the microbial load and promotes reepithelialisation, aiding in further defence against biofilms (Verbanic et al. 2020). Similarly, in the context of tooth brushing, the mechanical removal of plaque biofilm, including nutrients, is an important approach to maintaining good oral hygiene and reducing the occurrence of caries and periodontal diseases (Ashley 2001).

1.9.3 Chemical management of biofilms

The control and eradication of biofilms through chemical means involve a wide array of agents, each selected for specific efficacy against biofilm matrix components and the microbial constituents. Antimicrobial agents are the most significant example within this category. These substances are used to target microbial cells within biofilms, and depending on the mechanism of action, can kill or prohibit the multiplication of cells. The broad different classes of antimicrobials include antibiotics, antifungals, and antiviral agents (Di Martino 2022).

1.9.3.1 Antibiotic treatment of biofilms

Antibiotics are a subclass of antimicrobial agents that specifically target bacteria, and by interacting with essential bacterial cell components and processes can either kill bacteria (bactericidal) or inhibit their growth (bacteriostatic). Traditionally, the term antibiotic was reserved for agents that were products of other microorganisms, but some can now be chemically synthesised (Muller 2022). The classification of antibiotics is based on different aspects, including the source of the agent, mechanism of action and chemical structure. The following sections cover two of the most used antibiotic categories based on target of action.

1.9.3.1.1 Antibiotics targeting bacterial cell wall

β-lactam agents kill bacteria by targeting the cell wall. Specifically, these agents interfere with the synthesis of peptidoglycan through inhibition of transpeptidation (Turner et al. 2022). Transpeptidation is a process where fully formed peptide strands in the peptidoglycan of the bacterial cell wall are linked to each other to enhance cell wall structure and is catalysed by enzymes in the cytoplasmic membrane. β lactam agents bind to these enzymes leading to their inactivation, and subsequent cell death due to loss of cell contents or lysis caused by increased osmotic pressure (Catherwood et al. 2020). Similarly, glycopeptide antibiotics, such as vancomycin, also target the cell wall by preventing transpeptidation of peptidoglycan (Stogios and Savchenko 2020). However, glycopeptides have an additional mechanism that targets a stage in the formation peptidoglycans referred to as transglycosylation (Tonna and Tonna 2022). During the formation of peptidoglycans, subunits are incorporated into the backbone of peptidoglycans. Glycopeptides bind to these subunits inhibiting enzymatic activation leading to failure in forming peptidoglycans (Heijenoort 2001; Tonna and Tonna 2022).

1.9.3.1.2 Antibiotics targeting bacterial protein synthesis

Several classes of antibiotics exert their antimicrobial activity by targeting bacterial protein synthesis. These can act at different stages of protein production. By binding to the 30S subunit of bacterial ribosomes, aminoglycosides cause misreading of mRNA resulting in mistranslation leading to in incorrect amino acids incorporation into proteins, rendering them dysfunctional and cell death ensues (Krause et al. 2016). For certain aminoglycoside antibiotics, such as gentamicin, attachment to ribosomes is irreversible and sustained for multiple cycles leading to frequent translational errors (Drew 2010; Wohlgemuth et al. 2021). Tetracyclines and chloramphenicol are other examples of antibiotics that target protein synthesis (Drago 2019; Pearson et al. 2025). These agents bind to bacterial ribosomes blocking access of aminoacyl tRNA to mRNA. Aminoacyl tRNA carries the amino acids to be incorporated into the growing peptide chain thus blocking this step will stop protein synthesis (Krawczyk et al. 2024). Since this action is reversible tetracyclines are classified as bacteriostatic antibiotics, meaning they halt the growth of bacteria (Gaur and Bal 2022). Chloramphenicol selectively blocks the synthesis of specific codons, making their antimicrobial activity dependent on the protein sequence (Choi et al. 2020).

1.9.3.2 Antifungals

Antifungals are agents that target specific components of fungal cells. Like other antimicrobial agents, antifungals disrupt critical processes or structures in fungi, leading to cell death or growth inhibition. Since fungal cells are eukaryotic, identifying suitable targets that are absent from host cells is a greater challenge for antifungal development compared with antibiotics (Kumar and Srivastava 2023). There are several classes of antifungals, and these are summarised in Table 1.4.

1.9.3.2.1 Polyenes

Polyenes are a class of antifungals agents known for their broad spectrum against a wide range of fungi. Polyenes bind to ergosterol which an essential component of the cell membrane of most fungi (Sae-Tun et al. 2020). When polyenes, such as amphotericin B or nystatin, bind to ergosterol, pores and channels are formed which disrupt the integrity of the cell membrane and lead to leakage of ions compromising cell viability (Carolus et al. 2020). Polyenes are therefore fungicidal agents at suitably high enough concentrations.

1.9.3.2.2 Azoles

Azoles are antifungal agents that inhibit the biosynthesis of ergosterol (Teixeira et al. 2022). This occurs through the inhibition of lanosterol 14α-demethylase, which is an enzyme responsible for the catalysis of oxidative removal of a 14α-methyl group from sterol precursors, which is a crucial step in the ergosterol biosynthesis (Song et al. 2025). This inhibition leads to the reduction of ergosterol within the cell membrane, altering both structural and functional integrity of the fungal cell (Teixeira et al. 2022; Singh et al. 2023). Typically, azoles are fungistatic and therefore inhibit the growth of fungi, enabling the immune system to kill the colonising organisms (Ahmad et al. 2010). Frequently used azoles include fluconazole, itraconazole and voriconazole.

Table 1.4 A list of commonly used antifungal in fungal infections

Class	Antifungal	Mechanism of action	Route of administration	Reference
Polyene	Amphotericin B	Binds to ergosterol in the fungal membrane, disrupting structure and causing cell death	Systemic/Topical	(Carolus et al. 2020)
Azole	Fluconazole Itraconazole Voriconazole Posaconazole	Inhibits ergosterol synthesis by interfering with lanosterol 14-α-demethylase	Systemic	(Hof 2006)
Echinocandin	Caspofungin Micafungin Anidulafungin	Inhibits (1,3)-β-D-glucan synthase, weakening the fungal cell wall	Systemic	(Kofla and Ruhnke 2011)
Pyrimidine	Flucytosine	Interferes with DNA synthesis by inhibiting thymidylate synthetase and protein synthesis by altering amino acylation	Systemic, often combined with Amphotericin B	(Vermes et al. 2000)
Allylamine	Terbinafine	Inhibits the enzyme squalene epoxidase, disrupting ergosterol synthesis	Systemic	(Nakamura et al. 2024)

1.9.3.3 Chemical biocides

Chemical biocides play a vital role in controlling and eliminating biofilms across healthcare and industrial settings (Bridier et al. 2011). Among the most commonly used is sodium hypochlorite, a chlorine-based disinfectant renowned for its efficacy as an irrigation agent during root canal treatments (Cai et al. 2023). This efficacy is attributed to its broad-spectrum antimicrobial activity (Gonçalves et al. 2016) and its ability to dissolve necrotic tissue and organic debris within the root canal system (Stojicic et al. 2010). Other biocides, such as hydrogen peroxide, are widely used for disinfecting medical equipment (Assadian et al. 2021). Similarly, chlorhexidine is extensively employed in healthcare due to its broad-spectrum antimicrobial properties (Greenhalgh et al. 2019).

1.9.3.3.1 Chlorhexidine

Chlorhexidine (CHX) is a bisbiguanide antimicrobial agent that exhibits broad spectrum bactericidal and fungicidal activity (Cieplik et al. 2019). Chlorhexidine is composed of two biguanide groups connected by a hexamethylene chain, giving it strong cationic properties, which are crucial for its mechanism of action, which is disruption of the integrity of microbial cell membrane. The positively charged CHX interacts with negatively charged phospholipids on microbial cell surfaces and at low concentration, this leads to reversible biostatic activity. At higher concentrations or prolonged exposure, CHX exerts biocidal effects by binding with intracellular components such as adenosine triphosphate and nucleic acids, forming complex precipitation and coagulation leading to cell death (Lim and Kam 2008; Deus and Ouanounou 2022). CHX is insoluble in water, but when formulated with gluconic acid it forms water soluble salts (Thangavelu et al. 2020), which facilitate its incorporation into different applications and agents (Dinu et al. 2024). The broad antimicrobial spectrum of CHX means it is a significant

agent for a range of applications in dentistry and CHX is a valuable agent in biofilm control and periodontal disease prevention. CHX's ability to bind to surfaces in the oral cavity facilitates the prolonged activity after initial use, a process called substantivity (Solderer et al. 2019).

1.9.4 Targeting the EPS of biofilms

Due to the role of EPS in biofilm development and the increasing challenge of biofilm eradication, diverse strategies have been explored in biofilm research that target biofilm EPS. The approaches (outlined below) include the inhibition of EPS formation and its disruption in established biofilms.

1.9.4.1 Enzymatic treatment of EPS

An important approach to EPS inhibition is the use of enzymes to degrade the suspected major components of EPS. Researchers have used a wide variety of enzymes to assess activity against biofilms, with the aim of overcoming biofilm resistance. Depending on the desired target, different agents can be used, for example, proteinase for disrupting EPS proteins (Mugita et al. 2017). A combination of DNase I and proteinase K have been used to disrupt multispecies *in vitro* biofilms, significantly altering the composition and structural integrity of biofilms. DNase I degraded eDNA, a critical component for stability and cellular interactions, while proteinase K targeted extracellular proteins. Qualitative visual analysis of CLSM results revealed that the combined treatment led to greater disruption of biofilm compared to individual enzyme treatment. Furthermore, the *in vitro* biofilms, composed of *Actinomyces oris*, *Candida albicans*, *Fusobacterium nucleatum*, *Streptococcus mutans*, *Streptococcus oralis*, and *Veillonella dispar*, exhibited altered species dynamics following enzymatic treatment. The combined action of DNase I and proteinase K created an environment that favoured the growth of *S. mutans* and *S. oralis*, likely due to reduced nutritional competition (Karygianni et

al. 2020a). Another study demonstrated that a combined enzymatic treatment effectively disrupted *Pseudomonas aeruginosa in vitro* biofilms, including both laboratory strains and clinical isolates (Zhang et al. 2023). This approach utilised $AidH_{A147G}$, a mutant N-acylhomoserine lactonase quorum-quenching enzyme that degrades QS molecules, and PslG, a self-produced glycosyl hydrolase of *P. aeruginosa* that breaks down matrix polysaccharides. $AidH_{A147G}$ inhibited quorum sensing by degrading acyl-homoserine lactones, thereby suppressing virulence factor expression and biofilm-related gene activity, while PslG targeted extracellular polysaccharides, destabilising the biofilm structure. CLSM confirmed that the combination treatment eradicated biofilm presence on glass-bottom cell culture dishes. Furthermore, the enzymatic treatment enhanced antibiotic efficacy, with multidrug-resistant strains transitioning to intermediate or sensitive states when treated with antibiotics such as tobramycin or meropenem in conjunction with the enzymes (Zhang et al. 2023).

Selectivity of enzyme treatment is of value, when for example targeting the polysaccharides of biofilms involved in chronic wounds as it ensures that the enzymes are not detrimental to host tissues (Fleming et al. 2017). For enzyme targeting polysaccharides within the matrix a wide range of glycoside hydrolase enzymes have been investigated. The enzymes' ability to cleave glycosidic bonds of polysaccharides, results in them converting polysaccharides into simpler sugars and this disrupting the matrix (Wang et al. 2023). One such enzyme is dextranase, a glycoside hydrolase that targets α-1,6-linked glucans (dextran), which are key components of EPS in dental biofilms. In cariogenic biofilms, particularly those formed by *Streptococcus mutans*, dextran and related α-glucans contribute to biofilm cohesion, adhesion, and matrix architecture, making them suitable targets for enzymatic treatment (Pleszczyńska et al. 2015). A recent systematic review of *in vitro* studies further supports the use of dextranase as a non-biocidal strategy for biofilm control, demonstrating that

dextranase treatment can reduce cariogenic biofilm formation and destabilise established biofilms by degrading dextran-rich EPS matrices (Del Rey et al. 2024). Another example is dispersin B, a glycoside hydrolase enzyme produced by the bacterium *Aggregatibacter actinomycetemcomitans* (Kaplan et al. 2003), specifically hydrolyses poly-N-acetylglucosamine (PNAG), a polysaccharide commonly found in the biofilms of bacteria such as *Staphylococcus epidermidis, Escherichia coli* and *Staphylococcus aureus* (Breslawec et al. 2023). By breaking down PNAG, dispersin B (0.2 and 2 µg/mL) has prevented biofilm formation by the Gram-negative bacterium *Actinobacillus pleuropneumoniae* (Izano et al. 2007b). Studies have reported that dispersin B is effective in targeting biofilms from over 25 bacterial species, including both Gram-negative and Gram-positive bacteria. Its antibiofilm activity has been validated under controlled laboratory conditions and in animal models, highlighting its potential for broad-spectrum therapeutic applications (Kaplan et al. 2024).

Furthermore, DNase is a potent enzyme used in biofilm management due to its ability to degrade eDNA, which is an important component of EPS responsible for maintaining the stability of various microbial biofilms (Schlafer et al. 2017). Rikvold et al. (2023) assessed the effect of DNase treatment on oral biofilms, where healthy adult participants with good oral hygiene were fitted with jaw splints with glass slabs. The glass slabs were retrieved at different time points to assess efficacy of DNase on different stages of biofilm. DNase was found to disrupt *in situ* biofilms in the early stage of formation inhibiting the stability and coaggregation of cells. No significant effect on mature biofilms grown for over 7.5 h occurred (Rikvold et al. 2023).

1.9.4.2 Nanotechnology and photodynamic therapy in targeting EPS

Nanotechnology biofilm treatment involves application of nanoscale materials to prevent, control, and eradicate biofilm-associated infections, while offering a range of approaches to target EPS molecules (Asare et al. 2022). Examples include use of nano-enzymes that mimic DNase activity to degrade eDNA (Liu et al. 2019) or use of modified nanoparticles that can target polysaccharides (Gao et al. 2016). Another approach is to focus on overcoming the barrier of defence of EPS rather than targeting it. Lopes et al. (2019) investigated the use of glycerol monolaurate encapsulated within nano capsules with a mean diameter of 190.7 nm, demonstrating enhanced antimicrobial effectiveness against *Pseudomonas aeruginosa* biofilms. MIC testing, biomass reduction, and atomic force microscopy revealed that glycerol monolaurate nano capsules were more effective than free glycerol monolaurate in reducing biofilm biomass and levels of polysaccharides, proteins, and viable cells. These findings suggest that the nano capsules' size may have improved their ability to penetrate and disrupt biofilms (Lopes et al. 2019).

Other means of EPS targeting include use of photodynamic therapy, where light activated photosensitisers induce a toxic response through the generation of reactive oxygen species that can disrupt the matrix (Abdulrahman et al. 2020). Similarly, extracts from microorganisms can be considered a natural source of agents capable of disrupting and inhibiting biofilm formation, a study on the methanolic extract from the marine cyanobacterium *Oscillatoria subuliformis* revealed that it disrupts and inhibits *in vitro* biofilm formation of *P. aeruginosa*. Although the extract did not exhibit bactericidal activity compared to the control, results showed that a concentration of 5 µg/ml significantly inhibited biofilm formation by over 50%, reduced biofilm thickness, and decreased EPS production by 40% (LewisOscar et al. 2018).

1.10 Antimicrobial resistance

Despite the availability of a diverse array of antimicrobial agents, including those outlined above, microorganisms have developed sophisticated mechanisms to counteract these therapeutic interventions, and this is collectively defined by the term Antimicrobial Resistance (AMR) (Prestinaci et al. 2015). The global effect of AMR is escalating and significantly increasing healthcare costs, with billions of dollars spent annually to combat AMR (Naylor et al. 2025). AMR is associated with higher patient morbidity and mortality and this, together with associated costs of more intensive medical care and longer hospital stays, results in an unacceptable burden on both patients and the economies of healthcare systems (Naghavi et al. 2024). AMR poses a significant public health threat in Saudi Arabia, a recent systematic review reported high prevalence rates of major resistant pathogens, including methicillin-resistant *Staphylococcus aureus* (MRSA) at 38.7%, extended-spectrum β-lactamase (ESBL)-producing *Enterobacteriaceae* at 26.4%, and carbapenem-resistant *Enterobacteriaceae* (CRE) at 15.2% (Kiran et al. 2024). These findings underscore the urgent need for enhanced surveillance and the implementation of robust antimicrobial control policies to manage the growing burden of AMR. Consequently, the combined challenges of treatment and costs of AMR have resulted in widespread efforts to evaluate AMR mechanisms. The subsequent sections focus on the mechanisms of AMR expressed at cellular level, followed by the AMR mechanisms found in multicellular communities of biofilms.

1.10.1 Antimicrobial resistance mechanisms

1.10.1.1 Enzymatic inactivation of antibiotics

An important AMR mechanism employed by microorganisms is the production of enzymes that degrade antimicrobial agents. Examples are β-lactamases, which are enzymes that

inactivate penicillin type agents by binding to the antibiotic's β-lactam ring structure. β-lactamases have a structural similarity to penicillin binding proteins, the intended target of these antibiotics (Sanders and Sanders Jr 1992).

1.10.1.2 Modification of the antibiotic targets

Another AMR mechanism against β-lactam type antibiotics is the modification of the active site of the penicillin binding protein, as seen with MRSA (Ali et al. 2021). The modification of the peptidoglycan precursor involved in cell wall biosynthesis, confers resistance to glycopeptide antibiotics and is a further example of an AMR mechanism (Greule and Cryle 2020).

1.10.1.3 Multidrug efflux pumps

Multidrug efflux pumps play a key role in microbial AMR. Efflux pumps comprise of transporter proteins which expel harmful chemicals including antimicrobials out of the cell (Huang et al. 2022b). This has the effect of decreasing the concentration of harmful substances within the cell to below toxic levels and enhances the survival of microbes (Sreekantan et al. 2022). The Gram-negative bacterium *P. aeruginosa,* is a common cause of hospital-acquired infections, such as pneumonia, urinary tract infections, and infections in burns and wounds (Bodey et al. 1983) and frequently displays AMR mediated by multidrug efflux pumps. The overexpression of efflux pumps is often the cause of AMR and one such example is that of the MexAB-OprM, where its overexpression can reduce intracellular concentration of β-lactams, fluoroquinolones, and tetracyclines (Masuda et al. 2000; Lorusso et al. 2022).

1.10.2 Biofilm-specific antimicrobial resistance mechanisms

Biofilms exhibit significantly higher tolerance to antimicrobial treatments, with resistance levels often cited as being a thousand-fold higher compared to planktonic cells (Li et al. 2024). This profound increase in tolerance is highlighted in a study by Thöming and Häussler (2022), where researchers investigated 352 clinical isolates of *P. aeruginosa* to compare antimicrobial susceptibility profiles under biofilm and planktonic growth conditions. Even though the study revealed drug-specific killing activity, the reported biofilm tolerance levels of biofilms were up to 16,000-fold higher compared with planktonic cells (Thöming and Häussler 2022).

The reason for higher AMR in biofilms is multifactorial and attributed to both the biofilm cells and the surrounding EPS (Liu et al. 2024). For cells within biofilm, one contributing factor is the presence of dormant or slow-growing cells (Scribner et al. 2020). Many antimicrobials have higher activity against metabolically active and proliferating cells, making cell dormancy a protective feature for biofilms (Wainwright et al. 2021). In specific regions of a biofilm, cell dormancy and reduced activity is attributed to local environmental factors, such as limited nutrient availability, low oxygen levels, and adverse pH conditions (Behbahani et al. 2022). Additionally, due to the structural organisation of biofilms, which keeps cells in close proximity, there is a high frequency of HGT and uptake of eDNA which enables cells to acquire antimicrobial resistance genes (Michaelis and Grohmann 2023). Similarly, QS molecules benefit from this structural organisation of biofilms, by enabling coordinated responses to environmental challenges (Singh et al. 2017), including the upregulation of other resistance mechanisms such as increased expression of efflux pumps (Maseda et al. 2004).

An AMR mechanism associated with EPS is thought to be the reduced penetration of certain antimicrobials thereby reducing biofilm cell exposure (Flemming and Wingender 2010). The

EPS matrix can also sequester antimicrobial agents through electrostatic and hydrophobic interactions and reduce availability and action against the cell population (Singh et al. 2021b). The accumulation of antimicrobial inhibitory enzymes, *e.g.* ß-lactamases, in the biofilm matrix can also neutralise antimicrobial agents before they reach target cells thus contributing to elevated biofilm AMR (Hengzhuang et al. 2013).

Biofilm mediated AMR therefore involves complex interactions of multiple resistance mechanisms. Given that some of these AMR mechanisms are also exhibited by planktonic cells, their synergistic activity with biofilm specific components is important. The proximity of cells, surface attachment and the presence of the EPS promotes the effects of these different mechanisms, and the survival of the biofilm (Davies 2003; Hall-Stoodley et al. 2004; Singh et al. 2021a).

1.11 Methods and techniques used in biofilm research

To study the complex behaviour of biofilms including their responses to antimicrobial treatment, researchers have used an array of methods to grow and analyse biofilms. These techniques are crucial to allow subsequent analyses of biofilm structure, function, and behaviour, as well as evaluating the efficacy of treatment. The *in vitro* production and analyses of biofilms have involved use of high throughput methods, supporting sophisticated models of growth and the application of advanced analytical methods.

1.11.1 *In vitro* biofilm growth models

While *in vivo* studies are better representation of natural biofilm environments and associated clinical infections, they are also more complex and present specific challenges (Shi et al. 2019). *In vivo* experiments are associated with additional variables relating to the host and the immune response, that are difficult to standardise (Lebeaux et al. 2013). Often costs are high,

which limit the quantity of experiments and there are ethical considerations associated when using animals (Shi et al. 2019). In comparison, *in vitro* studies are typically of lower cost, have higher throughput, and have proven to be valuable in evaluating surface attachment of biofilms (Roberts et al. 2015). Therefore, to investigate the characteristics of biofilms, *in vitro* studies play an important role.

Numerous *in vitro* methods have been used to grow biofilms, each having their own distinct advantages and limitations. Biofilms can be grown in 'closed' or 'batch' systems, where there is no replenishment of culture medium. In contrast, continuous flow methods (also referred to as dynamic methods), can be used and are often considered superior as they enable medium replacement, removal of waste and introduction of shear forces. Typically, flow through models are performed in bioreactor systems (Crivello et al. 2023).

Growing biofilms under batch conditions frequently uses 96-well microtiter plates, and whilst the surface of the wells can be used as the substratum, other suitable surfaces in the form of coupons, can be used. In dynamic flow through models, such as the Centers for Disease Control and Prevention (CDC) biofilm reactor, biofilm growth is supported on coupons of various material types that can be removed from the bioreactor for subsequent analyses (Mendez et al. 2020). Another *in vitro* model is the Calgary Biofilm Device (CBD) which is an advanced system for studying biofilm formation and antimicrobial susceptibility (Subramanian et al. 2020). The device features a two-part reaction vessel, with a top component forming a lid that includes 96 pegs, each sealed to prevent contamination during removal. These pegs fit into the wells of a standard 96-well plate and are designed to sit in the channels of the bottom component of the vessel. This design channels the flow of medium across the pegs,

creating consistent shear forces and ensuring uniform biofilm formation on each peg (Ceri et al. 1999).

1.11.1.1 Batch systems for growing *in vitro* biofilms

Batch systems are considered the simplest and most widely used *in vitro* methods of growing biofilms. This approach involves introducing microorganisms in a liquid medium and allowing biofilm development on submerged surfaces. Whilst medium replenishment may not be a feature, manual and periodic medium exchange can be introduced. A batch system offers several advantages, including simplicity and minimal equipment requirement, high throughput, easy set up, and low cost. Standard laboratory materials *e.g.* the wells of a microtiter plate can provide the attachment surface. However, a batch system has limitations, most notable of which is the lack of control over the biofilm growth environment. Nutrient depletion and waste accumulation occurs with time, which can impact biofilm development and stability (Coenye and Nelis 2010).

1.11.1.2 The Centers for Disease Control and Prevention (CDC) biofilm reactor

The CDC biofilm reactor (Figure 1.2 C) is a dynamic system designed for *in vitro* biofilm culture. The system is adaptable, with adjustable settings for key parameters such as flow rate and surface of attachment (Guzman-Soto et al. 2021). The CDC biofilm reactor comprises a 1L cylindrical glass vessel, with an effluent port covered by a polyethene top which contains 3 ports and 8 holes for rods (Figure 1.2 D). The ports are used for inoculation and fresh medium injection, whilst an air filter port ensures sterile gaseous exchange. In the centre of the reactor's lid is a rod that descends to the bottom of the reactor and this attaches to a magnetic baffled stirrer, which is surrounded by peripheral rods when fitted. Inlet and outlet ports ensure circulation of culture medium into and out of the vessel. This design enables biofilm

growth under shear flow conditions which are generated by the baffled stir bar. The CDC biofilm reactor can be used in a batch phase, as stated by manufacturer's operator manual. Continuous flow conditions are enabled by introducing fresh medium through the inlet port and discarding spent medium through the effluent port.

The rods can be fitted with coupons of different materials including plastics, metals, and glass, each offering unique surfaces for biofilm attachment and growth (International 2007). The choice of coupon material is often determined by the specific requirements of the study, such as the type of biofilm being investigated or the conditions being mimicked, for example, the use of hydroxyapatite coupons to imitate a tooth surface (An et al. 2022) or titanium and zirconium to study implant colonising biofilms from common oral bacteria (Sánchez et al. 2014). Operating the CDC biofilm reactor requires additional equipment for nutrient supply and temperature control. Carboys are necessary for storing fresh media and for waste disposal, ensuring a consistent circulation (Figure 1.2). The bioreactor can also be placed on a magnetic stirrer to generate shear force.

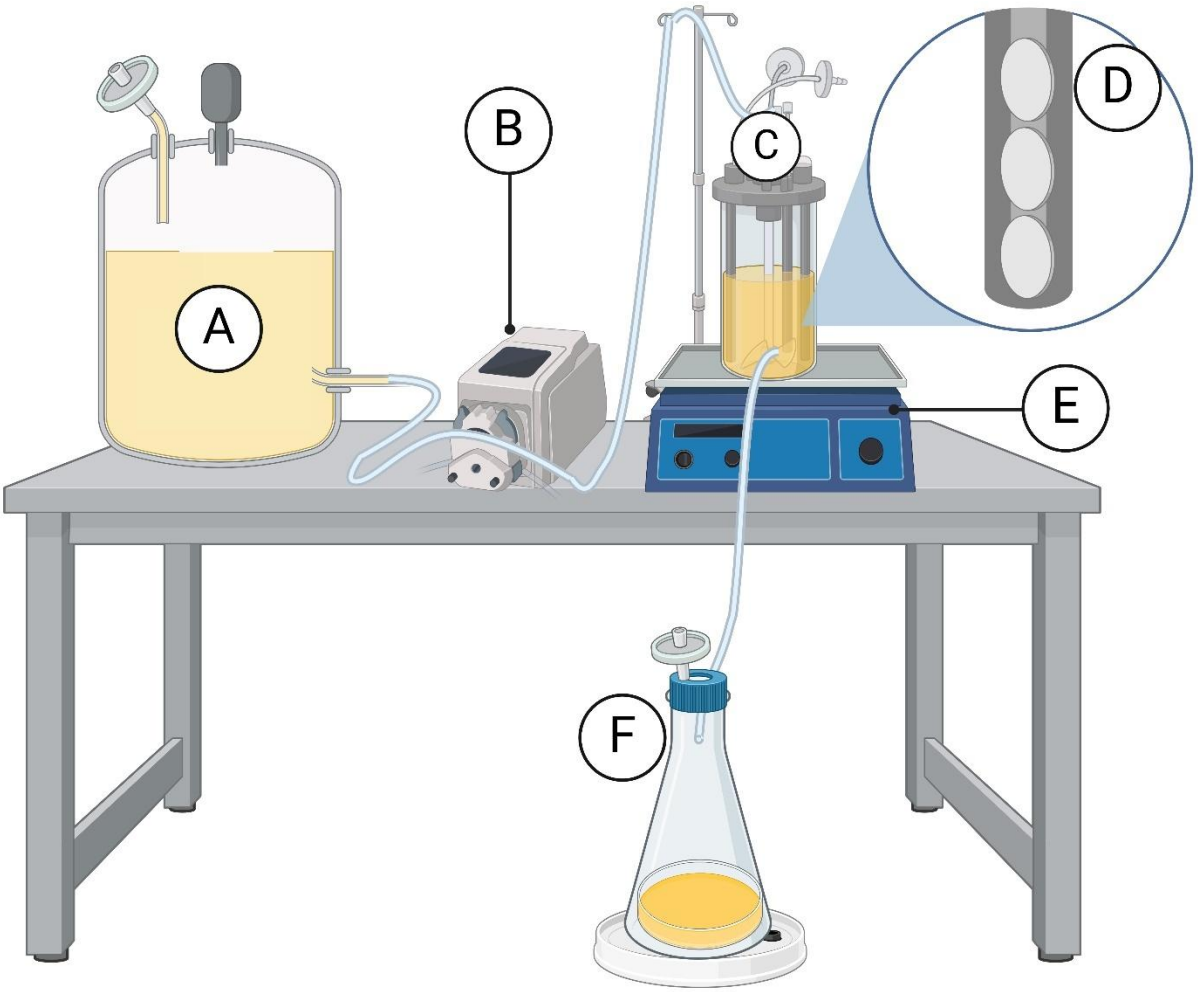

Figure 1.2 A full setup of a CDC biofilm reactor flow-through system fitted in temperature-controlled room.

A) Fresh media container. B) Peristaltic pump. C) The CDC biofilm reactor placed on magnetic stirrer (E). D) A close-up showing coupons fitted in the rod. F) Waste container of disposed medium (Created with BioRender.com).

Whilst these specifications and tools aid in precise control over the growth conditions, the assembled system introduces complexity in setup and operation, which are time consuming and labour intensive, particularly when compared to some batch systems, Table 1.5 summarise key differences between batch and flow-through systems (Azeredo et al. 2017).

Table 1.5 Comparison of the key differences between batch and flow-through biofilm systems

Batch system (microtiter plate)	Flow-through system (CDC biofilm reactor)
Closed/ Static	Open/ Dynamic
No or mild shear conditions	High and non-stop shear conditions
Manual replacement of media	The continuous flow of media
Accumulation of waste within the system	Continuous waste disposal out of the system
Easy assembly	More complicated assembly
Fewer consumables (reagents)	Higher volume of reagents
Low cost to run (equipment needed is usually common in laboratories)	Higher cost to run (a special type of equipment)

The importance of reproducing a biofilm's natural environment as near as possible is an important aspect of *in vitro* biofilm research. Introducing variables such as shear stress, nutrient gradients, and polymicrobial cultures can reveal important characteristics such as biofilm architectural complexity and specific metabolic activities (Shi et al. 2019). The overall result is a biofilm that better represents one occurring in clinical and natural settings, allowing for more accurate assessment of biofilms and antibiofilm testing. Nevertheless, it is impossible to fully replicate a biofilm in an oral environment, which is a significantly heterogeneous part of the body in the context of constituent microorganisms, surfaces for attachment, forces, and nutrition (Schönbächler et al. 2023). The oral cavity harbours hundreds of species of microorganisms existing in a biofilm state attached to the different surfaces of soft and hard tissues such as tongue, palate, gingival crevice, and teeth with

diverse nutrient sources from the host diet, secreted saliva and gingival crevicular fluid (Simon-Soro et al. 2013; Radaic and Kapila 2021). Considering cost, labour and time management, a batch system such as that provided by a microtiter plate can offer high throughput and low cost in the study of biofilm development and the study of biofilm prevention and disruption strategies (Azeredo et al. 2017).

1.11.1.3 Considerations for the selection and refinement of *in vitro* biofilm development conditions

In vitro biofilm development serves as a cornerstone for understanding microbial behaviour, interspecies interactions, and the impact of environmental factors. To ensure the relevance and accuracy of these models, several key considerations must be addressed, including species selection, surface conditioning, and incubation parameters, guided by the research aims and the specific environments under investigation.

The selection of microbial species is a fundamental consideration in biofilm research, as it directly impacts the relevance and applicability of the study's findings. Researchers often choose between single-species and polymicrobial biofilms depending on the study's objectives. Single-species biofilms are particularly valuable for understanding the specific behaviours, mechanisms, and responses of a single microorganism (Cleaver and Garnett 2023). They also facilitate the evaluation of how a single species behaves in planktonic versus biofilm states. Such studies provide controlled environments to dissect the contributions of individual species to biofilm formation, virulence, and antimicrobial susceptibility (Stewart et al. 2022).

In contrast, polymicrobial biofilms are increasingly recognised as more representative of natural and clinically relevant scenarios (Cleaver and Garnett 2023). They mimic the complex microbial communities found in environments such as the oral cavity, medical devices, and chronic wounds, more closely resembling of clinical infections, including caries, periodontitis, candidosis, otitis media, and wound infections (Anju et al. 2022). For example, a study on the *in vitro* virulence of *C. albicans* demonstrated that when grown with oral bacterial species in polymicrobial biofilms, its virulence was significantly enhanced (Morse et al. 2019). These biofilms included *C. albicans* alongside bacteria such as *Streptococcus sanguinis*, *S. gordonii*, *Actinomyces viscosus*, and *Actinomyces odontolyticus*. Interspecies interactions promoted the virulence of *C. albicans* by stimulating hyphal formation and upregulating virulence-associated genes, including those encoding adhesins and hydrolytic enzymes. The study underscored the critical role of interspecies interactions and highlighted the importance of selecting representative polymicrobial biofilms, as in this case, to more accurately mimic denture stomatitis, where *C. albicans* naturally coexists with oral bacteria (Morse et al. 2019).

Surface conditioning is commonly used in biofilm research to influence microbial attachment and biofilm development. This approach allows researchers to mimic natural environments where biofilms form on surfaces exposed to their surroundings, often covered by a film of macromolecules absorbed onto the surface (Dsouza et al. 2024). For instance, donor saliva (Martínez-Hernández et al. 2023) artificial saliva (da Silva et al. 2022) to replicate the natural occurrence of acquired pellicle formation on both host tissues (Chawhuaveang et al. 2021), and oral prosthetic devices (Souza et al. 2021).

The choice of material significantly influences biofilm growth and structure, as properties such as surface roughness, hydrophobicity, chemical composition, and surface charge affect

microbial adhesion and subsequent biofilm development (Zheng et al. 2021). The choice of surface for *in vitro* studies typically aligns with the environment of interest or application. For example, titanium is often used for studying implant-associated biofilms (Bevilacqua et al. 2018), while polymers like polyethylene and polymethyl methacrylate are used to represent catheters and dentures (Fang et al. 2016; Asker et al. 2021). Hydroxyapatite are of interest to mimic the tooth surface (Sangha et al. 2024). Therefore, selecting an appropriate surface material for *in vitro* studies is a crucial step in bridging the gap between experimental models and the complexities of *in vivo* environments. This choice plays a vital role in creating conditions that closely mimic *in vivo* settings, thereby enhancing the relevance and applicability of experimental findings.

The incubation duration is critically important in biofilm research, as it directly influences the stages of biofilm development. Incubation periods are often evaluated to assess their resemblance to natural dynamic environments or to ensure reproducibility (Pratten et al. 2003). Several factors, such as the microbial species, the environment being studied, and external conditions like temperature and nutrient availability, influence the appropriate duration. Consequently, characterising biofilm formation under different incubation periods is a common practice in biofilm research (Al-kafaween et al. 2019).

By addressing factors such as microbial species selection, surface conditioning, and incubation parameters, researchers can employ *in vitro* biofilm models in various ways that more closely replicate *in vivo* conditions. Such refinement is essential for generating meaningful insights into biofilm behaviour, enhancing the translational potential of biofilm research, and advancing strategies to manage biofilm-associated challenges.

1.11.2 Confocal Laser Scanning Microscopy (CLSM) in biofilm research

Important analytical methods in the study of biofilms are ones that enable assessment of biofilm quantity based on biofilm thickness and surface area coverage. For such analyses direct microscopical imaging of the biofilm is a valuable approach (Vyas et al. 2016). The advent of confocal laser scanning microscopy (CLSM) was an important development in this regard as in addition to the imaging of specific biofilm components through use of fluorescent labels, the method will also construct 3D views of biofilms (Huang et al. 2020). CLSM is non-invasive and can scan thick tissue or biofilms with excellent depth discrimination, which means it can focus on specific layers within the specimen, creating detailed images. Laser light passes through a pinhole that permits light to, and from, the targeted point while blocking 'out-of-focus' light enabling acquisition of sharp, high-resolution images at various depths within a sample. Multiple scans produce sequential 'layers' through the biofilm allowing for 3D reconstruction of the biofilm (Sharif et al. 2020; Kiziltoprak et al. 2021; Mhade and Kaushik 2023).

Fluorophores are integral to CLSM, and these are molecules that when excited by specific light wavelengths, then emit light at a longer wavelength. There are numerous fluorophores and associated applications (Elliott 2020). For example, green fluorescent protein (GFP) can be genetically incorporated into microbes, offering intrinsic cell labelling (Southward and Surette 2002). Another approach is the use of fluorescent dyes that selectively bind to targets of interest and then visualised via the re-emitted light (Yoon et al. 2021). Fluorescently conjugated labels or dyes can also be used to bind to biofilm components, illuminating specific structures or cells or the EPS (Schlafer and Meyer 2017). This allows spatial distribution of cells and biofilm organisation to be determined.

A frequent application of CLSM is the use of stains to assess cell viability in a sample (Grossman et al. 2021; Mountcastle et al. 2021). Typically, these involve a two-stain approach where one dye (*e.g.* Syto 9; green fluorescence) is cell-permeant and enters all cells, whilst the other dye (*e.g.* PI; propidium iodide) is cell impermeant, and only enters cells with damaged membranes. Both dyes typically bind to nucleic acids within cells. In the case of live/dead staining, differential fluorescence between cells is indicative of cell viability. The two dyes are excited at two different wavelengths, providing two distinct colours with clear visualisation (Boulos et al. 1999). Following acquisition of CLSM images, an image-processing program can be used to further analyse and measure different parameters of the sample. This includes assessing viability by quantifying the proportion of live versus dead cells and determining thickness and biomass of biofilms (Robertson et al. 2019).

Another CLSM application is to trace and locate EPS in a biofilm. This may be achieved using fluorochrome tagged molecules that target specific components. For example, Syto9 and Syto60 detect cells, while stains such as SYPROORANGE and SYPRORUBY can be used for detecting EPS proteins, and fluorescently conjugated lectins can detect polysaccharides (Wagner et al. 2009). Such approaches have previously been used with success in biofilm characterisation and evaluation of treatments (Xiao et al. 2012).

1.11.3 Scanning electron microscopy (SEM) in biofilm research

Using accelerated electron beams for illumination, the Scanning Electron Microscope (SEM) scans the surface of the sample and records topographical data using energy change signals (Mohammed and Abdullah 2018). SEM is recognised for its deep field, that aids in making the whole field of view in focus, at magnifications of up to x1,000,000 (Mohammed and Abdullah 2018). Thus, SEM is a valuable tool for generating high resolution images alongside additional

information, such as surface topography analysis and chemical composition (Vernon-Parry 2000). Therefore, SEM has potential use in analysing biofilms both qualitatively and quantitatively, and researchers have developed a quantitative method to assess biofilm removal of a surface by combining SEM and image analysis (Vyas et al. 2016). SEM is commonly used to observe the development of biofilm and characterise the constituent microorganisms (Rusu et al. 2020). Nevertheless, conventional SEM preparation methods are inherently destructive to biofilm samples due to dehydration process required for imaging (Chang and Rittmann 1986), which can cause morphological changes including shrinkage, distortion of delicate structures and alteration of EPS. The EPS is within a matrix naturally rich in water, transforms into a fibrous appearance after dehydration. Currently, advanced approaches such as cryo-SEM and high-pressure freezing that been developed to overcome these limitations (Hrubanova et al. 2018).

1.11.4 Chemical and molecular analytical techniques in biofilms research

Detailed analysis of biofilms benefits from combined use of a variety of technical methods in attempts to understand biofilm complexity and impact in healthcare and industrial settings. Researchers have used a range chemical analytical methods, to give insight into biofilm composition, structure, function, and inform on potential disruption strategies. Spectroscopic techniques have been described as the 'molecular explorers' of biofilms. Fourier-transform infrared spectroscopy (FTIR) has been used in studies investigating EPS composition, characterising the presence of carbohydrates, proteins, and their functional groups (Gieroba et al. 2020).

FTIR and Raman spectroscopy have enabled researchers to identify and characterise both microorganisms and EPS, as well as quantify components of oral biofilms (Shakeel et al. 2022).

These spectroscopic techniques offer non-destructive, label-free analysis making them useful in studying biofilms (Gieroba et al. 2020). As demonstrated by Gieroba *et al.* (2020), these methods can provide a chemical profile of both wet and dry biofilms, requiring no preparation. This includes detailed information on the presence of major EPS components such as polysaccharides, proteins and lipids.

Chromatographic techniques are considered to be molecular sorting methods (Kisley and Landes 2015). High-performance liquid chromatography (HPLC) is a qualitative and quantitative technique that aids identification of various components, such as monosaccharides and oligosaccharides with the ability to separate EPS components by size and hydrophobicity (Meisen et al. 2008). Gas chromatography-mass spectrometry (GC-MS) is used in biofilm research to analyse metabolic processes and identify metabolites involved in biofilm formation and development. GC-MS allows detection and quantification of volatile extracellular metabolites and has also been used to compare and identify patterns of metabolic profiles between planktonic, single, and dual species biofilms of *C. albicans* and *Klebsiella pneumoniae* (Galdiero et al. 2021), and *Salmonella enterica* Serovar typhimurium (Wong et al. 2015). Overall, GC-MS is a valuable tool for understanding metabolic processes and biofilms interaction, which can aid in the development of strategies to combat biofilm-associated diseases.

In biofilm research, molecular techniques can unravel the complexity of biofilm communities and their significant effect on health, industrial processes, and environmental science (Coppola et al. 2025). Sequencing of bacterial 16S rRNA is used to identify and characterise the diverse complex microbial constituents of biofilms by analysing the genetic sequences specific to different microbes. Importantly, molecular approaches based on phylogenetically

relevant molecules can identify microbes that cannot be traced by traditional cultural techniques (Kotaskova et al. 2019). Metagenomics takes this principle even further by sequencing the genetic material within the whole biofilm, allowing identification and evaluation of functional capabilities (Pérez-Cobas et al. 2020; Palanisamy et al. 2023). Also, it helps researchers understand the genomic basis of biofilm formation and behaviour, by distinguishing between genes expressed in health and disease, and can be applied to the study of the antimicrobial resistance of different biofilms (Ribeiro et al. 2017). These molecular techniques are vital to the unlocking of biofilm treatment strategies, helping in the assessment of new antimicrobial agents and evaluation of biofilm formation.

1.12 Project aims and objectives

Despite the significant body of research on biofilms, much of the focus has been on the cellular components, leaving the EPS underexamined. This research aims to explore and characterise EPS in selected clinically relevant biofilms and investigate its role in the antimicrobial tolerance of biofilms. Various techniques and methods of biofilm growth and EPS analyses will be used in these studies.

The specific aims of each experimental chapter are as follows:

Chapter 2: To optimise the development of selected clinically relevant *in vitro* biofilms, via the construction of mono and polymicrobial species biofilms on different substrata, conditions, and culture media environments.

Chapter 3: To identify EPS components within the developed biofilms using commercially available fluorescent probes in conjunction with confocal laser scanning microscopy. In addition, the role of Lig E in *N. gonorrhoea* biofilm formation as well as eDNA presence in EPS was assessed.

Chapter 4: To use chemical analyses such as coherent anti-Stokes Raman scattering microscopy and commercially available assays for the quantification of EPS components and evaluation of enzymatic disruption of EPS.

Chapter 5: To assess the effect of EPS disruption on the antimicrobial susceptibility of biofilms.

Chapter 2

In vitro development of clinically relevant biofilms

2.1 Introduction

The primary aim of the research in this PhD was to ascertain the role of extracellular polymeric substances (EPS) in altering susceptibility of biofilm microorganisms to antimicrobials. To undertake these investigations, it was first necessary to generate suitable *in vitro* biofilms for subsequent study. As discussed in Chapter 1, a plethora of approaches including *in vitro* and *in vivo* methods can be used to grow biofilms. Given the costs and ethical considerations in use of animals, *in vivo* models of biofilm development were not deemed appropriate for this research. Therefore, the focus of this chapter was to assess several *in vitro* models to produce biofilms for later study.

The ability to grow *in vitro* biofilms has been transformative to our understanding of the behaviour of biofilm microorganisms, particularly those involved in human infections. The development of standardised *in vitro* biofilms does however present a challenge, as they are inherently variable and influenced by complex environmental and biological factors. Therefore, establishing an approach to *in vitro* biofilm growth that was conducive to the generation of reliable results in a cost-effective manner was important.

2.1.1 *In vitro* biofilm growth methods

In vitro biofilm growth using models that are 'closed' to the continuous replenishment of medium or removal of waste are often referred to as 'batch' systems. Such approaches are amongst the simplest and most widely used methods for growing *in vitro* biofilms due to accessibility of equipment, ease of experimental setup, and potential for high-throughput experimentation (Whiteley et al. 1997). A microtiter plate is a frequently used format in batch biofilm studies (Allkja et al. 2021). A microtiter plate consists of multiple discrete wells that can simultaneously accommodate separate microbial cultures, making it possible to screen a

variety of conditions or compounds. In a typical setup, biofilm formation is initiated by introducing a microbial suspension into each well, allowing the cells to adhere to the plate's surface (Kwasny and Opperman 2010). This is then followed by a period of biofilm growth and subsequent analyses, which may or not require recovery of the biofilm from the well surface. The limitations of this method include the generation of biofilms that are of reduced complexity in their architecture compared with biofilms in their natural environment (Kragh et al. 2019). Furthermore, it has been reported that lower levels of EPS are produced in microtiter plate methods than those found in more complex systems, resulting in differences that may influence biofilm structure, behaviour and susceptibility (Allkja et al. 2021).

The need to study the effects of dynamic environmental conditions on biofilm growth have led to the introduction of flow-through techniques. Such approaches are a significant advancement in *in vitro* biofilm culture as they enable continuous flow of nutrients and waste removal, and the introduction of shear forces that effect biofilm structure, composition, and EPS production. All of these factors could be present in 'real-world' biofilm environments (Tsagkari et al. 2022).

The CDC biofilm reactor as described in section 1.11.1.2. overcomes the limitations of batch systems as it provides shear force and continuous flow of nutrition and waste. The controlled shear forces have reportedly led to thicker biofilms and with a more complex structure (Tsagkari et al. 2022). The system is designed to ensure an even distribution of shear force within the system exposing all coupons to similar conditions, regardless of their position (Johnson et al. 2021). The CDC biofilm reactor design can also accommodate a wide range of material coupons (Williams et al. 2019), which can also be used in certain well plate formats to allow batch biofilms study.

Within this system, operational parameters were selected to reflect physiologically relevant conditions while maintaining reproducible biofilm growth. Biofilms developed using the CDC biofilm reactor were selected to model dynamic conditions relevant to the oral environment, where salivary flow imposes hydrodynamic shear on developing biofilms. Reported whole saliva flow rates range from approximately 0.3–0.4 ml/min under unstimulated conditions to 4–5 ml/min during stimulated activities such as chewing (Iorgulescu 2009). A flow rate of 1.1 ml/min was therefore chosen as it falls within this reported physiological range and represents an intermediate flow condition compatible with stable biofilm development in the CDC biofilm reactor. In addition, this flow rate was selected to provide continuous medium turnover while avoiding excessive medium consumption during prolonged biofilm growth.

The use of a reduced (10%) growth medium concentration was included as an experimental option, as literature report that diluted media can yield more consistent, fully formed biofilms (Benoit et al. 2010) and are commonly employed to investigate biofilm behaviour under conditions of reduced nutrient availability (Luppens et al. 2002).

2.1.2 Material substrata and surface pre-conditioning for biofilm support

Variables in model systems that need to be considered are the types of substrata to support biofilm growth. Generally, the selection of coupon materials is based on their relevance to the area of clinical study and experimental applications. Hydroxyapatite is arguably a material that is representative of the surface of a tooth, and therefore could be the preferred substrate for studying biofilm formation in a dental context (Nobre et al. 2021). Similarly, polymethyl methacrylate (PMMA) is commonly used to construct acrylic dentures, and might therefore simulate the surfaces of oral prosthetics (dentures), for the colonisation and biofilm formation by *Candida albican*s. This would be of value in the context of studying oral candidosis in

denture wearers (Montoya et al. 2023). Polycarbonate coupons are also widely used in biofilm research due to their ability to support biofilm formation across a range of biofilm-related fields (Mendez et al. 2020), especially their involvement in medical devices, and high durability (Dygico et al. 2020).

Pre-conditioning of coupons surfaces with appropriate solutions that reflect relevant biological milieu could affect initial attachment of microorganisms. For *in vitro* development of oral biofilms, both filtered and artificial saliva are commonly used as pre-conditioning agents (Ayoub et al. 2020). The aim of saliva pre-conditioning is to allow formation of a coating layer that serves as an 'acquired pellicle' that typically forms on oral surfaces. The pellicle is a thin film that forms almost immediately upon exposure of enamel to saliva and plays a critical role in oral health by providing a protective and interactive layer on the tooth surface (Pedersen and Belstrøm 2019). The acquired pellicle is composed primarily of proteins, glycoproteins, and lipids including proline-rich proteins, mucins, and enzymes such as lysozyme (Chawhuaveang et al. 2021). This pellicle serves a protective function by acting as a barrier against external harms including those from acids and abrasion (Vukosavljevic et al. 2014). Furthermore, pellicle components aid in buffering pH and limiting dissolution of enamel minerals, maintaining enamel preservation (Amaechi and Higham 2001).

The pellicle components facilitate bacterial attachment by acting as binding sites for early colonisers such as species of *Streptococcus* and *Actinomyces* (Martínez-Hernández et al. 2023). For instance, salivary agglutinin, a glycoprotein present in the salivary pellicle, provides binding sites for P1, a surface protein found on *S. mutans* (Rezaei et al. 2023). The effect is therefore to facilitate adhesion and initiating of the first step in biofilm formation. Table 2.1 summarises the key differences and similarities between human saliva and artificial saliva,

focusing on aspects such as composition, pH range, stability, functionality, and associated challenges. The information is derived from a review of artificial saliva formulations and their applications in biological research (Pytko-Polonczyk et al. 2017).

Table 2.1 Comparison between human saliva and artificial saliva formulae

Aspect	Human Saliva	Artificial Saliva
Composition	Primarily water (99.5%) with minerals (e.g., sodium, potassium, calcium, and phosphates) and organic molecules like enzymes and proteins	Recreates the water content and key minerals, with some formulas including organic components like urea and mucins
pH Range	Naturally varies between pH 5.8 and 7.3 depending on flow and stimulation levels	Adjusted to fall within the physiological range, typically between pH 5.0 and 7.3
Stability	Highly variable due to individual health, diet, and environmental factors; prone to bacterial growth outside the body	Designed for consistency, resisting changes caused by external factors, and offers stability for experimental use
Functionality	Performs diverse roles, including digestion, protection against pathogens, and maintaining oral tissue health	Aims to replicate specific functional properties of natural saliva for research purposes, such as buffering and interaction with materials
Challenges	Difficult to use due to rapid changes in composition outside the mouth and the risk of contamination	Cannot fully replicate the biological complexity and dynamic nature of human saliva but offers standardisation

2.1.3 Assessment of biofilm formation

The methods of assessment of biofilm formation depends on the specific aims of experiments. Researchers have used a wide range of techniques to analyse biofilms, each tailored to address different objectives. For example, some methods focus on quantifying biofilm biomass, while others assess microbial diversity, metabolic activity, or resistance to antimicrobial agents. Despite the diverse objectives of assessment, some common techniques are indispensable such as basic viability tests, microscopic examination, biochemical assays, and genetic analyses (Azeredo et al. 2017).

Optimising *in vitro* biofilm development requires a comparative analysis of different conditions. A common approach is enumerating colony forming units (CFUs) derived from recovered biofilms (Chiou et al. 2023). CFU enumeration is typically based on the initial recovery of biofilms from surfaces followed by culture of the microorganisms on agar plates (Houchmandzadeh and Ballet 2023). The assumption made is that a single viable microorganism will proliferate to form a visible colony. The approach is indicative of biofilm levels, although the actual number of cells in a biofilm would require comprehensive disaggregation of all the biofilm cells prior to their culture on solid medium (Magana et al. 2018). Biofilms yielding higher CFU numbers could indicate that those biofilm culture conditions are favourable to biofilm formation. It is important to remove free floating or loosely attached planktonic cells prior to conducting such assessments (Thieme et al. 2021).

Fluorescent microscopy and particularly the use of confocal laser scanning microscopy (CLSM) is highly valuable in directly imaging biofilms. Such approaches allow detailed visualisation of biofilm structures that would otherwise be challenging to observe (Shailaja et al. 2022; Goulart et al. 2024). By tagging specific molecules or cellular components with fluorescent

dyes (fluorophores), insight into the organisation of complex microbial biofilm communities can be achieved (Van Hoogstraten et al. 2024). The selected fluorophore emits light upon excitation by a specific wavelength and then releases light at a longer wavelength, creating a visible image of the labelled structures. Emitted light is collected and amplified, allowing for a high-contrast, detailed view of the targeted cellular components (Zanacchi et al. 2014).

A commonly used application used in fluorescence microscopy is that of Live/Dead staining using fluorophores such as SYTO 9 and propidium iodide (PI) (Shailaja et al. 2022). Each fluorophore has unique properties that contribute to the effectiveness of this approach. SYTO 9 is a green fluorescent nucleic acid stain that is membrane permeable, allowing its penetration into intact as well as damaged cell membrane (Stiefel et al. 2015). SYTO 9 will allow all cells in a sample to emit green fluorescence. In contrast, PI is membrane impermeable stain, it emits red fluorescence upon binding to the nucleic acid of cells with a compromised cell membrane (Boulos et al. 1999). Intact cell membranes are impermeable to PI and ensure the stain does not lead to viable cell red fluorescence (Stiefel et al. 2015). When the two stains are used simultaneously on biofilms, with appropriate filter sets or excitation lasers, viable cells appear green, and non-viable cells appear red, due to the higher affinity of PI for nucleic acids, which displaces SYTO 9 from DNA (Stocks 2004). Additionally, PI quenches SYTO 9 fluorescence through fluorescence resonance energy transfer, preventing its green emission, resulting in only PI fluorescence (red) being detected in dead or cell wall-damaged cells (Stocks 2004). This differentiation enables researchers to observe and evaluate a biofilm population *in situ* and assess cell viability. Fluorescence microscopy results can therefore

provide a comparative analysis of biofilm growth under different conditions including assessment of the effectiveness of antimicrobial treatment (Mattern et al. 2024).

2.1.4 Aims

For the research presented in this Chapter, both quantification of CFUs as well live/dead imaging were used to achieve the following aims:

1. To assess the effect of specific environmental conditions on *in vitro* biofilm development of selected mono and polymicrobial species. Selected variables included different surface substrata, incubation time, pre-conditioning solutions, and use of batch culture or flow through systems.
2. To establish suitable conditions to grow each *in vitro* biofilms for subsequent biofilm analyses in later Chapters.

2.2 Materials and methods

2.2.1 Overview of microorganisms and growth conditions

Microorganisms used in these experiments represented those typically isolated from supragingival, subgingival and denture biofilms and that have also been linked to oral diseases. A summary of these microorganisms together with associated culture conditions used is presented in Table 2.2.

Table 2.2 Microorganisms used in this research for *in vitro* development of oral biofilms and corresponding medium

Microorganism	Strain Reference	Source of Isolation	Agar	Growth Medium
Streptococcus mutans	DSM 20523	Carious dentine	Tryptone Soya Agar (TSA, Oxoid)	Tryptone Soya Broth (TSB, Oxoid)
Streptococcus sanguinis	NCTC 7863	Subacute bacterial endocarditis	TSA	TSB
Streptococcus gordonii	NCTC 7865	Subacute bacterial endocarditis	TSA	TSB
Streptococcus salivarius	DSM 20560	Blood from patient with acute articular rheumatism	TSA	TSB
Candida albicans	SC5314	Candidemia	Sabouraud Dextrose Agar (SDA, Oxoid)	Sabouraud Dextrose Broth (SDB, Oxoid)

2.2.2 Standardisation of inocula for biofilms

The microbial suspensions used for seeding biofilm development were prepared by transferring a single colony of the microorganism into 10 ml of the corresponding medium, followed by incubation for 16 h. The suspensions were then standardised by optical density (OD) measurements obtained with a spectrophotometer at 600 nm wavelength (DiluPhotometer, Implen, Westlake Village, CA, USA). Sterile fresh medium was used to calibrate the spectrophotometer and to dilute the samples, if necessary. For *C. albicans* suspensions, a final OD_{600} of 1.00 (± 0.05) corresponding to approximately 1×10^7 cells/ml was used. For bacterial suspensions, dilution with TSB to an OD_{600} of 0.09 (± 0.01) corresponding to approximately 1.5×10^8 cells/ml was used.

2.2.3 Generating biofilm on coupon materials

Single and mixed-species biofilms were generated using the microorganisms listed in Table 2.2. The specific combinations of organisms used were as listed in Table 2.3

Table 2.3 Microbial combinations used for biofilm generation

Inoculum type	Microorganisms
Single species	*Candida albicans* SC5314, *Streptococcus mutans* DSM 20523
Mixed bacterial	*Streptococcus mutans* DSM 20523, *Streptococcus sanguinis* NCTC 7863, *Streptococcus gordonii* NCTC 7865, and *Streptococcus salivarius* DSM 20560
Mixed microbial species	*Candida albicans* SC5314, *Streptococcus mutans* DSM 20523, *Streptococcus sanguinis* NCTC 7863, *Streptococcus gordonii* NCTC 7865, and *Streptococcus salivarius* DSM 20560.

In the case of the mixed microbial species inocula, an equal volume of single species incubated for 16 h suspensions were combined after standardisation of the levels using the spectrophotometer. In addition to the above, selected experiments also used whole saliva as a source of biofilm microorganisms. The details of how this whole saliva was obtained and used is provided in Section 2.2.4.

2.2.4 Whole saliva collection

Whole unstimulated saliva was collected by expectoration from healthy adult volunteers (staff and students) based at the School of Dentistry, Cardiff University. Ethical approval for saliva collection was obtained from the Dental School Research Ethics Committee, Cardiff University (reference number: 2110), and all participants provided informed consent prior to sample donation.

Saliva collection was performed using a standardised protocol adapted from Navazesh (1993). Briefly, volunteers were seated comfortably with their head tilted slightly forward and instructed to allow saliva to accumulate naturally in the floor of the mouth. Saliva was expectorated directly into sterile polypropylene tubes until a volume of 5 ml was obtained per donor. (Navazesh 1993).

Saliva samples were collected from four individual volunteers. Each saliva sample was processed independently. Collected saliva was used immediately following collection and was not stored or frozen prior to use.

For standardisation across experiments, individual saliva samples were diluted using sterile Tryptone Soya Broth (TSB; Oxoid) to an optical density at 600 nm (OD_{600}) of 1.00, measured

using a spectrophotometer. The standardised saliva suspensions were then used immediately to seed in vitro biofilm models.

2.2.5 Preparation of coupons

Polycarbonate (PC) and hydroxyapatite (HA) coupons (diameter 12.7 mm and thickness 3.8 mm) were obtained from BioSurface Technologies (RD 128-PC, RD 128-HA, BioSurface Technologies Corporation, Bozeman, MT, USA). Polymethyl methacrylate (PMMA) coupons were prepared 'in house' using Oracryl Cold Cure polymer powder and Oracryl Cold Cure Liquid monomer (Bracon Dental Laboratory Products, Etchingham, UK). For the PMMA coupons, a 2:1 powder to liquid (w/v) ratio was mixed and poured into a 12.7 mm diameter disc mould made of polytetrafluoroethylene. A glass panel was placed on top of the exposed surface of the mould, pressure was applied to promote a smooth flat surface upon which the biofilm would subsequently be generated upon. The preparation was left to cure at room temperature for at least 1 h. After curing, coupons were removed from the mould and stored in distilled water for 1 week, to allow release of excess monomer. Sharp or rough edges of the coupons were removed by sanding, except on the area to be analysed.

All coupons were sterilised prior use by autoclaving at 121°C for 15 min. On manufacturer (BioSurface Technologies) advice, re-use of both polycarbonate and hydroxyapatite coupons was undertaken following autoclaving at 121°C for 15 min, with subsequent sonication, washing with distilled water and repeat autoclaving at 121°C for 15 min. PMMA coupons were discarded after a single use.

2.2.6 Pre-conditioning of coupons

Sterile coupons were immersed in sterile artificial saliva (AS) or sterile distilled water (control) and incubated at 37°C for 24 h before experiments. AS solution was prepared by mixing 2.5 g/L porcine stomach mucin, 0.35 g/L sodium chloride, 0.2 g/L potassium chloride, 0.2 g/L calcium chloride dihydrate, 0.2 g/L yeast extract, 1.0 g/L lab lemco powder, and 5.0 g/L protease peptone in sterile distilled water. The solution was then autoclaved at 121°C for 15 min. Post sterilisation, filter sterilised 40% (w/v) urea solution (final concentration of 1.25 ml/L) was added (Cavalcanti et al. 2015).

2.2.7 Batch culture biofilms

Pre-conditioned coupons were aseptically placed into the wells of a sterile 6-well plate (4 coupons in each well), and a 200 µl volume of inoculum was applied on the surface of each coupon. This was followed by addition of 8 ml of culture medium to each well. The plates were carefully placed in an incubator and incubated aerobically and statically at 37°C for 24, 48 or 72 h. The culture medium was replaced every 24 h. After each experiment, coupons were removed from the plates and washed gently with PBS, to remove any loosely or non-attached cells before analyses.

2.2.8 Biofilm development in the Centers for Disease Control and Prevention (CDC) biofilm reactor

A CDC biofilm reactor (CBR 90 Standard CDC Biofilm Reactor BioSurface Technologies Corporation, Bozeman, MT, USA) was used to grow biofilms in a flow-through method. The biofilm reactor was assembled and operated according to the instructions provided by the manufacturer. Briefly, the biofilm reactor consisted of a 1 L glass vessel with an effluent port.

The vessel was covered by a polyethylene top which contained 3 ports and 8 holes for coupon support rods. The ports enabled addition of inoculum, fresh medium injection, and air filtration. A baffled stirrer bar was positioned in the centre of the vessel base and was surrounded by the rods. Inlet and outlet ports ensured circulation of culture medium into and out of the vessel. Each rod supported 3 coupons for biofilm development. Coupons were fitted in rods, and the ports were secured and covered with aluminium foil. The vessel was filled with medium up to the effluent spout (around 400 ml) and was then clamped. The medium-filled biofilm reactor and tubing system, was then sterilised by autoclaving for 15 min at 121°C. All ports and connected tubes were covered with aluminium foil to maintain sterility until time of use.

For batch phase of biofilm development, the biofilm reactor was aseptically inoculated with 1 ml of prepared inoculum or collected saliva, placed on a magnetic stirrer, which was set at 150 rev/min. The inoculated biofilm reactor was incubated aerobically at 37°C for 24 h. For the flow-through phase, all tubes were connected, one tube from the fresh medium carboy through a peristaltic pump to the inlet port. A second tube was connected the effluent spout to the waste carboy. All clamps were removed, and the peristaltic pump was set at a flow rate of 1.1 ml/min, and incubated aerobically at 37°C for 48 h. Biofilms were grown for a total duration of 72 h, an initial 24 h batch phase followed by 48 h under flow-through conditions, with biofilm sampling performed at 24, 48, and 72 h.

Selected CDC biofilm reactor experiments were performed with a culture medium concentration of 3 g/L (10% of recommended concentration). After each experiment, the rods were aseptically removed and dipped gently in a tube filled with PBS to remove any non-attached cells before biofilm analyses were undertaken.

2.2.9 Analysis of developed biofilms

2.2.9.1 Recovery and enumeration of colony forming units (CFUs) from biofilms

To enumerate CFUs from biofilms, each coupon was washed gently with PBS and placed into a sterile petri dish. A sterile swab was used to thoroughly brush the surface, ensuring that the entire area 1.27 cm^2 was covered multiple times to optimise sample collection. Each swab was aseptically inserted into 10 ml of PBS and vortex mixed for 10 s, followed by serial dilution and deposition of 50 µl on agar plates using a spiral plater (Whitley Automatic Spiral Plater, Don Whitley Scientific, UK). After overnight incubation at 37°C colonies on plates ranging in number between 30 to 300 were enumerated.

2.2.9.2 Assessment of biofilm formation by direct fluorescence microscopy

Coupons were retrieved and 200 µl of stain was applied to the coupon surface. To stain bacteria, Live/Dead stain (LIVE/DEAD® BacLight™ Bacterial Viability Kits L7007 or FilmTracer™ LIVE/DEAD® Biofilm Viability Kit L10316, Fisher Scientific, Leicestershire, United Kingdom) was used according to the manufacturer's instructions by mixing equal volumes (3 µl) of Syto9 and PI in 1 ml of sterile water. In addition, 0.1% (w/v) calcofluor white in distilled water was used to stain *C. albicans* and was applied to the surface of coupons at room temperature in the dark for 30 min. The coupons were washed twice with sterile distilled water to remove planktonic or loosely attached cells as well as excess stain. The coupons were then positioned on a microscope slide using mounting putty. A glass cover slip was placed on the top surface of the coupon. Images were obtained using an Olympus Provis AX 70 fluorescence microscope, at x400 and x600 total magnification. Images from 15 randomly selected fields of view were acquired from each coupon surface and used for quantitative analysis.

2.2.9.3 Image analysis to measure the mean biofilm surface area coverage on coupons

Analysis of the mean biofilm surface area coverage based on fluorescence was undertaken using ImageJ software (version range 1.53o to 1.54f) (Schindelin et al. 2012). Using ImageJ, all images were converted to 8-bit (image:type:8-bit), followed by manually setting the threshold (image:adjust:threshold) to minimise background noise. To navigate the user interface on imageJ to measure the area of fluorescence, "Analyze" was selected followed by "Set measurements". Analysis "area" and "fraction area" were then selected and the decimal places set to "3". To run the analysis "measure" under the tab "Analyze", which displayed the results, the number under the box labelled "%Area" was the percentage that represented the area of fluorescence covered by biofilm in the image. Results were used to calculate the mean and standard deviation of the area of fluorescence (biofilm coverage) for 15 fields of view for each coupon and for different biofilm growing conditions.

2.2.9.4 Assessment of biofilm quantity by confocal laser scanning microscopy (CLSM)

Coupons supporting biofilm growth were gently rinsed using sterile distilled water to remove non-attached cells. Biofilm staining was then performed as described in section 2.2.9.2. After staining, the biofilm coupons were inverted and placed in a 24-well imaging plate (µ-Plate 24 Well Black, ibidi GmbH, Martinsried, Germany). This orientation ensured that the biofilm surface was in direct contact with the coverslip base of the well.

Biofilm imaging was done using a confocal laser scanning microscope (ZEISS Celldiscoverer 7 with LSM 900; Carl Zeiss, Germany) equipped with a range of objective lenses. Image acquisition and processing were performed using ZEN software (version 3.6; Carl Zeiss, Germany). For bacterial biofilms, imaging was conducted using a ×40 objective lens, while a ×20 objective lens was used for *C. albicans* biofilms. Laser excitation was at 405 nm for

calcofluor white, 488 nm for SYTO 9, and 561 nm for propidium iodide (PI). Random Z-stack images (n=15) of each condition were acquired and encompassed the full depth of the biofilm. No additional optical or digital zoom was applied. Images were acquired at scanning resolutions ranging from 1024 × 1024 to 1612 × 1612 pixels Line averaging was set to 2 to reduce background noise. Z-stacks were acquired using step sizes ranging from 0.5 µm to 1 µm, depending on the experiment, with consistent parameters maintained within each comparison group. All image datasets were analysed using COMSTAT software (Heydorn et al. 2000; Vorregaard 2008) version 2.1. Images were first converted to OME-TIFF, then COMSTAT2 plugin was started and desired images were selected and uploaded to observed directories. On the Comstat2 main menu (control panel), total biomass and maximum thickness parameters were selected.

2.2.10 Statistical analysis

Statistical analyses were performed using either GraphPad Prism 10.1.0 (GraphPad Software, Boston, Massachusetts USA, www.graphpad.com) or SPSS statistics 27.0 (IBM SPSS Statistics, IBM Corp., Armonk, New York, USA). Data were assessed for normality using Shapiro-Wilk test.

Kruskal–Wallis test with Dunn's post-hoc analysis for multiple comparisons was used to compare CFU, percentage of area coverage, biomass and thickness of the different groups.

Media concentration analysed using Welch's *t*-test for all CFU comparison, while comparisons based on percentage of area coverage, Welch's *t*-test was used for mixed bacterial and mixed microbial species biofilms, and Mann–Whitney *U* test for *C. albicans* and whole saliva biofilms.

2.3 Results

2.3.1 Recovery and enumeration of colony-forming units (CFUs) from biofilms

For mixed bacterial biofilms, preconditioning with AS resulted in higher numbers of recovered CFUs compared to preconditioning with water (Table 2.4). However, this difference was not significant ($p = 0.386$). The duration of culture (24, 48, or 72 h) did not significantly influence CFU recovery (Table 2.4). Surface type had a significant effect, with PMMA yielding significantly ($p < 0.001$) lower CFU counts compared to HA and PC. The system used also had a notable effect, with the batch system showing significantly ($p < 0.001$) higher CFU counts compared to the CDC biofilm reactor. Table 2.4 summarises the results of CFU counts for microorganisms recovered from mixed bacterial biofilms grown under different conditions.

For mixed microbial species biofilms, preconditioning with AS led to significantly ($p = 0.003$) lower numbers of recovered CFUs compared to preconditioning with water. CFU recovery for different culture durations (24, 48, and 72 h) showed no significant differences. At 72 h, PC coupons yielded significantly ($p < 0.001$) higher CFU counts compared to the other tested surfaces. The model used also significantly ($p = 0.011$) influenced CFU recovery, with flow through yielding higher counts than the batch system. Table 2.5 summarises the results of CFU enumeration for microorganisms recovered from mixed microbial species biofilms grown under different conditions

For *C. albicans* biofilms, preconditioning with AS did not significantly ($p = 0.254$) affect CFU recovery compared to preconditioning with water. CFU counts were significantly ($p < 0.001$) lower at 24 h compared to 72 h, while no significant difference was observed between 48 and 72 h. PMMA yielded significantly ($p < 0.001$) lower CFU counts compared to HA and PC. The model used also influenced CFU recovery, with the CDC biofilm reactor showing significantly

($p < 0.001$) higher counts compared to the batch system. Table 2.6 summarises the results of CFU counts of *C. albicans* biofilms grown under different conditions.

For whole saliva biofilms, preconditioning with AS resulted in significantly ($p = 0.005$) higher CFU recovery compared to water. CFU recovery at 24 h was significantly lower compared to 72 h ($p < 0.001$), while no difference was observed between 48 h and 72 h. Surface type had a significant effect, with PMMA biofilms yielding significantly ($p < 0.001$) lower CFU counts compared to HA biofilms. The CDC biofilm reactor produced significantly higher CFU counts compared to the batch system ($p = 0.005$). Table 2.7 summarises the results of CFU counts of whole saliva biofilms grown under different conditions.

Table 2.4 Recovered colony forming units (CFUs/cm^2) from mixed bacterial biofilms

Coupon material	Preconditioning	24 h		48 h		72 h	
		Batch	CDC biofilm reactor	Batch	CDC biofilm reactor	Batch	CDC biofilm reactor
PMMA	Water	3.6×10^5 ($\pm 2.6 \times 10^4$)	1.1×10^5 ($\pm 6.4 \times 10^3$)	2.7×10^5 ($\pm 1.3 \times 10^4$)	2.2×10^5 ($\pm 1.1 \times 10^4$)	1.9×10^5 ($\pm 1.1 \times 10^4$)	1.1×10^5 ($\pm 5.6 \times 10^3$)
	AS	1.0×10^5 ($\pm 6.4 \times 10^3$)	1.3×10^5 ($\pm 1.3 \times 10^4$)	4.9×10^5 ($\pm 2.7 \times 10^4$)	1.3×10^5 ($\pm 6.4 \times 10^3$)	1.7×10^6 ($\pm 5.6 \times 10^4$)	1.4×10^5 ($\pm 3.6 \times 10^3$)
PC	Water	1.3×10^5 ($\pm 1.1 \times 10^4$)	6.9×10^4 ($\pm 2.2 \times 10^3$)	2.4×10^5 ($\pm 1.1 \times 10^4$)	2.0×10^5 ($\pm 6.4 \times 10^3$)	1.1×10^5 ($\pm 5.6 \times 10^3$)	1.4×10^5 ($\pm 3.2 \times 10^3$)
	AS	3.3×10^6 ($\pm 2.1 \times 10^5$)	1.6×10^5 ($\pm 3.2 \times 10^4$)	9.4×10^5 ($\pm 2.8 \times 10^4$)	2.4×10^5 ($\pm 1.4 \times 10^4$)	2.8×10^6 ($\pm 2.6 \times 10^5$)	2.5×10^5 ($\pm 6.4 \times 10^3$)
HA	Water	3.1×10^5 ($\pm 1.7 \times 10^4$)	2.8×10^5 ($\pm 1.3 \times 10^4$)	3.3×10^5 ($\pm 2.7 \times 10^4$)	2.8×10^5 ($\pm 2 \times 10^4$)	3.1×10^5 ($\pm 2.9 \times 10^4$)	2.0×10^5 ($\pm 2.8 \times 10^3$)
	AS	3.3×10^5 ($\pm 1.9 \times 10^4$)	2.4×10^5 ($\pm 3.4 \times 10^4$)	6.8×10^5 ($\pm 2.1 \times 10^4$)	1.9×10^5 ($\pm 1.1 \times 10^4$)	2.8×10^6 ($\pm 5.6 \times 10^4$)	2.7×10^5 ($\pm 3.6 \times 10^3$)

Values are presented as the mean of three biological replicates, each analysed in triplicate (three technical replicates) ± standard deviation (SD). PMMA, polymethylmethacrylate; PC, polycarbonate; HA, hydroxyapatite; AS, artificial saliva.

Table 2.5 Recovered colony forming units (CFUs/cm^2) from mixed microbial species biofilms

Coupon material	Preconditioning	24 h		48 h		72 h	
		Batch	CDC biofilm reactor	Batch	CDC biofilm reactor	Batch	CDC biofilm reactor
PMMA	Water	8.7×10^4 ($\pm 3.2 \times 10^3$)	1.3×10^5 ($\pm 6.4 \times 10^3$)	2.8×10^5 ($\pm 3.6 \times 10^3$)	4.0×10^5 ($\pm 2.8 \times 10^3$)	1.9×10^5 ($\pm 1.4 \times 10^3$)	2.4×10^6 ($\pm 7.4 \times 10^4$)
	AS	2.2×10^6 ($\pm 2.4 \times 10^4$)	2.7×10^6 ($\pm 1 \times 10^4$)	1.7×10^6 ($\pm 7.4 \times 10^4$)	2.0×10^6 ($\pm 3.6 \times 10^4$)	3.5×10^5 ($\pm 1.3 \times 10^4$)	4.5×10^5 ($\pm 1.9 \times 10^5$)
PC	Water	1.4×10^6 ($\pm 1.2 \times 10^4$)	1.9×10^6 ($\pm 1.8 \times 10^4$)	4.1×10^6 ($\pm 8 \times 10^4$)	4.5×10^6 ($\pm 5.1 \times 10^4$)	3.0×10^6 ($\pm 3.7 \times 10^4$)	3.9×10^6 ($\pm 3.7 \times 10^4$)
	AS	3.5×10^6 ($\pm 2.5 \times 10^4$)	4.1×10^6 ($\pm 6 \times 10^4$)	3.8×10^6 ($\pm 9.4 \times 10^4$)	4.3×10^6 ($\pm 9.4 \times 10^4$)	1.3×10^6 ($\pm 4.1 \times 10^4$)	2.5×10^6 ($\pm 5.1 \times 10^4$)
HA	Water	4.7×10^5 ($\pm 3.3 \times 10^4$)	6.5×10^5 ($\pm 7 \times 10^4$)	2.5×10^6 ($\pm 2.4 \times 10^4$)	3.8×10^6 ($\pm 2.9 \times 10^4$)	1.9×10^6 ($\pm 2.2 \times 10^4$)	3.2×10^6 ($\pm 7.6 \times 10^4$)
	AS	8.7×10^4 ($\pm 4.2 \times 10^4$)	1.3×10^5 ($\pm 2.8 \times 10^3$)	2.8×10^5 ($\pm 3.1 \times 10^4$)	4.0×10^5 ($\pm 2.6 \times 10^4$)	1.9×10^5 ($\pm 1.7 \times 10^4$)	2.4×10^6 ($\pm 9.2 \times 10^4$)

Values are presented as the mean of three biological replicates, each analysed in triplicate (three technical replicates) ± standard deviation (SD). PMMA, polymethylmethacrylate; PC, polycarbonate; HA, hydroxyapatite; AS, artificial saliva.

Table 2.6 Recovered colony forming units (CFUs/cm^2) from *Candida albicans* biofilms

Coupon material	Preconditioning	24 h		48 h		72 h	
		Batch	CDC biofilm reactor	Batch	CDC biofilm reactor	Batch	CDC biofilm reactor
PMMA	Water	3.5×10^5 ($\pm 1.3 \times 10^4$)	4.1×10^5 ($\pm 2.3 \times 10^4$)	4.6×10^5 ($\pm 1.3 \times 10^4$)	5.4×10^5 ($\pm 3.1 \times 10^4$)	4.0×10^5 ($\pm 8.4 \times 10^3$)	5.0×10^5 ($\pm 3.2 \times 10^4$)
	AS	5.4×10^5 ($\pm 1.1 \times 10^4$)	4.6×10^5 ($\pm 1.3 \times 10^4$)	4.3×10^5 ($\pm 2.9 \times 10^4$)	4.9×10^5 ($\pm 2.5 \times 10^4$)	4.1×10^5 ($\pm 4.6 \times 10^3$)	4.7×10^5 ($\pm 6.6 \times 10^4$)
PC	Water	8.7×10^5 ($\pm 2.5 \times 10^4$)	2.5×10^6 ($\pm 4.2 \times 10^4$)	2.7×10^6 ($\pm 4.6 \times 10^4$)	4.1×10^6 ($\pm 3.4 \times 10^4$)	4.6×10^6 ($\pm 1.7 \times 10^6$)	6.1×10^6 ($\pm 1.5 \times 10^5$)
	AS	1.0×10^6 ($\pm 3.1 \times 10^4$)	2.3×10^6 ($\pm 8.4 \times 10^4$)	3.1×10^6 ($\pm 4.2 \times 10^4$)	4.7×10^6 ($\pm 7.2 \times 10^4$)	4.4×10^6 ($\pm 3.8 \times 10^5$)	5.7×10^6 ($\pm 9.1 \times 10^5$)
HA	Water	1.1×10^6 ($\pm 1.3 \times 10^4$)	2.0×10^6 ($\pm 3.9 \times 10^4$)	2.8×10^6 ($\pm 6.1 \times 10^4$)	3.5×10^6 ($\pm 7.2 \times 10^4$)	3.9×10^6 ($\pm 4.9 \times 10^4$)	5.4×10^6 ($\pm 5 \times 10^5$)
	AS	1.3×10^6 ($\pm 2.6 \times 10^4$)	2.4×10^6 ($\pm 7 \times 10^4$)	2.8×10^6 ($\pm 5.2 \times 10^4$)	5.2×10^6 ($\pm 9.5 \times 10^4$)	4.9×10^6 ($\pm 3.3 \times 10^5$)	5.5×10^6 ($\pm 7.8 \times 10^5$)

Values are presented as the mean of three biological replicates, each analysed in triplicate (three technical replicates) ± standard deviation (SD). PMMA, polymethylmethacrylate; PC, polycarbonate; HA, hydroxyapatite; AS, artificial saliva.

Table 2.7 Recovered colony forming units (CFUs/cm^2) from whole saliva biofilms

Coupon material	Preconditioning	24 h		48 h		72 h	
		Batch	CDC biofilm reactor	Batch	CDC biofilm reactor	Batch	CDC biofilm reactor
PMMA	Water	1.0×10^6 ($\pm 4.2 \times 10^4$)	1.4×10^6 ($\pm 4.2 \times 10^4$)	1.1×10^6 ($\pm 3.2 \times 10^4$)	1.3×10^6 ($\pm 3.7 \times 10^4$)	1.4×10^6 ($\pm 6.1 \times 10^4$)	1.6×10^6 ($\pm 1.5 \times 10^4$)
	AS	9.4×10^5 ($\pm 4.8 \times 10^4$)	1.3×10^6 ($\pm 6.8 \times 10^4$)	7.9×10^5 ($\pm 2.3 \times 10^4$)	9.4×10^5 ($\pm 5 \times 10^4$)	1.3×10^6 ($\pm 5.4 \times 10^4$)	1.4×10^6 ($\pm 8.8 \times 10^4$)
PC	Water	2.0×10^6 ($\pm 2.6 \times 10^4$)	1.9×10^6 ($\pm 8.1 \times 10^4$)	2.4×10^6 ($\pm 7.8 \times 10^4$)	3.3×10^6 ($\pm 4.9 \times 10^4$)	2.2×10^6 ($\pm 2.9 \times 10^4$)	3.0×10^6 ($\pm 4.7 \times 10^4$)
	AS	2.2×10^6 ($\pm 3.6 \times 10^4$)	1.7×10^6 ($\pm 1.9 \times 10^4$)	2.2×10^6 ($\pm 3.5 \times 10^4$)	2.8×10^6 ($\pm 7.4 \times 10^4$)	1.7×10^6 ($\pm 6.3 \times 10^4$)	2.2×10^6 ($\pm 3.2 \times 10^4$)
HA	Water	1.9×10^6 ($\pm 6.9 \times 10^4$)	1.6×10^6 ($\pm 3.7 \times 10^4$)	2.2×10^6 ($\pm 4.5 \times 10^4$)	2.4×10^6 ($\pm 5.9 \times 10^4$)	2.7×10^6 ($\pm 7.1 \times 10^4$)	1.9×10^6 ($\pm 2.9 \times 10^4$)
	AS	2.0×10^6 ($\pm 3.7 \times 10^4$)	1.7×10^6 ($\pm 7.2 \times 10^4$)	2.0×10^6 ($\pm 7.1 \times 10^4$)	2.5×10^6 ($\pm 4.6 \times 10^4$)	2.5×10^6 ($\pm 1.9 \times 10^4$)	2.2×10^6 ($\pm 9.8 \times 10^4$)

Values are presented as the mean of three biological replicates, each analysed in triplicate (three technical replicates) ± standard deviation (SD).
PMMA, polymethylmethacrylate; PC, polycarbonate; HA, hydroxyapatite; AS, artificial saliva

The effect of medium concentration on biofilm formation under flow through conditions varied with biofilm types. For *C. albicans*, the number of CFUs was 1.8-fold and significantly ($p < 0.001$) higher when using the manufacturer's recommended concentration. Conversely, mixed bacterial biofilms showed significantly ($p < 0.001$) higher CFU counts at 10% of the manufacturer's recommended concentration with CFU counts being 2.45-fold higher. No significant differences were observed between concentrations for whole saliva and mixed microbial species biofilms (Figure 2.1).

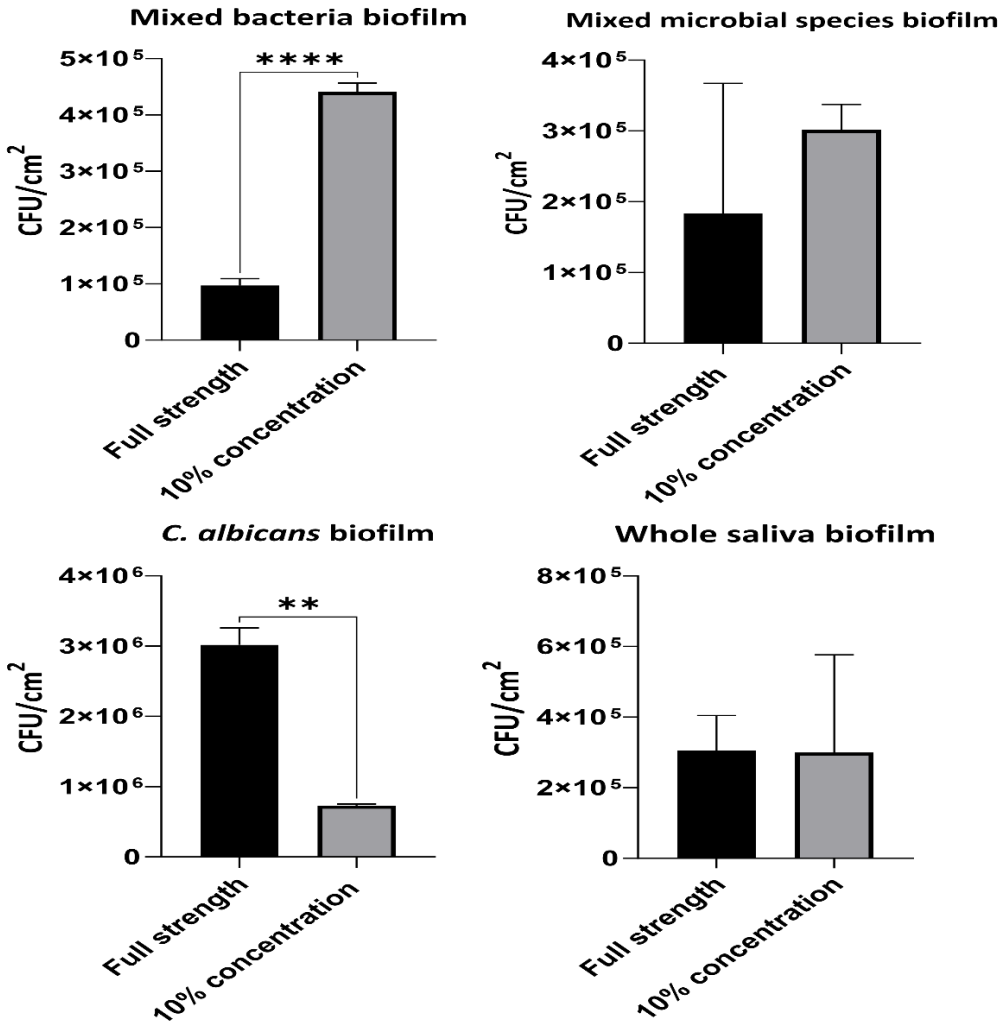

Figure 2.1 Comparison of biofilm formation in full and 10% medium concentration for different biofilm types.

Biofilm formation was assessed based on CFU recovery for whole saliva, mixed bacterial biofilms, mixed microbial species biofilms, and *C. albicans* biofilms.

2.3.2 Assessment of surface area coverage of *in vitro* biofilms by fluorescence microscopy

For bacterial biofilms (Figure 2.2), preconditioning with AS did not result in a significant difference in biofilm coverage compared to water preconditioned groups. Biofilm coverage was significantly ($p < 0.001$) lower at 24 h and 48 h ($p = 0.004$) compared to 72 h. PMMA surfaces exhibited significantly ($p < 0.001$) lower biofilm coverage compared to HA and PC. The batch system yielded a significantly ($p< 0.001$) higher percentage of biofilm area compared to the CDC biofilm reactor. Table 2.8 summarises the values of percentage of area covered by mixed bacterial biofilms.

For mixed microbial species biofilms (Figure 2.3A), preconditioning with AS resulted in a significant ($p = 0.015$) reduction in biofilm coverage compared to preconditioning with water. Coverage was significantly ($p < 0.001$) lower at both 24 h and 48 h compared to 72 h. PMMA exhibited significantly lower coverage compared to HA and PC ($p < 0.001$). The CDC biofilm reactor produced significantly higher biofilm coverage compared to the batch system ($p < 0.001$). Table 2.9 summarises the values of percentage of area covered by mixed microbial species biofilms.

For *C. albicans* biofilms (Figure 2.4), preconditioning with AS had no significant effect on biofilm coverage compared to water. Coverage was significantly ($p < 0.001$) lower at 24 h and 48 h compared to 72 h. PMMA showed significantly lower biofilm coverage compared to HA and PC. The CDC biofilm reactor yielded significantly ($p < 0.001$) higher coverage than the batch system. Table 2.10 summarises the values of percentage of area covered by *C. albicans* biofilms.

For whole saliva biofilms (Figure 2.3B), preconditioning with AS showed no significant difference in biofilm coverage compared to water. Coverage was significantly lower at 24 h ($p < 0.001$) and 48 h ($p = 0.002$) compared to 72 h. PMMA showed significantly ($p < 0.001$) lower coverage compared to HA and PC. The CDC biofilm reactor produced significantly ($p < 0.001$) higher biofilm coverage compared to the batch system. Table 2.11 summarises the values of percentage of area covered by whole saliva biofilms.

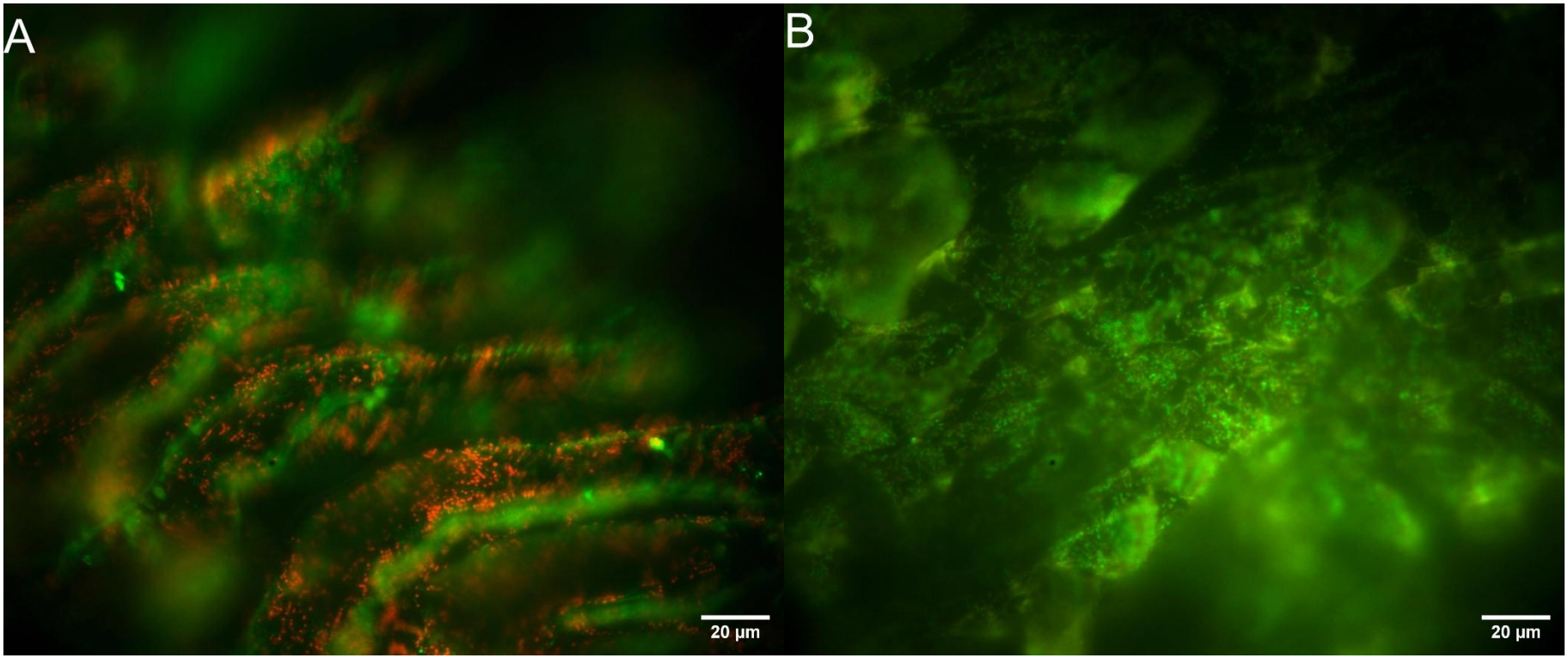

Figure 2.2 Fluorescence microscope image of mixed bacterial biofilms on water preconditioned polycarbonate coupons in the CDC biofilm reactor using tryptic soy broth (TSB) at different concentrations.

A) 10% TSB. B) 100% TSB. Biofilms were grown for 72 h Live/Dead BacLight stained (Invitrogen). Green fluorescence shows live cells stained by Syto9. Red fluorescence shows dead cells stained with propidium iodide. Images were acquired using a ×40 objective. Scale bar is 20 µm.

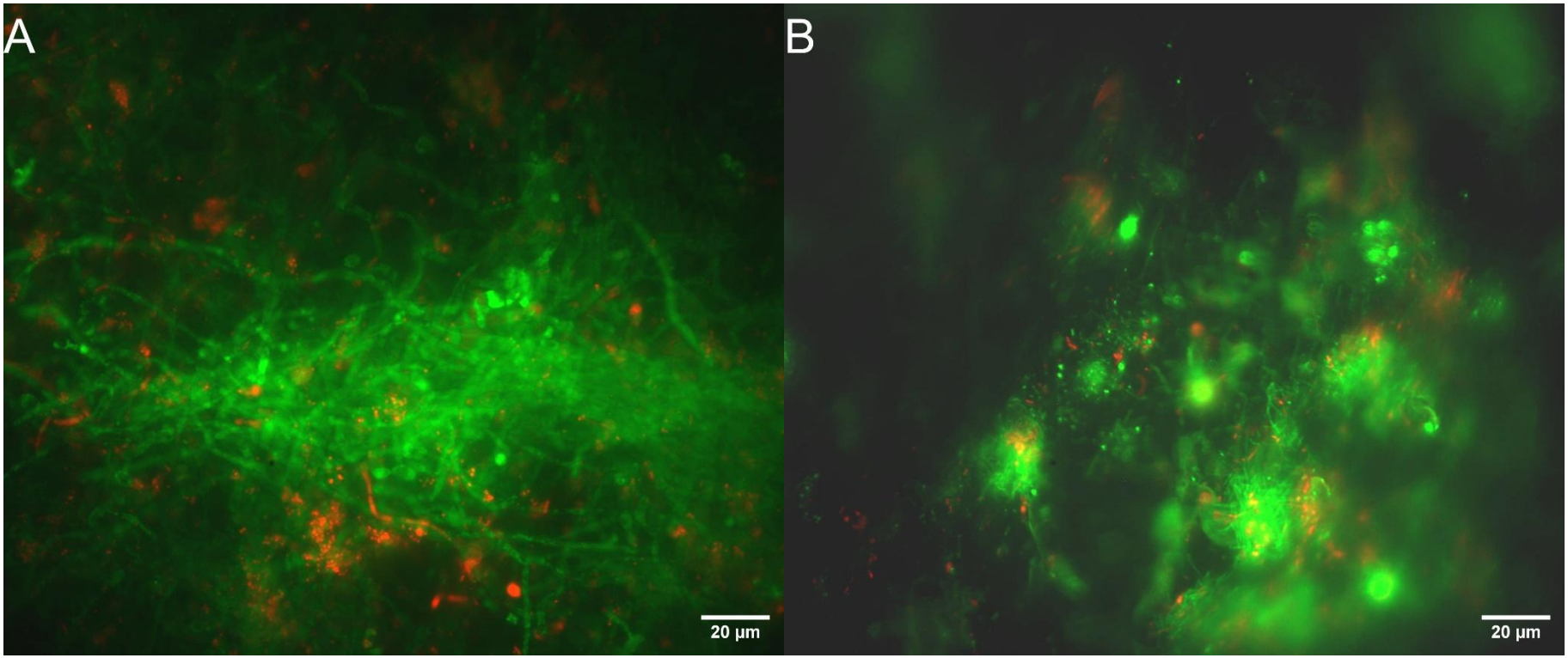

Figure 2.3. Fluorescence microscope image of biofilms developed using the CDC biofilm reactor and stained with Live/Dead BacLight (Invitrogen).

A) Mixed microbial species biofilm in 10% TSB medium. B) Whole saliva biofilm in full strength TSB medium. Green fluorescence shows live cells stained by Syto9. Red fluorescence shows dead cells stained with propidium iodide. Biofilms were grown for 72 h on water preconditioned polycarbonate coupons. Images were acquired using a ×40 objective. Scale bar is 20 µm.

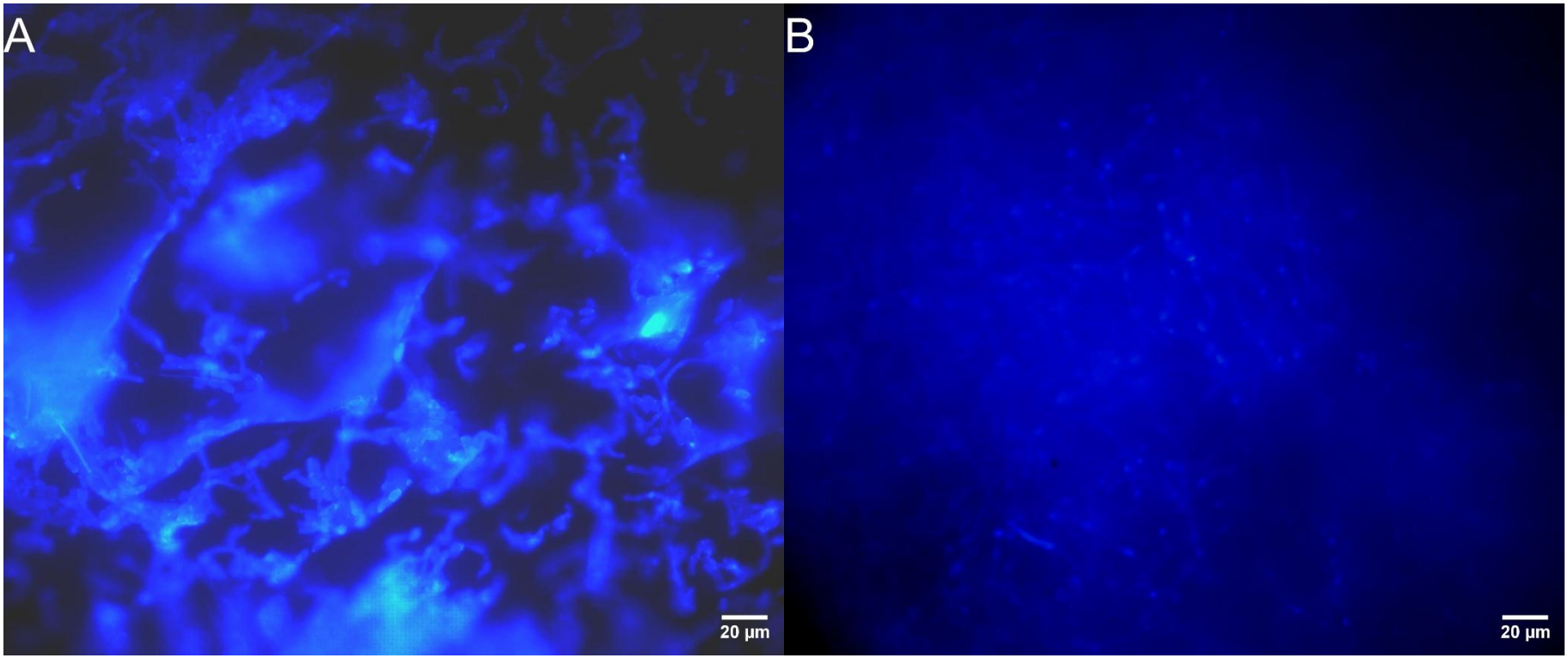

Figure 2.4 Fluorescence microscope image of *Candida albicans* biofilms developed in the CDC biofilm reactor in Sabouraud dextrose broth (SDB) at different concentrations.

A) 10% (w/v) SDB concentration. B) Full strength SDB. *Candida albicans* was stained with 1% (v/v) calcofluor white. Biofilms were grown for 72 h on water preconditioned polycarbonate coupons. Images were acquired using a ×40 objective. Scale bar is 20 µm.

Table 2.8 Percentage of area covered by mixed bacterial biofilm

Coupon material	Preconditioning	24 h		48 h		72 h	
		Batch	CDC biofilm reactor	Batch	CDC biofilm reactor	Batch	CDC biofilm reactor
PMMA	Water	14.92 (± 1.68)	8.23 (± 3.47)	24.31 (± 4.91)	12.47 (± 3.04)	19.02 (± 6.46)	12.74 (± 6.57)
	AS	13.99 (± 6.01)	7.93 (± 1.95)	12.44 (± 2.72)	15.08 (± 6.53)	13.29 (± 3.77)	15.23 (± 3.84)
PC	Water	15.65 (± 3.34)	11.95 (± 2.95)	23.48 (± 3.18)	13.02 (± 3.66)	27.43 (± 3.39)	13.26 (± 3.35)
	AS	19.15 (± 4.86)	9.86 (± 3.15)	13.78 (± 4.57)	16.45 (± 4.68)	26.46 (± 7.61)	16.63 (± 2.80)
HA	Water	15.78 (± 3.36)	13.04 (± 3.06)	23.80 (± 5.62)	13.57 (± 6.47)	29.84 (± 4.20)	13.75 (± 6.63)
	AS	20.20 (± 0.42)	11.61 (± 3.75)	25.35 (± 3.83)	14.16 (± 3.71)	30.76 (± 7.54)	14.50 (± 3.62)

Values are mean of 15 randomly selected images, three biological replicates, five technical replicates each ± standard deviation (SD). PMMA: polymethylmethacrylate, PC: polycarbonate, HA: hydroxyapatite, AS: artificial saliva.

Table 2.9 Percentage of area covered by mixed microbial species biofilms

Coupon material	Preconditioning	24 h		48 h		72 h	
		Batch	CDC biofilm reactor	Batch	CDC biofilm reactor	Batch	CDC biofilm reactor
PMMA	Water	7.35 (± 3.33)	10.11 (± 2.60)	3.72 (± 0.74)	6.44 (± 2.81)	12.13 (± 3.80)	15.15 (± 6.33)
	AS	9.98 (± 3.73)	12.98 (± 3.79)	19.39 (± 3.91)	22.11 (± 7.72)	9.47 (± 1.64)	14.00 (± 4.69)
PC	Water	19.26 (± 5.35)	21.76 (± 8.45)	32.54 (± 3.10)	36.54 (± 3.35)	42.28 (± 1.66)	46.81 (± 5.05)
	AS	20.25 (± 7.50)	23.19 (± 7.54)	26.66 (± 7.48)	19.14 (± 3.78)	33.99 (± 3.80)	38.24 (± 6.47)
HA	Water	28.13 (± 3.81)	30.85 (± 6.56)	35.11 (± 5.33)	35.04 (± 3.23)	44.72 (± 3.90)	49.32 (± 6.56)
	AS	25.90 (± 5.15)	36.84 (± 7.62)	37.64 (± 5.36)	39.09 (± 7.53)	41.76 (± 3.82)	47.41 (± 7.62)

Values are mean of 15 randomly selected images, three biological replicates, five technical replicates each ± standard deviation (SD). PMMA: polymethylmethacrylate, PC: polycarbonate, HA: hydroxyapatite, AS: artificial saliva.

Table 2.10 Percentage of area covered by *Candida albicans* biofilms

Coupon material	Preconditioning	24 h		48 h		72 h	
		Batch	CDC biofilm reactor	Batch	CDC biofilm reactor	Batch	CDC biofilm reactor
PMMA	Water	1.13 (± 0.18)	15.37 (± 3.83)	2.53 (± 0.45)	16.41 (± 4.83)	1.77 (± 0.21)	31.17 (± 12.62)
	AS	1.18 (± 0.16)	9.86 (± 3.81)	1.76 (± 0.21)	20.43 (± 6.22)	2.01 (± 0.25)	25.29 (± 11.87)
PC	Water	2.74 (± 0.19)	21.90 (± 2.60)	4.91 (± 2.64)	38.65 (± 3.76)	8.24 (± 1.98)	56.23 (± 6.22)
	AS	1.83 (± 0.19)	19.24 (± 4.58)	5.54 (± 2.08)	33.73 (± 4.24)	10.05 (± 2.40)	59.04 (± 2.35)
HA	Water	5.07 (± 1.11)	17.98 (± 3.81)	6.26 (± 2.38)	42.50 (± 3.73)	8.41 (± 2.29)	59.65 (± 4.72)
	AS	1.13 (± 0.18)	15.37 (± 3.83)	2.53 (± 0.45)	16.41 (± 4.83)	1.77 (± 0.21)	31.17 (± 12.62)

Values are mean of 15 randomly selected images, three biological replicates, five technical replicates each ± standard deviation (SD). PMMA: polymethylmethacrylate, PC: polycarbonate, HA: hydroxyapatite, AS: artificial saliva.

Table 2.11 Percentage of area covered by whole saliva biofilms

Coupon material	Preconditioning	24 h		48 h		72 h	
		Batch	CDC biofilm reactor	Batch	CDC biofilm reactor	Batch	CDC biofilm reactor
PMMA	Water	7.33 (± 3.59)	10.93 (± 2.75)	8.61 (± 2.83)	19.47 (± 6.00)	12.27 (± 6.73)	14.22 (± 5.42)
	AS	8.24 (± 3.41)	11.17 (± 5.41)	11.12 (± 3.62)	16.13 (± 6.32)	13.76 (± 4.82)	12.47 (± 4.23)
PC	Water	11.59 (± 2.34)	21.76 (± 5.87)	15.94 (± 3.33)	28.31 (± 4.12)	18.61 (± 6.28)	35.36 (± 4.69)
	AS	12.35 (± 3.30)	23.51 (± 0.21)	18.09 (± 2.86)	29.06 (± 6.93)	20.44 (± 7.61)	31.06 (± 5.99)
HA	Water	7.33 (± 3.59)	10.93 (± 2.75)	8.61 (± 2.83)	19.47 (± 6.00)	12.27 (± 6.73)	14.22 (± 5.42)
	AS	8.24 (± 3.41)	11.17 (± 5.41)	11.12 (± 3.62)	16.13 (± 6.32)	13.76 (± 4.82)	12.47 (± 4.23)

Values are mean of 15 randomly selected images, three biological replicates, five technical replicates each ± standard deviation (SD). PMMA: polymethylmethacrylate, PC: polycarbonate, HA: hydroxyapatite, AS: artificial saliva.

The effect of medium concentration on biofilm formation in the CDC biofilm reactor revealed that the percentage of biofilm coverage was significantly higher for *C. albicans* biofilms ($p < 0.001$) and whole saliva biofilms ($p = 0.0285$). Conversely, a 10% concentration of the manufacturer's recommendation resulted in significantly greater biofilm coverage in mixed bacterial and mixed microbial species biofilms ($p < 0.001$), as shown in Figure 2.5.

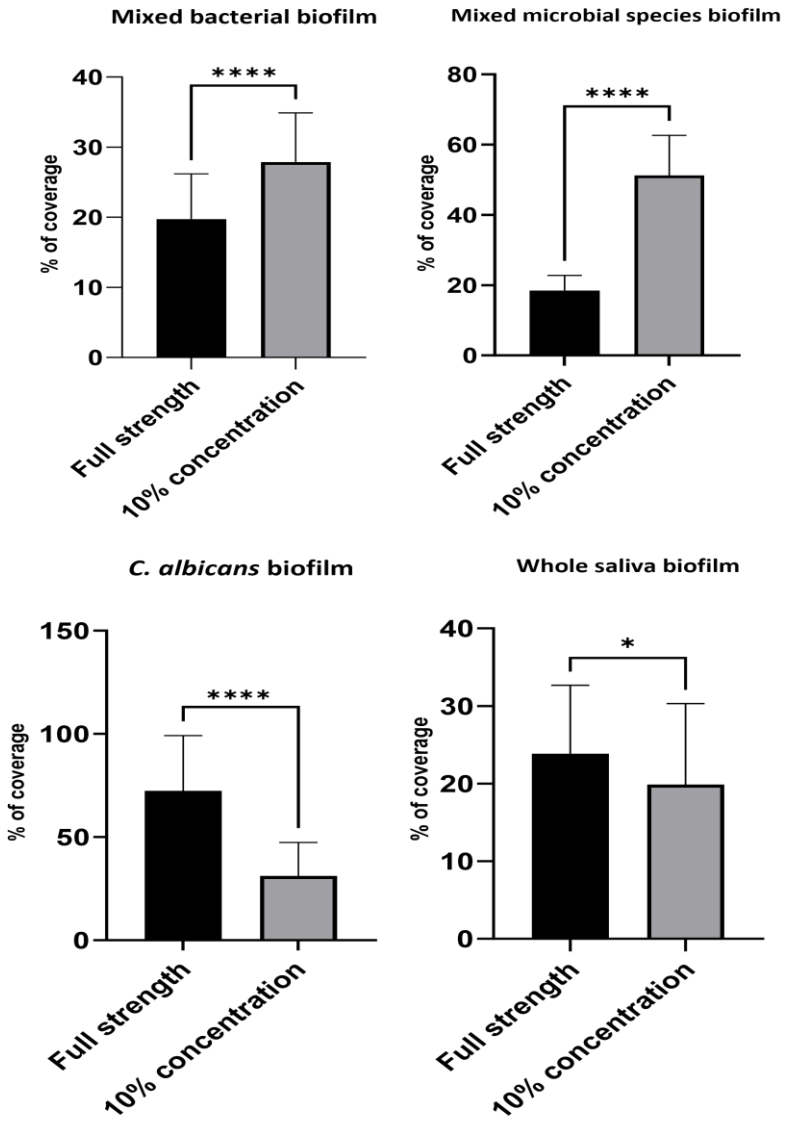

Figure 2.5 Comparison of biofilm formation under full and 10% medium concentration for different biofilm types.

Biofilm formation was assessed based on percentage of area covered by biofilm for whole saliva biofilms, mixed bacterial biofilms, mixed microbial species biofilms, and *Candida albicans* biofilms.

2.3.3 Assessment of *in vitro* biofilm biomass and thickness using CLSM

For mixed bacterial biofilms grown in full strength TSB, AS preconditioning (5.449 $\mu m^3/\mu m^2$) significantly ($p = 0.006$) increased biomass compared to using water (2.123 $\mu m^3/\mu m^2$). Surface type influenced biofilm biomass, with PMMA (1.950 $\mu m^3/\mu m^2$) yielding significantly ($p < 0.001$) lower biomass compared to HA (4.627 $\mu m^3/\mu m^2$) and PC (6.587 $\mu m^3/\mu m^2$). The model used did not significantly affect biomass levels.

For mixed microbial species biofilms (Figure 2.6) grown in full strength TSB, preconditioning had no significant ($p = 0.065$) effect on biomass. PC surfaces (5.758 $\mu m^3/\mu m^2$) yielded significantly ($p < 0.001$) higher biofilm biomass compared to HA (1.984 $\mu m^3/\mu m^2$) and PMMA (2.183 $\mu m^3/\mu m^2$). The CDC biofilm reactor (4.195 $\mu m^3/\mu m^2$) yielded significantly ($p < 0.001$) higher biofilm biomass compared to the batch system (1.495 $\mu m^3/\mu m^2$).

For *C. albicans* biofilms (Figure 2.7) grown in full strength SDB, preconditioning with AS did not affect biomass levels. PMMA surfaces (1.071 $\mu m^3/\mu m^2$) had significantly ($p < 0.001$) lower biofilm biomass compared to PC (4.435 $\mu m^3/\mu m^2$) and HA (3.438 $\mu m^3/\mu m^2$). The CDC biofilm reactor produced significantly ($p < 0.001$) higher biomass levels compared to the batch system.

For whole saliva biofilms grown in full strength TSB, preconditioning with AS did not significantly ($p = 0.775$) influence biomass. PC surfaces (7.665 $\mu m^3/\mu m^2$) yielded significantly ($p < 0.001$) higher biomass compared to HA (2.813 $\mu m^3/\mu m^2$) and PMMA (2.021 $\mu m^3/\mu m^2$). The CDC biofilm reactor (5.759 $\mu m^3/\mu m^2$) produced significantly ($p < 0.001$) higher biomass compared to the batch system (2.895 $\mu m^3/\mu m^2$).

Biofilm thickness results aligned with those obtained for biomass. AS pre-conditioning significantly ($p = 0.006$) increased thickness in mixed bacterial biofilms, while no differences

were observed for other biofilm types. The CDC biofilm reactor yielded significantly higher biofilm thickness levels for *C. albicans*, mixed microbial species, and whole saliva biofilms ($p < 0.001$), but no significant difference was observed in mixed bacterial biofilms.

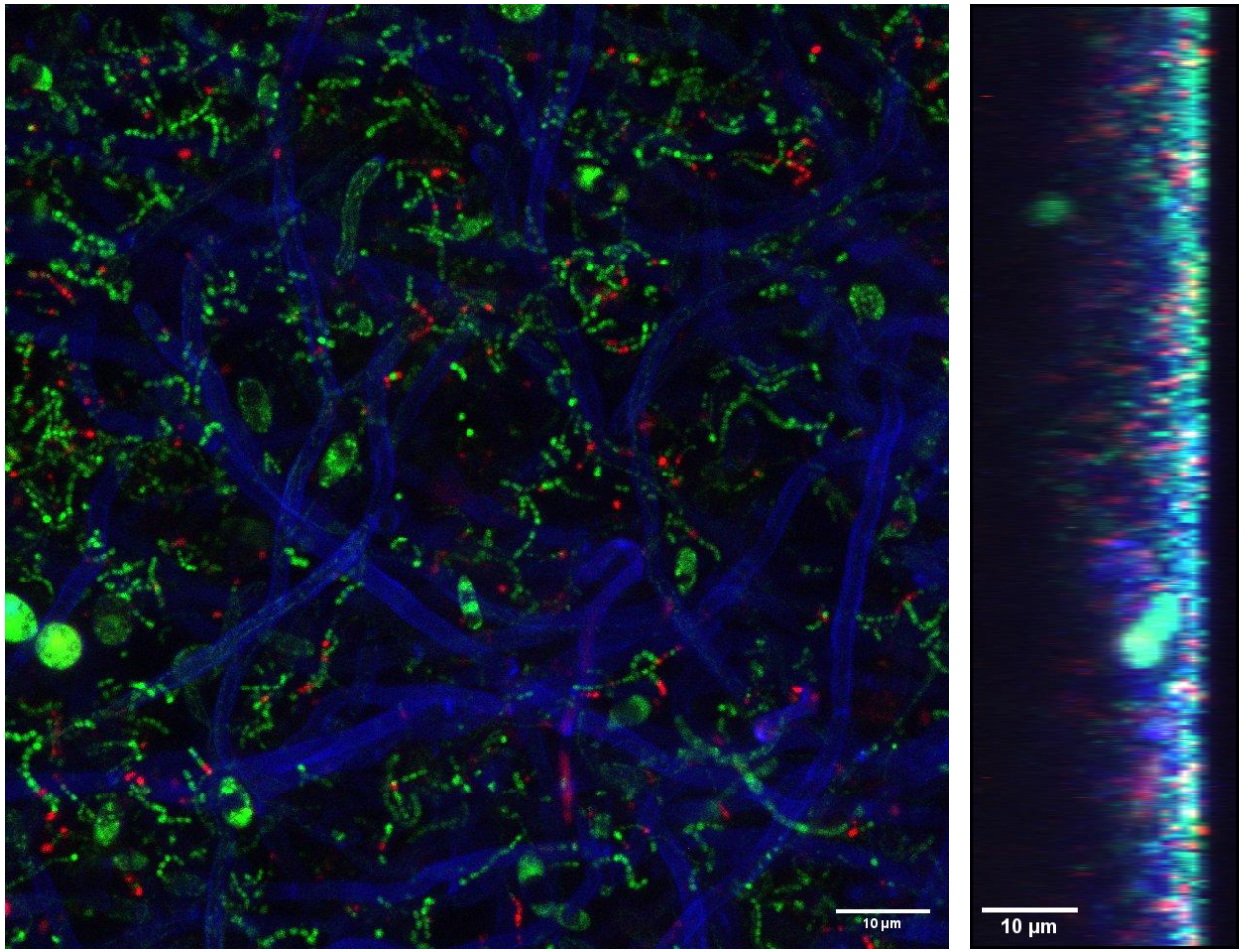

Figure 2.6 Image of mixed microbial species biofilms grown for 72 h on polycarbonate coupons in the CDC biofilm reactor using full strength tryptic soy broth (TSB) on polycarbonate coupons pre-conditioned with water.

Biofilms were Live/Dead BacLight stained (Invitrogen). Green fluorescence shows live cells stained by Syto9. Red fluorescence shows dead cells stained with propidium iodide. Blue fluorescence *Candida albicans* stained with 1% (v/v) calcofluor white. The orthogonal (YZ) view shown alongside the XY projection represents a single optical cross-section through the biofilm.

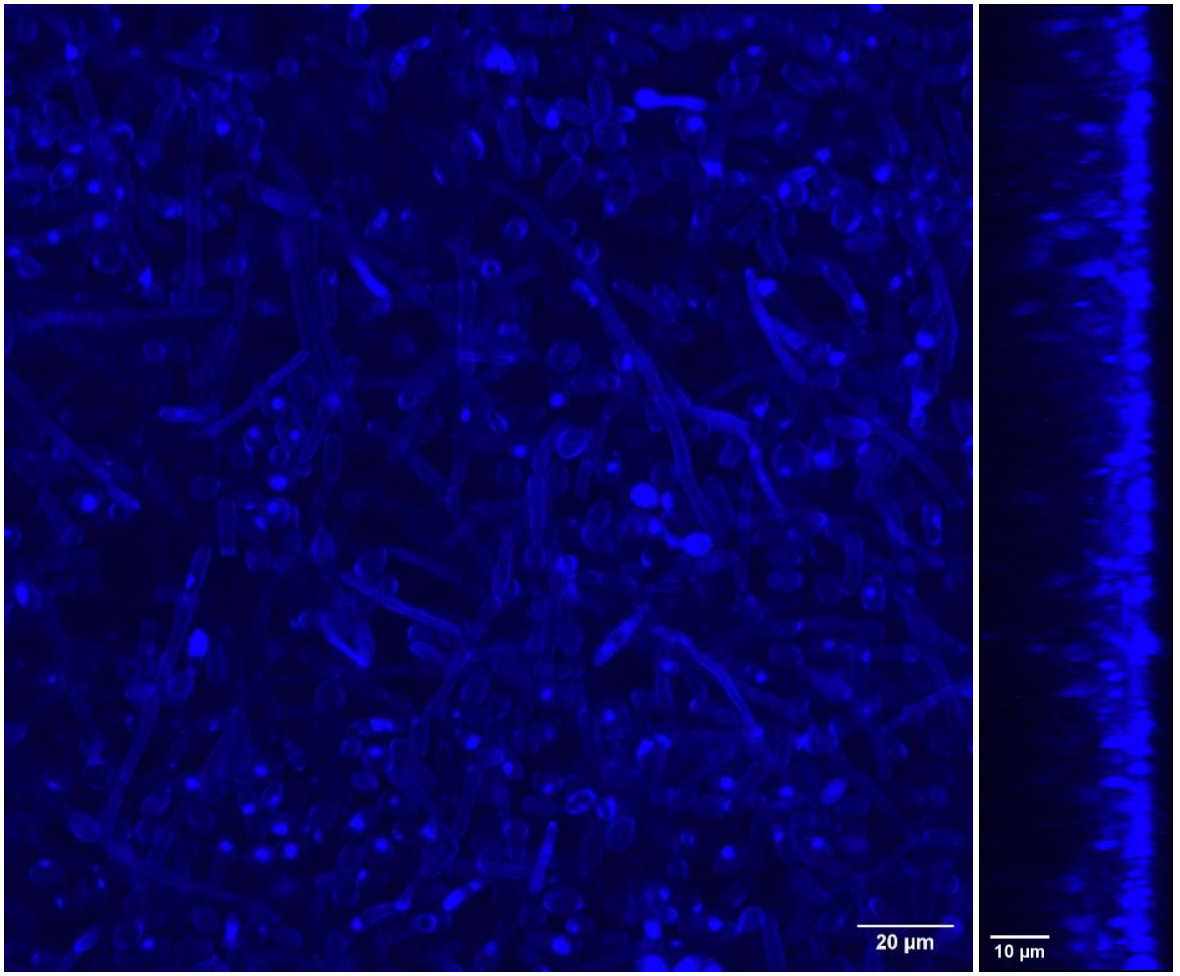

Figure 2.7 CLSM image of *Candida albicans* biofilm grown for 72 h using the CDC biofilm reactor culture in Sabouraud dextrose broth (SDB) full strength on polycarbonate coupons pre-conditioned with water.

Candida albicans was stained with 1% (v/v) calcofluor white. The orthogonal (YZ) view shown alongside the XY projection represents a single optical cross-section through the biofilm.

2.4 Discussion

The objective of this first experimental chapter of the thesis was to establish approaches to reliably grow *in vitro* biofilms for later studies that would permit the evaluation of EPS production and function in the context of antimicrobial resistance. Different types of microbial inocula were selected and included oral microorganisms recognised for their biofilm forming ability and association with disease (*i.e.*, *Streptococcus mutans* and *Candida albicans*). Also included, were commensal oral bacteria (*Streptococcus sanguinis, Streptococcus gordonii* and *Streptococcus salivarius*) recognised for biofilm formation and colonisation of oral surfaces. These microorganisms reportedly form biofilms on both hard (*e.g.* enamel of teeth) and soft tissues (*e.g.* surface of the tongue), and contribute to the complexity of oral biofilms (Baty et al. 2022). In addition, whole saliva was used for biofilm seeding, in the event that the other tested microbial inocula yielded limited *in vitro* biofilms levels. Whole saliva might have been expected to produce the highest quantity of biofilm based on the likely higher number of species present (Simon-Soro et al. 2022) and the likely presence of associated saliva components that could promote surface attachment (Chawhuaveang et al. 2021). However, the heterogeneous nature of whole saliva would also be a limitation, as this could lead to reduced standardisation between experiments in later research Chapters.

Establishing *in vitro* growth conditions was an important element of the research to meet the overarching aim of the PhD, and to identify suitable conditions for cultivating *in vitro* biofilms for subsequent analyses and the evaluation of EPS. The work outlined in this Chapter was also an important initial study to allow my own development of the required laboratory skills to successfully conduct subsequent research.

Batch and flow-through methods to culture *in vitro* biofilms are two fundamental approaches used in biofilm research. The CDC biofilm reactor is an apparatus that allows continuous flow of culture medium with provision of constant shear force generated by a baffled stirrer within the vessel. The CDC biofilm reactor's ability to maintain controlled flow and shear forces arguably replicates natural conditions, providing reproducible and insightful results. Previous studies have suggested use of the CDC biofilm reactor to grow *in vitro* biofilms resembling those on oral surfaces (An et al. 2022). An et al. (2021) demonstrated that the reactor, inoculated with pooled human saliva, supported the formation of stable and reproducible biofilms containing all six major bacterial phyla commonly found in the oral microbiota. While the present research similarly employed the CDC biofilm reactor testing the same inocula and substrata, a different growth medium (TSB instead of BHI) and a higher shear rate (1.1 ml/min vs. 0.5 ml/min) were used.

The ability of the CDC biofilm reactor to generate reproducible biofilms, despite these variations, underscores its robustness as a biofilm model. Furthermore, results presented demonstrate that the reactor can still support productive biofilm formation of a range of inocula (single and mixed species), growth conditions (medium concentrations) and substrata (PC coupons) reinforcing the suitability of the CDC biofilm reactor for oral biofilm development.

Moreover, the CDC biofilm reactor has been used to investigate biofilm interactions with various dental substrates (Rudney et al. 2012). By allowing controlled manipulation of environmental factors and substrata, the model facilitates the study of biofilm formation and responses to different dental materials, further reinforcing its relevance in oral biofilm research (Rudney et al. 2012). Additionally, the CDC biofilm reactor has been widely adopted

for different fields in biofilm research for testing efficacy of antimicrobial agents under dynamic conditions. For example, in dairy manufacturing, it has been used to culture robust biofilms of pathogens such as *Listeria monocytogenes* and *Staphylococcus aureus* on stainless steel surfaces. These biofilms simulate contamination scenarios to evaluate sanitiser efficacy (Lindsay et al. 2022).

The results in this current research showed that *C. albicans* produced significantly higher biofilm levels in the CDC biofilm reactor compared to the batch system. For example, biofilm levels grown using the CDC biofilm reactor for 72 h exhibited a up to 38% increase in CFUs compared to batch culture across all surfaces and pre-conditioning conditions, and up to 17-fold increase in biofilm area of coverage. These results reflect patterns noted in a previous study by Uppuluri et al. (2009) that compared *C. albicans* biofilms formed under static and flow conditions in which the authors used a simple flow-through system by fitting a silicone elastomer strip inside a conical tube, introducing fresh medium from the top, and allowing waste to drain from the bottom. Metabolic activity and biofilm biomass were quantified using an XTT reduction assay and dry weight measurement, while light microscopy, CSLM, and SEM were used to analyse biofilm structure. The findings revealed that biofilms grown under flow conditions developed three times faster, exhibited higher metabolic activity, and formed more complex architectures, including thicker and denser structures, compared to those grown under static conditions (Uppuluri et al. 2009).

Even though, *C. albicans* formed biofilms under the different conditions tested, it was evident that biofilms were in greater quantities in full strength SDB compared to a 10-fold diluted SDB medium. In such studies CFU counts were approximately 2-fold higher, and there was a 40 % increase in biofilm area coverage.

For mixed bacterial *in vitro* biofilms generated in the current research, the CDC biofilm reactor yielded lower CFUs (up to 90% reduction) and biofilm area coverage (up to 2-fold reduction) compared to batch culture.

It has previously been shown that *in vitro* biofilm development of *S. gordonii* biofilms was sensitive to the level of shear forces applied (Nairn et al. 2024). This study compared resulting biofilm biomass under different levels of shear and results showed significantly lower biomass levels at higher shear, and lower shear forces slightly increasing biomass. The shear stress generated by the CDC biofilm reactor (0.026 Pascal (Pa), as reported by the manufacturer) matches the shear stress of 0.02 Pa reported by Nairn et al. (2024), where fluid shear was shown to significantly influence biofilm biomass.

These observations indicated that *in vitro* biofilm formation was influenced by the magnitude of shear forces. Too much shear force will hinder initial microbial attachment, and this should be avoided. Ideally, shear force used in *in vitro* studies of biofilms should be at a similar level to those present in the environment aiming to be replicated. Although saliva flow has been reported to generate shear stress levels of approximately 0.076 Pa (Prakobphol et al. 1995), the mixed bacterial biofilms grown in the presented research were exposed to lower shear levels. This highlights the challenges of replicating identical biofilm conditions *in vitro* and the importance of optimising biofilm development to better reflect *in vivo* environments.

Results from this present study, comparing batch system and the CDC biofilm reactor, suggested that the shear applied in the CDC biofilm reactor was conducive to *C. albicans* biofilm formation, but was less beneficial for mixed bacterial biofilm development. Interestingly, the mixed microbial species biofilms that contained both *C. albicans* and bacteria exhibited higher biofilm formation using the CDC biofilm reactor compared to batch culture.

In the CDC biofilm reactor, CFU counts were significantly higher ($p = 0.01$), as was the area coverage ($p < 0.001$) and biomass ($p < 0.001$). These results could reflect the higher *C. albicans* biofilm growth under the shear provided by the CDC biofilm reactor.

Another factor that could contribute to the differences between mixed bacterial biofilm development in flow-through compared with the batch system was the orientation of the coupons to support biofilm growth. In the CDC bioreactor, the coupons were oriented vertically and subjected to high shear forces, simulating dynamic fluid flow conditions. In the batch well plate system the coupons were placed in a horizontal position, where initial attachment and biofilm formation were likely driven by gravity-mediated deposition. The difference in substrate orientation could also contribute to variations in developed biofilms (Malea et al. 2025), including heterogeneity in thickness and cellular density both on a single coupon and between coupons. Substrate orientation has been extensively studied in the context of biofouling and aquatic systems, where it is recognised as a significant factor influencing biofilm development (Glasby 2000). For instance, Bellou et al. (2012) research of *in situ* deep-sea biofilms showed that surface orientation effected biofilm growth under specific conditions (*e.g.* material for attachment, sea depth *etc*). Horizontally orientated surfaces had more microbial cells and higher biofilm growth compared to vertically orientated surfaces. This was attributed to differences in gravitational effects and cell attachment dynamics. Although deep-sea environments differ from *in vitro* systems, these findings emphasised the importance of the positioning of the supporting surface for biofilm growth (Bellou et al. 2012).

The rationale behind assessing pre-conditioning of coupons with AS stems from the aim to try to better represent the presence of a salivary acquired pellicle, which forms on all surfaces in

the oral cavity including dental materials such as titanium used in implants (Martínez-Hernández et al. 2023). As previously mentioned, (Section 2.1.2), the acquired pellicle provides receptor molecules for microbial attachment. Therefore, it was hypothesised that AS pre-conditioning of coupons would increase the resulting biofilm biomass and number of recovered CFUs. There was, however, no significant difference of CFU count and area of biofilm coverage between the water and AS preconditioned surfaces. In the case of biomass assessments, mixed bacterial biofilms that had been AS pre-conditioned were significantly elevated ($p = 0.006$) compared with water pre-conditioning.

The choice of surface material will affect microbial adhesion and biofilm formation because of surface properties (Kim et al. 2025). This could be through differences in surface roughness, hydrophobicity and charge that influence initial attachment of microorganisms and biofilm stability (Zheng et al. 2021). The coupons used in these experiments were constructed from PMMA, HA and PC and were compared for their ability to support *in vitro* biofilm growth. The surface roughness differs between these materials. PMMA coupons fabricated in the laboratory were previously characterised within our group to have a roughness around 3.06 µm (Williams 2023). A previous investigation that used the coupons from the same manufacturer reported the roughness of HA surfaces was 1.26 µm (Park et al. 2022). While the manufacturer reported the roughness of PC coupons to be 1.29 µm.

Previous studies on the role of surface roughness on microbial adhesion have identified key threshold levels for effective bacterial attachment which was a minimum of 0.2 µm in surface roughness for bacterial adherence (Bollen et al. 1996). Similarly, a study on *Porphyromonas gingivalis* indicated that increased roughness of titanium, particularly within a range of Ra of 0.8 to 1.2 µm, facilitated rapid colonisation and biofilm formation (Daw et al. 2013). This was

likely due to surface depressions and edges that enhance bacteria-surface contact and give protection against shear forces.

Surface hydrophobicity is a term that refers to the tendency of a surface to repel water, and this can significantly influence microbial attachment (Mu et al. 2023). For example, Yuan et al. (2017) assessed exposure of *E. coli* to surfaces of differing hydrophobicity, showed that adhesion was reduced at extreme levels of hydrophobicity (water contact angle ≈ 0°) or hydrophilicity (≈ 156°), with the highest bacterial adhesion occurring at an optimal value of ≈ 95°. This again highlights the sensitivity and complexity of microbial attachment, and that optimal conditions depend on multiple variables (Yuan et al. 2017). Furthermore, microorganisms themselves can exhibit either hydrophobic or hydrophilic surface properties, which influence their adhesion preferences. Research has demonstrated that hydrophobic microorganisms tend to adhere more to hydrophobic surfaces, while hydrophilic microorganisms preferentially attach to hydrophilic surfaces (Krasowska and Sigler 2014). For instance, *C. albicans* exhibits surface hydrophobicity, which plays a critical role in its adhesion to host tissues and abiotic surfaces. The level of hydrophobicity in *C. albicans* varies depending on environmental conditions, such as nutrient availability and growth phase, directly impacting its adhesive properties (Danchik and Casadevall 2021).

In this current research, results showed that for most cases there was no significant difference between biofilm formation on HA and PC surfaces. However, it was apparent that staining of biofilms on HA coupons resulted in a high degree of background fluorescence, which could compromise future analyses. PC coupons did not exhibit this background fluorescence and proved to be more physically robust for repeated experiments. Based on the overall results of the current studies, PC coupons were the preferred choice of substrate for biofilm development in subsequent investigations. It was also decided that the CDC biofilm reactor

with flow-through of culture would be used, based on its ability to produce of homogeneous biofilms and application of shear force (Goeres et al. 2005). The batch system was selected for production of mixed bacterial biofilms, as this showed higher biofilm CFU levels and area of biofilm coverage. Since surface pre-conditioning with AS and water yielded similar results in most conditions tested, it was decided that future experiments would be based on water conditioned surfaces for ease of use. Therefore, the chosen conditions for biofilm formation for subsequent analyses of biofilms and EPS development are summarised in Table 2.12.

Table 2.12 Summary of selected conditions for biofilm development for subsequent research

Inoculum	System	Concentration of medium	Growth duration	Substrate
Mixed bacterial biofilm	Batch system	Full strength	72 h	PC coupons
Mixed microbial species biofilm	CDC biofilm reactor	10% of recommended	72 h	PC coupons
Candida albicans biofilm	CDC biofilm reactor	Full strength	72 h	PC coupons
Whole saliva biofilm	CDC biofilm reactor	Full strength	72 h	PC coupons

PC, polycarbonate.

Chapter 3

Detection of extracellular polymeric substances in biofilms using fluorescently labelled probes and the role of LigE in *Neisseria gonorrhoea* pathogenicity

3.1 Introduction

Extracellular polymeric substance (EPS) is a defining feature of biofilms and constitutes the matrix that encases the microbial community and underpins structural integrity and functional capabilities of a biofilm (Sharma et al. 2023b). While the general role of EPS in maintaining biofilm structure and function is well established, detailed characterisation of individual matrix components remains challenging due to their chemical diversity and complex organisation within biofilms (Karygianni et al. 2020b). Key EPS constituents, including polysaccharides, proteins, extracellular DNA, and lipids, may be differentially distributed within the matrix and contribute distinctly to biofilm architecture, resilience, and antimicrobial tolerance (Flemming et al. 2023). Consequently, analytical approaches capable of resolving EPS composition *in situ* are required to improve understanding of matrix organisation within complex biofilms. Biofilm growth conditions are known to strongly influence EPS composition, structure, and spatial organisation (Saharan et al. 2024). Intermittent drying and desiccation have been shown to induce adaptive responses in biofilms, including increased EPS production and changes in matrix composition and architecture, which enhance structural stability and tolerance to environmental stressors (Gonzalez-Henao and Schrenk 2025). Extended growth allows biofilms to develop mature three-dimensional architecture and more established EPS matrix, which provide the structural basis for *in situ* visualisation and characterisation of matrix components (Sauer et al. 2022). Accordingly, intermittent drying and prolonged incubation were incorporated in this chapter to promote EPS development and enable detailed analysis of matrix composition using CLSM.

3.1.1 EPS components and function

Table 3.1 provides a summary of typical EPS components found in different biofilms, in addition to the potential function(s) provided by the components. Water is the main component of biofilms, but is strictly speaking not a 'polymeric' substance (Di Martino 2018). However, several EPS components such as certain carbohydrates are hydrophilic, and their presence can enhance retention of water within the biofilm matrix (Flemming and Wingender 2010). Water in the EPS provides an aqueous environment for solubilisation of substances for cell uptake and secretion (Galdino et al. 2020). It also serves as a fluid medium for movement of substances through the biofilm by diffusion and by flow (Quan et al. 2022). In cases where biofilm desiccation occurs, it has been reported that biofilm cells respond to this by increased production of hydrophilic EPS components to promote water retention (Or et al. 2007).

The EPS provides a scaffold for biofilm architecture, facilitates microbial adhesion, nutrient retention, and protection against environmental stressors (Huang et al. 2022a; Priyadarshanee and Das 2023; Flemming et al. 2025). In the case of the latter, the resilience of biofilms in the hostile environment of a living host could promote chronic and recurrent biofilm infection. An example of this would be the biofilms associated with dental implants, where if retained can lead to peri-implantitis (Costa et al. 2023).

Both the composition and structure of EPS varies with different microorganisms due to a combination of species-specific metabolic pathways (Oliva et al. 2025), genetic makeup, environmental factors and functional role (Hasan et al. 2024). Different species and strains have distinct pathways and regulatory systems, resulting in variation in the types of polysaccharides, proteins and other components incorporated into EPS (Netrusov et al. 2023). Similarly, nutrient availability influences both yield and composition of EPS (Oliva et al. 2025).

Additionally, production of EPS is dependent on the function required, whether for adhesion, protection against external stressors, nutrition retention, or structural support and remodelling. Therefore, multiple factors are involved in the diversity of EPS composition, structure and properties across different species and environments (Netrusov et al. 2023; Hasan et al. 2024).

The EPS not only promotes recruitment of microorganisms to the biofilm but also facilitates adhesion through specific components (Cugini et al. 2019; Guzmán-Soto et al. 2021). For example, for *Staphylococcus epidermidis*, the polysaccharide intercellular adhesin (PIA; also known as poly-β-1,6-N-acetylglucosamine [PNAG]) mediates cell-cell interactions allowing bacteria to accumulate into multilayered structures (Nguyen et al. 2020). Beyond structural roles, EPS enhances antimicrobial resistance (AMR) by limiting antimicrobial penetration into biofilms as well as providing protection against immune defences (Singh et al. 2021a). Additionally, EPS facilitates interspecies and cross-kingdom interactions by enabling matrix sharing within polymicrobial biofilms. An example is the Psl produced by *P. aeruginosa*, which provides protection against colistin to susceptible species such as *E. coli* and *S. aureus* that may also be present in the biofilm (Billings et al. 2013). Similarly, the EPS of *C. albicans*, particularly β-1,3-glucan, confers protection to *S. aureus* against vancomycin by acting as a physical barrier with β-1,3-glucan coating the bacterial cells (Kong et al. 2016). These attributes increase the likelihood of microbial cell survival within biofilms, contribute to biofilm virulence and plays a direct role in promoting damage to host cells, as seen in peri-implantitis (Costa et al. 2020). *Shigella flexneri*, which forms biofilms in the intestine, has an EPS that is mainly polysaccharides , and interactions between these components stabilise the biofilm matrix (Nickerson et al. 2017). In particular, the exopolysaccharide, S-EPS 2-1, has been

shown to significantly enhance *S. flexneri* biofilm formation and pathogenicity in intestinal infections (Song et al. 2022).

EPS plays a central role in AMR with multiple reported mechanisms reported. These include the formation of physical and chemical barriers that protect embedded microbial cells from environmental stressors such as antimicrobial agents (Nahum et al. 2024). EPS can limit the movement of antibiotics through the biofilm and reduce their efficacy by lowering antibiotic concentrations in the biofilm (Liu et al. 2024). Diffusion of charged antimicrobials through the EPS can be impeded by sequestration by oppositely charged EPS components (Koo et al. 2017). In addition, antimicrobial degrading enzymes retained in the EPS may also reduce the effective levels of the agent in the biofilm (Karygianni et al. 2020b). Chemical gradients within the biofilm are maintained by EPS and these may impact on antimicrobial function (Jo et al. 2022). Additionally, the EPS surrounding the cells can facilitate horizontal gene transfer (which may involve genes associated with resistance) between constituent cells, further contributing to the development and propagation of resistance (Liu et al. 2024). This arises due to retention of released DNA (including DNA encoding antimicrobial resistance genes; ARGs) in the EPS which can then be more readily acquired by microbial cells in close proximity.

3.1.2 EPS characterisation

Characterising and identifying EPS components is key to understanding and addressing the unique properties of biofilms. Whilst the literature highlights the general functions of EPS, such as providing structural integrity, nutrient retention, and protection against antimicrobials, biofilms are highly diverse, with their composition varying significantly across environments and microbial communities. This diversity emphasises the need for targeted studies to establish knowledge specific to the biofilm under investigation. Understanding the

specific components of EPS is also crucial for effectively targeting and disrupting biofilms. Identifying these components forms the basis for developing precise strategies to undermine the structural integrity and protective functions of EPS. Furthermore, this knowledge provides valuable insights into biofilm ecology, the mechanisms of AMR, and the persistence of biofilms in challenging conditions. A comprehensive characterisation of EPS provides the basis for innovative strategies to prevent, disrupt, and treat biofilm-associated infections (Lu et al. 2024).

3.1.3 The composition and function of EPS for selected clinical biofilm-forming microorganisms

3.1.3.1 EPS production by *Candida albicans*

The EPS produced by *C. albicans* is reported to contain typical components commonly found in microbial biofilms, including polysaccharides, proteins, eDNA, and lipids (Wall et al. 2019). Among the polysaccharides, β-1,3-glucan, β-1,6-glucan, and α-mannan are key constituents that form a mannan-glucan complex (MGCx) (Nickerson et al. 2017). The MGCx accounts for approximately 20% of the total carbohydrate content of the matrix (Zarnowski et al. 2014). The MGCx plays a critical role in maintaining biofilm structural integrity and contributes to antifungal resistance by sequestering antifungal drugs, such as fluconazole, through binding and retention within the matrix, thereby reducing the drug's availability to target cells (Dominguez et al. 2018). Proteins in the EPS include both fungal-derived proteins, such as glycolytic enzymes (Wu et al. 2024) (*e.g.,* enolase and alcohol dehydrogenase) and host-derived proteins such as fibrinogen, fibronectin, and albumin (Nett et al. 2015). Additionally, the EPS matrix exhibits remarkable diversity in fungal-derived proteins, with studies

identifying up to 458 distinct polypeptides and proteins constituting approximately 55% of the EPS' dry weight (Zarnowski et al. 2014).

Lipids in the EPS of *C. albicans* include neutral and polar glycerophospholipids and sphingolipids, which can comprise up to 15% of the EPS (Kumar and Kumar 2023). These lipids contribute to biofilm resistance and structural organisation. Notably, the lipid composition varies with environmental conditions, enhancing the biofilm's adaptability. Extracellular DNA, primarily derived from autolysis, is another significant component of the EPS (Martins et al. 2010). It is largely noncoding and plays a role in maintaining biofilm structural integrity and resistance to antifungal treatments (Mitchell et al. 2016).

3.1.3.2 EPS production by oral streptococci

In oral biofilms, particularly those formed by streptococci such as *S. mutans* and *S. sanguinis*, the EPS primarily consist of polysaccharides, including both soluble and insoluble glucans (Díaz-Garrido et al. 2022; Costa et al. 2023; Scaffa et al. 2023). These glucans are synthesised by glucosyltransferases (GTFs) and can mediate adhesion, microbial aggregation and further matrix development (Bowen and Koo 2011). Glucans are polysaccharides composed of glucose monomers linked by glycosidic bonds and are classified based on solubility and the type of glycosidic linkages (Chen et al. 2021). The type and arrangement of these bonds determine the physical and chemical characteristics of the polymer. For instance, consecutive α-1,3 linkages result in tightly packed structures that are water-insoluble, whereas linear α-1,6 glucans form less dense and more flexible arrangements, making them primarily soluble (Ernst et al. 2024).

In addition to glucans, oral streptococcal biofilms contain other matrix components, such as eDNA, proteins, and lipids (Jakubovics et al. 2021). eDNA contributes to biofilm integrity by

interacting with glucans, particularly under the low pH conditions characteristic of cariogenic biofilms (Liao et al. 2014; Cugini et al. 2019). This interaction strengthens the matrix, facilitates microbial adherence to tooth enamel and protects the biofilm community from antimicrobial agents (Jakubovics and Burgess 2015). Similarly, proteins in the EPS, including glucan-binding proteins and regulatory enzymes, play essential roles in adhesion, biofilm formation, and AMR (Besingi et al. 2017). These proteins contribute to cell-cell interactions and binding with other EPS components, enhancing the structural integrity of the biofilm. Lipids, such as lipoteichoic acids, are integral to matrix stability and participate in synthesising insoluble glucans (Wu et al. 2022). Additionally, they influence the viscoelastic properties of the biofilm, aiding its resilience and adaptability to environmental changes (Cugini et al. 2019; Zuber and Kreth 2023).

3.1.3.3 *Neisseria gonorrhoeae* EPS and DNA ligases

The EPS of *N. gonorrhoeae* is distinct from that of many other bacterial species in that it lacks extracellular polysaccharides and is instead predominantly composed of eDNA, which originates from membrane blebs (Steichen et al. 2011). Moreover, eDNA is actively secreted as single stranded DNA, which has been implicated in the early stages of biofilm development, promoting initial surface adhesion and intercellular connectivity (Zweig et al. 2014). eDNA not only provides structural support, but also contributes to the cohesion both *in vitro* and *in vivo*, such as during cervical infections where it colocalises with neutrophil extracellular traps, suggesting a role in pathogenesis and immune evasion (Buzzo et al. 2021). Together, these findings highlight the central role of eDNA as a major component in the matrix architecture and function of *N. gonorrhoeae* biofilms.

DNA ligases are enzymes capable of repairing breaks within the DNA backbone (Bilotti et al. 2022). These enzymes are essential for all living cells as they participate in DNA replication and repair (Tomkinson et al. 2006). DNA ligases are categorised based on the cofactor used to catalyse the ligation process. The most common cofactor is adenosine triphosphate (ATP), which is used by ATP-dependent ligases (ADLs). These enzymes are widespread and found in both eukaryotes and prokaryotes (Shi et al. 2018). In bacteria, however, most DNA ligases use β-nicotinamide adenine dinucleotide (NAD) as a cofactor to catalyse the ligation process (Weller and Doherty 2001). Such ligases are referred to as NAD-dependent ligases (NDLs). Unlike the prevalent ADLs, the unique cofactor in NDLs presents an opportunity for developing antibiotics that selectively target bacteria while being harmless to eukaryotic cells (Pergolizzi et al., 2016).

Although all bacteria possess NDLs, some also encode ADLs, indicating that certain species maintain both types of enzymes (Wilkinson et al. 2001). One group of particular interest is Lig E, due to its predicted periplasmic location (Williamson et al., 2016) and its presence in bacteria known to form biofilms rich in eDNA (Pan et al., 2024). Pan et al. (2024) evaluated the involvement of Lig E from *N. gonorrhoeae* in biofilm formation and concluded that deletion of Lig E reduced biofilm formation without affecting the viability of planktonic cells compared to the wild type.

3.1.4 EPS characterisation involving CLSM

Advances in imaging techniques, particularly fluorescence labelling in conjunction with CLSM, has enabled the quantitative, non-destructive analysis of EPS. CLSM approaches facilitate high-resolution, three-dimensional imaging of biofilms, leveraging the specificity of dyes to target and identify EPS components (Pan et al. 2022). In a study by Neu and Kuhlicke (2022),

a wide selection of fluorescently labelled lectins was used to identify EPS components across a diverse range of biofilms sourced from environments such as rivers, wastewater treatment reactors, and marine systems. The study showed how lectins could comprehensively screen and characterise the polysaccharide content of biofilm EPS. By using over 80 lectins targeting polysaccharides, glycoproteins, and glycolipids, variation in EPS composition between different biofilms was demonstrated (Neu and Kuhlicke 2022). Other researchers have used stains to detect specific non-polysaccharide EPS components. Extracellular proteins have been identified using protein-specific fluorescent dyes (Rooney et al. 2020). Whilst dimeric cyanine nucleic acid stains, which are cell-impermeable, have been used to localise eDNA within biofilm EPS (Evans et al. 2025). This approach offers a powerful tool to study the spatial arrangement and contribution of eDNA to the structural stability and resilience of biofilms (Kanampalliwar and Singh 2020).

3.1.5 Aims

EPS characterisation of selected biofilms using CLSM coupled with fluorescently labelled molecular probes and SEM. In addition, through collaboration with the University of Waikato, an evaluation of *N. gonorrhoea* biofilm formation and eDNA production on both biotic (*in vitro* infection model) and abiotic (polycarbonate) surfaces were used to address the following aims:

1. Providing both qualitative and quantitative analyses of EPS of selected biofilms, establishing a baseline for subsequent evaluation of EPS disruption described in later chapters
2. Assess the role of Lig E in *N. gonorrhoea* biofilm formation as well as eDNA presence in EPS.

3.2 Material and methods

3.2.1 Microorganisms and growth conditions

The microorganisms and specific conditions used for planktonic and biofilm culture were as previously described in **Chapter 2**, sections 2.2.2 and 2.2.3, under conditions presented in Table 2.12**.** Additional culture modifications were introduced to investigate their effects on EPS production. These modifications included: 1) use of intermittent biofilm drying, which was achieved by removing the liquid culture medium and incubating the biofilms at 37°C for up to 24 h; 2) extending the incubation times to 7 and 28 days; and 3) supplementing the culture medium with 1% sucrose. Where indicated, biofilms were grown in culture media supplemented with 1% (w/v) sucrose and 1 µM dextran, with supplementation present from inoculation and maintained throughout biofilm formation.

In the case of *Neisseria gonorrhoea,* all strain variants (Table 3.1) had previously been generated from *N. gonorrhoea* MS11 (ATCC: BAA-1833™) by Pan *et al.* (2024) at the University of Waikato, New Zealand. Strains included 1) the wild type *N. gonorrhoea* MS11, 2) a *Δngo-Lig E* mutant (containing a disruption of the *ngo-Lig E* gene (NGFG_01849) via a kanamycin resistance cassette, 3) an *opaB-ngo-Lig E* mutant with increased Lig E expression and 4) a *ngo-Lig E-His* mutant (containing a 6-His-tag at the C-terminus of the intact *ngo-Lig E* gene as well as an additional kanamycin resistance cassette behind the gene). The latter strain served as a control for the antibiotic resistance gene included in the knockout.

Neisseria gonorrhoea strains were grown at 37°C in 5% CO_2 for 16-17 h in gonococcal base liquid medium (15 g/L proteose peptone #3, 4.0 g/L K_2HPO_4, 1.0 g/L KH_2PO_4, 1.0 g/L NaCl) or on gonococcal base agar (Difco). Both the liquid and solid media were supplemented with 1%

Kellogg's supplement (22.22 mM glucose, 0.68 mM glutamine, 0.45 mM cocarboxylase, 1.23 mM $Fe(NO_3)_3$) (Dillard 2011).

Table 3.1 *Neisseria gonorrhoea* variants used in this study and their abbreviation.

Strain	Description
Wt *Neisseria gonorrhoea* MS11	Wild-type *N. gonorrhoea*
Δngo-Lig E	knockout of the Lig E gene
ngo-Lig E-His	control for the knockout since both contain the same insertion
opaB-ngo-Lig E	Increased expression of Lig E

3.2.2 *In vitro Neisseria gonorrhoea* biofilm development

Neisseria gonorrhoea biofilms were grown in batch culture as described in section 2.2.7, or in the CDC biofilm reactor as described in section 2.2.8**,** in gonococcal medium.

3.2.3 Characterisation of biofilm EPS using molecular probes

Coupons supporting biofilm growth were retrieved from the culture medium and gently washed in distilled water before being stained with a panel of commercially available molecular probes conjugated with specific fluorochromes (Table 3.2).

Fluorescent probes were prepared immediately prior to use according to the manufacturers' instructions and diluted to the recommended working concentrations. In cases where a working concentration was not provided, probes were used at a final concentration of 100 µg/ml. Staining solutions were protected from light throughout preparation and use.

For staining, each coupon was incubated with sufficient volume of the prepared staining solution to fully cover the biofilm surface and incubated at room temperature in the dark for

a minimum of 30 minutes. Following incubation, coupons were gently rinsed with sterile distilled water to remove unbound dye, then placed in the wells of a 24-well imaging plate (µPlate 24 Well Black, ibidi GmbH, Martinsried, Germany). CLSM (ZEISS Celldiscoverer 7 with LSM 900; Carl Zeiss Germany) was used to generate biofilm images as described in section 2.2.9.4. The microscope used objective lens magnification up to ×100 and laser lines at 405 nm, 488 nm, 561 nm, and 640 nm.

Table 3.2 Overview of fluorescently tagged molecular probes and their targets used to assess EPS

Molecular probe	Target	Description (Excitation/Emission)
SYTO™ 9	Nucleic acids (Cell-permeant)	LIVE/DEAD™ BacLight™ Bacterial Viability Kit, Invitrogen™ (480/500)
Propidium iodide (PI)	Nucleic acids (Cell-impermeant)	LIVE/DEAD™ BacLight™ Bacterial Viability Kit, Invitrogen™ (490/635)
TOTO™-3 Iodide	Nucleic acids (Cell-impermeant)	Invitrogen™ (633/660)
FilmTracer™ SYPRO™ Ruby Biofilm Matrix Stain	Proteins	Invitrogen™ (450⁄610)
Lectin (PNA) From *Arachis hypogaea* (peanut)	Carbohydrates (terminal β-galactose residues of glycoproteins)	Invitrogen™ Alexa Fluor™ 647 Conjugate (650/668)
Concanavalin A (ConA)	Carbohydrates (α-mannopyranosyl and α-glucopyranosyl)	Invitrogen™ Alexa Fluor™ 633 Conjugate (632/647)
Lectin (GS-II) From *Griffonia simplicifolia*	Carbohydrates (α- or β-linked N-acetyl-D-glucosamine)	Invitrogen™ Alexa Fluor™ 647 Conjugate
Lectin (SBA) From Glycine max (soybean)	Carbohydrates (α- and β-N-acetylgalactosamine and galactopyranosyl residues).	Invitrogen™ Alexa Fluor™ 647 Conjugate

Table 3.3 (Continued) Overview of fluorescently tagged molecular probes and their targets used to assess EPS

Maclura pomifera Lectin (MPA) Osage Orange	Carbohydrates (Gal-β3-GalNAc)	TCS Biosciences TRITC Conjugated (522/578)
Pisum sativum Lectin (PSA) Garden Pea	Carbohydrates (α-Mannose, α-Glucose)	TCS Biosciences TRITC Conjugated
Lectin (HPA) From *Helix pomatia* edible snail	Carbohydrates (N-acetylgalactosamine)	Invitrogen™ Alexa Fluor™ 647 Conjugate
Lycopersicon esculentum (Tomato) Lectin (LEL)	Carbohydrates (1,3-N-acetylglucosamine)	Invitrogen™ Texas Red (595/613)
Calcofluor white stain (CFW)	Carbohydrates (Cellulose and chitin)	Sigma-Aldrich (350/432)
Dextran	The stain was added to culture media at concentration 1 µM during the growth and formation of biofilm.	Invitrogen™ Alexa Fluor™ 647; 10,000 MW, Anionic, Fixable

3.2.4 Imaging of biofilms and associated EPS using scanning electron microscopy (SEM)

For SEM sample preparation, biofilms on coupons were initially fixed in 3% glutaraldehyde for a minimum of 1 h. Following fixation, samples were gently washed (×2) for 10 min in PBS to remove residual fixative. Sample dehydration was achieved by 15 min immersion in an ascending ethanol concentration series (50%, 70%, 90%, and 100%). The 100% ethanol step was repeated with a fresh application of ethanol for an additional 15 min to ensure complete dehydration. The coupons were then transferred to a new well plate, biofilms were covered with 100% ethanol and left in a fume cupboard for 18 h to allow evaporation and air drying. An alternative approach was also employed, where samples were allowed to air dry without use of ethanol. In this method, samples were kept in a warm and dry room to facilitate air drying. After drying, the dehydrated samples were mounted on to SEM stubs, sputter-coated with gold, and imaged using a Tescan VEGA SEM system (TESCAN, Brno, Czech Republic).

3.2.5 Infecting tissue models of human vaginal epithelium (HVE) with *Neisseria gonorrhoea*

Tissue models of Human Vaginal Epithelium (SkinEthic™ HVE/S/5) were obtained from EpiSkin (Lyon, France). The tissue model comprised of A431 cells derived from squamous cell carcinoma (Naglik et al. 2008). Tissues from each batch had undergone quality assurance checks by the manufacturer which included assessment for the absence of bacterial and fungal contamination.

Upon tissue receipt, inserts were placed into the wells of well plates filled with fresh maintenance medium and incubated for a minimum of 4 h before use. For *N. gonorrhoea* infection, cultures of the different strains were adjusted to an OD_{600} of 0.05 in maintenance

medium without antibiotics (EpiSkin). Each of the four strains was introduced to the inserts holding the HVE tissue model at a concentration of $1x10^8$ CFU/cm^2 of HVE, and incubated overnight at 37°C in 5% CO_2. Analysis was performed on three tissues for each strain. Post infection, the supernatant was collected, and the tissues were retrieved by approaching the insert from underside and carefully cutting around the outer edge between membrane and plastic ring with a sterile scalpel. As the tissue separated, it was gently supported on a sterile Petri dish to facilitate the remaining excision. Once fully detached, tissues were used for histopathological analysis.

3.2.6 Lactate dehydrogenase (LDH) activity of *Neisseria gonorrhoea* infected HVE

The supernatant of the HVE culture medium for each insert was collected for analysis of cell damage using a CyQUANT™ LDH Cytotoxicity Assay (Invitrogen™ C20300, Fisher Scientific, Leicestershire, United Kingdom) following the manufacturer's instructions. The assay was a colourimetric approach that measured cellular cytotoxicity by detecting and quantifying LDH activity.

3.2.7 Histological preparation of infected human vaginal epithelium (HVE) tissues

Damage to the HVE and invasion of *N. gonorrhoea* was assessed by CLSM. Tissues were retrieved, and a bio-wrap was carefully placed around each tissue sample before placement into cassettes. The samples were fixed in 10% (v/v) neutral buffered formalin for 4 h, followed by a dehydration process involving sequential ethanol treatments: 90% ethanol for 1 h, 95% ethanol for 1 h, and 100% ethanol (×4) for 1 h. This was followed by three 1-h treatments in xylene. Dehydrated tissues were then sent to the histology department in the School of Biosciences (Cardiff University) for sectioning where multiple sections (5 µm and 20 µm thick), were obtained from various depths of each tissue.

Tissue sections were dewaxed in xylene and rehydrated with water. For CLSM preparation, sections were treated with 1 mg/ml lysostaphin and incubated at 37°C for 60 min in a humidified container. Citrate buffer was then applied to the sections and incubated at 55°C for 30 min, with two PBS washes performed after each step. To stain tissues and bacteria, 20 mg/ml of pan-Cytokeratin Antibody (C11) Alexa Fluor® 647 (Santa Cruz Biotechnology, Heidelberg, Germany) was added, followed by a universal bacterial Cy3-labelled peptide nucleic acid (PNA) probe (BacUni1CY3; 300 nM; probe sequence: CTGCCTCCCGTAGGA) targeting bacterial 16S rRNA. The sections were incubated at 55°C for 60 min in a humidified container. Finally, the slides were mounted using 20 µl of VECTASHIELD (Antifade Mounting Medium with DAPI, H-1200-10, Vector Laboratories, Newark, USA).

3.2.8 Image 3D reconstruction and COMSTAT analysis

CLSM images of HVE infections were acquired using a Zeiss LSM880 Airyscan Fast confocal laser scanning microscope equipped with a ×40/1.3 oil immersion objective, and image acquisition was performed using ZEN Microscopy Software (Carl Zeiss Microscopy GmbH, Germany). Z-stacks were collected to span the full depth of the tissue, and COMSTAT analysis was done as described in section 2.2.9.4.

3.2.9 Statistical analysis

Statistical analyses were performed using GraphPad Prism 10.1.0 (GraphPad Software, Boston, Massachusetts USA, www.graphpad.com). Data were assessed for normality using Shapiro-Wilk test. One-way analysis of variance (ANOVA) with Tukey Post-Hoc test was used to compare the different groups.

3.3 Results

3.3.1 Characterisation of EPS in biofilms using molecular probes and CLSM

Table 3.3 summarises the results of the screened fluorochromes tested on biofilms grown under the selected conditions. Representative images of the staining are shown in Figure 3.1. Analysis of CLSM images showed that EPS production in biofilms was variable and dependent on growth conditions. Some of the fluorochrome conjugates used in this study were known to target cells within biofilms. However, the focus of the assessment was to evaluate their ability to detect EPS in biofilms. The results revealed three distinct patterns of staining. Firstly, in some cases, there no detectable labelling, suggesting absence of the targeted EPS component. Secondly, certain stains generated a labelling pattern that was closely associated with the cellular structure of the biofilm and following the contours and arrangement of the bacterial cells. This may indicate presence of the target on cell surface or a thin layer of EPS covering the cells. Thirdly, staining produced distinct and spatially separated signals clearly localised within the EPS and consistent with successful EPS labelling.

Intermittent drying and prolonged incubation of biofilms did not result in increased EPS production (Figure 3.2). In contrast, medium supplementation with 1% sucrose and 1 µM of Alexa fluor 647 conjugated dextran did increase EPS production for all biofilms containing oral bacteria (Figure 3.3). *Streptococcus mutans* biofilms showed the highest production of EPS in supplemented medium as shown in Figure 3.4.

Table 3.3 Summary of extracellular polymeric substances (EPS) detection using different fluorochromes for *in vitro* biofilms

Fluorochrome	Mixed Bacterial	*C. albicans*	Mixed microbial species	Whole saliva
SYTO 9	-	-	-	-
PI	-	-	-	-
TOTO-3	-	-	-	-
CFW	*	-	-	*
SBA	*	*	*	*
SYPRO Ruby	*	*	*	*
Con A	*	-	-	*
PNA	*	*	*	*
GS-II	*	*	*	*
MPA	*	*	*	*
PSA	*	*	*	*
HPA	*	*	*	*
LEL	*	*	*	*
Dextran	+	-	+	+

* the stain was mainly associated with cellular components; - the stain used did not label EPS; + the stain labelled EPS.

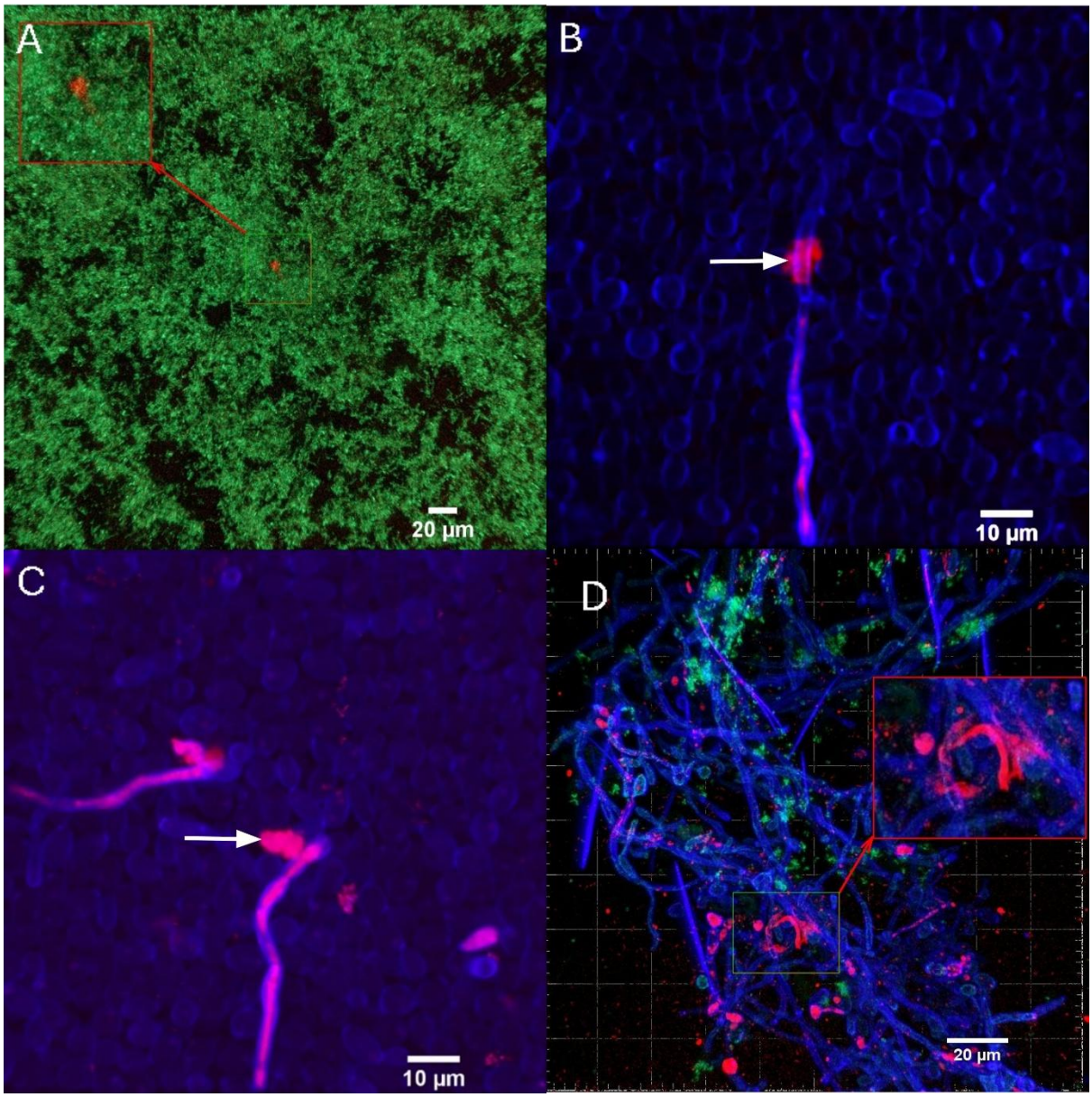

Figure 3.1 CLSM characterisation of EPS in *in vitro* biofilms.

A) Mixed bacterial biofilms stained with *Pisum sativum* (PSA Garden Pea) lectin (Red), which binds to α-mannose and α-glucose; x100 magnification. **B)** *Candida albicans* biofilms stained with *Maclura pomifera* agglutinin (MPA) Osage Orange lectin (Red), seen here associated with hyphal structures, and EPS detection surrounding the cell (arrowed); x400 magnification. **C)** *C. albicans* biofilms stained with PSA Garden Pea lectin (Red), seen here associated with the hyphal structure, and extracellular detection surrounding the cell (arrowed); x400 magnification. **D)** Mixed microbial species biofilm stained with soybean agglutinin (SBA) lectin (Red), which binds to α- and β-N-acetylgalactosamine and galactopyranosyl residues; x200 magnification. *In all images green represents Syto 9, which binds to nucleic acid of bacterial cells. Blue represents calcofluor white, which binds to the cell wall of *Candida albicans*.

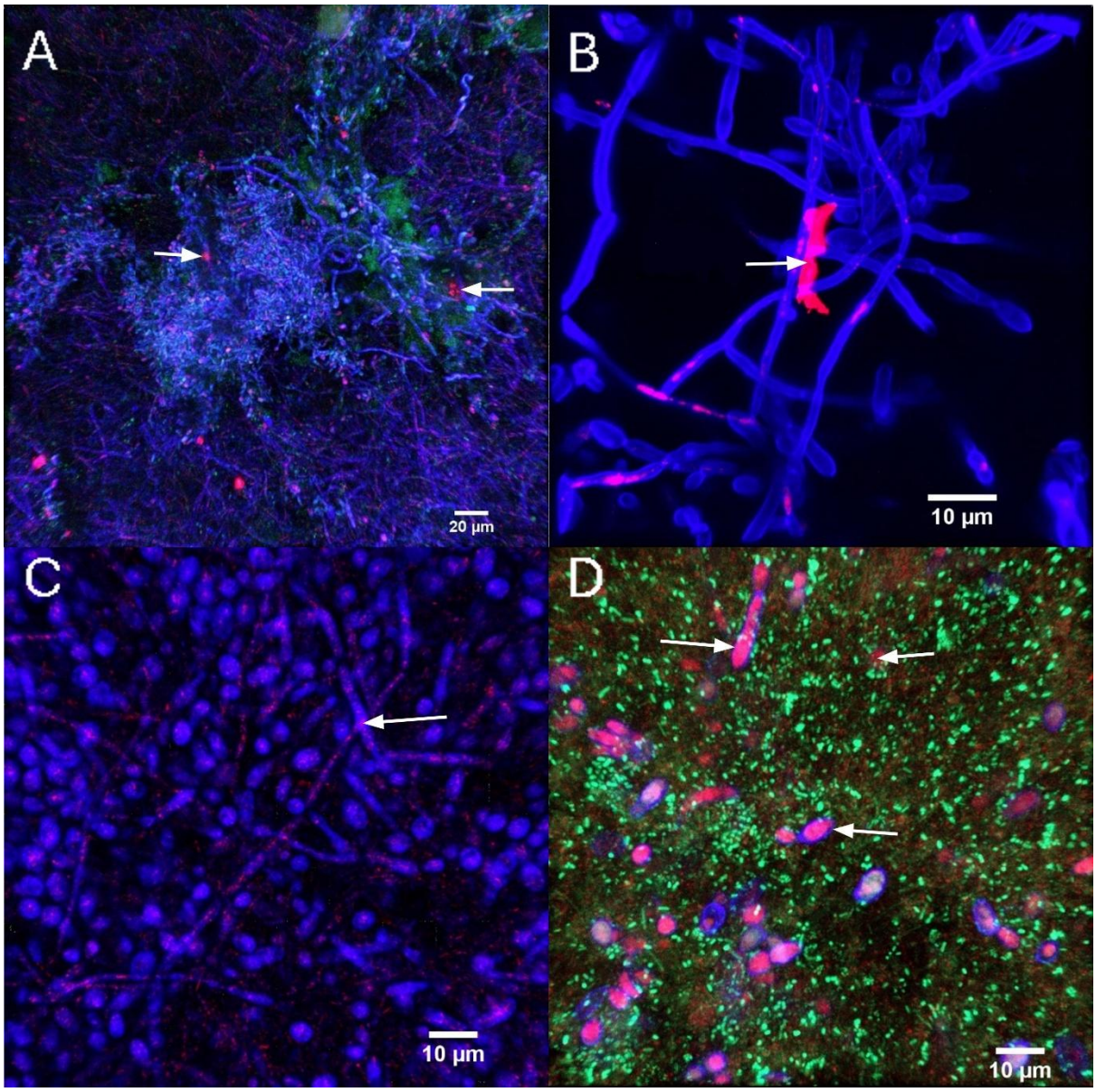

Figure 3.2 CLSM imaging of EPS in *in vitro* biofilms grown under modified conditions.

A) Mixed microbial species biofilm exposed to drying and stained with soybean agglutinin (SBA) lectin (Red; arrowed), seen bound to cellular components mainly yeast cells. x100 magnification. **B)** *Candida albicans* biofilm grown for 7 days stained with *Griffonia simplicifolia* (GS-II) lectin (Red) seen here associated with the hyphal structure, and extracellular detection (arrowed); x500 magnification. **C)** *Candida albicans* biofilm grown for 28 days and stained with GS II lectin (Red) seen here associated with the hyphal structure (arrowed); x400 magnification. **D)** Mixed microbial species biofilm grown for 28 days and stained with *Helix pomatia* agglutinin (HPA; edible snail) lectin, primarily associated with yeast cells (arrowed); x400 magnification.

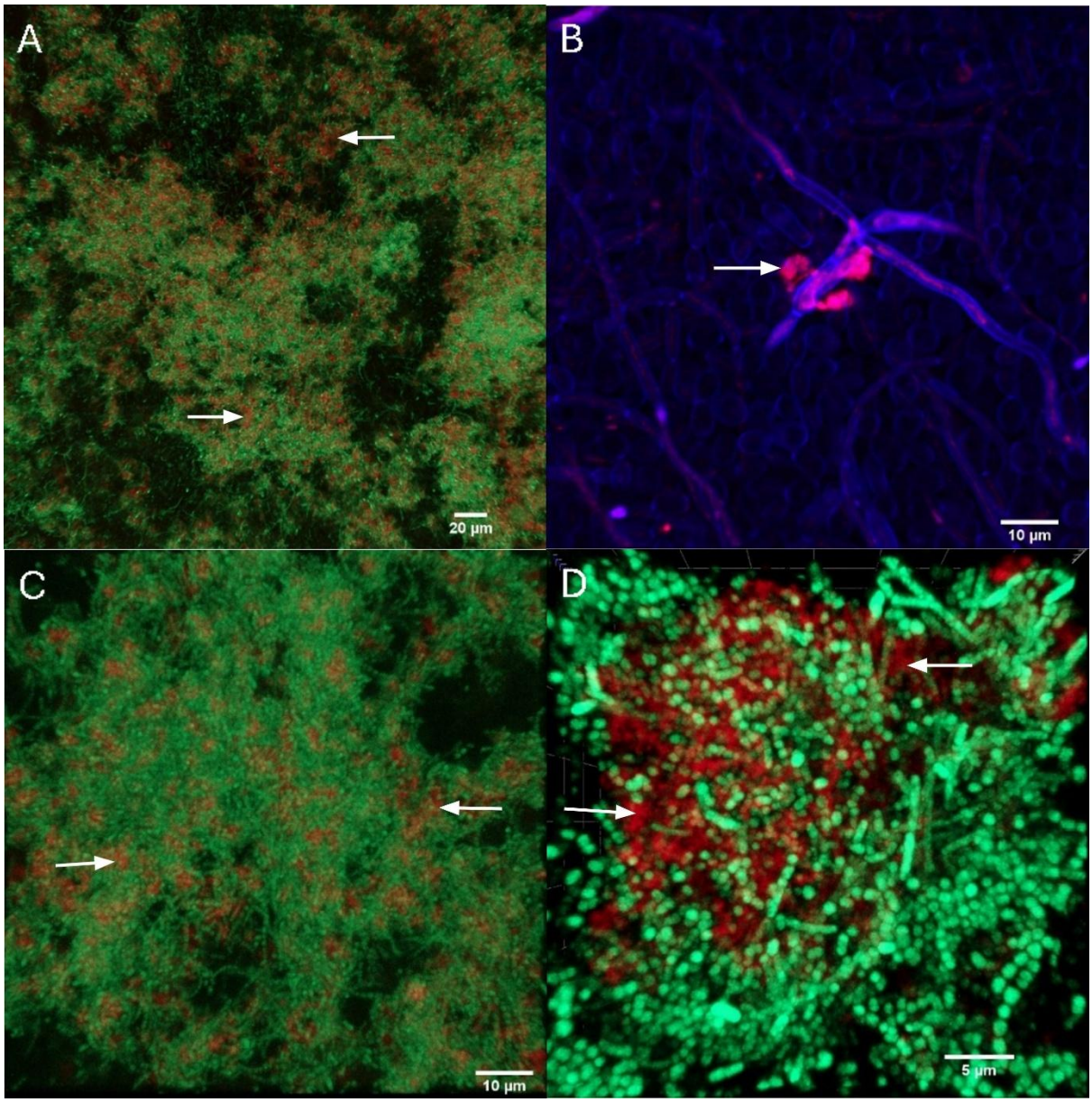

Figure 3.3 CLSM characterisation of EPS in biofilms grown in supplemented medium.

Biofilms supplemented with 1% (w/v) sucrose and 1 µM Alexa fluor 647 conjugated dextran. **A)** Mixed bacterial biofilm x100. **B)** *Candida albicans* biofilm x400. **C)** Mixed microbial species biofilm x400. **D)** Whole saliva biofilm x1000. Green: Syto9, Blue: Calcofluor white, Red: Glucan EPS incorporating Alexa Fluor 647 conjugated dextran (arrowed).

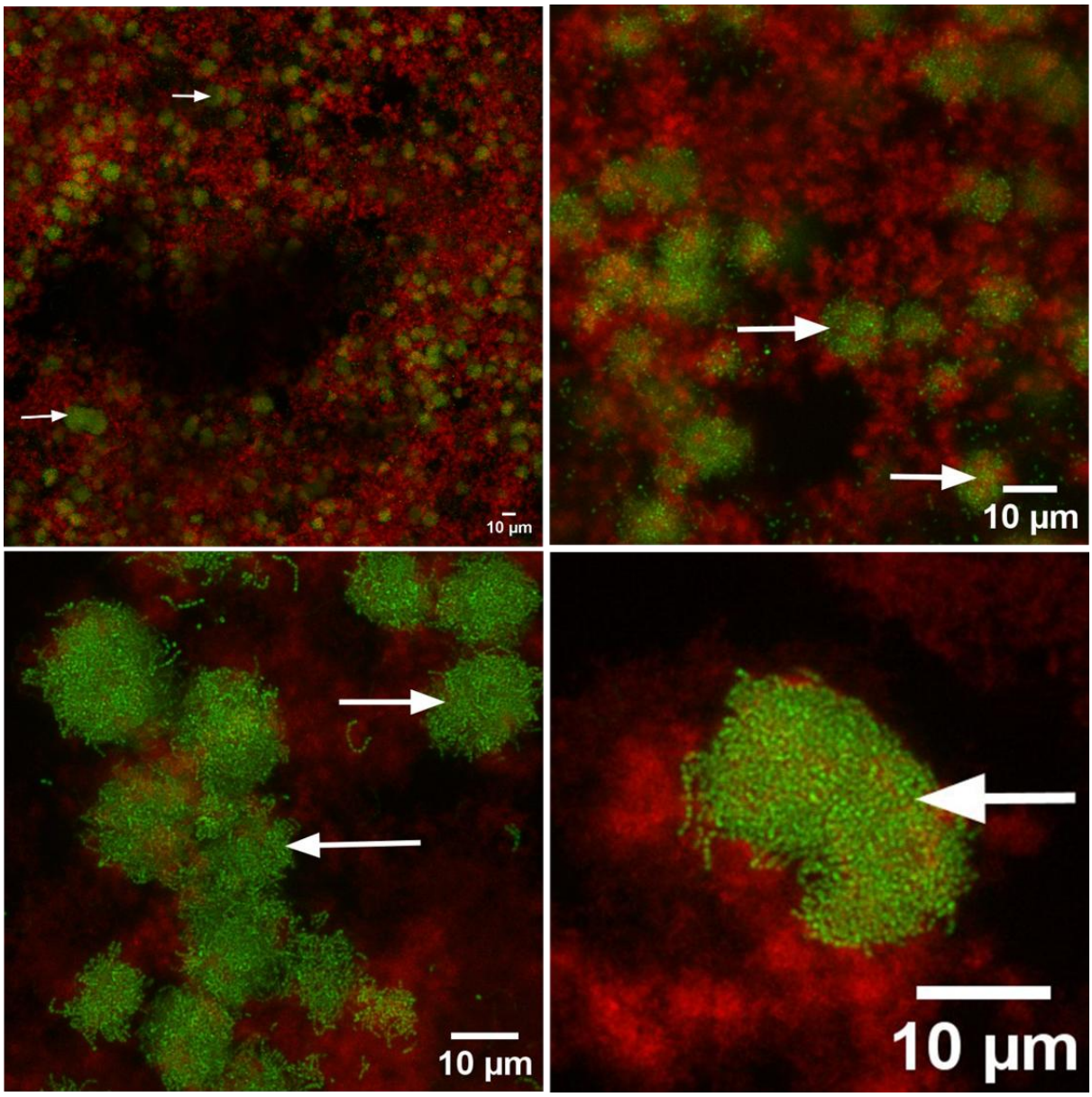

Figure 3.4 CLSM detection of EPS in *Streptococcus mutans* biofilms grown in supplemented medium.

Streptococcus mutans biofilm supplemented with 1% (w/v) sucrose and 1 µM Alexa fluor 647 conjugated dextran under different magnifications. Green (arrowed): Syto9, which binds to nucleic acids. Red: Glucan EPS incorporating Alexa Fluor 647 conjugated dextran.

3.3.2 Imaging of biofilms using SEM

SEM images presented in this section were obtained from biofilms prepared using the ethanol dehydration protocol described in section 3.2.4. Images revealed that *C. albicans* biofilms had a dense and complex structure. However, no evidence of EPS was observed (Figure 3.5 & Figure 3.6). Similarly, mixed bacterial and whole saliva biofilms had no detectable EPS, but displayed biofilm formation on the coupon surfaces, characterised by thinner layers and voids that exposed the underlying polycarbonate surface (Figure 3.7 & Figure 3.8). In contrast, *S. mutans* biofilm (grown in medium supplemented with 1% (w/v) sucrose and 1 µM dextran) showed an abundance of EPS, forming a smooth layer that encapsulated the microcolonies. This EPS layer was evident from the presence of bulges corresponding to the underlying cellular architecture (Figure 3.9 & Figure 3.10).

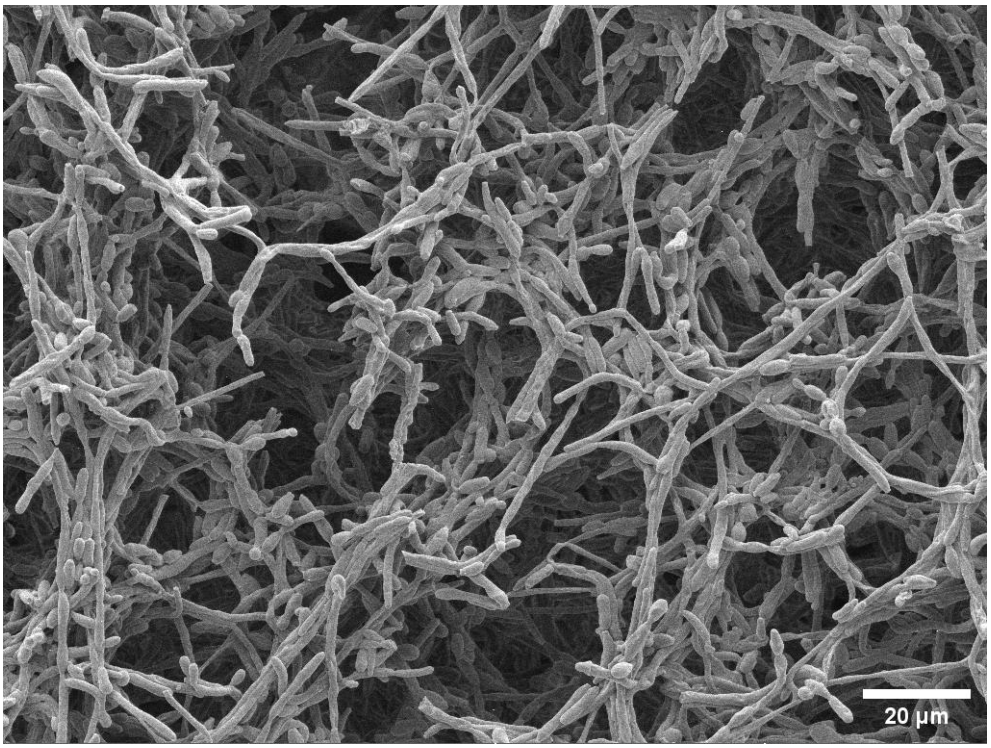

Figure 3.5 Scanning electron micrograph of *Candida albicans* biofilm grown on polycarbonate coupons in the CDC biofilm reactor using Sabouraud dextrose broth (Oxoid) for 72 h (x1510 magnification).

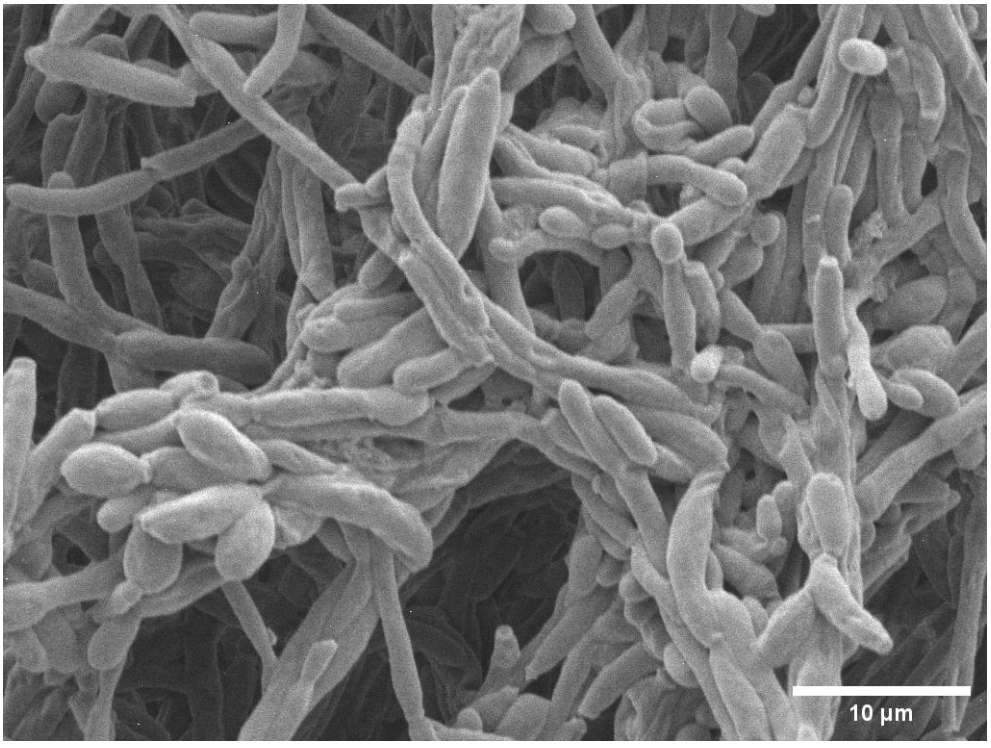

Figure 3.6 Scanning electron micrograph of *Candida albicans* biofilm grown on polycarbonate coupons in the CDC biofilm reactor using Sabouraud dextrose broth (Oxoid) for 72 h (x5000 magnification).

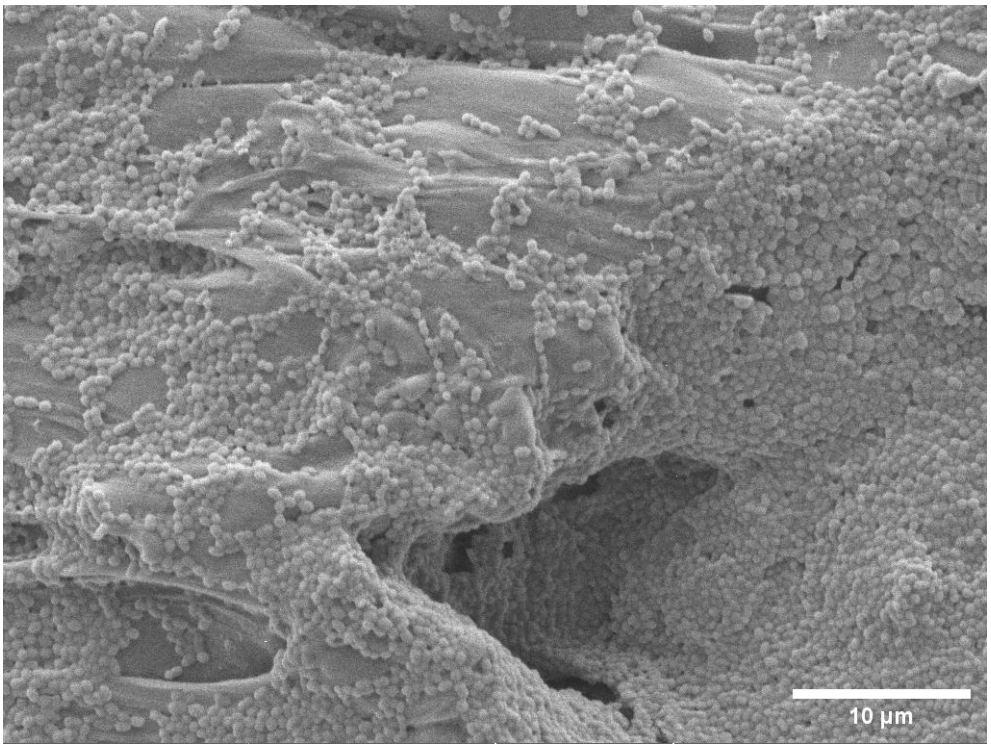

Figure 3.7 Scanning electron micrograph of mixed bacterial biofilm grown on polycarbonate coupons in batch culture using tryptone soy broth (Oxoid) for 72 h (x5000 magnification).

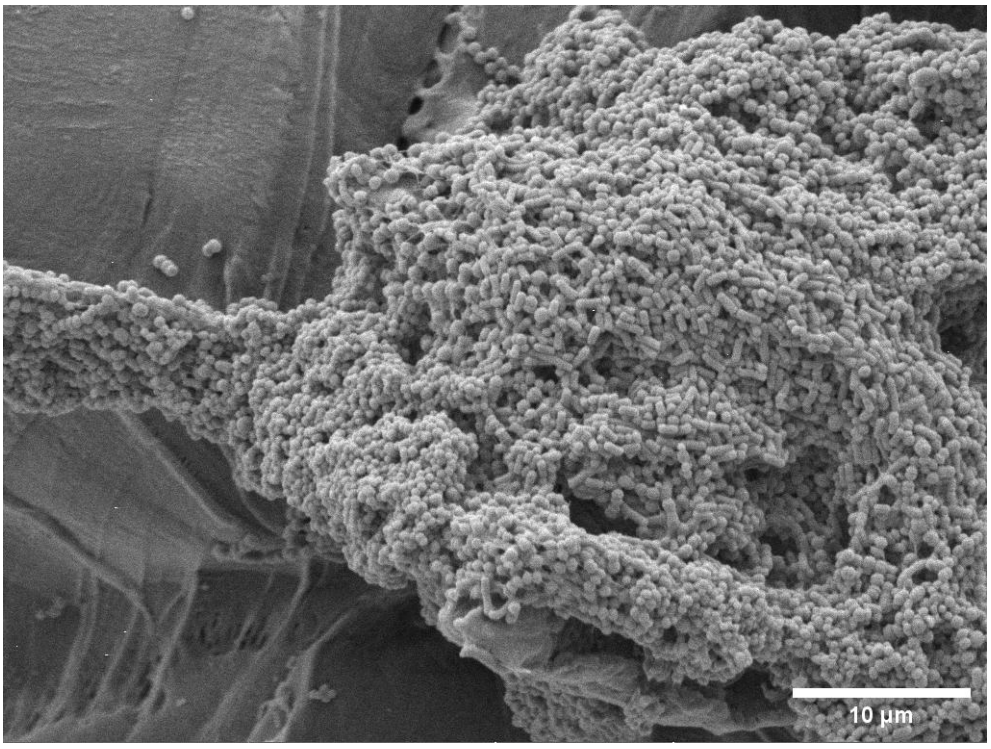

Figure 3.8 Scanning electron micrograph of whole saliva biofilm grown on polycarbonate coupons in the CDC biofilm reactor using tryptone soy broth (Oxoid) for 72 h (x5000 magnification).

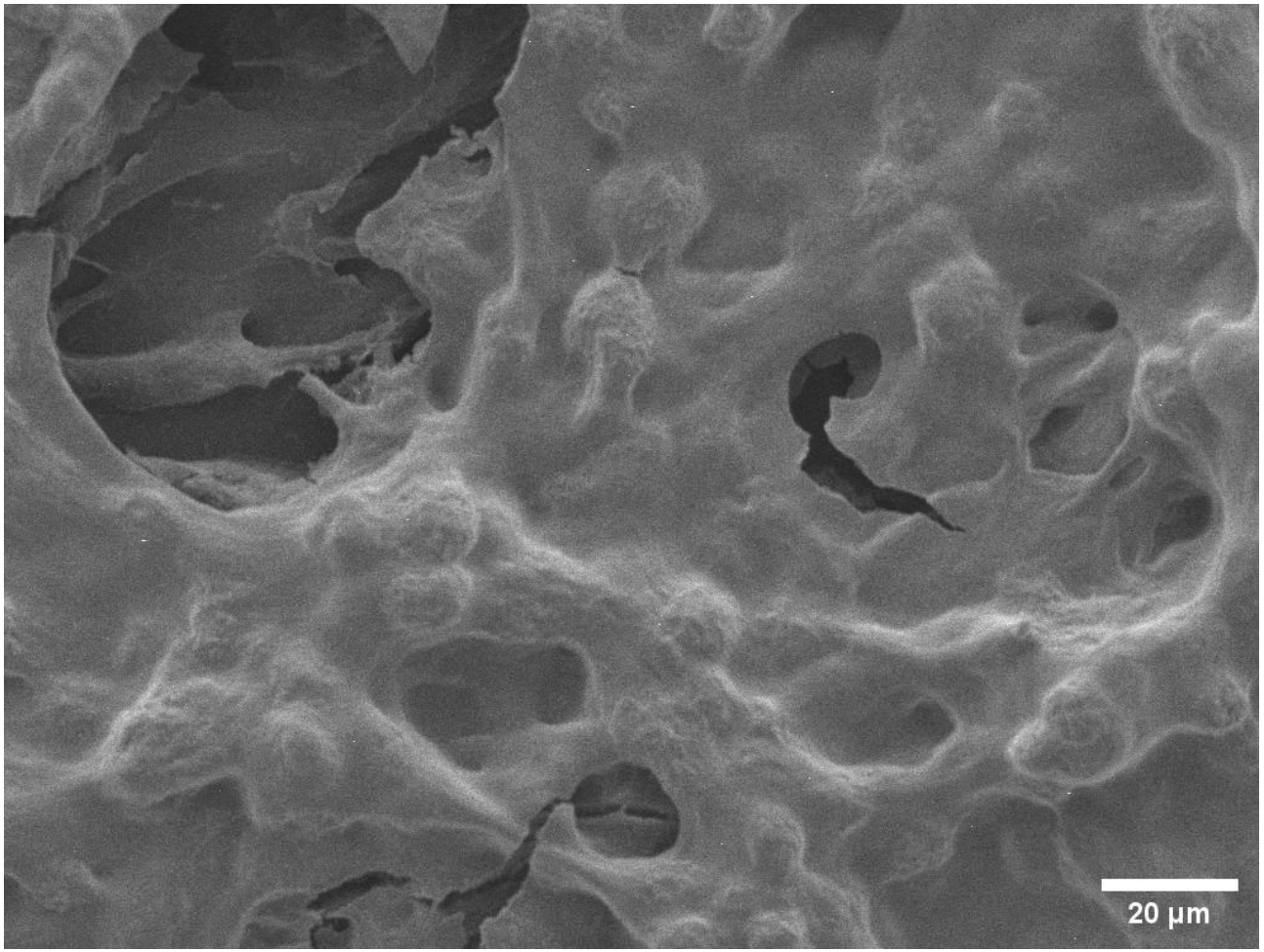

Figure 3.9 Scanning electron micrograph of *Streptococcus mutans* biofilm grown on polycarbonate coupons in batch culture using tryptone soy broth (Oxoid) (supplemented with 1% (w/v) sucrose and 1 µM dextran) for 72 h (x1500 magnification).

EPS can be observed covering the bacterial cells, attached to the surface and forming a network linking the distinct microcolonies.

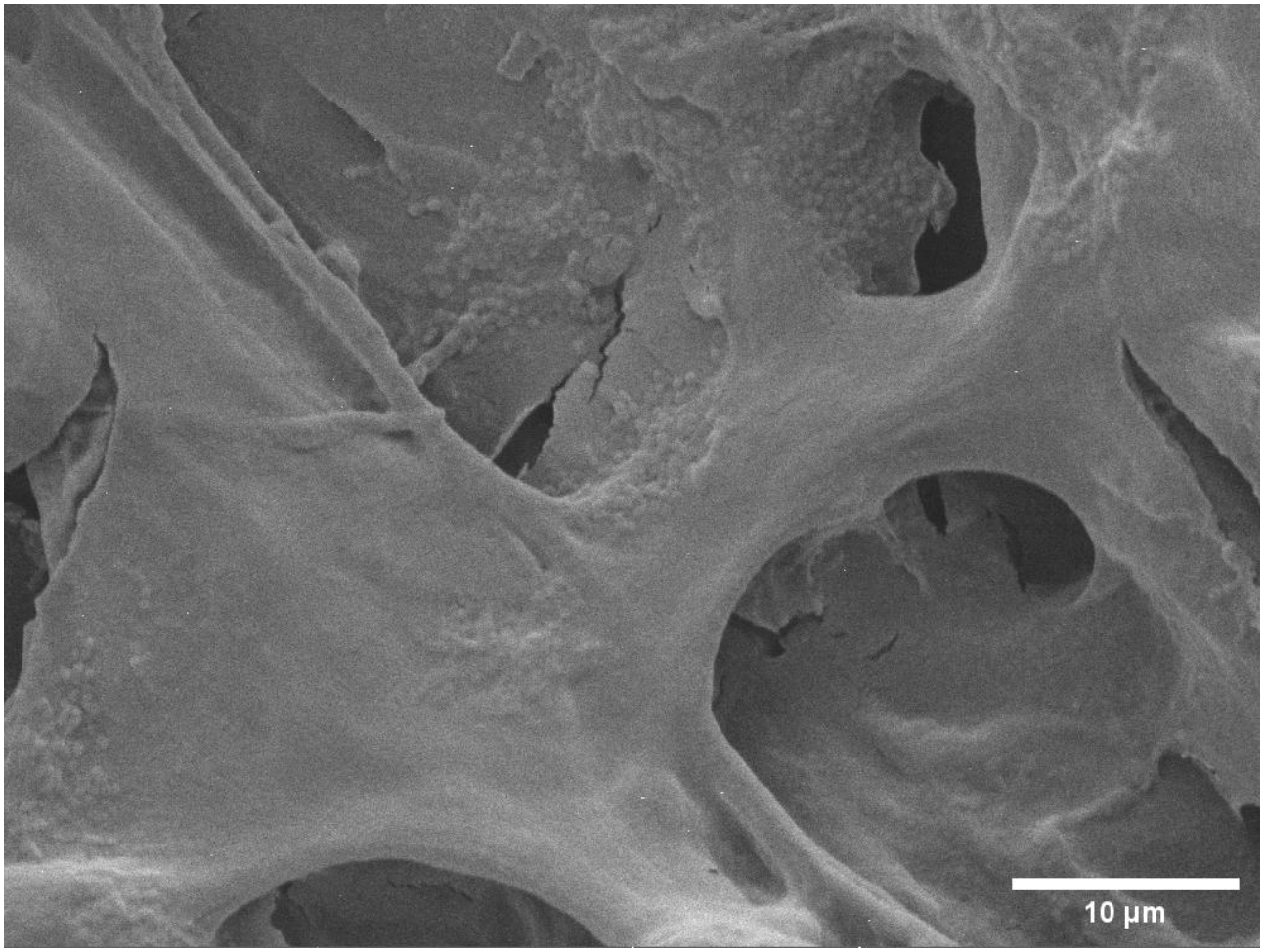

Figure 3.10 Scanning electron micrograph of *Streptococcus mutans* biofilm grown on polycarbonate coupons in batch culture using tryptone soy broth (Oxoid) (supplemented with 1% (w/v) sucrose and 1 µM dextran) for 72 h (5000 X magnification).

EPS can be observed covering the bacterial cells, attached to the surface and forming a network linking the distinct microcolonies

3.3.3 *In vitro* biofilm development by *Neisseria gonorrhoeae* on polycarbonate coupons and HVE infection

For *N. gonorrhoea, in vitro* biofilm formation on coupons proved to be limited in quantity, and resulted in no detection of eDNA. Figure 3.11 shows the biomass measurement of *N. gonorrhoea* variants grown in the CDC biofilm reactor, indicating low levels of biofilm formation on coupons with no significant difference between strain variants. Nevertheless, biofilm formation on tissues (Figure 3.12) showed significant ($p = 005$) reduction in biomass of the Lig E knockout strain ($p < 001$) and *opaB-ngo-Lig E* strain compared to the wild type. EPS staining did not however reveal distinct eDNA for any of the biofilms and variants tested (Figure 3.13). Full dataset of biomass values used to assess biofilm formation on polycarbonate coupons and HVE tissues are provided in Appendix II.

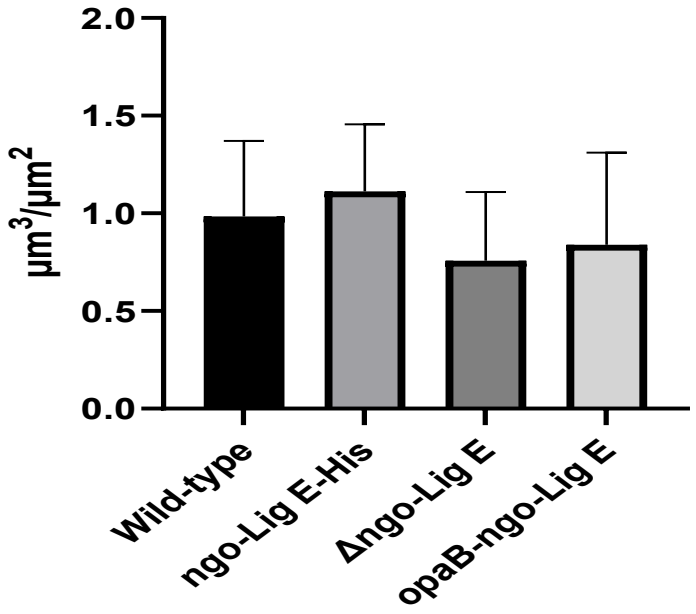

Figure 3.11 COMSTAT biomass measurement of biofilm formed by *Neisseria gonorrhoeae* variants on polycarbonate coupons in CDC biofim reactor.

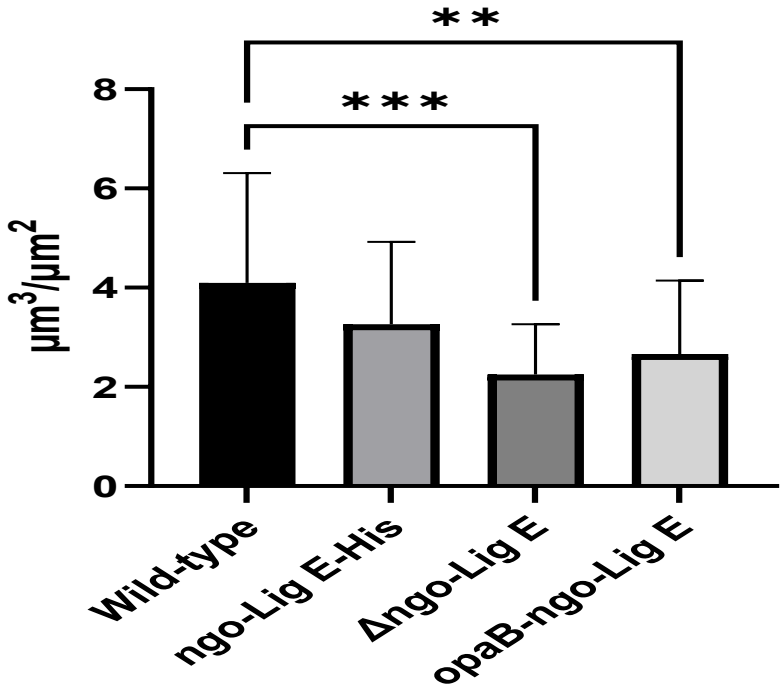

Figure 3.12 COMSTAT biomass measurement of biofilm formed by *Neisseria gonorrhoeae* variants on reconstructed human vaginal tissue.

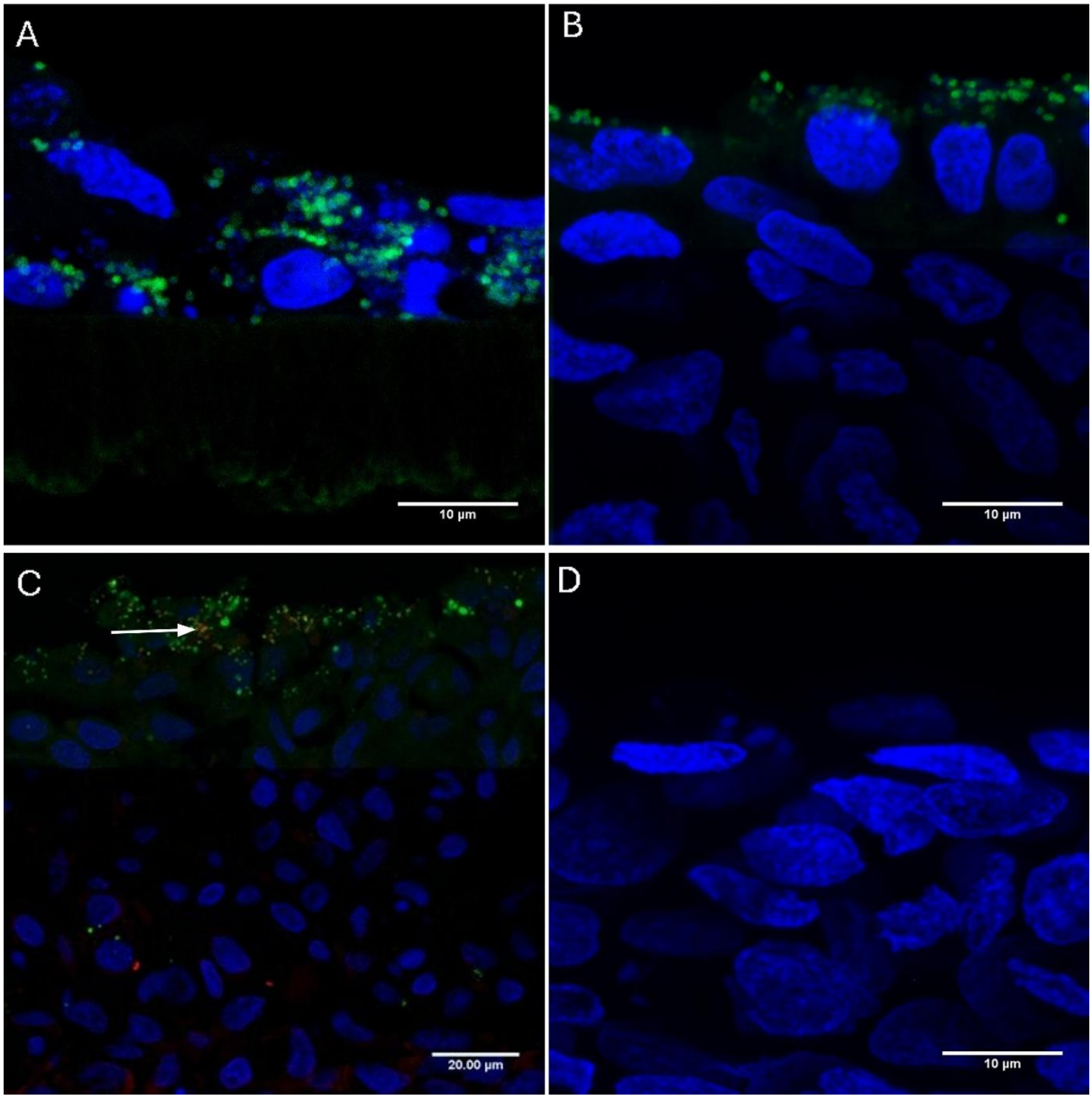

Figure 3.13 CLSM characterisation of EPS in *Neisseria gonorrhoeae* biofilms in reconstructed human vaginal epithelium.

A) Wild-type strain (x600) showing microbial cell invasion to deep layers of the epithelium. **B)** Knockout strain (*Δngo-Lig E*) showing biofilm formation at top layer of epithelium (x600). **C)** Knockout strain (*Δngo-Lig E*) showing biofilm formation at top layer of epithelium (x200). **D)** uninfected reconstructed human vaginal epithelium. * Green: GFP *Neisseria gonorrhoeae*, Blue: DAPI staining epithelial cells, Red: TOTO-3 to detect eDNA (arrowed).

3.3.4 Tissue damage caused by *Neisseria gonorrhoea* as assessed by LDH activity measurement

The assessment of tissue damage, measured by lactate dehydrogenase (LDH) activity, revealed that the damage induced by the knockout strain was significantly reduced ($p < 0.05$) compared to other strains. Although the *opaB-ngo-Lig E* strain caused more damage than the knockout strain, the extent of damage was significantly less than that observed for the wild-type strain ($p < 0.001$) and the *ngo-Lig E-His* strain ($p = 0.002$) (Figure 3.14).

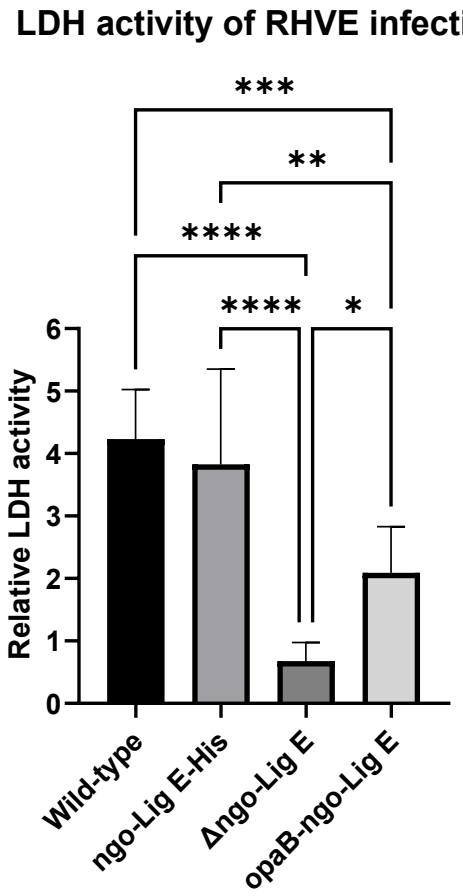

Figure 3.14 LDH measuring the induced damage on reconstructed human vaginal tissue caused by *Neisseria gonorrhoeae* strain variants.

3.4 Discussion

The ability to characterise EPS is key to understanding its role in AMR and could be important for the development of novel therapeutics against biofilms and *in vitro* testing platforms. By determining the composition and functions of EPS, researchers can identify potential targets for disrupting biofilm structure and overcoming the protective barrier provided by EPS against antimicrobial agents. Furthermore, a deeper understanding of EPS could inform strategies to mitigate biofilm-associated infections, guiding the development of effective preventive measures and treatments tailored to specific biofilm environments. Such insights are particularly valuable for addressing persistent biofilm-related challenges in clinical and industrial settings (Joshi et al. 2021).

Microscopy plays an important role in biofilm analyses. In this regard, CLSM is a useful tool for EPS detection due to its ability to image within thick biological samples, as evident in biofilms. Thin optical sections can then be reconstructed into 3D images of the biofilm. This ability, combined with the elimination of 'out-of-focus' light and the use of fluorochromes that target specific components, makes CLSM an effective tool for studying EPS. It has previously provided potentially valuable information on the spatial distribution of components within biofilms (Reichhardt and Parsek 2019). Various commercially available probes have been used with CLSM to detect and characterise EPS in biofilms, including fluorochrome tagged probes that target the major components of EPS polysaccharides, proteins, and eDNA (Moshynets et al. 2022; Neu and Kuhlicke 2022).

In this current research, a range of lectins were used to target potential polysaccharide components within biofilm EPS. Proteins were targeted using FilmTracer™ SYPRO™ Ruby Biofilm Matrix Stain (Invitrogen™ F10318, Fisher Scientific, Leicestershire, United Kingdom), a

stain with high affinity for most protein classes making it useful for protein content screening of biofilm EPS. For eDNA detection, most stains were cell-impermeant and could not penetrate cells with intact cell walls. These stains were able to bind to dead cells, cells with impaired membranes, and eDNA. Initial evaluation of eDNA was performed using propidium iodide, which predominantly stained dead cells. To achieve a potentially more sensitive assessment, the cyanine dimer nucleic acid stain TOTO™-3 Iodide was used, as it is reported to have higher sensitivity for eDNA (Okshevsky and Meyer 2014).

Results showed that in all biofilms grown under initial culture conditions, fluorochrome signal was primarily seen in close proximity to the cells and in low quantities (Figure 3.1). These findings suggested that EPS production under the tested conditions was lower than expected. This outcome could be attributed to several factors, however intermittent drying was introduced in an attempt to induce environmental stress, and longer incubation periods were also tested to determine if they would promote increased EPS production. The hypothesis was that incorporating stress into the growth conditions would trigger EPS generation. However, the results indicated that the quantity of EPS remained similar to that observed previously, with fluorochrome signals targeting EPS remaining scarcely detectable and often localised near the cells within the biofilms.

These findings suggest that the success of fluorescent probes screening depends primarily on binding affinity and the presence and quantity of the target. This is supported by findings by Neu and Kuhlicke (2022), where the authors reported some lectins failed to produce detectable signals despite the likely presence of their targets. This outcome can be attributed to factors such as weak binding affinity, staining technique, or the inaccessibility of glycoconjugates within the matrix. In other cases, lectins failed to produce any detectable

staining in the biofilm samples. This absence of signal suggests that the specific glycoconjugates recognised by those lectins were either not produced by the microorganisms under the tested conditions or were present at concentrations below the detection threshold of the lectin.

For oral biofilms, a previous study investigated the carbohydrate composition of *in situ* oral biofilms and the impact of sucrose exposure on matrix structure (Dige et al. 2022). A selection of lectins was used to screen the EPS of biofilms grown on glass slabs embedded in custom-designed splints, which human participants wore for 48 h. One side of each splint was treated with a 4% sucrose solution (eight treatments per day), while the other side was exposed to water as a control. Ten fluorescently labelled lectins were tested using CLSM and digital image analysis to quantify the biovolumes of biofilms. Some lectins exhibited weak or intermediate fluorescence signals and were less effective in staining biofilm matrix volumes. However, three lectins, *Morniga agglutinin* G, *Aleuria aurantia* lectin, and *Allium sativum* agglutinin were selected for further analysis due to strong fluorescent signals and the ability to bind to targets of interest, specifically galactose, fucose, and mannose. The study reported successful staining of biofilm samples with some lectins, although sucrose exposure led to a non-significant increase in the biovolumes of mannose and fucose, as indicated by the fluorescence of their respective lectins. Results also revealed notable variations between subjects and replicate samples, highlighting the complexity and variability of biofilm matrix composition (Dige et al. 2022). These results indicate that, in addition to the inherent complexity of biofilms, several other factors critically influence the success of fluorescent probes for EPS staining. Biologically, the composition and spatial distribution of EPS vary not only between strains, but also as a result of environmental conditions, biofilm maturation and heterogeneity of biofilm structure. Therefore, specific EPS components may be entirely absent or confined to certain biofilm

regions, limiting probe accessibility (Turonova et al. 2016). Other factors include the type of fluorescent label, lectin specificity, probe concentration, incubation time, and the sequence of probe application can significantly alter staining outcomes (Neu et al. 2001).

To address the limited EPS production in previous test conditions, additional approaches were used in an effort to generate sufficient quantities of EPS for subsequent quantification and analysis of disruption techniques. One approach involved supplementation of the growth medium to induce and detect EPS under CLSM. Certain *Streptococcus* species, particularly *S. mutans*, are known to metabolise a variety of carbohydrates (Priya et al. 2021). *Streptococcus mutans* possesses multiple pathways for sucrose catabolism, leading to acid production, and for this purpose expresses at least three glycosyltransferases (Gtfs) capable of synthesising both water-soluble and water-insoluble glucans. Specifically, GtfB primarily produces water-insoluble glucans, GtfD synthesises water-soluble glucans, and GtfC produces both (Bowen and Koo 2011). The synergistic activity of Gtfs has been well-documented. For instance, GtfD-produced glucan enhances the activity of GtfB in synthesising water-insoluble glucans (Vacca-Smith and Bowen 1998). Dextran, acting as a primer for glucosyltransferases, is subsequently incorporated into the insoluble glucan synthesised by GtfB (Lemos et al. 2019). Expanding on this, Klein et al. (2009) demonstrated that fluorescently labelled dextran, when added to sucrose-supplemented medium, was incorporated into the glucan matrix and fluoresced under CLSM, enabling glucan detection (Klein et al. 2009).

In the present research, medium supplementation with sucrose resulted in comparatively high amounts of EPS, particularly for *S. mutans* biofilms (Figure 3.4), and was also used with other biofilms. Given that biofilms are typically polymicrobial, *S. mutans* was co-inoculated with other microorganisms, as well as in whole saliva inoculum. It has been suggested that all

streptococci produce Gtfs (Kreth et al. 2008), which can bind to other microbial cells and transfer the capacity to produce glucans (Falsetta et al. 2014). Although EPS production was not as prominent as in *S. mutans* only biofilms, CLSM images (Figure 3.3) revealed the presence of EPS in all tested biofilms except for *C. albicans* biofilms. EPS accumulation at certain sites covered some of the constituent cells within colonies and may contribute to their survival during biofilm targeting treatments.

Glucans play a pivotal role in the structural stability and integrity of oral biofilms, providing mechanical stability and the binding of bacterial cells to form a cohesive extracellular matrix that supports 3D architecture. Glucans enhance biofilm adhesion to surfaces and promote bacterial aggregation, facilitating microcolony formation and vertical growth (Xiao and Koo 2010).

A study by Li et al. (2023) used subgingival plaque samples collected from human volunteers to demonstrate the critical role of glucans in biofilm formation. *In vitro* oral biofilms were grown on collagen-coated hydroxyapatite discs in a medium supplemented with labelled dextran under anaerobic conditions. An abundant presence of EPS was detected and attributed to incorporation of dextran into glucans. The study also investigated biofilm characteristics at different maturation stages, focusing on EPS matrix volume, surface roughness, and bacterial adhesion properties. Mature biofilms (three weeks old) exhibited significantly higher EPS volumes compared to younger biofilms (one week old), underscoring the importance of EPS in biofilm development. Additionally, atomic force microscopy (AFM) revealed increased adhesion forces at cell-cell interfaces in mature biofilms, likely due to EPS accumulation (Li et al. 2023). The results of this research, alongside findings from the literature, emphasise that glucans are a major component of oral biofilms, playing a critical

role in their structural and functional dynamics. Ensuring their retention and survival in the diverse environments within the oral cavity.

In the present research SEM did not show distinct EPS features for *in vitro* biofilms of *C. albicans*, mixed microbial species, mixed bacterial, and whole saliva generated biofilms (Figure 3.5-Figure 3.8). The lack of EPS seen by SEM can be attributed to two factors. Firstly, EPS production could be limited, resulting in low levels. Secondly, the preparation process of samples for SEM could compromise the structure of biofilm, leading to partial or complete loss of EPS (Dassanayake et al. 2020). However, such damage was not observed in *S. mutans* biofilms, which indicates that the preparation process including fixation and dehydration was not a major influence on the lack of EPS. Nevertheless, SEM provided detailed imaging of the structural organisation of biofilms. For instance, *C. albicans* biofilms grown in the CDC biofilm reactor had a complex 3D architecture comprising of densely packed hyphal and yeast forms. The observed budding of yeast cells was notable, and a feature previously reported as being a critical component of biofilm dispersion and colonisation dynamics (Uppuluri et al. 2010). This highlights the role of structural transitions in biofilm life cycles and their potential impact on dispersal and subsequent biofilm formation. Similarly, biofilms from mixed microbial species, mixed bacterial, and whole saliva had morphological features characteristic of the species and structural organisation; however, EPS presence was not evident. In contrast, *S. mutans* biofilms grown in sucrose-supplemented medium exhibited an abundance of EPS that extensively covered the biofilm structure (Figure 3.9 & Figure 3.10). These findings were consistent with previous reports in the literature (Koo et al. 2010; Liu et al. 2013; Cai et al. 2016; Hwang et al. 2016; Zhang et al. 2022b).

A study by Weber et al. (2014) assessed SEM techniques to evaluate *S. mutans* biofilms grown in a medium supplemented with 1% sucrose. Three types of SEM techniques were compared: conventional SEM, SEM with ruthenium red, and variable pressure SEM. Conventional SEM, which involved dehydration and sputter-coating, was sufficient for visualising the biofilm structure and EPS, but resulted in some loss of EPS. SEM with ruthenium red, a variation that uses ruthenium red to stabilise polysaccharides in the EPS during dehydration, showed no improvement in preserving EPS in *S. mutans* biofilms. In contrast, variable pressure SEM, which operates under lower vacuum and higher humidity conditions, eliminated the need for dehydration and provided superior preservation of the EPS (Weber et al. 2014). A separate study investigated the role of the *vicK* gene in *S. mutans*, focusing on its impact on biofilm formation, EPS production, and cariogenicity. The study demonstrated that deletion of *vicK* resulted in thinner, sparser biofilms with altered EPS production and composition. Using a combination of techniques, SEM in particular revealed that biofilms formed by the wild-type strain displayed dense EPS encasing the cells and filling the spaces between microcolonies. In contrast, the *vicK* mutant biofilms exhibited a scattered architecture with visibly reduced EPS (Deng et al. 2021). Together, the findings of Weber et al. (2014) and Deng et al. (2021) highlighted use of SEM as a suitable tool for biofilm research, particularly in visualising EPS and biofilm structure. Notably, these findings align with the results of this research, where *S. mutans* biofilms grown in sucrose supplemented medium produced visually apparent large volumes of EPS. The EPS formed dense, continuous layers that enveloped the microcolonies, interlinked adjacent aggregates, and extended into the interstitial spaces, creating a cohesive and protective biofilm matrix.

For *N. gonorrhoeae* biofilms, different variants were used to investigate the role of Lig E in eDNA production, given its prevalence in bacteria known to form biofilms rich in eDNA. Notably, previous

studies evaluated the involvement of Lig E in biofilm formation in *N. gonorrhoeae* and concluded that the deletion of Lig E significantly reduced biofilm formation without affecting the viability of planktonic cells compared to the wild type (Pan et al. 2024).

The limited biofilm formation by *N. gonorrhoeae* on polycarbonate coupons posed challenges in tracing eDNA within the *in vitro* biofilms. Although dimeric cyanine nucleic acid stains have been shown to be effective in detecting eDNA within the biofilm matrix (Seper et al. 2011), the results indicated that eDNA staining was typically reported in biofilms with a substantial quantity of eDNA. Similarly, attempts to detect EPS in the HVE using TOTO™-3 on prepared slides did not provide distinct evidence of eDNA (Figure 3.13). This suggests that, if present, the eDNA quantities were below the threshold required for detection by fluorescence microscopy. One challenge in eDNA tracing is background fluorescence. While various factors may contribute to this issue, a key variable in this part of the study compared to earlier sections was the fixation step, which could induce background fluorescence (Baschong et al. 2001). In contrast, the assessment of biofilm formation revealed a significant reduction in biomass values for the knockout strain (*Δngo-Lig E)* and overexpresser *opaB-ngo-Lig E* strains compared to the WT. Additionally, LDH activity measurements of supernatants from infected tissues showed a decrease for infections by the Lig E knockout and *opaB-ngo-Lig E* strains (Figure 3.14), suggesting reduced pathogenicity. These findings suggest that Lig E plays an important role in biofilm pathogenicity.

In conclusion, fluorescently labelled molecular probes and CLSM allowed for qualitative visualisation and quantitative assessment of EPS in tested biofilms. Variation in EPS abundance and distribution was observed under different growth conditions, indicating that medium composition can influence matrix development. Supplementation with 1% sucrose was associated with increased EPS presence in *Streptococcus mutans* biofilms, which supported its selection as a suitable model for subsequent chapters focused on EPS disruption

and antimicrobial susceptibility. Findings from *N. gonorrhoeae* biofilms highlighted the role of Lig E in biofilm formation and pathogenicity.

Chapter 4

Detection of extracellular polymeric substances in biofilms and assessment of glucan disruption by chemical analyses and Raman microscopy

4.1 Introduction

Conventional treatment of biofilm infections has largely focused on targeting the microbial cells embedded within the biofilm using traditional antimicrobials (Mirghani et al. 2022). The effectiveness of administered antimicrobials to treat infections is often determined based on laboratory tests against planktonic cultures (Coenye 2023). The presence of a biofilm as the source of an infection has historically not been considered (Martins et al. 2019). However, the effectiveness of antimicrobials can be reduced against microbial cells in a biofilm, and this is, in part, associated with protective properties afforded by extracellular polymeric substances (EPS) (Abebe 2020).

EPS can act as a physical and chemical barrier to the movement of antimicrobials and can also neutralise their activity before reaching target cells (Pinto et al. 2020; Abdelhamid and Yousef 2023). The protective features of biofilms are evident when the inability to effectively treat an infection leads to recurrent and chronic episodes (Mendhe et al. 2023). Coupling EPS disruption with antimicrobial therapy could, theoretically, increase delivery of the agent to the target microorganisms leading to the inhibition of both exposed and dispersing cells (Dhiman et al. 2024).

Studies have explored the benefits of combining EPS targeting enzymes with antimicrobials to effectively combat biofilm associated infections. For example, *in vitro* research has investigated the effects of trypsin, β-glucosidase, and DNase on dual species biofilms of *Staphylococcus aureus* and *Pseudomonas aeruginosa* formed in a 'wound like' medium (Fanaei Pirlar et al. 2020). Results showed that enzymatic treatment significantly disrupted the biofilm matrix when targeting proteins, eDNA, and polysaccharides. Notably, the combination of trypsin and DNase at concentration below their individual effective levels

achieved complete biofilm disruption, indicating a synergistic effect between the two enzymes. Furthermore, enzymatic treatment lowered the minimum biofilm eradication concentrations (MBECs) of antibiotics including meropenem and amikacin, by up to 5-fold against biofilm embedded bacteria. This combined approach highlights the benefit of targeting EPS components to improve therapeutic outcome of antimicrobials in biofilms relevant to wound infections (Fanaei Pirlar et al. 2020).

In the case of oral biofilms, research has investigated the role of EPS in contributing to biofilm architecture and pathogenicity of mixed species biofilms containing *Streptococcus mutans*, *Actinomyces naeslundii*, and *Streptococcus oralis* (Xiao et al. 2012). This study found that the EPS matrix facilitated the generation of localised acidic pockets (pH < 5.5), which promoted enamel demineralisation. To assess the structural role of insoluble glucans in the EPS matrix, mutanase, an enzyme targeting α-(1-3)-linkages of glucans was applied to biofilms. Quantitative analysis confirmed that EPS disruption with mutanase led to a significant reduction in both EPS and cellular biomass (Xiao et al. 2012). While both mutanase and dextranase hydrolyse glycosidic bonds of glucan, they differ in the specific glucan linkage they target, dextranase targets α-(1-6)-linkages and mutanase targets α-(1-3)-linkages (Cortez et al. 2023).

Based on the findings presented in **Chapter 3**, *Streptococcus mutans* was selected as the biofilm model for this chapter. Among the species and growth conditions assessed previously, *S. mutans* produced abundance of EPS and exhibited extensive and well-defined matrix architecture, making it the most appropriate system for investigating enzymatic EPS disruption. The growth conditions established in **Chapter 2** were retained to enable direct comparison of EPS composition between biofilm and planktonic populations.

Dextranase was selected as a targeted proof of concept enzyme to investigate the susceptibility of the dominant glucan component of the *S. mutans* EPS matrix to enzymatic disruption. The EPS produced under the sucrose supplemented conditions used in this study is rich in α-(1→6)-linked glucans (dextran), which play a key role in biofilm cohesion and structural stability (Cifuente et al. 2024). Dextranase concentration and incubation time used in this chapter were selected based on published studies demonstrating effective disruption of pre-formed *S. mutans* biofilms under comparable conditions (Yano et al. 2010). The selection of 1 h dextranase incubation time falls within the range commonly reported in literature and allows the evaluation of short-term exposure, which is more relevant to clinical application (Del Rey et al. 2024).

To effectively target the EPS of biofilms, knowledge of its composition is key, and the complexity and heterogeneity of EPS necessitates use of robust analytical methods to achieve this. Various chemical techniques have been used to advance our understanding of EPS chemistries, molecular structure and functional properties (Lu et al. 2024). Researchers have used colorimetric assays, that rely on chemical reactions to produce a measurable colour change proportional to the concentration of a specific target. Phenol sulphuric acid assays have been used to determine polysaccharide levels in EPS (Wickramasinghe et al. 2020). Similarly, protein quantification assays have been applied to the study of biofilms involved in marine biofouling (Richards et al. 2020), wastewater biology (Felz et al. 2019), and in endodontic infection (Chen et al. 2016).

Confocal laser scanning microscopy (CLSM), coupled with specific fluorescent probes, has been a popular approach for EPS analysis due to its non-destructive features and ability to be used *in situ* (Achinas et al. 2020). Such approaches have enabled both qualitative and

quantitative assessments of biofilm EPS structure and composition. Quantitative assessments using CLSM and analysis software allow researchers to evaluate enzymatic disruption by measuring specific EPS components before and after disruptive treatment, permitting insight into susceptibility of targets to interventions (Lu et al. 2024). For example, the effect of combining enzymatic disruption of EPS with antibiotics on the viability of *P. aeruginosa* and *S. aureus* in 'wound-like' *in vitro* biofilms has been assessed (Rubio-Canalejas et al. 2022). Various enzymes, including DNase, both in solution and immobilised on silver nanoparticles, have been evaluated for EPS degradation and enhancing antibiotic penetration. CLSM was used to image and quantify subsequent EPS disruption. Using TOTO-1 staining, soluble and immobilised DNase treatments of dual species wound-like biofilms were shown to significantly reduce eDNA quantity by 55% and 74%, respectively, resulting in increased penetration of antimicrobials within the biofilm (Rubio-Canalejas et al. 2022).

Raman spectroscopy is another technique that has been used to analyse biofilm EPS (Shakeel et al. 2022; Shen et al. 2022). Raman spectroscopy is a non-destructive analytical method that can theoretically provide details of the molecular composition and structure of a sample (Talari et al. 2015). Raman spectroscopy detects the inelastic scattering of monochromatic light caused by molecular vibrations when exposed to laser energy. This scattering provides a unique spectral fingerprint for an analysed material (Félix-Rivera and Hernández-Rivera 2012). Raman spectroscopy has been applied to characterise EPS components, including glucans, proteins, and lipids, for single and mixed species biofilms of different strains of *Streptococcus* (*S. mutans, S. sanguis and S. sobrinus*) (Gieroba et al. 2020). The technique provided detailed insights into the distribution and composition of EPS, allowing for direct comparison between single species and mixed species biofilms. The results showed that lipid saturation varied with

strains and species, with *S. sobrinus* and *S. mutans* exhibiting higher levels, and distinct polysaccharides signatures in biofilms (Gieroba et al. 2020).

Confocal Raman Microscopy (CRM) is an advanced Raman-based imaging technique that enables chemically specific, high-resolution spatial mapping of biological and material samples. Unlike conventional Raman spectroscopy, CRM incorporates confocal microscopy where a pinhole rejects out of focus light, thereby improving depth resolution and contrast (Gurram et al., 2017). CRM is particularly useful in analysing heterogeneous biological structures within biofilms, where spatial organisation of EPS components is crucial. The core components of a CRM system include an excitation laser, optical filtering system, confocal microscope, spectrometer, and detector. A monochromatic laser is used to excite the sample, with the beam focused through a high numerical aperture objective lens to ensure precise targeting of a small sample volume. The Raman scattered light is then filtered using an edge filter (which removes the intense Rayleigh scattering) allowing only the Raman shifted photons to pass through. A critical feature of CRM is the pinhole aperture in front of the detector, which blocks out-of-focus light and significantly enhances depth resolution, making it possible to selectively collect Raman signals from a defined focal plane. The collected spectral data undergoes pre-processing to remove noise, followed by spectral analysis to identify key molecular components. The processed data provides chemical maps and quantitative measurements, and information on spatial distribution (Pan et al. 2025b).

Liu et al. (2022) used CRM for *in situ*, label free characterisation of hydrated biofilm matrices of *P. aeruginosa* and *P. putida*. The researchers integrated Non-Negative Matrix Factorization (NMF), a computational technique that decomposes complex hyperspectral data into fundamental spectral components, allowing separation of biologically relevant signals from

interfering background noise. This approach effectively subtracted the water background signal, which constitutes up to 95% of the hydrated biofilm matrix and is a major limitation in traditional Raman analysis. As a result, it was possible to resolve and spatially map biomolecular components within the biofilm, including proteins, bacterial cells, glycolipids, and polyhydroxyalkanoates. Results showed that glycolipids were predominantly found in the lower layers of *P. aeruginosa* biofilms, whilst polyhydroxyalkanoates accumulated in the basal regions of the *P. putida* biofilms, and these findings correlated with the specific physiological functions of these microorganisms. The study highlighted the value of CRM in biofilm research, demonstrating its ability to distinguish spatially heterogeneous EPS components and bacterial cells (Liu et al. 2022).

In this current research, an opportunity arose to access a Lightsheet Confocal Raman Microscope (LCRM) (Figure 4.1). The LCRM was custom built by the research group of Professors Paola Borri and Wolfgang Langbein in the School of Biosciences, Cardiff University. A supporting data analysis algorithm called Factorization into Susceptibilities and Concentrations of Chemical Components (FSC^3), had previously been developed by the research group (Masia et al. 2013). The algorithm enables measured Raman spectra to be split up into individual chemical components (*e.g.* water, proteins, lipids *etc*) with corresponding quantitative concentration maps. These maps provide spatial organisation of molecules in complex systems without requiring prior knowledge of the sample's composition (Pope et al 2021).

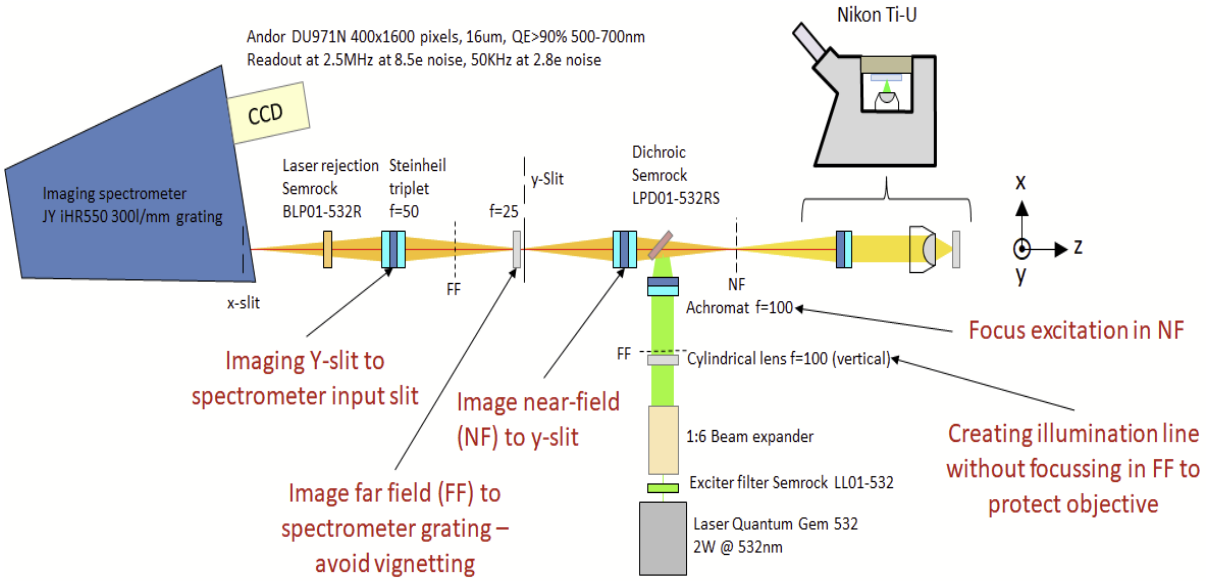

Figure 4.1 Schematic of the Lightsheet confocal Raman setup in the School of Biosciences at Cardiff University.

A laser beam (532 nm) is focused into a line through cylindrical lenses and directed onto the sample through the microscope. This creates a narrow line of illumination, reducing background signal and protecting the objective lens. The Raman scattered light from the sample passes through filters that remove unwanted light, and only the relevant Raman signal is focused onto the spectrometer slit. The spectrometer disperses the light by wavelength, and a sensitive CCD camera records the Raman spectra, allowing chemical mapping of the sample.

4.1.1 Aims

The aim of the research in this Chapter was to use colorimetric assays to first quantify suspected major components of EPS in *in vitro* biofilms and compare to equivalent populations of planktonic cells. Additionally, this Chapter used CSLM and LCRM to assess EPS and investigate the efficacy of enzymatic EPS disruption by dextranase.

4.2 Material and methods

4.2.1 Biofilm preparation for EPS chemical analysis

Biofilms were prepared as previously described in section 2.2.3. To assess the protein and carbohydrate matrix content, biofilms were first detached from the surface of coupons using a scraper and resuspended in distilled water. Overnight cultures of the inocula (section 2.2.2) used to produce biofilms, served as planktonic controls. A minimum of three biological replicates was included for each condition.

Additionally, *S. mutans* biofilms were grown on polycarbonate coupons using overnight cultures adjusted to an OD_{600} of 0.1 into tryptone soy broth (TSB; Oxoid) supplemented with 1 µM dextran conjugated with Alexa Fluor™647 (Invitrogen, Fisher Scientific, Leicestershire, United Kingdom) and 1% (w/v) sucrose. Incubated under static conditions at 37 °C in a 5% CO_2 atmosphere for 72 h, with daily replacement of freshly supplemented medium. The resulting biofilms were evaluated for subsequent EPS disruption by dextranase. For LCRM, the medium was supplemented with 'label-free' 1 µM dextran (Invitrogen™ D1860, Fisher Scientific, Leicestershire, United Kingdom) to avoid undesired fluorescence.

4.2.2 DNA extraction from biofilm and planktonic samples

DNA was extracted from biofilms using the DNeasy PowerBiofilm Kit (Qiagen) based on the manufacturer's protocol. Briefly, biofilms were transferred to a collection tube and centrifuged at 13,000 x *g* for 1 min and the supernatant was removed. The biofilm was resuspended in 350 µl of lysing reagent (MBL solution) and transferred to a PowerBiofilm bead tube. FB solution (100 µl), which contains a chaotropic agent that aids in lysis, was added, and the mix were incubated at 65°C for 5 min. Mechanical disruption was achieved by bead-beating at 6 m/s for 30 s using a FastPrep-24 Sample Preparation System Homogenizer (MP

Biomedicals). Following this, 100 µl of IRS solution was used to remove non-DNA organic and inorganic material and incubated at 2-8°C for 5 min prior to centrifugation (13,000 x *g* for 1 min). The supernatant was discarded, and 900 µl of MR solution (a concentrated salt solution that allows binding of DNA to silica) was added. A 650-µl volume of supernatant was placed on an MB spin column (which contains a silica membrane that binds DNA while discarding non-DNA components) and centrifuged (13,000 x *g* for 1 min). The flow through was discarded and the step repeated until the supernatant was fully processed. This was followed by a wash step using 650 µl of PW solution to remove residual salts and other contaminants. The solution was centrifuged (13,000 x *g* for 1 min) and subjected to a 650 µl ethanol wash and centrifugation (13,000 x *g* for 1 min). The flow through was discarded and the tube was centrifuged (13,000 x *g* for 2 min) to ensure residual ethanol removal. Finally, the column was placed in a new collection tube, and 100 µl of EB solution (which allows release of DNA bound to the filter membrane) was added and centrifuged (13,000 x *g* for 1 min). The resultant flow through, which contained the extracted DNA, was used for subsequent analysis.

4.2.3 Quantitative real-time polymerase chain reaction (qRT-PCR) for assessing numbers of bacteria and *Candida*

To allow comparisons between samples it was necessary to standardise biofilms for cell content. To do this, qRT-PCR was used as it was considered more appropriate than enumeration of biofilm CFUs. Briefly, planktonic cultures of *C. albicans* alone and mixed bacterial population (*Streptococcus mutans* DSM 20523, *Streptococcus sanguinis* NCTC 7863, *Streptococcus gordonii* NCTC 7865, and *Streptococcus salivarius* DSM 20560) were serially decimal diluted, and the number of colony forming units (CFUs) determined by culture on agar medium (as described in section 2.2.9.1). DNA was extracted from each of the planktonic

dilutions and subjected to qRT-PCR. Precision FAST SY qRT-PCR Master mix (PrimerDesign) on the QuantStudio™ 6 Flex Real-Time PCR System (Applied Biosystems) was used for qRT-PCR. All reactions were in total volumes of 20 µL, each containing 10 µl of master mix, 2 µl of each forward and reverse primer, 5 µL of template DNA, and 1 µl nuclease-free water. Bacterial qRT-PCR used universal bacterial primers targeting 16S rRNA gene (16S-341_F: 5'-CCT ACG GGN GGC WGC AG-3' and 16S-805_R: 5'-GAC TAC HVG GGT ATC TAA TCC-3') (Galazzo et al. 2020). *Candida albicans* qRT-PCR used L18 primers (L18F: 5'-CTC GTA GTT GAA CCT TGG-3' and L18R: 5'-GCC TGC TTT GAA CAC TCT-3') (White et al. 2004). qRT-PCR cycling conditions were initial denaturation at 95°C for 2 min, followed by 40 cycles of annealing at 95°C for 5 s and primer extension at 60°C for 20 s. All reactions were performed in triplicate. Negative controls of nuclease-free water were included with all qRT-PCR experiments to confirm absence of contamination. Following qRT-PCR, the log transferred known cell number of planktonic cultures was plotted against the Ct values obtained from the qRT-PCR. A linear regression model was used to generate a standard curve, which was used to determine the number of cells in the biofilms. Biofilms could then be standardised based on cell number and compared for EPS content.

4.2.4 Total protein quantification in biofilm and planktonic cultures

Measurement of total protein content used either a Pierce™ BCA Protein Assay Kit or a Micro BCA™ Protein Assay Kit (Thermo Scientific™ 23227 and 23235, Fisher Scientific, Leicestershire, United Kingdom). For each biofilm, three technical repeats were included in accordance with the manufacturer's instructions. The assays were performed in 96 well plates with three biological replicates per sample.

A 25-µl volume of the test sample or supplied protein standard was mixed with 200 µl of the working reagent (provided with the kit). The plate was incubated at 37°C for 30 min, followed by equilibration to room temperature for up to 10 min. Absorbance was measured at 562 nm using a plate reader (FLUOstar, BMG Labtech, Aylesbury, United Kingdom). Protein concentration was then determined by comparison with a standard curve prepared using bovine serum albumin (provided with the kit). All measurements were performed within 10 min of equilibration to minimise potential variations caused by continued colour development.

4.2.5 Total carbohydrate quantification in biofilm and planktonic cultures

Measurement of carbohydrate content was done for three technical repeats using a total carbohydrate assay kit (MAK104, Sigma-Aldrich, Burlington, Massachusetts, United States) in accordance with the manufacturer's instructions. The assay was performed in the wells of a 96 well plate using glucose standards and test samples (30 µl). To the test volumes, 150 µl of concentrated sulphuric acid was added and mixed thoroughly by repeat pipetting. The mixture was then incubated in the dark at 90°C for 15 min. After incubation, 30 µl of the provided developer solution was added and incubated for 5 min on a shaker at room temperature. The plate was mixed for a further 1 min immediately prior to absorbance measurements at 490 nm.

4.2.6 Preparation of dextranase for use in EPS disruption

Dextranase from *Chaetomium erraticum* (D0443, Sigma-Aldrich, Burlington, Massachusetts, United States) was diluted with distilled sterile water to a concentration of 0.25% (v/v). To target the glucan matrix, biofilms were immersed in 0.25% dextranase for 1 h at 37°C. For controls, biofilms were treated in distilled water instead of dextranase.

4.2.7 Assessment of dextranase efficacy using confocal laser scanning microscopy (CLSM) and COMSTAT analysis

For biofilms cultured in medium supplemented with 1% (w/v) sucrose and 1 µM dextran Alexa Fluor™647 conjugate, the resulting glucan EPS was incorporating the labelled dextran during EPS formation, and this would then be detectable by CLSM. Microbial cells could also be imaged by SYTO 9 staining. Briefly, polycarbonate coupons supporting biofilm growth were retrieved and washed using distilled water to remove planktonic or loosely attached cells. The biofilms were then incubated at 37°C for 1 h in 1 ml of either 0.25% dextranase or distilled water. After incubation and washing, biofilms were stained with 3.3 µM of SYTO®9 green-fluorescent nucleic acid stain (Invitrogen™ L7007, Fisher Scientific, Leicestershire, United Kingdom). The coupons were then placed in a 24-well plate (µ-Plate 24 Well Black, ibidi GmbH, Martinsried, Germany) and protected from light. Images were acquired using a ZEISS Celldiscoverer 7 with LSM 900 (Carl Zeiss, Germany) as described in section 2.2.9.4. For COMSTAT analysis, CLSM images were analysed using COMSTAT 2.1 software (Heydorn et al. 2000; Vorregaard 2008). Images were converted to OME-TIFF according to COMSTAT 2.1 manual and analysed as described in section 2.2.9.4. For each condition, a minimum of three independent biological replicates with five image stacks per each replicate was analysed.

4.2.8 Scanning electron microscopy (SEM) assessment of dextranase disruption of glucan

To image the effect of dextranase treatment on *S. mutans* biofilms, SEM was also used. Biofilm samples were grown in supplemented medium for 72 h, and dextranase treatment applied as described previously 4.2.6. Following treatment, biofilms were gently immersed in tissue culture plate wells filled with sterile water to remove planktonic or loosely attached cells.

Biofilms were air dried by incubation for 24 h at 37°C and then left at room temperature for prior to SEM as described previously 3.2.4.

4.2.9 Lightsheet Confocal Raman Microscopy (LCRM) analysis to characterise EPS and assess its disruption by dextranase

Streptococcus mutans biofilms were grown on polycarbonate or hydroxyapatite (BioSurface technologies, Montana, USA) coupons, or on 35 mm glass bottom dishes (MATTEK P35G-1.5-14-C, Massachusetts, USA). These biofilms were used to identify EPS components and evaluate the effect of dextranase treatment on the glucan matrix. Biofilms were cultured for 72 h at 37°C in medium supplemented with 1% (w/v) sucrose and containing unlabelled 1 µM dextran. After washing gently with sterile distilled water, a 2-ml volume of 0.25% dextranase solution (v/v) was applied to the biofilms and incubated for 1 h at 37°C. Control samples were treated with 2 mL of distilled water. Following incubation, biofilms were gently rinsed with distilled water to remove any remaining enzyme.

LCRM was used to identify EPS components and evaluate effects of dextranase treatment on the glucan matrix of *S. mutans* biofilms. LCRM apparatus included a 532 nm laser, a cylindrical lens creates the light sheet which was directed onto the biofilm using a ×40, 1.15 NA objective lens, acquiring a 200 × 200 µm area, and high-resolution spatial coverage of the biofilm surface. Acquisition and processing were performed using ImageJ software (version range 1.53o to 1.54f)

The LCRM's spectral resolution was optimised to target the relevant vibrational range. The Raman signal was collected in the epi direction using the same objective used to excite the sample, allowing backscattered Raman photons to be collected along the same optical path as the excitation laser. The collected signal passed through a longpass dichroic filter (Semrock,

LPD01-532RS) and focused on to the entrance slit of an imaging spectrometer (Horiba Jobin-Yvon, iHR 550), fitted with a 300 l/mm grating. A Charge-Coupled Device (CCD) camera (Andor, Newton DU 971N – BV) was fitted to the exit of the spectrometer to record Raman spectra. The acquired hyperspectral data were analysed using FSC³ algorithm. Analysis focused on the fingerprint region (450 to 2000 cm^{-1}), which contained vibrational signatures of molecular components.

Raman spectra were extracted from the fingerprint region and analysed using KnowItAll software (KnowItAll software, (version 24.1.65.0). Wiley & Sons, Hoboken, New Jersey, USA) to characterise and identify the molecular component(s). Identification was based on spectral comparisons made against reference libraries, whilst quantitative concentration maps were generated to visualise and analyse spatial organisation of glucans, before and after dextranase treatment.

The spectral component maps corresponding to regions with minimal cellular content and a predominant glucan matrix, typically found between microcolonies, were analysed using ImageJ software. The intensity values of the images were rescaled to 16-bit. For each sample, the spectral component of interest was selected, and average intensity values were measured for 9 different images for each condition.

4.2.10 Statistical analysis

Statistical analyses were performed using GraphPad Prism 10.1.0 (GraphPad Software, Boston, Massachusetts USA, www.graphpad.com). Data were assessed for normality using Shapiro-Wilk test. For total protein comparisons between biofilm and planktonic cultures, Welch's *t*-test was used for *Candida* and whole saliva samples. A Student's *t*-test was applied for mixed microbial samples, while the Mann–Whitney *U* test was used for bacterial cultures.

Carbohydrate comparisons between biofilm and planktonic cultures were analysed using the Mann–Whitney *U* test for *Candida*, mixed microbial and bacterial cultures. Welch's *t*-test was used for whole saliva samples. Total carbohydrate content in *Streptococcus mutans* biofilms (untreated vs 0.25% dextranase treated) was analysed using Welch's *t*-test.

CLSM and COMSTAT glucan biomass comparisons between untreated and dextranase treated biofilms were analysed using Welch's *t*-test for *S. mutans* and dual species biofilms, and the Mann–Whitney *U* test for whole saliva biofilms. Glucan average thickness was analysed using Welch's *t*-test. Cellular biomass was analysed using the Mann–Whitney *U* test.

CRM mean intensity values of glucan concentration maps in untreated and dextranase-treated *S. mutans* biofilms were analysed using Student's *t*-test.

4.3 Results

4.3.1 Quantitative real-time polymerase chain reaction (qRT-PCR) for bacteria and *Candida albicans*

The 10-fold dilution series of planktonic *C. albicans* for generating a standard curve from qRT-PCR, ranged from 3.2×10^8 to 3.2×10^3 CFU/ml, while the dilution series for bacteria ranged between 4×10^8 to 4×10^2 CFU/ml. For the purpose of standardisation, CFU/ml were deemed to be equivalent to cells/ml.

Following DNA extraction and qRT-PCR on the diluted preparations, the resulting Ct values were plotted against the logarithmic cell concentrations to generate a standard curve, fitted using linear regression. The equation of the standard curve for *C. albicans* was Ct = -5.2099 × log (cell number) + 60.875, with a coefficient of determination (R^2) value of 0.99, indicating a strong linear relationship between log (cell number) and Ct value (Figure 4.2). Similarly, the equation of the standard curve for the bacteria preparations was Ct = -4.2858 × log (cell number) + 46.254, with an R^2 value of 0.99, indicating a strong linear relationship (Figure 4.3).

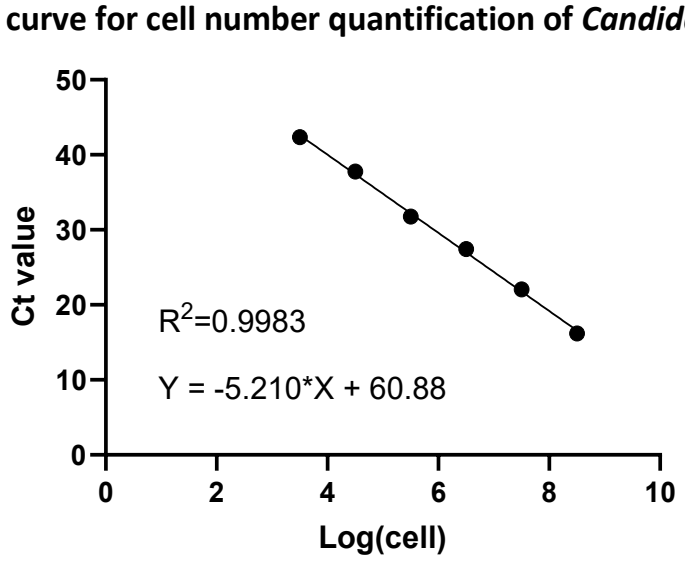

Figure 4.2 Standard curve of *C. albicans* cells cell number quantification against Ct value obtained from qRT-PCR.

The relationship between Ct value and log (cell number) for serial dilutions of planktonic samples is shown. The equation of the best-fit line is Y = -5.210 × X + 60.88, with an R^2 value of 0.99. This equation was used to determine the cell numbers in test samples with unknown cell numbers.

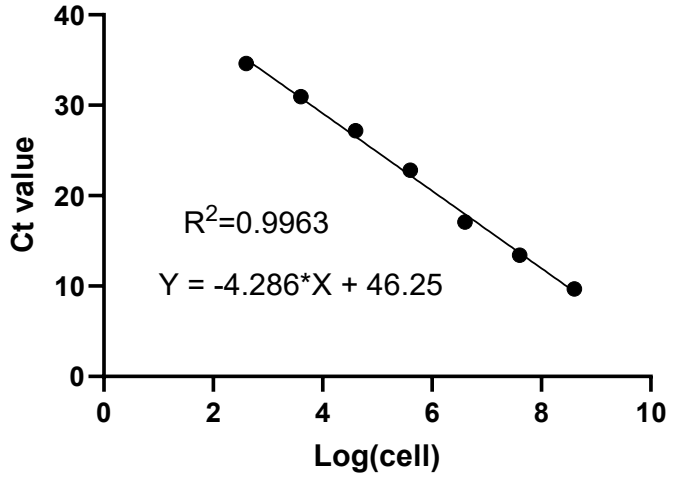

Figure 4.3 Standard curve of mixed bacteria cell number quantification against Ct value obtained from qRT-PCR.

The relationship between Ct values and log (cell number) for serial dilutions of planktonic mixed bacteria samples is shown. The equation of the best-fit line is Y = -4.286 × X + 46.25, with an R^2 value of 0.99. This equation was used to determine the cell numbers in test samples with unknown cell numbers.

4.3.2 Total protein quantification in biofilms and planktonic cultures

Biofilms exhibited significantly higher ($p<0.001$) protein concentrations per 1×10^6 cells compared to planktonic equivalents for all tested microorganisms. Specifically, the mean protein concentration for biofilm samples was *C. albicans* (6 µg/10^6 cells), bacteria (2.5 µg/10^6 cells), mixed microbial species (3.7 µg/10^6 cells) and whole saliva (17.5 µg/10^6 cells). In comparison, planktonic cultures had mean protein concentrations of *C. albicans* (2.6 µg/10^6 cells), bacteria (1.27 µg/10^6 cells), mixed species (1.2 µg/10^6 cells) and whole saliva (0.25 µg/10^6 cells). Figure 4.4 compares protein content of biofilms and planktonic cultures. Table 4.1 presents the total protein quantification values of each microorganism and compares biofilm and planktonic cultures. In the case of *S. mutans* biofilms grown in 1% sucrose supplemented medium, the mean total protein content was 1.11 µg/10^6 cells.

Table 4.1 Compiled total protein quantification values of biofilms and planktonic cultures of tested microorganisms

Microorganism	*C. albicans*		Mixed bacteria		Mixed species		Whole saliva		*S. mutans*	
Sample	Planktonic	Biofilm	Planktonic	Biofilm	Planktonic	Biofilm	Planktonic	Biofilm	Planktonic	Biofilm*
1	2.444	5.728	1.595	2.164	1.029	3.737	0.336	16.831	0.021	1.067
2	2.586	5.817	1.579	1.916	1.253	3.696	0.310	13.305	0.017	0.844
3	2.464	6.319	1.624	2.123	1.208	3.771	0.327	17.206	0.018	0.759
4	2.531	4.560	1.616	1.886	1.106	3.707	0.337	18.543	0.017	0.316
5	2.658	5.510	1.663	2.135	1.104	3.648	0.320	14.099	0.017	1.149
6	2.714	5.151	1.576	2.293	1.225	3.944	0.370	18.556	0.018	1.127
7	2.668	6.746	1.051	2.182	1.233	3.661	0.198	15.024	0.017	0.617
8	2.734	5.362	1.031	2.505	1.200	4.054	0.192	13.887	0.018	1.357
9	2.621	6.305	1.074	2.780	1.322	3.917	0.201	21.691	0.022	1.247
10	2.782	5.791	1.018	2.857	1.125	3.548	0.185	19.131	0.021	0.909
11	2.831	6.476	1.069	2.931	1.356	3.613	0.189	18.704	0.017	0.785
12	2.762	7.043	0.994	3.021	1.482	3.607	0.192	19.100	0.019	1.856
13	2.907	6.220	1.070	3.124	1.164	3.686	0.184	18.893	0.019	0.881
14	2.579	6.638	1.056	2.919	1.283	3.552	0.185	17.661	0.016	1.594
15	2.452	6.709	1.069	3.100	1.298	3.859	0.194	19.939	0.021	2.237
Mean	2.649	6.025	1.272	2.528	1.226	3.733	0.248	17.505	0.018	1.116

All values are reported as µg/ml after standardisation based on cell number. * *Streptococcus mutans* biofilm grown in 1% sucrose and 1 µM dextran supplemented tryptone soy broth.

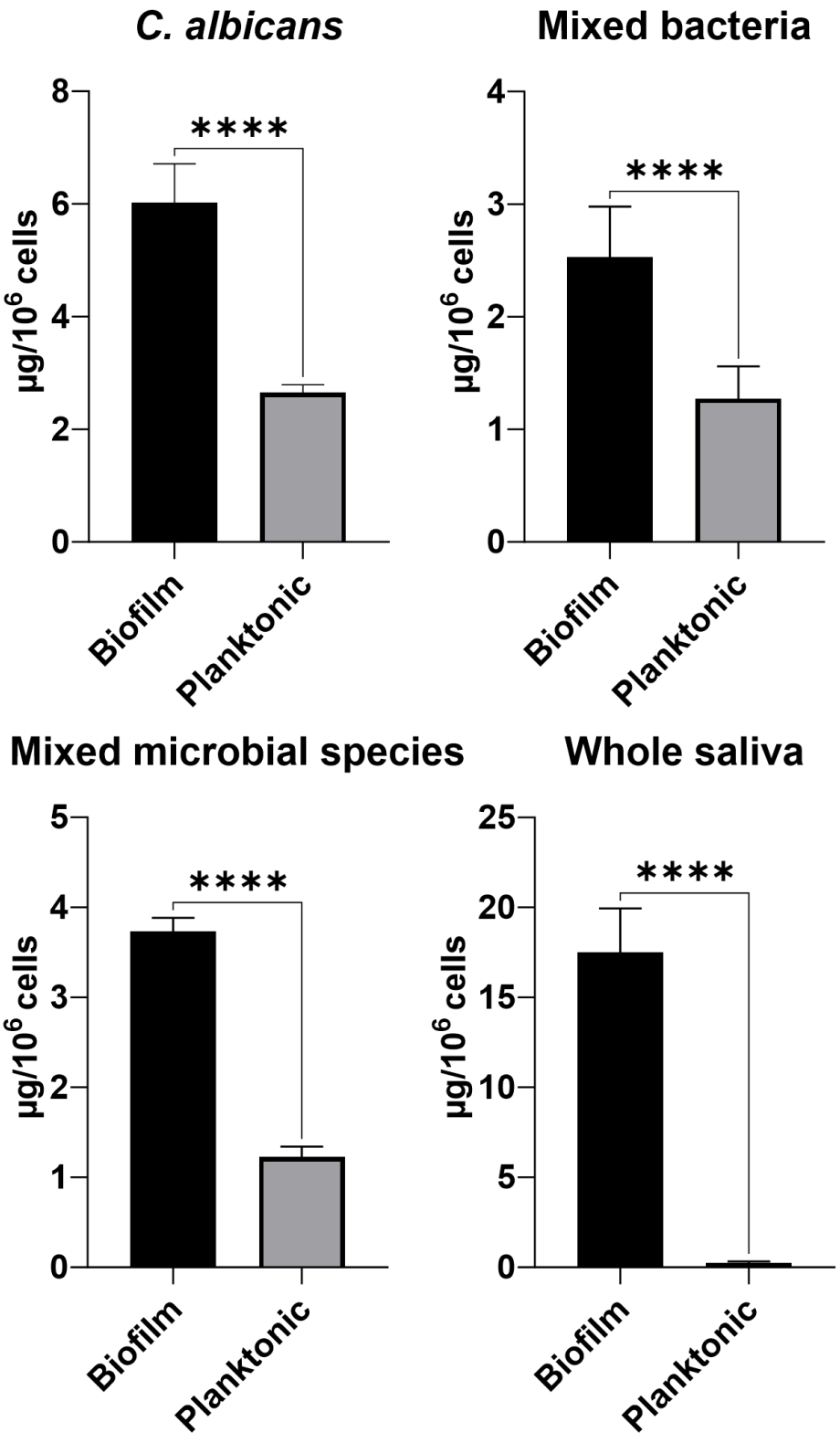

Figure 4.4. Total protein levels in biofilm and planktonic cultures for different tested cultures.

Protein concentrations were standardised based on cell number. Protein content is expressed as µg/10^6 cells. Data represent the mean ± standard deviation (n=10 per group).

4.3.3 Total carbohydrate quantification in biofilms and planktonic cultures

Total carbohydrate content in biofilms produced by *C. albicans* and from whole saliva was significantly ($p<0.001$) higher than their planktonic equivalents. The mean carbohydrate concentration was 4.9 $\mu g/10^6$ cells in *C. albicans* biofilms, 3.8 $\mu g/10^6$ cells in mixed species biofilms and 2.3 $\mu g/10^6$ cells in whole saliva derived biofilms. For planktonic cultures, total carbohydrate was at a mean level of 3.9 $\mu g/10^6$ cells for *C. albicans*, 0.5 $\mu g/10^6$ cells for mixed species and 0.4 $\mu g/10^6$ cells for whole saliva cultures. There was no significant difference in the carbohydrate concentrations for bacteria only biofilms (0.48 $\mu g/10^6$ cells) and planktonic cultures (0.51 $\mu g/10^6$ cells).

Figure 4.5 presents the carbohydrate concentrations in biofilm and planktonic cultures. Table 4.2 lists the total carbohydrate quantification values of each microorganism and condition tested.

Table 4.2 Compiled total carbohydrate quantification values of biofilms and planktonic cultures of tested microorganisms

Microorganism	*C. albicans*		Mixed bacteria		Mixed species		Whole saliva		*S. mutans*	
Sample	Planktonic	Biofilm	Planktonic	Biofilm	Planktonic	Biofilm	Planktonic	Biofilm	Planktonic	Biofilm*
1	4.530	3.990	0.393	0.452	0.382	3.529	0.278	2.066	0.028	2.936
2	3.708	3.990	0.425	0.582	0.603	2.789	0.646	2.094	0.062	3.339
3	3.858	3.990	0.598	0.548	0.496	4.481	0.425	2.229	0.035	3.390
4	5.542	3.990	0.388	0.416	0.740	2.893	0.299	0.605	0.024	4.211
5	5.154	3.990	0.677	0.511	0.765	4.798	0.545	0.519	0.048	3.934
6	4.111	3.990	0.398	0.437	0.572	2.659	0.423	0.431	0.043	3.830
7	3.686	5.465	0.682	0.402	0.313	4.518	0.344	2.480	0.057	3.740
8	3.173	4.595	0.590	0.553	0.588	3.707	0.631	4.105	0.025	4.090
9	3.544	5.566	0.437	0.422	0.363	2.905	0.515	3.506	0.072	1.802
10	3.090	5.892	0.657	0.639	0.357	3.553	0.605	2.880	0.040	3.898
11	4.246	5.899	0.442	0.409	0.895	4.921	0.316	3.402	0.037	3.325
12	3.335	5.899	0.389	0.605	0.457	2.959	0.729	2.400	0.051	2.884
13	3.483	5.430	0.553	0.488	0.296	5.025	0.510	2.496	0.030	7.935
14	3.656	5.899	0.430	0.195	0.451	4.727	0.364	3.411	0.066	5.521
15	3.645	5.841	0.654	0.541	0.309	4.914	0.639	2.790	0.034	6.868
Mean	3.917	4.962	0.480	0.514	0.506	3.892	0.484	2.361	0.044	4.453

All values are reported as µg/ml after standardisation based on cell number. * *Streptococcus mutans* biofilm grown in 1% sucrose and 1 µM dextran supplemented tryptone soy broth.

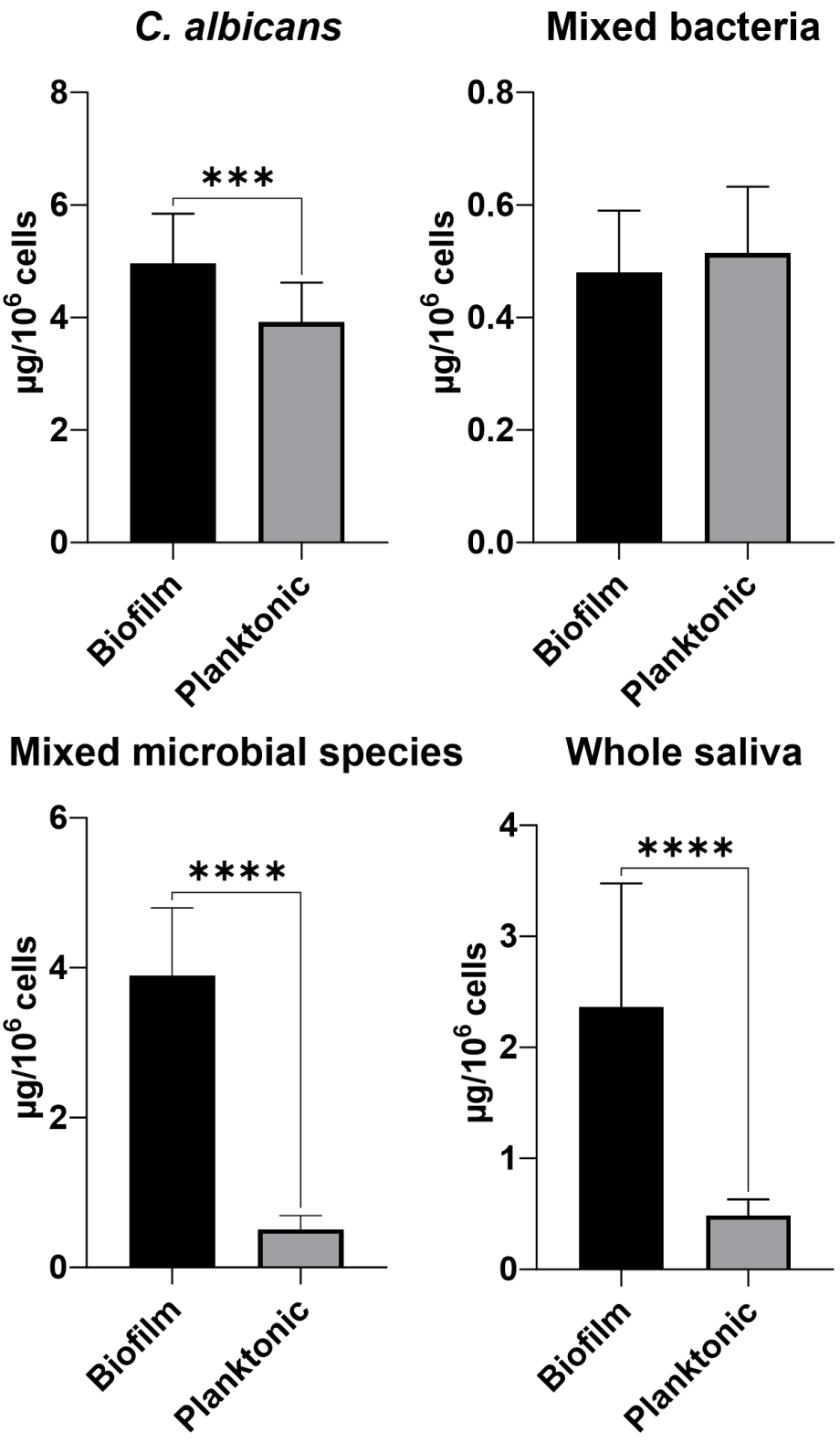

Figure 4.5. Total carbohydrate levels in biofilm and planktonic cultures for tested cultures.

Carbohydrate concentrations were standardised based on cell number. Carbohydrate content is expressed as µg/10^6 cells. Data represent the mean ± standard deviation (n=10 per group).

4.3.4 Evaluation of 0.25% dextranase efficacy as disruption agent of biofilms containing glucan EPS

4.3.4.1 Assessment of dextranase efficacy by quantifying carbohydrate content

To assess the efficacy of dextranase treatment on *S. mutans* biofilms, carbohydrate content determination of treated and untreated samples revealed a 34.2% reduction in biofilms treated with 0.25% dextranase, as shown in Figure 4.6. Statistical analysis determined this as being significant ($P<0.001$). Full dataset of carbohydrate content for all replicates is listed in Appendix II.

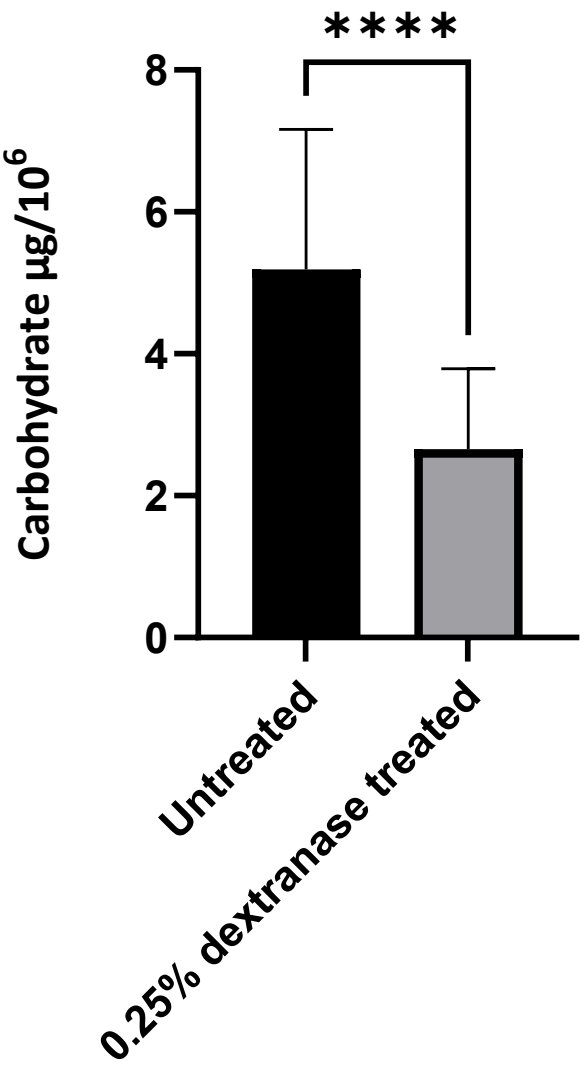

Figure 4.6 Total carbohydrate content in untreated (5.19 µg/10^6) and 0.25% dextranase treated (2.65 µg/10^6) *Streptococcus mutans* biofilms, measured in µg/10^6 cells.

Biofilms were grown 1% (w/v) sucrose and 1 µM Alexa Fluor™ conjugated dextran supplemented medium for 3 days on polycarbonate coupons, with 0.25% dextranase (v/v) treatment applied for 1 hour for treated group. Data represent the mean ± standard deviation (n = 25 per group).

4.3.4.2 Assessment of dextranase disruption of glucan using confocal laser scanning microscopy and COMSTAT analysis

CLSM of dextranase treated *S. mutans* biofilm cultures showed a reduction in the glucan matrix. *Streptococcus mutans* biofilms grown in 1% (w/v) sucrose and 1 µM of Alexa fluor™ 647 conjugated dextran supplemented medium, but untreated with dextranase, exhibited a dense matrix of microcolonies of bacterial cells embedded within and EPS matrix (Figure 4.7). In the case of established biofilms being treated with dextranase, there was a noticeable reduction in the EPS matrix, as seen by comparatively large spaces devoid of fluorescence between bacterial cells (Figure 4.8). Interestingly when dextranase treatment occurred during biofilm development, apparent inhibition of the formation of the matrix occurred with the prevention of microcolony aggregation. This resulted in a more homogenous and distributed biofilm structure (Figure 4.9).

COMSTAT analysis revealed a significant reduction in matrix volume for all three biofilm types *i.e.*, *S. mutans*, whole saliva and dual species, following dextranase treatment. For *S. mutans* biofilms (Figure 4.10A), matrix biomass was found to decrease by 74%, a significant ($p<0.001$) reduction compared to untreated biofilms. Furthermore, analysis of biomass showed an 80% reduction in the glucan matrix of dextranase treated whole saliva biofilms ($p<0.001$; Figure 4.10B) and a 50% reduction in dual species biofilms ($p=0.016$; Figure 4.10C). Results showed that the average thickness of glucan matrix in *S. mutans* biofilm decreased significantly ($p<0.001$) post dextranase treatment, from 35.3 µm to 9.8 µm, a decrease of approximately 72% (Figure 4.11). In contrast, dextranase treatment did not result in a significant reduction ($p = 0.806$) in *S. mutans* cellular biomass, as assessed by SYTO™9 staining, with mean biomass

values of 2.621 µm³/µm² in untreated biofilms and 2.192 µm³/µm² following dextranase treatment (Figure 4.12).

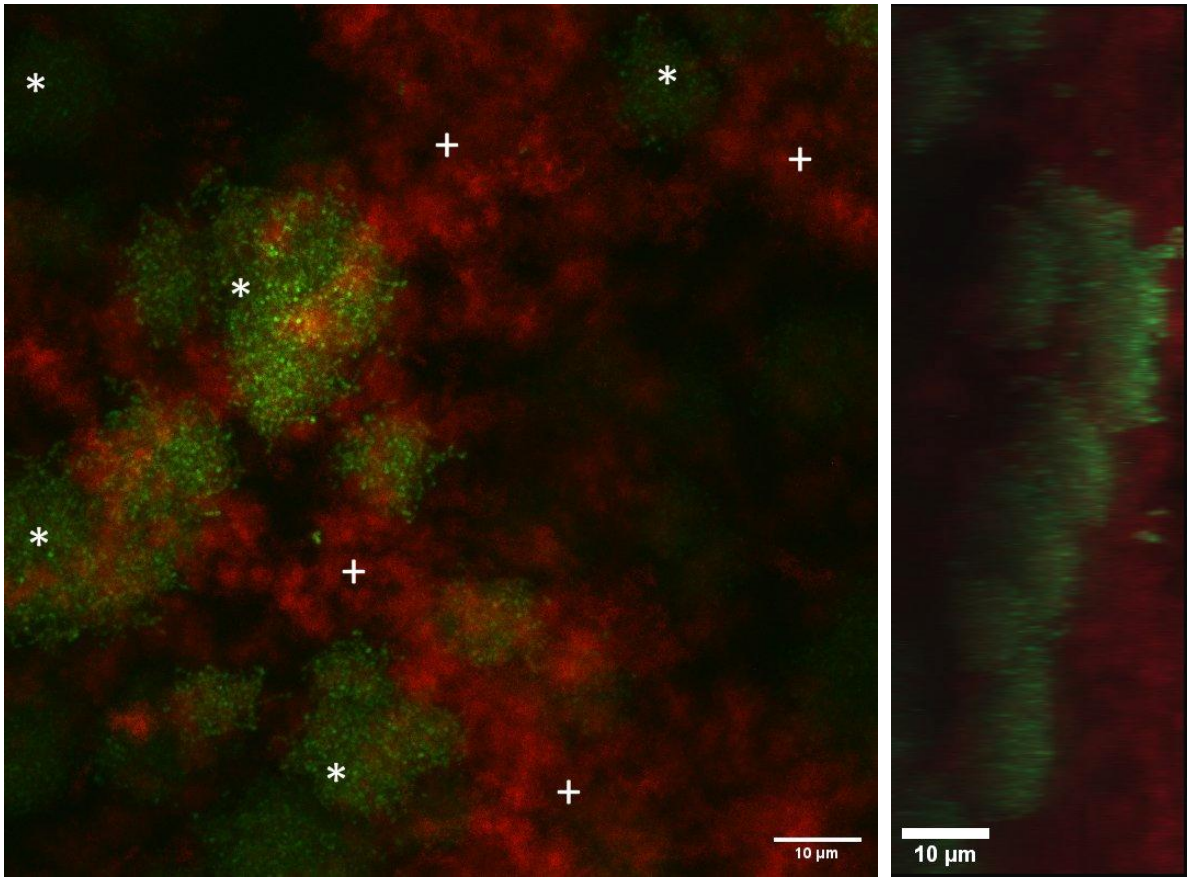

Figure 4.7 CLSM image of *Streptococcus mutans* control biofilm without dextranase treatment.

The biofilm was cultured in 1% (w/v) sucrose and 1 µM Alexa Fluor™ conjugated dextran supplemented medium for 3 days on polycarbonate coupons and was imaged at x40 objective magnification. Green represents cells stained with Syto 9(*), while red fluorescence corresponds to matrix stained by incorporation of Alexa Fluor™ 647 labelled dextran (+). The image shows an abundance of glucan matrix (+) embedding microcolonies (*). . The orthogonal (YZ) view shown alongside the XY projection represents a single optical cross-section through the biofilm, scale bar = 10 µm.

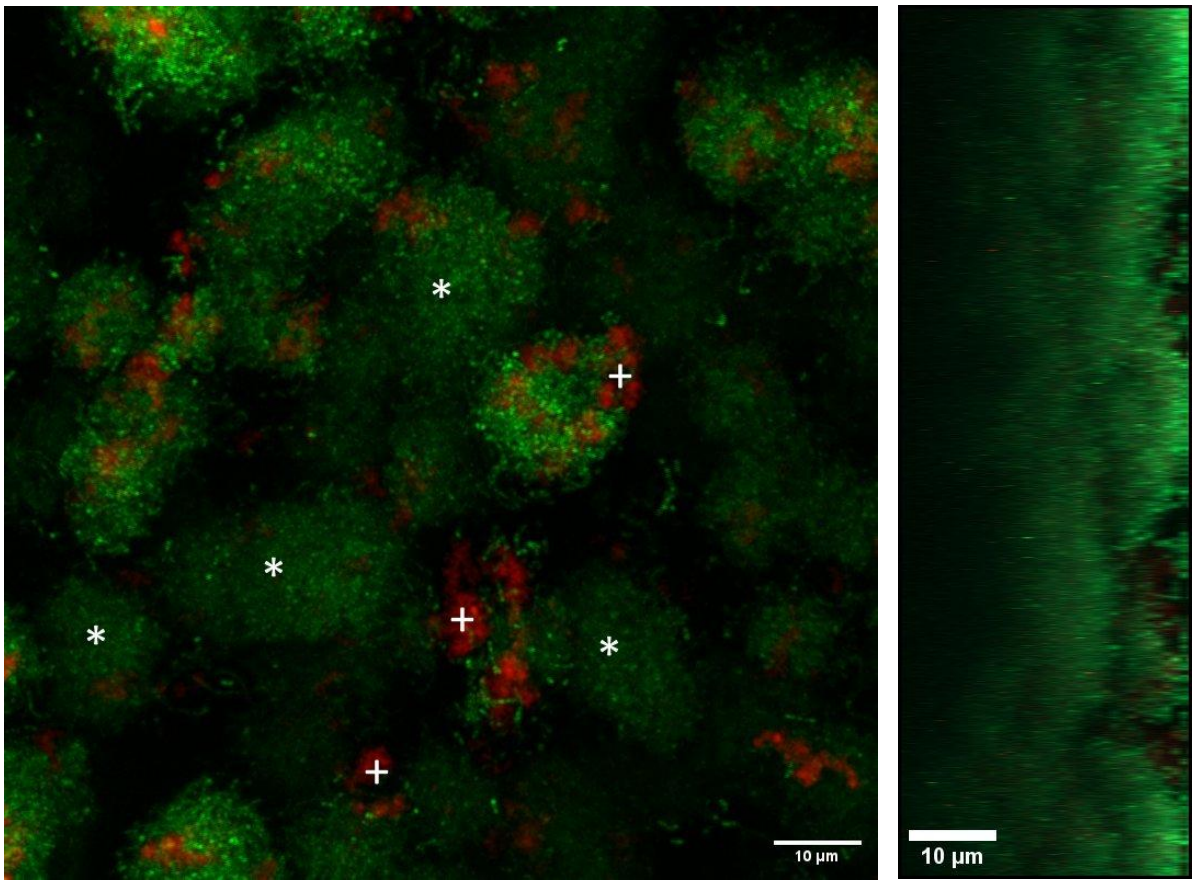

Figure 4.8 CLSM image of *Streptococcus mutans* biofilm, treated with 0.25% dextranase (v/v) for 1 h post growth.

Prior to disruption biofilms were grown in 1% (w/v) sucrose and 1 µM Alexa fluor conjugated dextran supplemented medium for 3 days on polycarbonate coupons at x40 magnification. Green represents cells stained with Syto 9 (*), while red corresponds to matrix stained by incorporating Alexa Fluor™ 647 labelled dextran (+). The image shows reduced amount of glucan matrix (+), exposing the microcolonies (*). The orthogonal (YZ) view shown alongside the XY projection represents a single optical cross-section through the biofilm, scale bar = 10 µm.

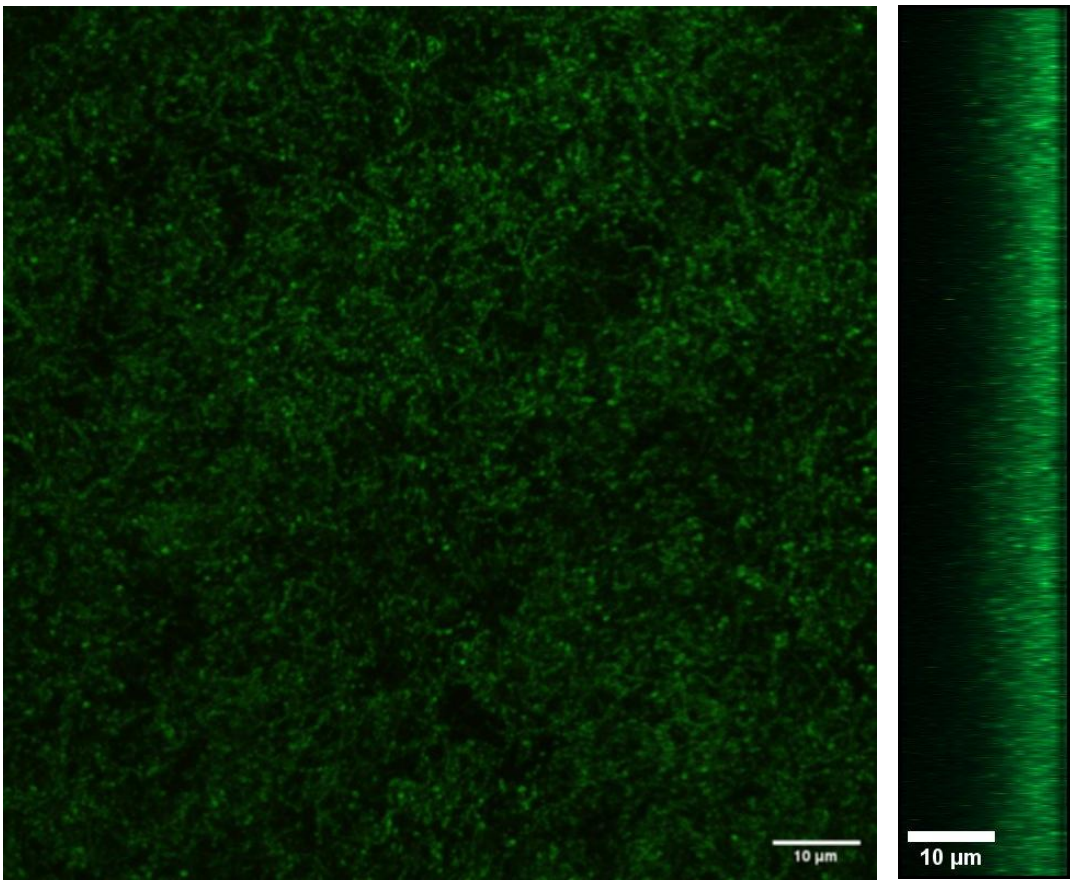

Figure 4.9 CLSM image of *Streptococcus mutans* biofilm with dextranase added during biofilm formation.

Biofilms were grown in medium supplemented with 0.25% dextranase (v/v), 1% (w/v) sucrose and 1 µM Alexa Fluor™ 647 conjugated dextran for 3 days on polycarbonate coupons and scanned at x40 magnification. Green represents cells stained with Syto 9; the red channel was viewed but no signal of Alexa Fluor™ 647 labelled dextran was detected. The image shows the absence of any detectable matrix and structural change from microcolony to more uniform layer of biofilm. The orthogonal (YZ) view shown alongside the XY projection represents a single optical cross-section through the biofilm, scale bar = 10 µm.

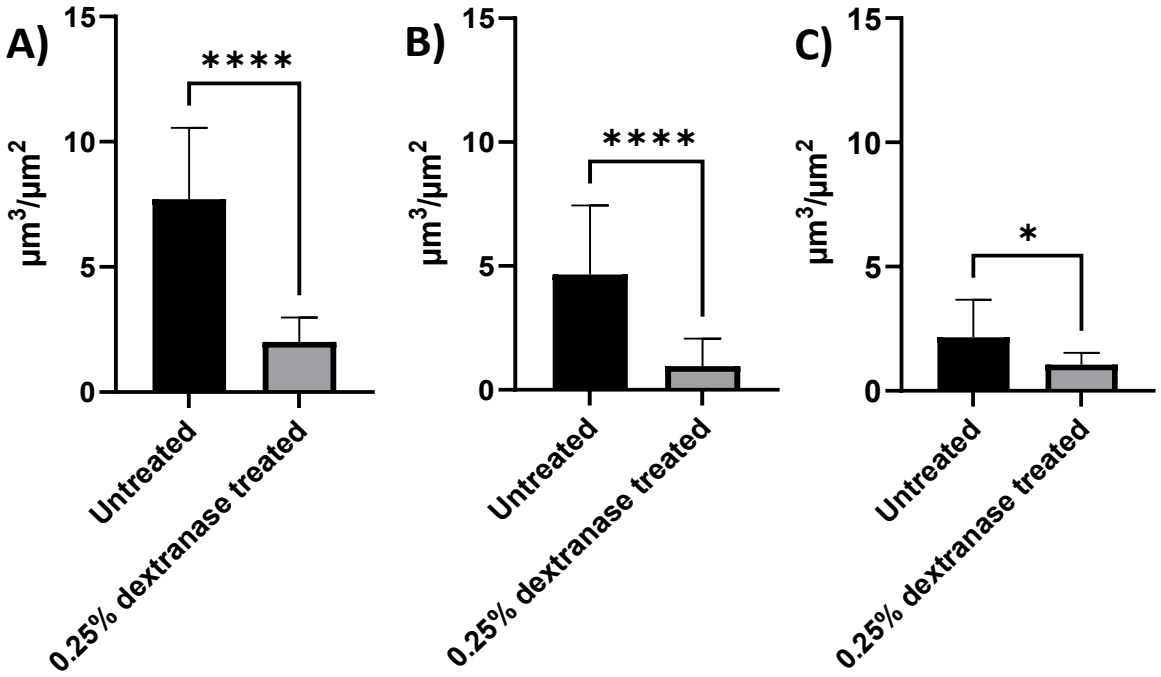

Figure 4.10 Comparison of glucan biomass in untreated and 0.25% dextranase treated biofilms. measured by COMSTAT analysis of CLSM images.

Biofilms were grown for 3 days on polycarbonate coupons in 1% (w/v) sucrose and 1 µM Alexa Fluor™ 647 conjugated dextran supplemented medium, with 0.25% dextranase (v/v) applied for 1 h in the treated group. Data represent the mean ± standard deviation (n = 15 per group). A) *Streptococcus mutans* biofilms showing a significant reduction ($p<0.001$) in dextranase treated (2.001 $\mu m^3/\mu m^2$) compared to untreated (7.71 $\mu m^3/\mu m^2$) biofilms. B) whole saliva biofilm, showing a significant reduction ($p<0.001$) in dextranase treated (4.652 $\mu m^3/\mu m^2$) compared to untreated (0.958 $\mu m^3/\mu m^2$) biofilms. C) dual species (*S. mutans* and *Candida albicans*), showing a significant reduction ($p=0.016$) in dextranase treated (2.157 $\mu m^3/\mu m^2$) compared to untreated (1.056 $\mu m^3/\mu m^2$) biofilms.

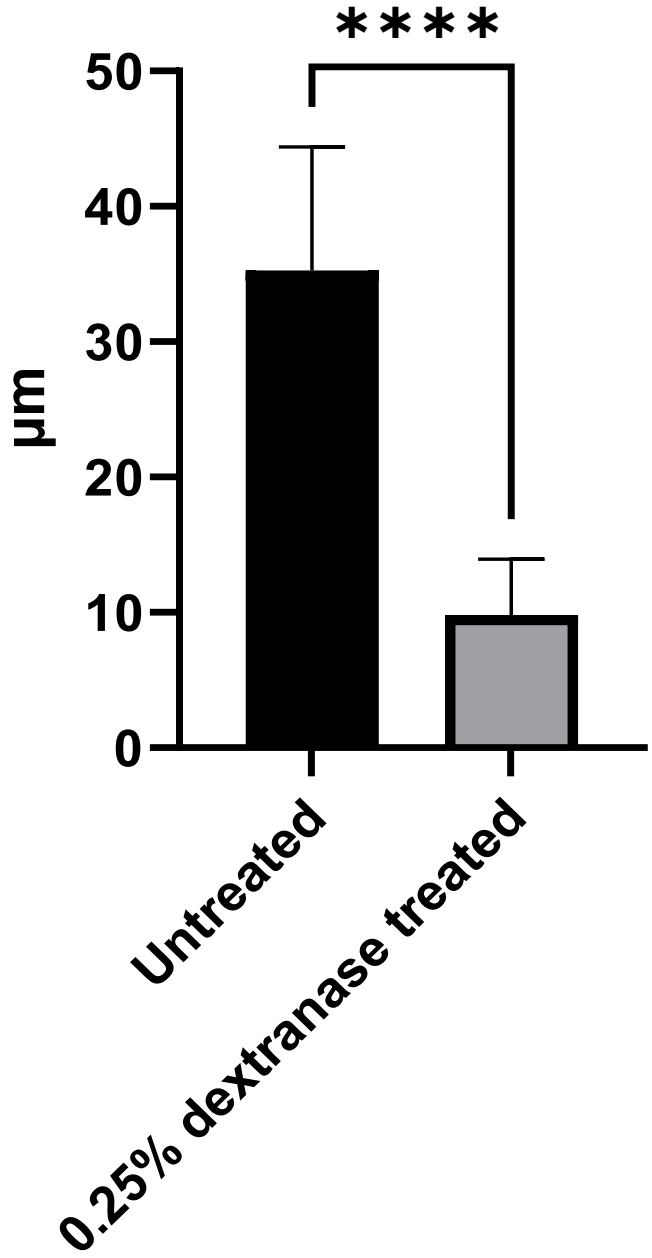

Figure 4.11 Comparison of glucan average thickness in untreated and 0.25% dextranase treated *Streptococcus mutans* biofilms.

A significant reduction ($p<0.001$) in thickness of dextranase treated biofilms (9.819 µm) compared to untreated biofilms (35.282 µm). Values were measured by COMSTAT analysis of CLSM images. Biofilms were grown for 3 days on polycarbonate coupons in 1% (w/v) sucrose and 1 µM Alexa Fluor™ 647 conjugated dextran supplemented medium, with 0.25% dextranase applied for 1 h in the treated group. Data represent the mean ± standard deviation (n = 15 per group).

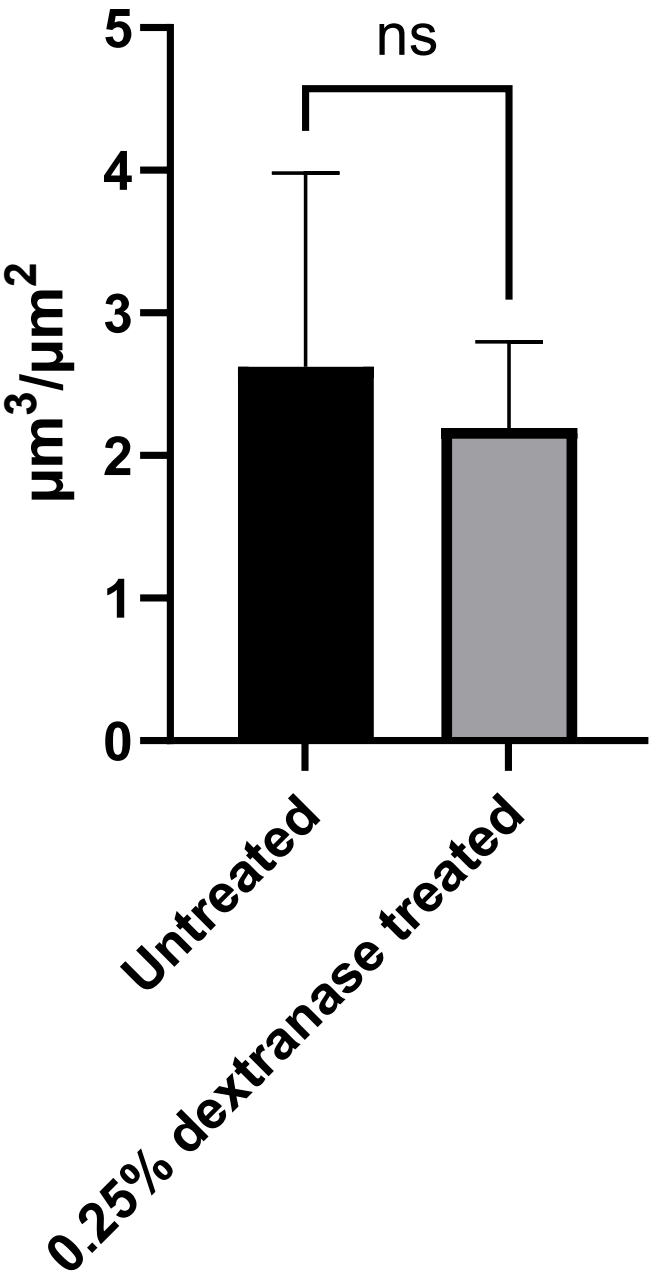

Figure 4.12 Comparison of cellular biomass (stained with SYTO9™) in untreated and 0.25% dextranase treated *Streptococcus mutans* biofilms.

Dextranase treatment did not significantly reduce the biomass of cells. Values measured by COMSTAT analysis of CLSM images. Biofilms were grown for 3 days on polycarbonate coupons in 1% (w/v) sucrose and 1 µM Alexa Fluor™ 647 conjugated dextran supplemented medium, with 0.25% dextranase applied for 1 h in the treated group. Data represent the mean ± standard deviation (n = 15 per group).

4.3.4.3 Assessment of dextranase efficacy using scanning electron microscopy

SEM of *S. mutans* biofilms before and after dextranase treatment revealed clear changes in the biofilm structure. Prior to enzyme treatment, biofilms exhibited a dense, compact structure, with tightly aggregated microcolonies fully covered by the matrix (Figure 4.13). The matrix visibly surrounding the microcolonies, effectively covering the bacterial cells within, suggesting a robust and well-established biofilm architecture. In contrast, after dextranase treatment, there was a notable reduction in the observed matrix, resulting in the exposure of cellular components within the biofilm.

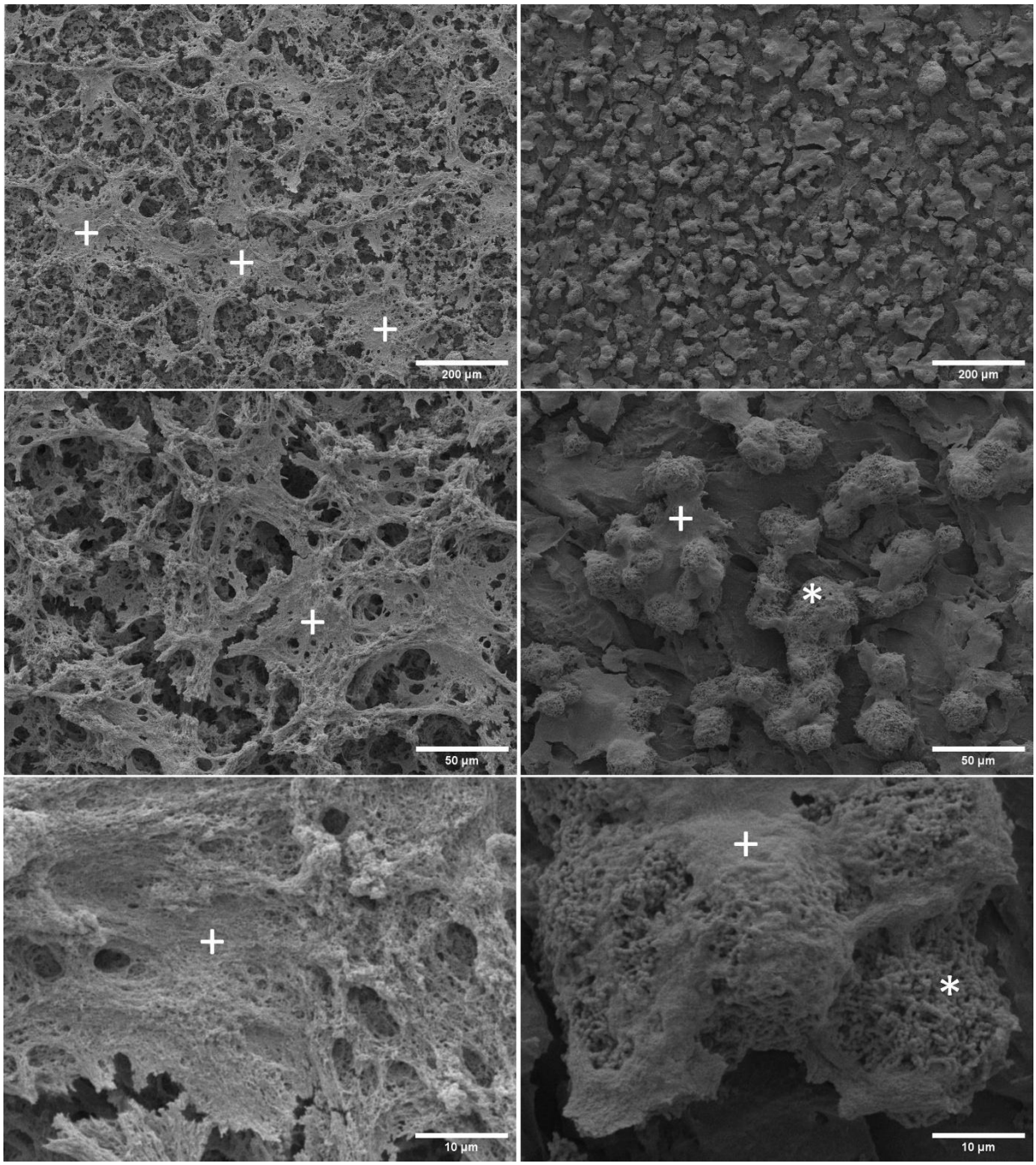

Figure 4.13 SEM micrographs of *Streptococcus mutans* biofilms before and after dextranase treatment.

Biofilms were grown in 1% (w/v) sucrose and 1 µM Alexa Fluor™ conjugated dextran supplemented medium. The images on the left show untreated biofilms (at different magnifications) and reveal a complex arrangement and coverage by an extensive extracellular matrix (+). The images on the right show biofilms following 0.25% dextranase treatment, with notable disruption of the matrix and exposure of microcolonies (*). Each row pair of images represents identical magnification, demonstrating the degradation of the matrix and the altered biofilm structure after treatment.

4.3.4.4 Lightsheet Confocal Raman Microscopy analysis to characterise the EPS and assess the efficacy of dextranase disruption

LCRM and FSC³ algorithm, enabled the generation of spectral component maps representing distinct chemical structures within the biofilm. After data acquisition (Figure 4.14A), the FSC³ algorithm was applied to the fingerprint region (450–2000 cm^{-1}) to decompose the hyperspectral dataset into individual spectral components (Figure 4.14B). Raman spectra were analysed using KnowItAll software to compare the obtained spectral data with reference libraries. However, no direct matches were found within the database, indicating that the detected spectral features did not correspond to any compounds available in the software's spectral library. The spectral components retrieved via FSC^3 did however closely resemble the Raman spectra of *S. mutans* measured by Gieroba et al. (2020), providing confidence in the FSC^3 results.

The spatial concentration maps generated from CRM and the FSC^3 algorithm (Figure 4.14 C&D) were used to analyse the efficacy of dextranase treatment on *S. mutans* biofilms. The component selected for analysis was primarily localised in regions between microcolonies (Figure 4.14D), where the glucan network was expected to be most prominent. Quantitative image analysis was performed using ImageJ to measure the intensity of this component across dextranase treated and untreated samples. The results revealed significant ($p = 0.009$) reduction in the intensity of the glucan-associated spectral component following 0.25% dextranase treatment, indicating enzymatic degradation of the biofilm matrix (Figure 4.15).

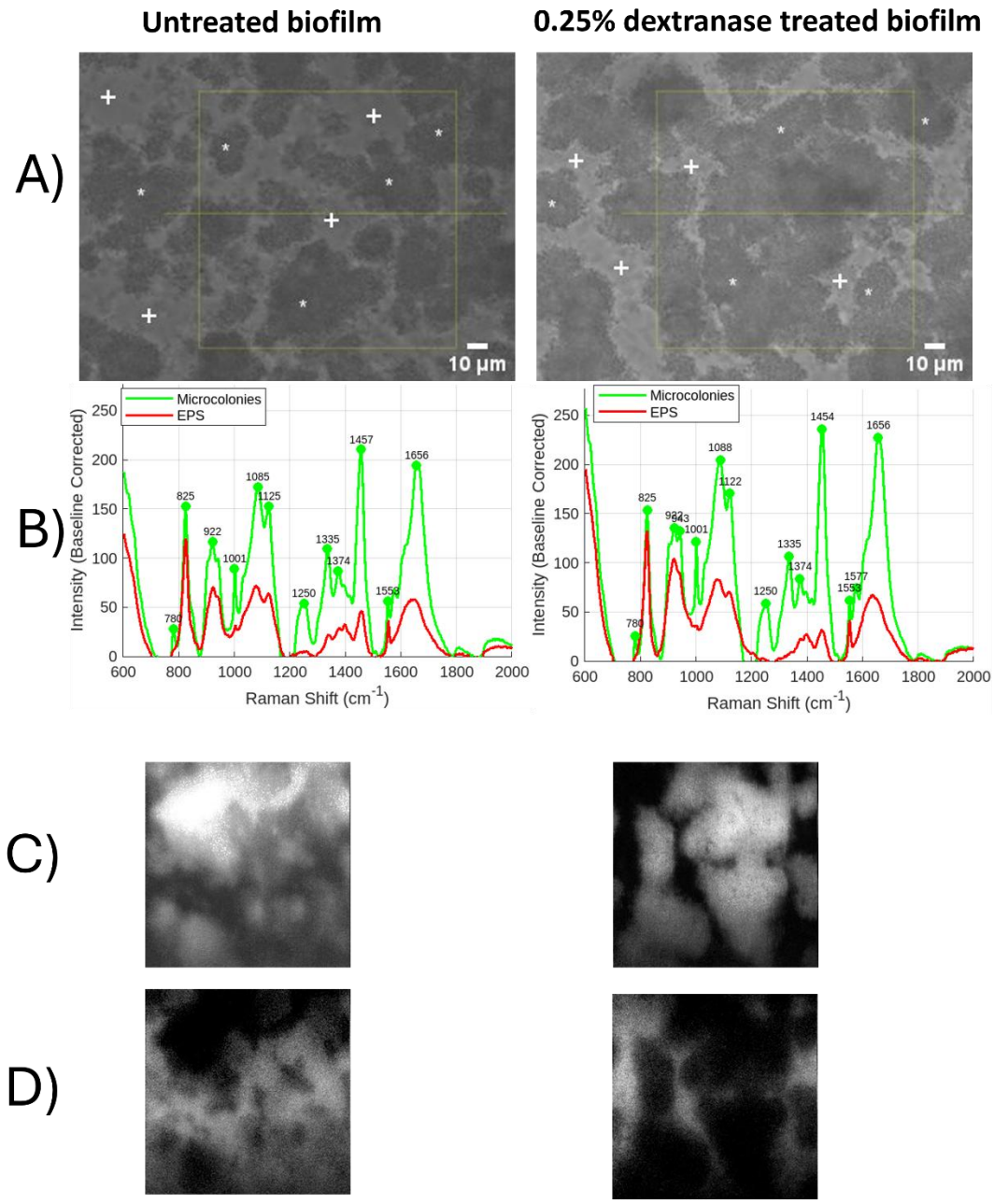

Figure 4.14 Representative Confocal Raman Microscopy analysis of dextranase treatment on *Streptococcus mutans* biofilms.

Biofilms grown in tryptone soy broth supplemented with 1% (w/v) sucrose and 1 µM dextran comparing untreated and 0.25% dextranase treated biofilms. (A) Brightfield images (40× magnification) of untreated (left) and 0.25% dextranase treated (right) biofilms with white asterisks (*) indicating Raman acquisition points of microcolonies region, while crosses (+) indicate points of EPS region. (B) Raman spectra retrieved from microcolony regions (green) and EPS regions (red). (C) Concentration maps derived from CRM analysis showing spatial distribution of selected components within microcolony regions of untreated (left) and treated (right) biofilms. (D) Concentration maps derived from CRM analysis showing spatial distribution of selected components within EPS regions of untreated (left) and treated (right) biofilms.

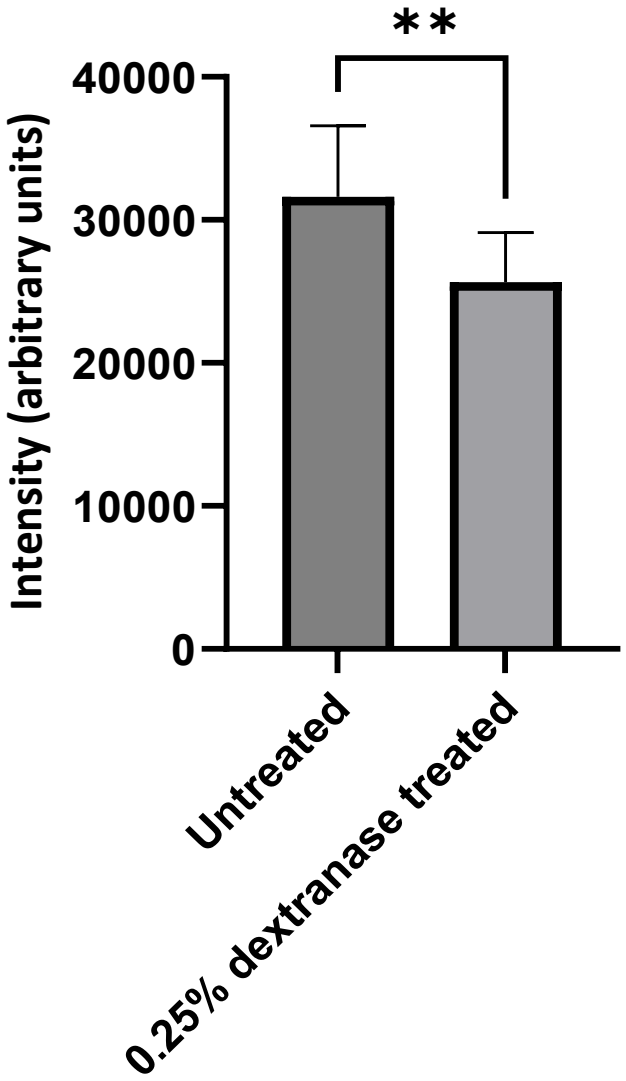

Figure 4.15 Mean intensity values of chemical glucan concentration maps generated using Confocal Raman Microscopy and FSC³ of untreated and 0.25% dextranase (v/v) treated *Streptococcus mutans* biofilms.

Biofilms were grown in 1% (w/v) sucrose and 1 µM dextran supplemented medium. Data represent the average intensity ± standard deviation. A significant reduction in intensity was observed in enzyme-treated biofilms compared to controls ($p = 0.009$), highlighting dextranase degradation of the glucan matrix.

4.4 Discussion

The EPS of biofilms is recognised as a fundamental component of biofilm architecture, providing structural integrity, and facilitating adhesion and protection for microbial communities (Serrage et al. 2021). The research presented in this Chapter sought to detect and quantify the EPS in biofilms and assess the ability of enzymatic treatment to disrupt it. This would then inform subsequent research (Chapter 5) on assessing EPS' role in antimicrobial resistance of biofilms.

Results showed that tested biofilms exhibited significantly higher protein ($p < 0.001$, in all conditions) and carbohydrate levels ($p < 0.001$), in all tested conditions except for mixed bacteria cultures ($p = 0.69$) per unit cell compared to planktonic equivalents, suggesting an increased EPS production during biofilm formation. Carbohydrates and proteins are recognised as major components of the EPS matrix in oral biofilms, where they contribute to structural stability, adhesion, and enzymatic activity (Karygianni et al. 2020b; Jakubovics et al. 2021; Costa et al. 2023). EPS components such as polysaccharides, proteins, and eDNA contribute to biofilm resilience by creating a viscoelastic matrix with water retentive properties, providing protection against environmental stressors including antimicrobial agents and shear forces (Karygianni et al. 2020b).

In the present study, carbohydrate content was elevated in biofilms compared to planktonic cells. This finding was expected, as polysaccharides are well established as the main component of the EPS matrix in oral biofilms (Cugini et al. 2019). Glucan is considered to be the main EPS component in cariogenic biofilms (Chen et al. 2020), and acts as the primary structural framework, particularly in biofilms containing oral streptococci, facilitating microbial adhesion to surfaces and promoting microbial coaggregation, leading to the

formation of a dense, protective biofilm (Leme et al. 2006; Bowen et al. 2018). In the oral cavity, glucan is synthesised from sucrose by glucosyltransferases (Gtfs) that bind to enamel surfaces coated with the salivary pellicle (Koo et al. 2013; Guo et al. 2015). Glucan can facilitate microbial cell adhesion to the tooth surface through interactions with adhesins such as glucan-binding proteins (Gbps) expressed on the bacterial surface (Marin et al. 2025).

The increased protein content (relative to cell number) in biofilms compared with planktonic cultures suggests involvement of proteins in the EPS matrix. In the EPS, proteins contribute to cell-cell interactions, enzymatic activity, and biofilm maturation, playing roles in structural integrity and adaptation to external physical forces (Flemming et al. 2023). In contrast, planktonic cells exist in a 'free floating' state where extensive EPS production would not be necessary for persistence, as the cells do not require matrix scaffolding or surface adhesion (Shree et al. 2023). Instead, these cells prioritise mobility and adaptability to locate favourable conditions, rather than investing resources in EPS synthesis (Moore-Ott et al. 2022). This would explain the lower protein and carbohydrate concentrations (per cell) observed in planktonic cultures. The observed differences between biofilm and planktonic EPS aligns with previous research, which showed that planktonic cells produced less EPS compared to their biofilm counterparts (Kives et al. 2006). This study of *Pseudomonas fluorescens* employed EPS extraction methods prior to quantification using colorimetric assays, revealing that biofilms produced significantly more EPS with 3-to-4-fold increase in polysaccharides and proteins. The authors report that their data were normalised based on dry weight of remaining sample after extraction (Kives et al. 2006).

A recent study of *Nitrosomonas europaea*, an aerobic ammonia oxidising bacterium involved in nitrification, compared EPS production in biofilms and planktonic cells (Oshiki et al. 2023).

The bacterium was grown in two different media, with biofilm formation occurring in nutrient rich medium, while planktonic growth was obtained using a medium that does not promote surface attachment or biofilm formation. Their results showed that biofilm associated cells produced significantly more EPS than planktonic cells, with statistically significant increase in carbohydrate, protein, and uronic acid content per wet biomass weight (mg/g wet cells).

As proteins are recognised as key component of EPS in oral biofilms, a study by Klein et al. (2012) examined protein synthesised by *S. mutans* during development of mixed species biofilm containing *S. oralis* and *Actinomyces naeslundii*. The research identified several proteins involved in EPS production and biofilm formation and remodelling, including glucosyltransferases that synthesise glucans and fructosyltransferase and fructan hydrolase which contribute to fructan metabolism, which act as nutrient reserves and contributes to biofilm hydration. Also, surface associated glucan-binding, such as GbpB, facilitate adhesion and attachment within the biofilm, as well as dextranase involved in glucan remodelling (Klein et al. 2012).

When comparing the extent of change in EPS components from planktonic to biofilm states, *S. mutans* grown in the presence of sucrose demonstrated an increase in carbohydrate content relative to protein. Carbohydrate content of *S. mutans* biofilms increased by more than 100-fold compared to planktonic, whereas protein content increased approximately 60-fold. This highlights the targeted production of polysaccharides in presence of sucrose, as it is a key factor in synthesis of glucan (Decker et al. 2014). Presence of sucrose allows for glucan production along with it being an energy source for *S. mutans* cells (Costa Oliveira et al. 2021). In contrast, protein content increase could be reflective of biomass increase, or accumulation

and retention of enzymes within biofilms, as enzymes can be detected using BCA assays (Mrigwani et al. 2023).

The EPS used in this Chapter was not extracted from cellular material, which is experimentally challenging, and demands chemical, physical, or physicochemical treatments that can compromise the integrity of the EPS or result in co-extraction of intracellular materials (Hasan et al. 2024). Since the aim of the study was to compare biofilms with their planktonic counterparts, EPS extraction was avoided to prevent introducing inconsistencies by such procedures. Biofilm quantities were normalised to cell number by applying qRT-PCR to determine bacterial cell numbers. qRT-PCR-based approaches offer several advantages, including high sensitivity, specificity, and rapid detection of target organisms (Rudi et al. 2005). Importantly, they are valuable in quantifying cells within biofilms, as culture based CFU counts underestimate the number of cells in biofilm samples due to bacterial aggregation, where a group of cells could result in a single colony (Ammann et al. 2013). In contrast, a potential limitation of using qRT-PCR to quantify cells within complex biofilms with a rich matrix is the potential bias introduced during DNA extraction, as incomplete cell lysis or DNA fragmentation, can undermine the accuracy of quantification (Galazzo et al. 2020). However, DNA extraction assays and commercial kits have been developed to mitigate such limitations by introducing mechanical disruption via bead beating and enzymatic agents that selectively degrade non-DNA components of samples (Corcoll et al. 2017). Furthermore, in a mixed species biofilm primer bias may occur, where sequence variations between species lead to preferential amplification of certain taxa over others, resulting in inaccurate representation of species abundance (Piñol et al. 2019; Zhang et al. 2020; Noh et al. 2021). Nevertheless, such limitation can be addressed by validation of universal primers (Nakano 2018).

Based on standardised biofilms, it was evident that biofilms contained more carbohydrate and protein than planktonic cultures. It was assumed that the increased levels of protein and carbohydrate was attributed to EPS production. Furthermore, results indicated that within *S. mutans* biofilms grown in 1% (w/v) sucrose containing medium, carbohydrates constituted a more prominent component of the EPS matrix compared to proteins. This was evident from the higher carbohydrate content of 5.11 µg/10^6 cells relative to protein content of 1.11 µg/10^6 cells.

Given the structural and protective roles of glucan polysaccharides in oral biofilms, enzymatic degradation of glucans would be a promising strategy for EPS disruption. This is particularly relevant in the present study, as sucrose and dextran supplemented biofilms were shown to be rich in glucans, as demonstrated in section 3.3. In this study, dextranase was explored for its ability to degrade glucans and disrupt the biofilm EPS.

Dextranase is an enzyme that degrades dextran, a key glucan component of the EPS in oral biofilms (Hayacibara et al. 2004). Dextranase catalyses the endohydrolysis of α-1,6-glycosidic linkages, degrading dextran into smaller oligosaccharides, such as isomaltose and isomaltotriose (Khalikova et al. 2005; Juntarachot et al. 2020). Dextranase is predominantly produced by bacteria and fungi (Wang et al. 2024). Fungal dextranases are widely used due to their stability and efficiency in degrading high molecular weight dextran. Commercial preparations of dextranase are often derived from species of the fungal genus *Chaetomium*, such as *Chaetomium erraticum* (Eggleston and Monge 2005) *Talaromyces* (Ebaya et al. 2020) and *Penicillium (Wang et al. 2022)*. Notably, *S. mutans* produces dextranase, which is important in glucan metabolism and biofilm regulation (Zheng et al. 2023). By hydrolysing

dextran, smaller oligosaccharides are then ingested by bacteria to produce glucose (Klahan et al. 2018).

In this research, dextranase proved to be an effective enzyme for targeting glucan in the biofilm matrix. CLSM, LCRM and colorimetric assays showed that dextranase significantly reduced the quantity of glucan in treated biofilms. A commercial colorimetric assay showed carbohydrate reduction in the EPS of *S. mutans* biofilms after 0.25% dextranase treatment for 1 h 2.65 µg/10^6 compared to untreated biofilms 5.19 µg/10^6. Furthermore, CLSM and COMSTAT showed that 0.25% dextranase treatment for 1 h, reduced glucan biomass by 74.06% in *S. mutans*, and 79.38% in whole saliva biofilms, and 50.88% in dual species *S. mutans* and *C. albicans* biofilms. However, although EPS was significantly reduced, CLSM images showed no alteration in the structure of microcolonies highlighting that dextranase treatment did not disrupt the cells that had aggregated. This was further supported by COMSTAT analysis, which showed no reduction in the volume of cells between dextranase treated and untreated *S. mutans* biofilms. This agrees with the work undertaken by Juntarachot et al. (2020), who demonstrated that fungal dextranase produced by *Penicillium roquefortii* significantly reduced *S. mutans* biofilm formation. The enzyme exhibited antibiofilm activity, reducing biofilm formation and bacterial cell adhesion, resulting in lower number of cells within the biofilm, as confirmed by CLSM imaging. The antibiofilm effect of dextranase was assessed in a 96-well microplate assay, where *S. mutans* biofilms were grown in presence of crude dextranase. Biofilm biomass reduction was quantified by crystal violet staining, while CLSM imaging provided visual confirmation of biofilm disruption. The authors explored potential use in oral care applications by encapsulating dextranase in sodium alginate beads, with enzyme activity assays showing encapsulated dextranase retained its

function for at least three months at 40°C, demonstrating potential for integration into toothpaste formulations.

LCRM provided complementary, label-free chemical insight into EPS matrix of *S. mutans* biofilms and its susceptibility to enzymatic disruption. Unlike fluorescence-based approaches, Raman spectroscopy enabled the detection of intrinsic molecular vibrations, allowing assessment of EPS associated chemical components without the need for exogenous staining. In this study, FSC³ analysis of the Raman hyperspectral data resolved spectral components predominantly localised to regions between microcolonies, consistent with areas enriched in extracellular glucan matrix rather than cellular biomass.

Although direct sample identification was not achieved through comparison with existing spectral libraries, the extracted spectral profiles closely resembled Raman spectra previously reported for *S. mutans* biofilms (Gieroba et al. 2020). This similarity supports the assignment of the analysed spectral component, while also highlighting a limitation of Raman library-based identification for complex biological samples, where reference spectra for heterogeneous biofilm are limited. However, quantitative analysis of the FSC³ derived concentration maps demonstrated a significant reduction in intensity of regions with glucan-associated spectral component following dextranase treatment. Importantly, the Raman-based observations corroborate trends identified using CLSM and colorimetric assays, providing independent chemical evidence of EPS disruption.

It is widely reported that single enzyme approaches often show limitations in targeting mature biofilms (Olaimat et al. 2024). While enzymes such as DNase I, glycoside hydrolases, and proteases can effectively degrade specific EPS components, they are rarely successful in complete biofilm removal (Upadhyay et al. 2023). As a result, some researchers have explored

the potential of combining multiple enzymes to target the major components of the EPS. One study investigated the effects of DNase I and proteinase K on biofilm integrity and microbial composition of multispecies oral biofilms grown in a batch culture system (Karygianni et al. 2020a). The inoculum included equal proportions of *S. mutans, S. oralis, Actinomyces oris, Fusobacterium nucleatum, Candida albicans*, and *Veillonella dispar*. To simulate dynamic nutrient conditions, 0.3% glucose was provided for the first 16 h, followed by 0.15% glucose + 0.15% sucrose from 16 to 64 h, and biofilms were grown on hydroxyapatite coupons. CLSM results demonstrated that combined DNase I and proteinase K treatment was more effective than single enzyme treatment. The combined treatment led to a more pronounced disruption of the biofilm structure, with less matrix and fewer remaining cells compared to individual enzyme applications.

In a separate study, the effectiveness of mutanase, β-glucanase, and DNase, both individually and in combination, was assessed for preventing and removing saliva derived biofilms *in vitro* (Dukanovic Rikvold et al. 2024). The study explored whether targeting multiple EPS components simultaneously would enhance biofilm disruption compared to single-enzyme treatments. Saliva collected from healthy donors was used to grow biofilms on polystyrene 96-well plates under aerobic conditions for 24 h in 5% sucrose and sterile saliva supplemented medium. Experiments assessed biofilm inhibition, where enzymes were added during growth, in addition to biofilm disruption, where enzymes were applied after biofilm development and maturation. Results showed that mutanase was the most effective enzyme, reducing biofilm formation by over 90% and removing up to 73.2% of established biofilms. DNase and β-glucanase had moderate effects on biofilm inhibition (36.9% and 48.2% reduction, respectively), whilst when used in combination there was an additive effect, reducing biofilm formation by 81.0%. For biofilm disruption, DNase alone had no significant impact, while β-

glucanase led to 25.6% biofilm reduction, and their combination did not enhance biofilm disruption. CLSM analysis showed that enzymatic treatments significantly reduced polysaccharides (glucans), particularly with mutanase, but eDNA abundance remained unchanged, suggesting it played a minor role in the structural integrity of these biofilms. Additionally, enzyme treatments did not inhibit planktonic bacterial growth, confirming that their effects were due to matrix degradation rather than direct bactericidal activity (Dukanovic Rikvold et al. 2024).

In the current study, application of dextranase to developed biofilms primarily reduced the matrix without significantly altering the cellular structure of biofilms, suggesting that single enzyme treatment using dextranase was not sufficient for complete biofilm eradication. Although a single enzyme approach could be considered limited, due to its limited disruption of cells, it does propose a benefit in clinical settings; uncontrolled bacterial release from an established biofilm could lead to systemic infections or colonisation of new sites, making treatments less effective and potentially worsening infections (Yu and Chua 2020).

A study by Fleming & Rumbaugh (2018) highlighted the potential dangers of biofilm dispersal in wound infections. The research investigated the effects of glycoside hydrolases, enzymes that degrade biofilm exopolysaccharides, on *Pseudomonas aeruginosa* and *Staphylococcus aureus* biofilms in a mouse wound model. While enzymatic treatment successfully disrupted the biofilm structure, it also triggered rapid bacterial dispersal, leading to lethal septicaemia in the absence of antibiotics. However, combining enzymatic treatment with antibiotics effectively prevented septicaemia. When glycoside hydrolases were administered alongside systemic or topical meropenem, bacterial dissemination was controlled, and infection clearance occurred significantly faster compared to antibiotic treatment alone. This highlights

the importance of pairing enzymatic biofilm disruption with antimicrobial agents to prevent dispersed bacterial cells evading immune surveillance or colonising new sites (Fleming and Rumbaugh 2018).

Dextranase disruption of glucan is well established as it randomly cleaves glycosidic bonds (Barzkar et al. 2022). Work presented in this Chapter aligns with existing literature regarding the ability of dextranase to disrupt biofilm structure by degrading the matrix, however, dextranase may also offer a preventative strategy, interfering with biofilm formation at an early stage. In the present study, results showed that adding dextranase during biofilm formation inhibited both microcolony aggregation and glucan assembly as shown in Figure 4.9, suggesting that dextranase mediated biofilm control extends beyond glucan degradation alone.

In a study by Lynch et al. (2007), glucan binding proteins (Gbps) were shown to play a crucial role in *S. mutans* biofilm architecture. This research demonstrated that GbpC, a surface-bound protein, was essential for dextran dependent aggregation, and facilitating bacterial clustering and microcolony formation. The loss of GbpC in mutant strains led to a significant reduction in biofilm height and bacterial aggregation (Lynch et al. 2007). Similarly, Senpuku et al. (2018) examined the role of GbpC in dextran mediated aggregation and found that dextranase treatment completely abolished aggregation by *S. mutans*. This effect mirrored the loss of aggregation observed in GbpC deficient mutants, suggesting that dextran degradation disrupted GbpC-mediated cell clustering. The findings highlight that GbpC requires intact dextran structures to facilitate bacterial adhesion, reinforcing the idea that dextranase prevents bacterial clustering by interfering with GbpC glucan interactions (Senpuku et al. 2018).

The enzymatic activity of dextranase allows for various established and potential applications across multiple industries. Both the experimental findings presented in this Chapter and the existing literature highlight dextranase's potential in oral healthcare, making it a strong candidate for incorporation into toothpastes and mouthwashes to aid in plaque control by targeting biofilm-associated glucans.

Beyond oral health, dextranase is widely used in the sugar industry, where microbial dextran contamination presents challenges during sugar cane and beet processing (Martínez et al. 2021). Dextran accumulation increases juice viscosity, disrupts crystallisation, and reduces sucrose recovery, affecting overall efficiency (Eggleston and Monge 2005). The enzymatic degradation of dextran significantly enhances processing efficiency and improves product quality (Jiménez 2009). In pharmaceutical and medical applications, dextranase plays a key role in the enzymatic synthesis of low molecular weight dextran, which is used in treatment of anaemia and as a blood plasma expander (Gan et al. 2014). These diverse applications underscore the broad use of dextranase clinically and further support its potential in biofilm control strategies.

In conclusion, carbohydrate and protein levels were found to be higher in biofilms compared to their planktonic counterparts, highlighting the enriched EPS associated with the biofilm development. Dextranase was able to inhibit glucan production and microcolony aggregation in biofilms of *S. mutans*. Furthermore, dextranase was found to disrupt established glucan matrices in *S. mutans*, dual species (*S. mutans* and *C. albicans*) and whole saliva biofilms thereby, exposing embedded cells. In terms of using LCRM in the study of biofilms, this novel technique was able to profile chemical differences within a biofilm. However, identification of components within EPS was challenging since it relies on existing entries in reference libraries.

Nevertheless, LCRM proved to be a valuable approach for assessing EPS degradation using dextranase and is advantageous as non-destructive method in situations where fluorochrome based detection of EPS is not applicable.

Chapter 5

Antimicrobial susceptibility of biofilms and impact of extracellular polymeric substances

5.1 Introduction

Biofilms typically have higher tolerance to antimicrobials compared to planktonic cells (Ciofu et al. 2022) and multiple factors have been associated with this. These biofilm factors include an increased efficiency of horizontal gene transfer including those genes involved in resistance (Madsen et al. 2012), the occurrence of quorum sensing (QS) and physiological heterogeneity of biofilm growth rate that alters metabolism of cells embedded deep within the biofilm resulting in slower growing or dormant cells (Olsen 2015). The latter has relevance as many antimicrobials are more effective against actively growing cells (Liu et al. 2024). QS enhances biofilm tolerance by coordinating the expression of genes involved in stress responses, EPS production, and antimicrobial resistance (AMR), thus promoting a collective defence mechanism against hostile conditions (Elias and Banin 2012; Markowska et al. 2024). However, it is the presence of EPS that is often considered the primary contributor to increasing biofilm antimicrobial tolerance (Hobley et al. 2015).

As described previously, EPS facilitates the persistence of biofilm cells in hostile environments as it promotes surface attachment, cell recruitment, and retention of water, nutrients and enzymes (Liu et al. 2024). In the case of antimicrobial tolerance, EPS has been reported to limit and slow the movement of an antimicrobial through a biofilm through physical/chemical entrapment, electrostatic interaction or enzymatic degradation (Goel et al. 2021).

Chlorhexidine (CHX) is a widely used antimicrobial agent in oral healthcare, particularly in controlling dental plaque and targeting of oral microorganisms (Seguya et al. 2022). CHX has been beneficial in the control of periodontal disease and in the reduction of dental plaque (Brookes et al. 2021). CHX is a cationic bisbiguanide antiseptic that works primarily by degrading bacterial cell membranes (Lim and Kam 2008). The CHX molecule has two positively

charged biguanide groups (Figure 5.1) which allow interaction with negatively charged bacterial surfaces, especially the phospholipid parts of the cytoplasmic membrane (Cieplik et al. 2019). This interaction damages the membrane causing ions, metabolites, ATP and other low-molecular-weight substances to leak out of cells (Cheung et al. 2012). As CHX induced membrane damage progresses, it becomes irreversible and leads to cell death (Deus and Ouanounou 2022). Anionic lipids present in microbial cell membranes promote strong electrostatic interactions with chlorhexidine, whereas such lipids are absent in human cells, conferring selective activity of chlorhexidine against microbial cells (Hubbard et al. 2017).

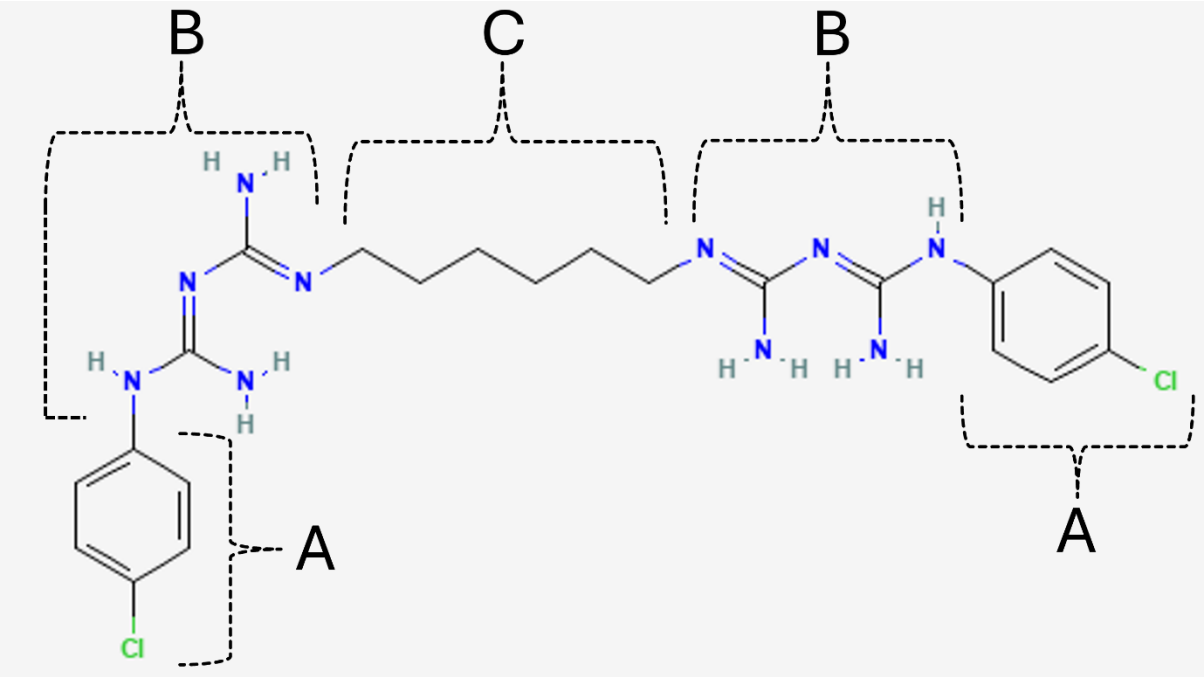

Figure 5.1 Chemical structure of Chlorhexidine (CHX) base.

CHX is a bisbiguanide compound composed of two p-chlorophenyl rings (A), connected by positively charged biguanide groups (B) and a hexamethylene linker (C) (PubChem Identifier: CID 9552079).

Fluconazole (Figure 5.2) is an azole antifungal that is often used to treat both localised and systemic *C. albicans* infections (Barantsevich and Barantsevich 2022). Fluconazole has widely documented efficacy, broad tissue distribution, a wide antifungal spectrum, and low host cell toxicity even in immunocompromised individuals (Martin 1999). Fluconazole antifungal activity occurs via the inhibition of lanosterol 14-α-demethylase, which is an enzyme encoded by the *ERG11* gene (Fandilolu et al. 2024). This enzyme is involved in ergosterol biosynthesis (Song et al. 2004; Silva et al. 2012). The enzyme contains a haem moiety in its active site, with a central iron atom essential for catalysing the oxidative demethylation of lanosterol (Sheng et al. 2009). Fluconazole inhibits the enzyme by means of an unhindered nitrogen, and binding directly to the iron atom, thereby preventing oxygen activation and subsequent demethylation of lanosterol (White et al. 1998). Although mammalian cells express lanosterol 14-α-demethylase as part of cholesterol biosynthesis, fluconazole exhibits lower binding affinity for the mammalian form, due to a water molecule retention of the haem iron of the mammalian enzyme which prevents direct coordination with the drug (Strushkevich et al. 2010).

Despite the antifungal effectiveness of fluconazole, *C. albicans* can develop fluconazole resistance through various mechanisms, including overexpression of efflux pumps, mutations or upregulation of the target, matrix mediated limitation and activation of stress-response pathways (Lu et al. 2021).

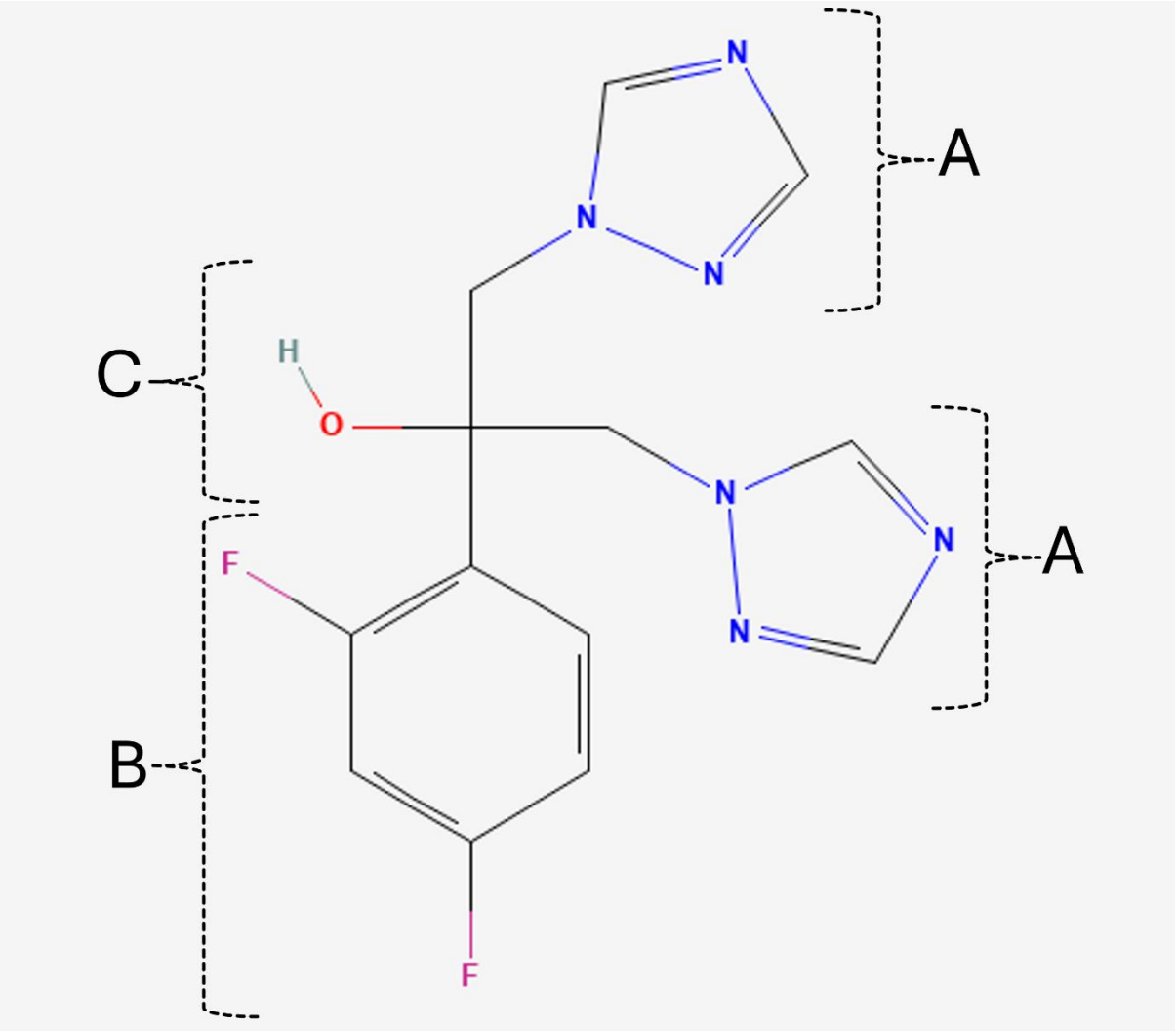

Figure 5.2 Chemical structure of fluconazole.

Fluconazole is an azole antifungal containing A) two triazole rings that essential for interaction with lanosterol 14-α-demethylase, B) a difluoro phenyl group contributing to hydrophobic interactions, and C) a hydroxyl group that enhances solubility (PubChem Identifier: 3365).

While CHX and fluconazole are widely used in clinical settings, evidence shows that AMR can occur (Gow et al. 2022; Van den Poel et al. 2022). The protective and structural qualities provided by EPS to biofilms have proven to be key factors in biofilm associated tolerance. This is increasingly recognised by researchers (Colvin et al. 2011; Ragupathi et al. 2024) and various approaches have been explored to overcome the protective effects of EPS (Pinto et al. 2020). One approach is to use specific enzymes to target EPS, promoting its removal as a barrier and

weakening the integrity of biofilm structure, thereby increasing antimicrobial susceptibility (Upadhyay et al. 2024).

Several approaches have been used to assess AMR and these include use of agar diffusion, gradient diffusion and microdilution assays (Hossain 2024) to measure minimum inhibitory concentrations (MICs) and minimum bactericidal concentrations (MBCs). The MIC is the lowest antimicrobial concentration that inhibits visible growth of a microorganism under defined conditions and can reflect microbiostatic as well as microbiocidal activity. In contrast, the MBC is the minimum concentration required to kill (microbiocidal) microorganisms (Schrader et al. 2023).

While the MIC and MBC are used to measure antimicrobial action against planktonic cells, the minimum biofilm eradication concentration (MBEC) is used to measure the lowest antimicrobial concentration required to eradicate a biofilm. The MBEC is arguably a more relevant measure than the MIC in the context of biofilm-associated infections, as it reflects the higher drug concentrations required to eliminate biofilm embedded cells (Di Bonaventura and Pompilio 2021). In addition to standard antimicrobial assays, the use of fluorescent viability staining with CLSM has proven useful in assessing viability of biofilms. These approaches can quantify both live/dead biofilms cells in conjunction with open-source software (Mountcastle et al. 2021).

5.1.1 Aims

The aims of this Chapter were to investigate the antimicrobial activity of CHX and fluconazole against *Streptococcus mutans* and *Candida albicans*, respectively. The effectiveness of these agents against biofilms was then assessed and the role of EPS in increasing antimicrobial

tolerance of biofilms was determined. The methods of assessment included MIC, MBC, and MBEC assays, alongside enumeration of colony forming units and live/dead staining.

5.2 Material and methods

5.2.1 Susceptibility of *Streptococcus mutans*

5.2.1.1 Minimum Inhibitory Concentration (MIC) of CHX against *Streptococcus mutans*

The minimum inhibitory concentration (MIC) of CHX against *S. mutans* DSM 20523 was measured using a broth microdilution method based on the M07-A10 protocol by Clinical and Laboratory Standards Institute (CLSI 2018).

Four different growth media were used for susceptibility tests and were: (1) Tryptic Soy Broth (TSB), (2) TSB supplemented with 1 µM dextran, (3) TSB with 1% (w/v) sucrose, and (4) TSB supplemented with 1 µM dextran and 1% sucrose. A two-fold serial dilution of CHX was prepared in each of the four types of culture media to give final CHX concentrations ranging from 0.0000125% to 0.0128% v/v (equivalent to 0.125 to 128 µg/ml).

A total of 100 µl of each CHX dilution was added to the wells of a sterile 96-well microtiter plate. An overnight culture of *S. mutans* was standardised by adjusting its optical density with fresh culture medium to 0.1 ± 0.01 at 600 nm (OD_{600}) using a spectrophotometer (DiluPhotometer, Implen, Westlake Village, CA, USA). A 100-µl volume of this bacterial suspension was added to each well, generating in a final volume of 200 µl per well. Growth controls (bacteria in media without CHX) and negative controls (media only) were included in triplicate for each growth condition. Plates were incubated at 37 °C for 24 h. The MIC was identified as the lowest concentration of CHX where no visible change in turbidity was observed compared with controls without organisms. The MIC was also confirmed by adding 30 µl of 0.015% of resazurin dye to each well and incubation for at least 2 h at 37°C. After incubation, the lowest antimicrobial concentration at which no colour change occurred

confirmed the MIC value (Elshikh et al. 2016). MIC measurements were conducted in triplicates on at least three independent occasions for reproducibility.

5.2.1.2 Minimal bactericidal concentration (MBC) of CHX against *Streptococcus mutans*

Resuspended contents from the same wells used to establish the MICs were transferred to sterile tubes containing 2 ml of antimicrobial free TSB, ensuring that chlorhexidine was diluted beyond MIC value, and incubated at 37 °C for 24 h. Following incubation, samples were spread onto antimicrobial-free TSB agar plates and incubated at 37 °C for a further 24 h. The lowest antimicrobial concentration where there was no subsequent regrowth was determined as the MBC.

5.2.1.3 Minimum biofilm eradication concentration (MBEC) of CHX against *Streptococcus mutans*

To establish the MBEC, biofilms were grown by inoculating 100 µl of *Streptococcus mutans* DSM 20523 overnight culture, standardised to OD_{600} = 0.1 ± 0.01 (DiluPhotometer, Implen, Westlake Village, CA, USA), in 96-well flat-bottom microtiter plates. Biofilms were grown in base Tryptic Soy Broth (TSB) medium as well as three supplemented media. The supplemented media were: (1) TSB with 1 µM dextran, (2) TSB with 1% sucrose, and (3) TSB containing 1 µM dextran and 1% sucrose. Biofilm growth was achieved by incubation at 37°C for 24 h to allow biofilm formation. After incubation, the medium was removed, and the wells gently washed (x3) with 100 µl sterile phosphate-buffered saline (PBS) to remove non adherent cells. CHX was serially diluted two-fold to produce a concentration range of 0.0000125% to 0.0128% (v/v) (equivalent to 0.125 to 128 µg/ml) and these concentrations were added to the biofilms in the microtiter plate well. Plates were then incubated for an additional 24 h at 37°C. Following incubation, the wells were washed (x3) with PBS to remove residual CHX.

Subsequently, 200 µl of fresh TSB was added to each well, and plates were incubated for an additional 24 h at 37°C.

Bacterial regrowth was assessed by scraping each well content and resuspended in 2 ml of fresh medium. The MBEC was the lowest antimicrobial concentration that yielded no visible growth. All assays were performed in biological triplicates and repeated three times for reproducibility.

To evaluate the effect of disrupting EPS on CHX susceptibility, biofilms were either treated with 0.25% dextranase during or after growth. In the former, dextranase was added directly to the inoculum at the start of biofilm growth. In the case of the latter, the biofilms were gently washed with PBS and 200 µl of 0.25% dextranase (or sterile distilled water as a control) was added and incubated at 37 °C for 1 h. After dextranase treatment, the wells were washed (x3) with PBS prior to CHX treatment described earlier in this section.

5.2.1.4 Live/dead staining and confocal laser scanning microscopy assessment of CHX treatment

Analysis of the role of EPS in *S. mutans* DSM 20523 viability in CHX treated biofilms using live/dead staining and CLSM. Biofilms were grown on sterile polycarbonate (PC) coupons with cultures of *S. mutans* adjusted to an optical density of 0.1 ± 0.01 at 600 nm (OD_{600}) prepared using a spectrophotometer (DiluPhotometer, Implen, Westlake Village, CA, USA). Biofilms were incubated at 37°C for 24 h under static conditions in 24 well plates in TSB, or TSB supplemented with 1% sucrose and label-free dextran (Invitrogen™ D1860, Fisher Scientific, Leicestershire, United Kingdom Scientific). After incubation, coupons were carefully rinsed with sterile PBS to remove planktonic cells. Coupons were then immersed in either 0.25% dextranase (v/v) or sterile distilled water (control) and incubated at 37 °C for 1 h. For

dextranase added during biofilm formation, 0.25% (v/v) dextranase was added to medium prior to incubation. Following treatment, coupons were again washed gently with PBS and exposed to 16 µg/mL CHX for an additional 24 h. Following treatment, coupons were stained using the LIVE/DEAD BacLight Bacterial Viability Kit (Invitrogen™ L7007, Fisher Scientific, Leicestershire, United Kingdom) following the manufacturer's instructions and visualised using a confocal laser scanning microscope (Carl Zeiss, Germany). Z-stack images were acquired and analysed as described in section 2.2.9.4.

5.2.2 Susceptibility of *Candida albicans*

5.2.2.1 Minimum Inhibitory Concentration (MIC) of CHX and fluconazole against *Candida albicans*

To assess antifungal susceptibility of *C. albicans* SC5314, fluconazole (F8929, Sigma-Aldrich, Burlington, Massachusetts, United States) was dissolved in water to a two-fold dilution series ranging from 256 to 0.125 µg/ml, and CHX concentrations ranging from 0.0000125% to 0.0128% v/v (equivalent to 0.125 to 128 µg/ml). The MIC of CHX and fluconazole were determined by broth microdilution method using different media conditions as described in 5.2.1.1.

5.2.2.2 Minimum fungicidal concentration (MFC) of CHX and fluconazole against *Candida albicans*

Resuspended contents from the same wells used to establish the MICs were transferred to sterile tubes containing 2 ml of antimicrobial free TSB, ensuring that antimicrobial agent was diluted beyond MIC value, and incubated at 37 °C for 24 h. Following incubation, samples were spread onto antimicrobial-free TSB agar plates and incubated at 37 °C for a further 24 h. The

lowest antimicrobial concentration where there was no subsequent regrowth was determined as the MFC.

5.2.2.3 Minimum biofilm eradication concentration (MBEC) of CHX and fluconazole against *Candida albicans*

The MBEC of both CHX and fluconazole against *C. albicans* SC5314 was determined as described in section 5.2.1.3.

5.2.3 *Streptococcus mutans* and *Candida albicans* dual species biofilm susceptibility

5.2.3.1 Enumeration of *Candida albicans* colony forming units to assess fluconazole activity against dual species biofilms

Overnight growth of *Streptococcus mutans* DSM 20523 and *C. albicans* SC5314 were respectively standardised using Tryptic Soy Broth (TSB) to OD_{600} = 0.10 ± 0.01 and *C. albicans* growth to OD_{600} = 1.00 ± 0.10 (DiluPhotometer, Implen, Westlake Village, CA, USA). Equal volumes of these standardised cultures to prepare the inoculum for biofilm growth. A 200 µl volume of the mixed suspension was added to each well of a sterile 96-well flat-bottom plate containing TSB supplemented with 1% sucrose. Plates were statically incubated at 37°C for 24 h for biofilm formation.

Following incubation, non-adherent cells were removed, and biofilms were gently washed (x3) with sterile PBS. Then, 200 µl of 0.25% dextranase or sterile distilled water (control) was added for 1 h at 37°C, followed by washing (x3) in PBS. A 200-µl volume of fluconazole (256 µg/ml) in 1% dimethyl sulfoxide (DMSO) was added to each well, while control wells received an equivalent volume of the corresponding medium containing 1% DMSO, and incubated for 24 h at 37°C. After treatment, wells were washed again, and biofilms were mechanically

resuspended by repeat pipetting and scraping. The contents of each well were transferred to tubes containing 1 ml of TSB and incubated for an additional 24 h at 37°C. The preparations were then serial decimally diluted and plated on using an on Sabouraud dextrose agar (SDA) automatic spiral plater (Whitley Automatic Spiral Plater, Don Whitley Scientific, UK), which was incubated at 37°C for 24 to 48 h. Colony forming units (CFU) were enumerated and used as a measure of *C. albicans* viability after treatment. All experiments were done in triplicate and repeated on three separate occasions.

5.2.4 Statistical analysis

Statistical analyses were performed using GraphPad Prism 10.1.0 (GraphPad Software, Boston, Massachusetts USA, www.graphpad.com). Data were assessed for normality using Shapiro-Wilk test. One-way analysis of variance (ANOVA) with Tukey Post-Hoc test was used to compare the different groups.

5.3 Results

5.3.1 Susceptibility of *Streptococcus mutans*

5.3.1.1 Minimum Inhibitory Concentration (MIC) of chlorhexidine (CHX) against *Streptococcus mutans*

The MIC for CHX against *S. mutans* DSM 20523 cultured in different media are summarised in Table 5.1. Results showed that the MIC of *S. mutans* cultured in tryptic soy broth (TSB) alone was 0.25 μg/ml, and was not altered in medium supplemented with sucrose and/or dextran did not alter the MIC (0.25 μg/ml).

5.3.1.2 Minimal bactericidal concentration (MBC) of CHX against *Streptococcus mutans*

MBC of CHX against *S. mutans* was consistent among the different media conditions tested with a concentration of 2 μg/ml (Table 5.1).

5.3.1.3 Minimum biofilm eradication concentration (MBEC) of CHX against *Streptococcus mutans*

Susceptibility of *S. mutans* to CHX was higher for biofilms compared to planktonic growth as shown by increased concentration of MBEC required to eradicate biofilms (Table 5.1). The MBEC of *S. mutans* in TSB medium alone and in TSB supplemented with dextran was 16 μg/ml. In medium supplemented with 1% sucrose with or without dextran, the MBEC was 32 μg/ml (Table 5.1).

Whilst dextranase (0.25%) treatment post biofilm growth did not alter the MBEC, addition of dextranase during biofilm growth resulted in lower MBEC (4 or 16 μg/ml) compared with that of no dextranase treatment (16 or 32 μg/ml; Table 5.1).

Table 5.1 Susceptibility of *Streptococcus mutans* to chlorhexidine digluconate (CHX)

Medium	MIC[1]	MBC[1]	MBEC[1]		
			No dextranase treatment	0.25% dextranase treatment post growth	0.25% dextranase treatment during growth
Tryptic Soy Broth (TSB)	0.25	2	16	16	4
TSB + Dextran (1 µM)	0.25	2	16	16	4
TSB + Sucrose (1%)	0.25	2	32	32	16
TSB + Dextran + Sucrose	0.25	2	32	32	16

[1] Values are in µg/ml; MIC, minimum inhibitory concentration; MBC, minimal bactericidal concentration; MBEC, minimum biofilm eradication concentration; TSB, tryptic soy broth. Each condition was tested in triplicate at three different occasions.

5.3.1.4 Live/dead staining assessment of *S. mutans* susceptibility to chlorhexidine

Live/dead staining using CLSM was used to evaluate the effect EPS degradation on the susceptibility of *S. mutans* biofilms to CHX (Figure 5.3). Biofilms grown in Tryptic Soy Broth (TSB) medium supplementation with 1% (w/v) sucrose and 1 µM dextran developed a more complex and structured architecture, consistent with enhanced EPS production as established in Chapter 3. When these sucrose supplemented biofilms were exposed to 0.25% dextranase for 1 h prior to 16 µg/ml CHX treatment (Figure 5.3A), a proportion of red stained cells was observed, indicating cell death. In comparison, biofilms grown under the same conditions but treated with CHX alone (16 µg/ml), without prior dextranase exposure (Figure 5.3B), displayed less red fluorescence, indication reduced antimicrobial effects. Biofilms grown in TSB and treated with CHX (16 µg/ml), exhibited a less complex structure and predominantly red staining (Figure 5.3C), indicating a higher degree of cell killing. The untreated control biofilm grown in 1% sucrose supplemented TSB (Figure 5.3D) had a dense, viable structure with minimal red fluorescence.

Statistical analysis showed that biofilms without dextranase treatment prior to CHX treatment had a significantly higher percentage of viable biomass compared to biofilms treated with 0.25% dextranase post biofilm formation, and both biofilms had significantly higher percentage of viable biomass compared to biofilms grown with dextranase added during formation ($p < 0.001$; Figure 5.4). Full dataset of values showing viability percentage of *Streptococcus mutans* biofilms treated with dextranase and CHX is listed in Appendix II.

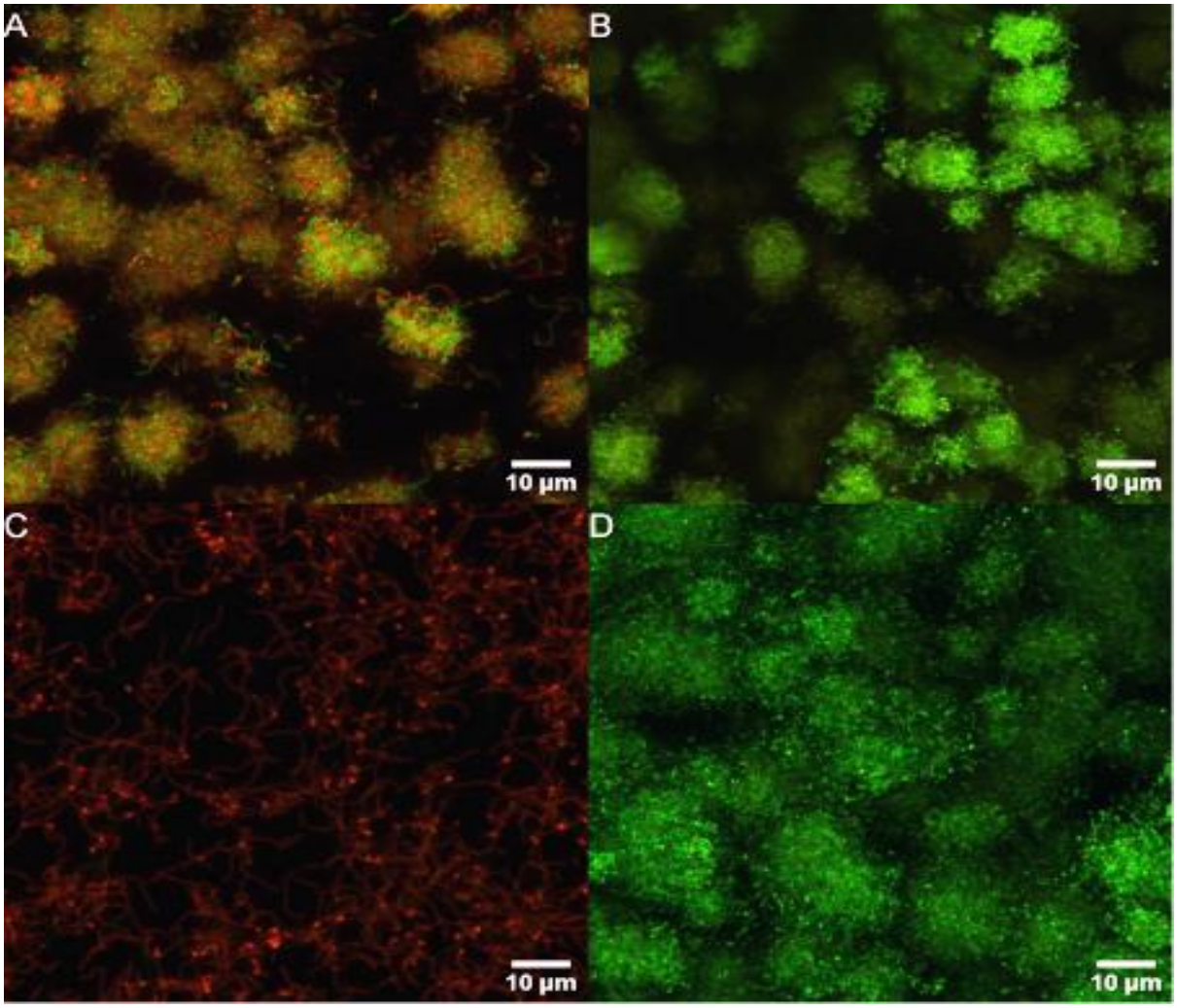

Figure 5.3 Effect of 0.25% dextranase treatment on *Streptococcus mutans* biofilms treated with chlorhexidine (CHX).

A) Biofilm grown in sucrose supplemented TSB for 24 h then exposed to 0.25% dextranase for 1 h followed by CHX (16 µg/ml) for 24 h. **B)** Biofilm grown in 1% (w/v) sucrose supplemented TSB for 24 h then exposed to water for 1 h followed by CHX (16 µg/ml) for 24 h. **C)** Biofilm grown in 1% sucrose supplemented TSB and 0.25% dextranase added during growth for 24 h then treated with CHX (16 µg/ml) treatment for 24 h. **D)** Untreated biofilm grown in 1% sucrose supplemented medium for 24 h. Biofilms were stained with Live/Dead BacLight (ThermoFisher) and viewed under x400 magnification.

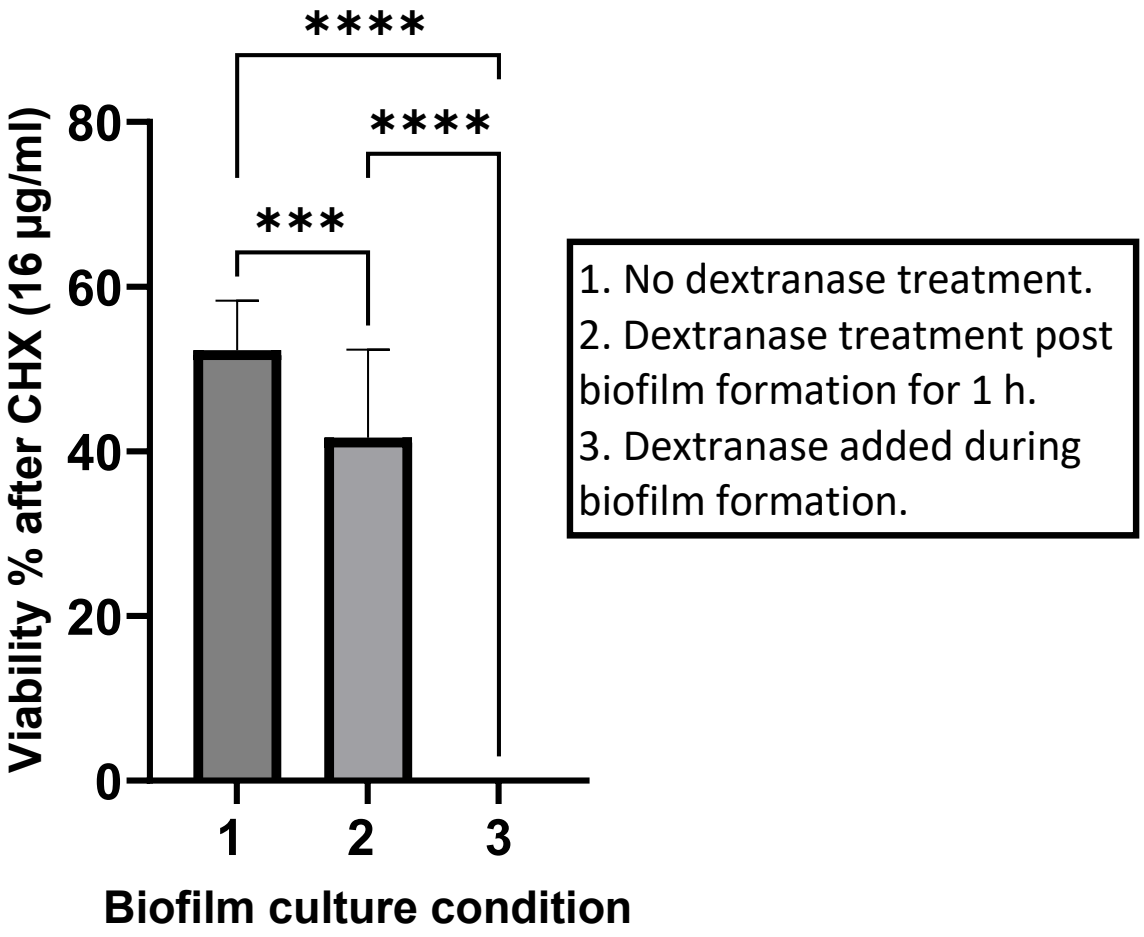

Figure 5.4 Percentage biofilm cell viability of *Streptococcus mutans* after chlorhexidine (CHX; 16 µg/ml) treatment.

Biofilms without dextranase treatment prior to CHX treatment had a significantly higher percentage of viable biomass compared to biofilms treated with 0.25% dextranase post biofilm formation, and both biofilms had significantly higher percentage of viable biomass compared to biofilms grown with dextranase added during formation ($p < 0.001$). Viability was calculated using COMSTAT analysis of CLSM images as the ratio of live cells (stained with SYTO9) to total biomass (live cells stained with SYTO9 and dead cells stained with propidium iodide. Data represent the mean ± standard deviation independent Z stacks (n = 15).

5.3.2 Susceptibility of *Candida albicans*

5.3.2.1 Minimum Inhibitory Concentration (MIC) of CHX and fluconazole against *Candida albicans*

The MICs for CHX against *C. albicans* SC5314 cultured in different media are summarised in Table 5.2. Results show that MICs were the same in tryptic soy broth (TSB) and in TSB supplemented medium with sucrose and/or dextran (8 µg/ml).

Fluconazole ranging from 256 to 0.125 µg/ml was not found to inhibit planktonic *C. albicans* growth in any tested media, thereby yielding no MIC value.

5.3.2.2 Minimum fungicidal concentration (MFC) of CHX and fluconazole against *Candida albicans*

The MBC of CHX against *C. albicans* SC5314 was the same for different media and was 8 µg/ml (Table 5.2). Tested concentrations ranging from 256 to 0.125 µg/ml of fluconazole did not eradicate planktonic cells of *C. albicans* in the tested media, resulting in no MFC value.

5.3.2.3 Minimum biofilm eradication concentration (MBEC) of CHX and fluconazole against *Candida albicans*

Susceptibility of *C. albicans* to CHX was higher in biofilms compared with planktonic growth as shown by increased concentration of 32 µg/ml required to eradicate biofilms (Table 5.2). Tested concentrations of fluconazole ranging from 256 to 0.125 µg/ml did not eradicate *C. albicans* biofilms in any of tested media, resulting in no MBEC.

Table 5.2 Susceptibility of *Candida albicans* to chlorhexidine digluconate (CHX)

Medium	MIC[1]	MFC[1]	MBEC[1]
Tryptic Soy Broth (TSB)	8	8	32
TSB + Dextran (1 µM)	8	8	32
TSB + Sucrose (1%)	8	8	32
TSB + Dextran + Sucrose	8	8	32

[1] Values are in µg/ml; MIC, minimum inhibitory concentration; MBC, minimal fungicidal concentration; MBEC, minimum biofilm eradication concentration; TSB, tryptic soy broth. Each condition was tested in triplicate at three different occasions.

5.3.3 Enumeration of *Candida albicans* colony forming units to assess fluconazole activity against dual species biofilms

To assess the role of EPS in dual species biofilm, *C. albicans* SC5314 cultured with *S. mutans* DSM 20523 in 1% sucrose supplemented medium was treated with fluconazole (256 µg/ml). This concentration was selected as increasing fluconazole concentrations produced a progressive reduction in visible growth despite no definitive MIC, MFC or MBEC was established. Resulting CFU results of recovered biofilms were significantly lower ($p < 0.001$) for biofilms treated with 0.25% dextranase and biofilms grown in absence of sucrose, compared with control treated with distilled water (Figure 5.5).

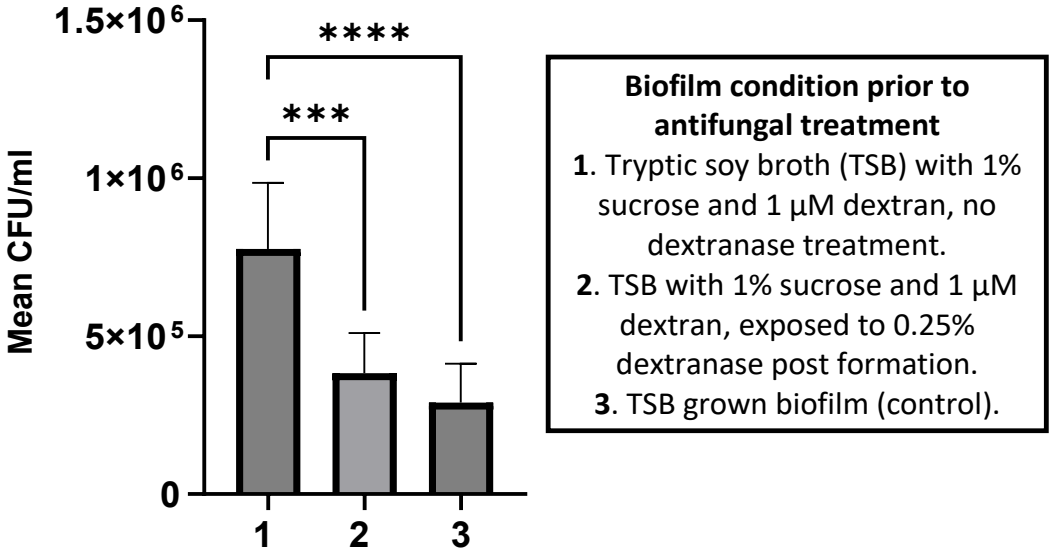

Figure 5.5 Mean number of colony forming units (CFUs)/ml of *Candida albicans* recovered from dual species biofilms with *Streptococcus mutans* and treated with fluconazole (256 µg/ml).

Condition 1 biofilm was grown in 1% sucrose and 1 µM dextran supplemented tryptone soy broth (TSB) and exposed to distilled water for 1 h prior to fluconazole treatment. Condition 2 biofilm was grown in 1% sucrose and 1 µM dextran supplemented TSB and exposed to 0.25% dextranase after EPS accumulation for 1 h prior to fluconazole treatment. Condition 3 biofilm was grown in TSB medium with no supplementation and no prior enzymatic treatment. Both condition 2 and 3 were significantly lower than condition 1 ($p < 0.001$).

CLSM imaging of dual species biofilms revealed the spatial distribution of *C. albicans* and *S. mutans* and their association with the glucan matrix under sucrose supplemented conditions (Figure 5.6). Biofilms were grown in TSB supplemented with 1% sucrose and 1 µM Alexa Fluor™ 647 conjugated dextran to visualise EPS production. Calcofluor white staining identified *C. albicans* yeast and hyphal cells, while green represents cells of *S. mutans* biofilm forming microcolonies clusters stained with SYTO9. Notably, both *S. mutans* microcolonies and fungal structures were embedded within a red stained glucan matrix.

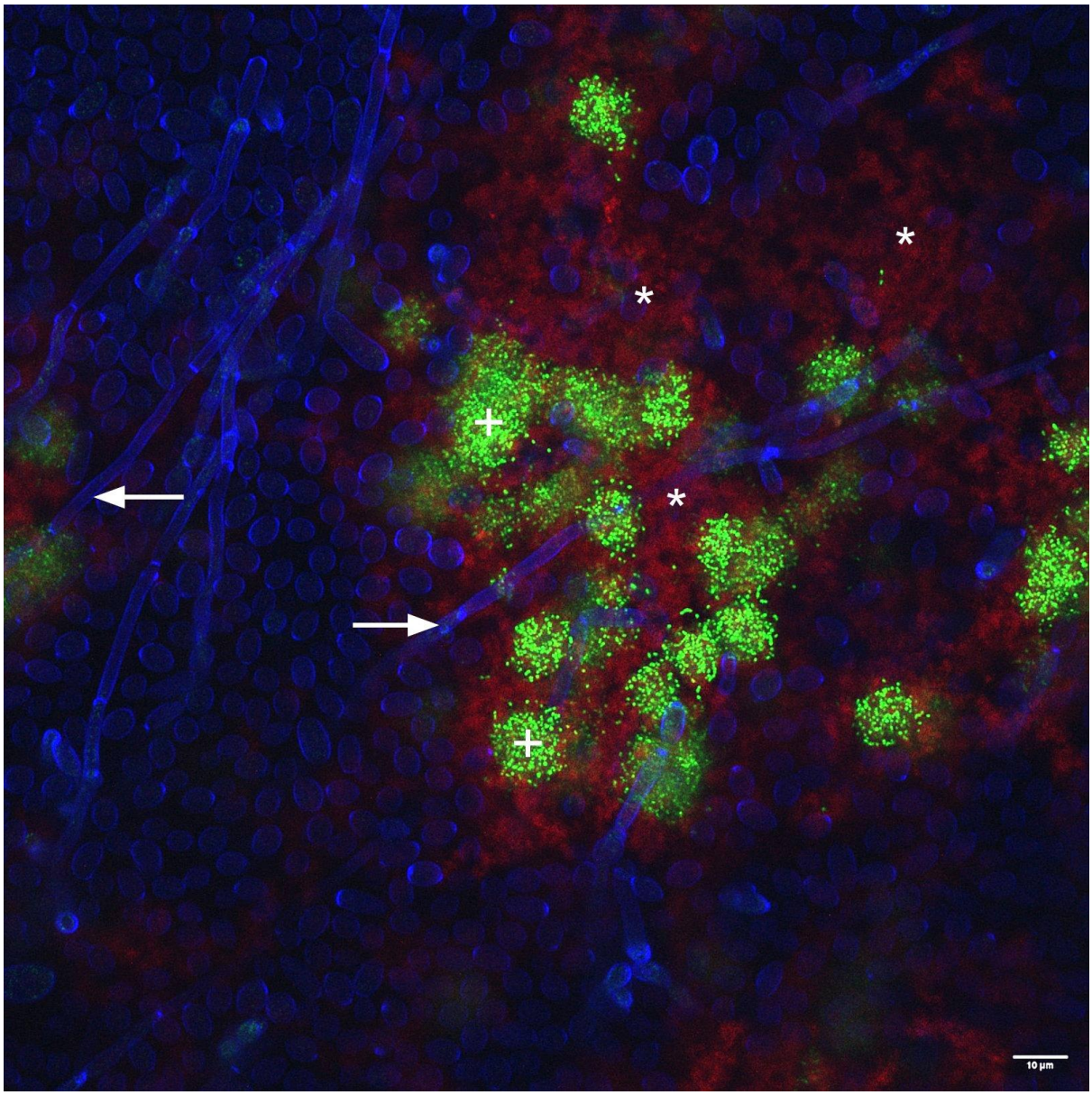

Figure 5.6 CLSM image of dual species biofilm (*Candida albicans* and *Streptococcus mutans*).

Biofilm was grown in 1% sucrose and 1 µM Alexa Fluor™ 647 conjugated dextran supplemented tryptone soy broth (Oxoid). The image shows calcofluor white (blue) stained yeast and hyphae (arrowed) of *Candida albicans* covered in glucan matrix (Alexa Fluor™ 647conjugated dextran Red, *) and aggregated green Syto9 stained *Streptococcus mutans* cells (+), magnification atx400.

5.4 Discussion

This study focused on *Streptococcus mutans* and *Candida albicans*, which are two oral microorganisms that are frequently co-isolated from dental biofilms, particularly in cases of early childhood caries (Sridhar et al. 2020; Garcia et al. 2021). *Streptococcus mutans* is a primary coloniser known for its acidogenicity, aciduricity, and robust EPS production, which contribute to its cariogenic potential (Guo et al. 2013; Moon et al. 2025). The opportunistic fungal pathogen *C. albicans* is implicated in superficial and systemic infections, posing a significant clinical challenge due to its ability to cause severe infections, especially in immunocompromised individuals (Koehler et al. 2019; Costa-Barbosa et al. 2025).

Chlorhexidine (CHX) was studied because of its widespread use in clinical dentistry, where it is the most used oral antiseptic (Ozmeric et al. 2025). CHX is incorporated into mouthrinses, gels, and varnishes for management of dental plaque and the prevention of gingivitis and dental caries (James et al. 2017). Similarly, fluconazole is the first line systemic antifungal for mucosal and invasive *Candida* infections due to its efficacy and oral availability (Marzucco et al. 2024). This makes it a suitable agent for assessing the role of EPS in antimicrobial susceptibility, particularly in the context of dual species biofilms. Its targeted activity against *C. albicans* allows for the evaluation of potential protection conferred by the *S. mutans* derived glucan matrix, providing insight into EPS mediated tolerance. However, antimicrobial agent effectiveness against cells within biofilm can be significantly reduced by the presence of extracellular polymeric substances (EPS) (Liu et al. 2024). EPS can sequester or inactivate antimicrobials before they reach their microbial targets. Negatively charged polymers within the matrix electrostatically bind to cationic agents like CHX, resulting in delayed or limited penetration into the biofilm (Singh et al. 2021c).

The aims of this chapter were to evaluate the contribution of biofilm EPS in antimicrobial resistance. To assess this, both single and dual species biofilms of oral microorganisms were used and their susceptibility to CHX and fluconazole was evaluated.

The study initially evaluated susceptibility of *S. mutans* planktonic cells to CHX. MIC and MBC values were the same for all tested media conditions, including tryptic soy broth (TSB) with no supplements and TSB supplemented with 1% sucrose and/or 1 µM dextran, with an MICs of 0.25 µg/ml and an MBC of 2 µg/ml. These values confirmed the susceptibility of *S. mutans* to CHX under planktonic conditions, regardless of medium supplementation. However, when assessed in biofilm state, *S. mutans* had reduced susceptibility with MBEC values ranging from 16 µg/ml for TSB with no supplements and TSB with 1 µM dextran to 32 µg/ml for biofilms grown in presence of 1% sucrose. This difference between planktonic and biofilm susceptibility highlights the increased tolerance of cells growing in biofilm.

Dextranase was used to degrade the EPS of *S. mutans* biofilms permitting evaluation of the role of glucan EPS in reducing biofilm susceptibility to CHX. Initially, disrupting an established glucan matrix did not alter MBEC of *S. mutans* biofilms, indicating that EPS presence might not be the only factor involved in causing increased tolerance. However, when dextranase was added during biofilm formation, the MBEC of CHX was reduced and comparable to that for *S. mutans* biofilms grown only in TSB (limited to no EPS). Dextranase treatment during biofilm formation was thus hypothesised to have inhibited EPS assembly and the formation of complex 3D biofilm aggregates as discussed in section 4.3.4.2. These results indicate that inhibiting both EPS accumulation and formation of clusters of cell aggregation enhanced CHX activity.

An MBEC measurement requires complete eradication of biofilm viable cells, as even the persistence of a single viable cell post treatment will be sufficient to generate growth and not provide an MBEC. As a result, further assessment of antimicrobial activity was undertaken by live/dead staining and CLSM. Reduced viability of biofilms that had been treated with dextranase compared to biofilms with no dextranase treatment, indicates a protective role of EPS, since both tested groups (i.e. biofilm with no dextranase treatment and biofilms exposed to 0.25% dextranase post biofilm formation for 1 h) had similar microcolony aggregations. Differences in CHX susceptibility could most likely be attributed to sequestering by the EPS, where ionic interactions between the positively charged CHX (Gränicher et al. 2021) and negatively charged glucan matrix (Guo et al. 2015) occurs.

As established in previous Chapters, the presence of sucrose in the culture medium resulted in a more complex structure of *S. mutans* biofilms. In these biofilms, cells were seen to occur as aggregates in microcolonies and embedded in glucan EPS. The presence of glucan EPS surrounding the cells can link different microcolonies on the surface, allowing further accumulation and structural complexity (Rainey et al. 2019). In contrast, biofilms grown in TSB without sucrose, seemed largely lacking in EPS and as a result the biofilm was more homogeneous in appearance.

Results of this research agree with those in a previous study where the structural arrangement of both cells and EPS in a biofilm could be limiting factors for CHX diffusion (Xiao et al. 2012). The researchers used a mixed species biofilm of *S. mutans, Actinomyces naeslundii* and *Streptococcus oralis* which was grown on saliva coated hydroxyapatite coupons in medium containing 1% sucrose. Sucrose induced a complex 3D structure of cells in microcolonies with accumulation of EPS and a localised acidic environment. Live/dead staining showed that cells

embedded in EPS-rich biofilm had higher tolerance to 0.12% (v/v) CHX with 10% of cells being killed after 15 min exposure. This compared to 60 to 75% of cells being killed after 15 min by 0.12% (v/v) CHX for EPS-deficient biofilms grown in 1% glucose. It was concluded that occurrence of cells in microcolonies surrounded by EPS restricted penetration by CHX. It was hypothesised that the accumulation of negatively charged lipoteichoic acid in the matrix contributed to impeding the diffusion of CHX (Xiao et al. 2012).

EPS' role in antimicrobial tolerance of biofilms is not exclusive to bacteria and can influence other microorganisms including *Candida albicans*. It was found that β-1,3-glucan, a major EPS component of *Candida* biofilms on rat central venous catheters, limited the diffusion of fluconazole into biofilms. This effect was negated after EPS disruption using glucanase (Nett et al., 2007).

Most biofilms are polymicrobial and contain several microbial species able to produce EPS (Willems et al. 2016). In these polymicrobial biofilms, the EPS produced by certain microorganisms can provide protection to neighbouring non-EPS producers through the shared matrix properties. This could lead to enhanced tolerance of non EPS producing microorganisms to antimicrobials (Billings et al. 2013).

In this research, susceptibility of *C. albicans* to fluconazole was evaluated in the presence of EPS produced by *S. mutans* in dual species biofilm. Results showed that *C. albicans* had increased fluconazole tolerance when co-cultured with *S. mutans* in glucan rich biofilms, compared to *C. albicans* in dual species biofilm grown in TSB medium alone which had no detectable glucan, indicating that the bacterial EPS conferred protective effects to *C. albicans*. This was confirmed by CFU enumeration when the EPS was disrupted using 0.25% dextranase,

and the susceptibility of *C. albicans* to fluconazole returned to levels observed in biofilms without glucan.

A mechanism by which glucan EPS imparts biofilm tolerance to fluconazole was investigated in a previous study of *S. mutans* and *C. albicans* biofilms (Kim et al. 2018). Fluorescently labelled fluconazole was added to biofilms after EPS production, and was shown to concentrate in the EPS and was restricted from reaching fungal cells. Treatment with dextranase degraded the EPS and restored fluconazole penetration, leading to increased antifungal activity (Kim et al. 2018).

Lobo et al. (2019) evaluated CHX tolerance of dual and single species biofilms of *S. mutans* and *C. albicans* in sucrose rich conditions. Increased biofilm biomass, protein content for dual species compared with single species biofilms occurred when treated with 0.12% CHX. This increased tolerance was attributed to biofilm structure and the EPS produced by *S. mutans*. Results were supported by CLSM, which showed *S. mutans* glucan embedded cells and hyphae. Gene expression also showed that *C. albicans* downregulated certain EPS genes (*BGL2* and *PHR1*) in co-culture, suggesting a reduced need to produce its own EPS (Lobo et al. 2019).

Enzymatic disruption of polymicrobial biofilms is an important area of biofilm research in the development of approaches to overcome biofilm mediated antimicrobial resistance. Results from this chapter and previous studies show the potential of enzymatic disruption of EPS in dual species biofilms on reducing resistance. Gränicher et al. (2021) assessed synergy between CHX, DNase I and proteinase K in a multispecies oral biofilm model. The biofilm comprised of *S. mutans*, *C. albicans*, *Streptococcus oralis*, *Actinomyces oris*, *Veillonella dispari* and *Fusobacterium nucleatum* and was constructed on hydroxyapatite discs. Comparing the effectiveness of CHX treatment alone or combined with enzymes revealed that the latter

reduced total viable cells of five of the microorganisms, including *S. mutans* and *C. albicans*. CLSM also revealed that enzyme treatment disrupted biofilm structure and reduced cell density, thereby facilitating CHX penetration into the biofilm (Gränicher et al. 2021).

The research described in this Chapter showed that *S. mutans* biofilms had increased tolerance to CHX compared to planktonic cells. *S. mutans* planktonic culture was susceptible to CHX regardless of medium supplementation type with all growth conditions having the same MIC and MBC. However, compared to planktonic *S. mutans*, biofilms were less susceptible as assessed by MBEC. This was particularly evident in sucrose supplemented medium. Dextranase-mediated degradation of EPS matrix was found to lower the tolerance of *S. mutans* biofilms, particularly when added during biofilm formation.

In dual species (*S. mutans* and *C. albicans*) biofilm, *C. albicans* had higher tolerance to fluconazole when cultured with *S. mutans* in glucan rich biofilm indicating a bystander protective effect mediated by EPS. Dextranase treatment enhanced antifungal activity of fluconazole, reducing *C. albicans* viability to levels similar to those observed in biofilms lacking glucan matrix. These findings highlight the contribution of EPS to antimicrobial tolerance in biofilms and support the potential of combinational therapy using enzymes and antimicrobials in the treatment of biofilms.

Chapter 6

General Discussion

Historically, the *in vitro* study of microorganisms was undertaken in liquid broth culture, where the organisms grow as free swimming or planktonic cells. However, since the 1970s there has been recognition that away from the laboratory, most microorganisms grow attached to surfaces in cell aggregates that are embedded in extracellular polymeric substance (EPS); these growth forms are referred to as biofilms (Donlan and Costerton 2002).

Biofilms are now regarded as the predominant mode of microbial growth in natural, industrial, and clinical environments (Penesyan et al. 2021). Importantly, microbial cells in biofilms typically have higher tolerance to environmental stresses than their planktonic counterparts including the exposure to antimicrobial agents (Manavathu and Vazquez 2017).

In clinical environments, biofilms are responsible for numerous chronic and recurrent infections (Grari et al. 2025). For example, in the oral cavity, dental plaque biofilms are the source of the causative agents of dental caries, and periodontal disease (Cugini et al. 2021; Yekani et al. 2025), and denture stomatitis (Le et al. 2024). Such biofilm-associated infections are difficult to treat with conventional antimicrobials and are major global challenges (Grooters et al. 2024).

A distinctive and defining feature of biofilms is the presence of microbial-produced extracellular polymeric substance (EPS), which is an important contributor to the structural and functional behaviour of a biofilm (Flemming and Wingender 2010). The EPS matrix is typically a complex mixture of polysaccharides, proteins, lipids, and extracellular DNA (eDNA) that provides mechanical stability, cohesion (Hasan and Aggarwal 2025), nutrient retention (Limoli et al. 2015), surface adherence (Gong et al. 2024), and facilitates communication between microbial cells (Lu et al. 2024).

In recent years, there has been growing interest in EPS as a core component of biofilm lifestyle (Powell et al. 2018; Lu et al. 2024; Joos et al. 2025). Investigations using various clinical and environmental models have revealed that EPS plays a central role in orchestrating microbial behaviour, biofilm development, and resilience (Saharan et al. 2024). One of the most clinically relevant functions of EPS is its contribution to antimicrobial tolerance, which has multifactorial mechanisms including reducing the penetration of antimicrobial agents through the biofilm by chemically binding and sequestering active compounds (Ciofu et al. 2017).

Research in this PhD focused on characterising the biofilm EPS produced *in vitro* by specific clinically relevant microorganisms and to assess its contribution to antimicrobial tolerance. Oral streptococci, including *S. sanguinis*, *S. salivarius* and *S. gordonii*, are early colonisers of tooth surfaces, and constitute up to 80% of dental plaque communities (Aruni et al. 2015). Unsurprisingly, oral streptococci strongly influence the development and behaviour of oral biofilms (Rosan and Lamont 2000). *Streptococcus mutans* was selected for study as it is regarded as a primary causative microorganism of dental caries and under these conditions it is a prevalent member of the dental plaque biofilm (Fang et al. 2024). *S. sanguinis*, *S. salivarius* and *S. gordonii* were also included as they are frequent constituents of dental plaque and are early colonisers that promote subsequent attachment of both commensal and pathogenic bacteria through specific coaggregation interactions (Abranches et al. 2018). Additionally, the fungus *Candida albicans*, which is an opportunistic pathogen was included, as it is a leading cause of denture stomatitis and an adept biofilm former on denture acrylic (Abuhajar et al. 2023). *Candida albicans* is also often isolated with *S. mutans* in early childhood caries biofilms (Lu et al. 2023). *Neisseria gonorrhoeae* was included as it is both a biofilm former and the causative agent of gonorrhoea, a sexually transmitted infection that can lead to urethritis, cervicitis, pelvic inflammatory disease and infertility (Belcher et al. 2023). *Neisseria*

gonorrhoeae forms resilient biofilms on mucosal tissues, a trait that contributes to its persistence, reduced susceptibility to antibiotic treatment (Greiner et al. 2005) and host immune evasion (Darville 2021). Of note, biofilms of *N. gonorrhoeae* reportedly contain high levels of eDNA which would represent a different target compared with the carbohydrate dominated EPS of oral biofilms (Steichen et al. 2011).

6.1 *In vitro* biofilm development

Initial experiments, described in **Chapter 2**, aimed to evaluate methods of *in vitro* biofilm development which could be used to produce biofilm material for subsequent study. Research conducted in **Chapter 2** also facilitated acquisition of biofilm analytical approaches including methods based on culture and microscopy. Experiments compared biofilm growth under continuous flow in the CDC biofilm reactor and in static cultures in microtiter plates. In addition, different surface materials to support biofilm growth including polycarbonate, hydroxyapatite, and polymethyl methacrylate (PMMA) were evaluated. Furthermore, the merits of preconditioning these surfaces with an artificial saliva pellicle was examined (Mutahar et al. 2017).

Biofilm was quantified by several measures including enumerating colony forming units, (CFUs), assessing surface area coverage by biofilms based on fluorescent microscopy, and total biovolume and thickness analysis from confocal laser scanning microscopy (CLSM)images. Enumerating CFUs of cells recovered from biofilms provides an indicator of biofilm viability. However, tenaciously attached bacterial cells might be underestimated by this method. Furthermore, aggregates of cells would be prevalent in biofilms and likely lead to a further underestimation of total cells present by cultural methods. Nevertheless, CFU enumeration has frequently been used to assess biofilm viability, either alone or in combination with

imaging methods (Kohno et al. 2021; Wang et al. 2021). In contrast, fluorescence microscopy provides a direct assessment of biofilm levels and can inform on the spatial distribution of cells and their viability if appropriate dyes are used (Wilson et al. 2017). CLSM provides detailed imaging of biofilm architecture and allows for non-destructive analysis of biomass, viability, and EPS components (Wilson et al. 2017). Both fluorescence microscopy and CLSM rely on the use of molecular probes conjugated with fluorochromes, which can target different components allowing for imaging of specific biofilm features such as live and dead cells, or EPS constituents (Alovisi et al. 2022; Hong et al. 2022; Ren et al. 2023; Bijle and Abdalla 2024; Chen et al. 2024; Gerardi et al. 2024; Xu et al. 2024). CLSM combined with fluorescence staining is well established for live/dead staining and EPS, particularly in oral biofilm research (Schneider-Rayman et al. 2021; Li et al. 2023; He et al. 2024). While other studies have used widefield fluorescence microscopy to evaluate viability and biofilm coverage (Reda et al. 2021).

Taken together, combined use of culture based and imaging approaches in Chapter 2 enabled an assessment of biofilm development across the tested conditions, while also highlighting limitations of relying on any single analytical method. This exploratory phase showed that *in vitro* biofilm development was sensitive to growth system, surface material, and medium composition, with marked differences observed in cell density, surface coverage, and biofilm biomass. The optimisation strategy in **Chapter 2** established a reproducible *in vitro* biofilm model, although EPS was not directly quantified, the working assumption being that a higher cell density and thicker biofilm would contain more EPS. An evaluation of EPS in developed biofilms was the focus of the research presented in **Chapter 3**.

6.2 Assessment of EPS in *in vitro* biofilms using fluorescently labelled molecular probes

Since polysaccharides are known to be a major component of oral biofilm matrices (Jakubovics et al. 2021), several carbohydrate specific probes and fluorescent lectins that bind to particular sugar moieties were selected to interrogate the EPS of *in vitro* biofilms. In addition, eDNA and the presence of protein in EPS was explored respectively using cell impermeable nucleic acid stains, and SYPRO™ Ruby, a protein stain that labels most classes of proteins (Bie et al. 2025). Multiplex staining of EPS and cellular targets was undertaken to enable spatial distribution of EPS to be made.

Surprisingly, the conditions that produced highest biofilm quantities in **Chapter 2**, showed limited quantities of EPS detected by the molecular probes. Most fluorescence was associated with microbial cell surfaces, with limited fluorescence outside of cells where the presence of EPS was expected. In the case of lectin probes, a possible reason could be that the specific carbohydrate moieties targeted by the lectins were not present or were masked in the biofilm. As such when using highly specific probes without prior knowledge of the EPS composition, a range of lectins should be screened to avoid potential oversight of EPS components. In contrast, eDNA and proteins stains typically have a broader binding profile, allowing for general detection of targeted polymers, if present. However, the signals obtained indicated that protein and eDNA were also present in low abundance. The absence of EPS could indicate that *in vitro* culture conditions are not good inducers of EPS. Potentially, use of traditional culture media provides favourable growth conditions where needless production of EPS would be metabolically wasteful. It was therefore thought that use of more 'hostile' conditions could trigger greater EPS production.

In an attempt to induce EPS production, environmental stress conditions were applied to the biofilms. Intermittent drying was introduced, as it has been reported that biofilms can synthesise EPS as a protective mechanism against desiccation (Choudhari et al. 2023). It was hypothesised that repeated drying cycles would therefore stimulate increased EPS production. Additionally, extended incubation periods were used, as prolonged biofilm maturation has been associated with increased EPS accumulation (He et al. 2024). However, neither approach yielded a noticeable increase in EPS. Finally, supplementation of the growth medium with sucrose (1% w/v) was explored to promote glucan EPS production and this proved to be successful.

Sucrose (a disaccharide of glucose and fructose) is recognised as a substrate that *S. mutans* along with other oral streptococci use to synthesise large quantities of extracellular glucan polymers via glucosyltransferase (Gtf) enzymes (Hoshino and Fujiwara 2022). In fact, frequent intake of dietary sucrose is a key driver of cariogenic biofilm development *in vivo*, primarily due to its fermentation by *Streptococcus* species into lactic acid, which lowers local pH and promotes enamel demineralisation (Anderson et al. 2018), leading to biofilms with rich EPS that enhances microbial adhesion and biofilm cohesion (Du et al. 2020). Consistent with this, biofilms grown in medium supplemented with 1% sucrose had an abundance of EPS, that could be imaged by the inclusion of fluorescently labelled dextran in the sucrose supplemented medium. In this medium, the labelled dextran serves as an acceptor for Gtfs facilitating initiation of glucan polymerisation (Venkitaraman et al. 1995). As Gtfs convert sucrose to glucan, the fluorescent dextran is incorporated into growing glucan chains (Koo et al. 2010). This incorporation confirms that the EPS detected in tested biofilms was predominantly glucan, which aligns with previous reports identifying glucans as major

structural components of EPS in oral biofilms, particularly those formed by *S. mutans* (Moon et al. 2025).

CLSM images revealed increased EPS production in biofilms grown in presence of sucrose, which appeared to envelop microcolonies, often connecting neighbouring cell clusters into a larger network. Furthermore, glucan detection was observed not only in *S. mutans* biofilms, but also in biofilms of mixed bacterial species, mixed microbial species (where *S. mutans* was co-cultured with other oral microorganisms), dual species of *S. mutans* and *C. albicans*, and in biofilms from whole saliva. These observations confirmed that sucrose increased EPS production and its presence led to formation of structurally complex biofilms, characterised by microcolonies embedded in glucan matrix.

6.3 Assessment of Lig E and eDNA role in *Neisseria gonorrhoeae* biofilm

In contrast to biofilms produced by oral microbial species, where polysaccharides are the primary component of EPS (Bowen et al. 2018), *N. gonorrhoeae* forms biofilms characterised by an extracellular matrix dominated by extracellular DNA (eDNA) (Steichen et al. 2011). The absence of polysaccharide components in *N. gonorrhoeae* occurs due to the lack of required genes responsible for polysaccharides production (Falsetta et al. 2011). The eDNA originates largely from outer membrane blebbing and active secretion of single stranded DNA (Anderson et al. 2016). The focus of recent investigations has been the role of DNA ligases in regulating eDNA dynamics within biofilms, DNA ligase is an enzyme that catalyses the formation of phosphodiester bonds between DNA strands, joining ends and fixing breaks in DNA backbone during processes such as replication, repair and recombination (Wilkinson et al. 2001; Pergolizzi et al. 2016). In particular, the ATP dependent DNA ligase Lig E has been reported to have a role in biofilm formation and adhesion (Pan et al. 2024).

In this present study, a Lig E knockout of *N. gonorrhoeae* was used to evaluate the role of eDNA in EPS. *In vitro N. gonorrhoeae* biofilm growth on polycarbonate coupons was limited with no significant differences between strains with different Lig E expressing ability. However, infection of reconstructed human vaginal epithelial (HVE) tissues with Lig E deficient strains revealed lower biofilm biomass with less tissue damage compared to the wild-type strain. This reduction in biofilm formation was evident in HVE model, where COMSTAT analysis of CLSM images revealed lower biomass of biofilm in Lig E knockout compared to wild type. Reduction in biomass was accompanied by lower cytotoxicity, as measured by lactate dehydrogenase (LDH), suggesting that Lig E contributes not only to biofilm formation but also to host tissue damage. The research conducted with *N. gonorrhoeae* in **Chapter 3** provided the basis of a publication from this PhD (Pan et al. 2025a). While attempts to visualise eDNA by CLSM were inconclusive, which was likely due to low eDNA abundance or interference from fixation induced background fluorescence, the functional assays provided evidence for the contribution of Lig E to biofilm formation and virulence. While the role of DNA ligases in *N. gonorrhoeae* remains underexplored, the need to characterise such virulence factors has been emphasised in recent literature (Kurzyp and Harrison 2023), supporting the rationale for investigating Lig E in the context of biofilm formation and infection.

6.4 Characterisation and quantification of extracellular polymeric substances in biofilms and planktonic cells

To complement the largely microscopical analyses undertaken in **Chapter 3** and to obtain quantitative insight, **Chapter 4** compared the chemical composition of biofilms and planktonic cultures. For carbohydrates, their reaction with phenol in the presence of concentrated sulfuric acid, produces a coloured product that can be measured spectrophotometrically (DuBois et al. 1956). The Bicinchoninic Acid (BCA) assay is based on reduction of Cu^{2+} to Cu^{+}

by proteins in an alkaline environment. The generated Cu^{+} ion reacts with bicinchoninic acid to produce a purple-coloured product that absorbs light at 562 nm and the value is proportional to the protein concentration (Smith et al. 1985).

Comparing planktonic and biofilm yields directly could be misleading, as one form could contain more cells, leading to a perceived higher presence of measured substances, therefore, results had to be normalised to the number of cells in each type of sample. Cell number was estimated by quantitative real-time polymerase chain reaction (qRT-PCR), as it provided a means to overcome the limitations of CFU enumeration in biofilms, where cells often exist in dense aggregates or within protective matrix components that can hinder accurate plating and colony recovery (Ammann et al. 2013). After normalisation, biofilms were found to contain more polysaccharides and protein compared to planktonic cultures of the same microorganism. When examining the extent of protein and carbohydrate change from planktonic cultures to biofilm cultures, protein levels increased more substantially than carbohydrates in biofilms of *C. albicans* (2-fold), mixed bacteria (2-fold), and whole saliva (70-fold). In contrast, mixed species and *S. mutans* showed a greater increase in carbohydrate content. This was especially evident for *S. mutans*, where carbohydrate levels increased over 100-fold in biofilm supplemented with sucrose, which is associated with increased glucan production, compared to 60-fold increase in protein level of *S. mutans* biofilm compared to planktonic. The increase in carbohydrate content indicates a targeted production of carbohydrate in EPS of *S. mutans* biofilms grown in presence of sucrose. The observed increase is largely attributed to Gtfs activity especially GtfB and GtfC, which catalyse the extracellular synthesis of glucan (Decker et al. 2014). This is driven by sucrose presence as it provides both energy for fermentation and glycosyl units for polymer synthesis (Costa Oliveira et al. 2021).

The increase in protein content could be attributed to presence of enzymes within the biofilm, such as Gtfs, the accumulation of enzymes can be detected and quantified using BCA assays (Mrigwani et al. 2023). In contrast to protein content, which could increase as biomass increases, production of glucan in response to sucrose is amplified, as the matrix becomes mostly polysaccharides as a result of sucrose metabolism (Duarte et al. 2008).

A relatively novel approach of analysing biofilm EPS in **Chapter 4** was the use of Confocal Raman Microscopy (CRM). CRM is a label free, non-destructive approach that has potential to identify biofilm components (Keleştemur et al. 2018). In principle, Raman spectra from different regions within the biofilm can be matched to known spectra of biological molecules to identify EPS constituents. In tested biofilms, the retrieved spectra showed some distinctive features, but identification required matching each spectrum to a spectral library, but identifications of specific EPS compounds were unsuccessful. This could be due to the fact that accurate identification by spectral analysis is dependent on the availability of relevant reference spectra in the database (Cialla-May et al. 2021). If EPS components were not in the database, the spectra would be unrecognisable or misidentified.

Previous studies have demonstrated successful application of CRM for EPS analysis in oral biofilms, particularly in systems characterised by well-defined polysaccharide structures or simplified experimental models. For example, a study characterised water-insoluble α-glucans and their spatial distribution within *Streptococcus mutans* biofilms using in situ Raman spectroscopy, supported by extensive calibration against purified reference compounds (Pezzotti et al. 2023). However, Raman scattering may be affected by background fluorescence, and substantial spectral overlap between proteins, carbohydrates, lipids, and

nucleic acids complicates peak assignment and limits the specificity of spectral interpretation within chemically heterogeneous EPS matrix (Liu et al. 2022).

6.5 Extracellular polymeric substances disruption using dextranase

Having established a reproducible biofilm rich with detectable EPS, enzymatic targeting of EPS was done using dextranase. Dextranase hydrolyse glycosidic bonds of glucan by targeting α-(1-6)-linkages (Cortez et al. 2023). When 72 h old biofilms grown in sucrose enriched media was treated with dextranase for 1 h, the glucan EPS was degraded, as shown by the different methods of assessment. Quantitative image analysis of CLSM images confirmed a decrease in total glucan biovolume. However, interestingly, the overall architecture of the biofilm's cellular component remained largely intact. Bacterial cells, visualised by use of a fluorescence cell stain (SYTO9), still formed microcolony clusters, and the total biomass of cellular part as measured by cell associated signal was not different from control biofilms. Dextranase therefore removed most of the glucan within the biofilm thereby exposing the cells, and this was also supported by scanning electron microscopy.

Importantly, adding dextranase during biofilm growth resulted in *S. mutans* cells forming a less dense biofilm with no detectable glucan. Essentially, the enzyme prevented the bacteria from establishing the rich polysaccharide scaffold seen in the presence of sucrose. This observation was consistent with the established role of EPS glucans as a structural scaffold that promotes cell clustering and surface adhesion (Schilling and Bowen 1992). The results align with previous studies reporting that degradation of EPS compromises biofilm architecture and impairs microcolony formation in *S. mutans* (Paula et al. 2020). However, while Paula et al. (2020) observed the absence of EPS and failure to form microcolonies after degradation of EPS, they reported a reduction in total biovolume of bacterial cells. Which was

not the case in the current research. Paula et al (2020), used a combination of dextranase and mutanase to target multiple glucan linkages, whereas only dextranase was employed in the present study.

Another study conducted a screening of EPS degrading enzymes to evaluate their ability to disrupt oral biofilms formed from human saliva (Nielsen et al. 2024). The authors tested 321 combinations of 44 different enzymes, including dextranase, mutanase, glucanase, cellulase, xylanase, amylase, DNase, and lipase. Biofilm disruption was assessed by measuring reduction in total biofilm biomass using crystal violet staining. Most enzymes showed limited efficacy when applied individually except for mutanase which significantly reduced the biofilm by approximately 40%. However, the most effective treatments involved combinations containing mutanase, particularly with dextranase or glucanase, which achieved biofilm reductions of up to 69% (Nielsen et al. 2024).

Use of dextranase in this current research effectively degraded the EPS matrix, but did not lead to complete biofilm removal, highlighting the complexity and resilience of biofilm structures. While studies have employed combination of enzymes targeting multiple EPS components to maximise biofilm eradication, this work focused on the selective removal of the EPS as a strategy to expose the underlying microbial cells. This distinction is important, as dispersal of viable cells without adequate killing poses potential clinical risk, as dispersed bacteria can exhibit increased expression of virulence and adhesion factors compared to both planktonic and biofilm embedded counterparts, and that dispersal may act as the initiating step in systemic infections (Guilhen et al. 2017). In present study, using dextranase alone allowed selective modification of EPS while largely preserving overall biofilm structure, facilitating the evaluation of its role in antimicrobial tolerance in an EPS-disrupted biofilm

state. From a clinical perspective, approaches that modulate the biofilm matrix without extensive dispersal followed by conventional antimicrobial agent treatment, may offer advantages by limiting the release of viable cells associated with enhanced virulence and recolonisation. Adding dextranase during the formation of the biofilm resulted in preventing the establishment of glucan matrix and aggregation clusters typically formed in presence of sucrose. This observation was consistent with the known role of EPS glucans as a structural scaffold that promotes cell clustering and surface adhesion (Schilling and Bowen 1992).

Stability of dextranase has been characterised under controlled conditions. Dextranase from *Chaetomium erraticum* was shown to undergo first-order irreversible thermal inactivation, with enzyme activity decreasing over time in a temperature-dependent manner and a measurable half-life (Virgen-Ortíz et al. 2015). Dextranase exhibits optimal activity at mildly acidic pH and retains sufficient activity over the duration of typical experimental treatments. In a study that assessed the use of dextranase in oral and biofilm-related applications, they reported the ability of dextranase to disrupt biofilm structure and reduce bacterial adherence during short exposure periods, rather than fully eliminating the biofilm (Juntarachot et al. 2020).

Incorporating dextranase into oral care formulations has been actively explored as a strategy to target the extracellular polysaccharide of dental plaque. Encapsulation-based approaches have demonstrated that dextranase can be incorporated into toothpaste while retaining enzymatic activity and antibiofilm efficacy during storage, despite the presence of surfactants and other destabilising components (Juntarachot et al. 2020). However, another study has highlighted enzyme instability as a key limitation and proposed immobilisation or encapsulation as necessary strategies to preserve activity in toothpaste environments (Lee,

2022). Taken together, reported literature coupled with findings of present study, indicate that further assessment of dextranase as strategy for inhibiting biofilm development is needed. Additional work is required to determine whether clinically relevant EPS disruption using dextranase enhances the antimicrobial susceptibility of biofilms to agents such as chlorhexidine. Finally, further assessment is required to establish the suitability of dextranase as a functional ingredient in oral care formulations.

6.6 Assessment of extracellular polymeric substances role in antimicrobial susceptibility

With the ability to degrade EPS and prevent its formation, the role of EPS in biofilm antimicrobial tolerance could be assessed, and this was the focus of **Chapter 5**. Chlorhexidine (CHX) is a broad-spectrum cationic antiseptic commonly used in oral healthcare (Deus and Ouanounou 2022) and known for its antimicrobial and antiplaque activity (Liang et al. 2024). CHX was therefore selected as suitable test agent to explore whether the EPS produced by oral bacteria could impede its activity. The minimum inhibitory concentration (MIC) and minimum bactericidal concentration (MBC) of CHX against planktonic *S. mutans* were initially determined using four different media: tryptic soy broth (TSB), TSB supplemented with 1 µM dextran, TSB supplemented with 1% sucrose, and TSB supplemented with both 1 µM dextran and 1% sucrose. In addition, an assay to determine the minimum biofilm eradication concentration (MBEC) was also used to assess susceptibility of *S. mutans* biofilms to CHX.

Results showed that *S. mutans* biofilms exhibited higher tolerance to CHX compared with planktonic equivalents. This was expected as it is considered one of the main characteristics of biofilm mode of growth (Zhao et al. 2023), such phenomena is documented in both traditional antibiotic and novel antibacterial compounds (Folliero et al. 2022).

The MIC obtained for *S. mutans* in the present study (0.25 µg/ml) is within the typical range reported in literature. Although growth conditions differ, MICs of clinical isolates (Järvinen et al. 1993; Järvinen et al. 1995; Yeon and Young 2019) range from 0.25 up to 1 µg/ml. While others report MICs below 2 µg/ml (Ermer et al. 2018).

For MBC, the CHX concentration required to kill *S. mutans* was 2 µg/ml regardless of culture medium supplementation, which also falls in the range reported by a study on clinical isolates of *S. mutans* resulting in an MBC range of 1.95 to 15.63 µg/ml (Yeon and Young 2019). However, Yeon and Young (2019) reported higher MBEC (62.5 µg/ml) of clinical *S. mutans* isolates compared to this research, which was 32 µg/ml.

In contrast, when comparing MBECs using different media conditions, results showed that sucrose presence reduced susceptibility of *S. mutans* to CHX. Notably, MIC and MBC values for planktonic cells were unaffected by the presence of sucrose, indicating that the media supplements did not inhibit CHX activity directly. This aligns with the study by Kreth et al. (2008), where it was reported that sucrose increased the antimicrobial tolerance of *S. mutans*. The researchers suggested that the increased tolerance appeared to be linked to activity of Gtf enzymes, as when they used a *gtfB, gtfC* and *gtfD* mutant strain of *S. mutans*, no increased tolerance was found, revealing that this effect was not due to intracellular sucrose metabolism (Kreth et al. 2008).

Next, dextranase was used to assess the role of EPS in antimicrobial tolerance of *S. mutans* biofilms. Exposure to 0.25% dextranase 1 h, prior to CHX treatment, did not alter MBEC of any tested medium conditions (TSB alone, TSB and dextran, TSB and sucrose, and TSB with sucrose and dextran). In contrast, when dextranase was introduced into the culture medium during biofilm formation, MBECs were reduced under all conditions. Importantly, biofilms grown in

the presence of 1% sucrose showed reduced CHX tolerance when dextranase was included during biofilm formation, compared to biofilms with no dextranase and biofilms exposed to dextranase post biofilm formation, reaching levels of susceptibility comparable to biofilms formed in the absence of sucrose and without dextranase treatment (conditions that produce biofilms with limited glucan EPS).

As reported in **Chapter 4**, addition of dextranase during biofilm formation inhibited glucan assembly, resulting in biofilms lacking a glucan matrix and these biofilms were more thinly distributed across the surface. Inhibiting EPS assembly rendered the biofilm more susceptible to CHX treatment, results that suggest that glucan plays a critical role in the increased tolerance of biofilms. This was consistent with a study by Xiao et al. (2012), who assessed the role of EPS in virulence of a mixed species oral biofilm. The study demonstrated that biofilms grown in sucrose rich medium resulting in bacterial cells located within microcolony complexes displayed enhanced survival following CHX exposure compared to those outside the structures, or in biofilms lacking EPS. The researchers concluded that increased tolerance to antimicrobials, such as CHX, was attributed to the structural organisation and spatial distribution of EPS. It was suggested that the EPS allowed the formation of protective microenvironments, along with facilitating electrostatic interaction of negatively charged EPS and positively charged CHX molecules, which limited CHX's diffusion within the biofilm (Xiao et al. 2012).

Having established that EPS contributes to antimicrobial tolerance in *S. mutans* biofilms and considering that MBEC determination is a strict method requiring complete eradication of viable cells, live/dead staining combined with CLSM was employed to further investigate the effects of dextranase treatment. CLSM imaging of CHX treated biofilms provided visual

evidence supporting the protective role of the EPS matrix, while quantitative analysis using COMSTAT enabled direct comparisons of cell viability between treatment conditions.

All biofilms in this experiment were grown in 1% sucrose and subsequently treated with CHX (16 µg/mL). In control biofilms, a relatively low proportion of dead cells (stained red) was observed, with the majority of the biofilm composed of live (green) cells, indicating bacterial survival following CHX treatment. In contrast, biofilms that were exposed to dextranase for 1 hour after formation and then treated with CHX displayed a higher proportion of red stained (dead) cells throughout the biofilm. This suggests that partial degradation of the EPS enhanced CHX penetration and efficacy. Notably, biofilms exposed to dextranase during their formation, followed by CHX treatment at the same concentration (16 µg/mL), showed complete red staining, indicating total bacterial death, which agrees with MBEC data. COMSTAT analysis of CLSM image revealed significant differences ($p < 0.001$) in percentage of viable cells between treatment groups, further reinforcing the impact of EPS degradation on CHX efficacy.

When evaluating the antifungal susceptibility of *C. albicans* in the different media supplementation, fluconazole did not yield a definitive MIC, MFC or MBEC values. This may be attributed to using tryptic soy broth, which is not RPMI 1640, the recommended medium for antifungal susceptibility testing (CLSI 2018), as Bartizal and Odds (2003) demonstrated that, among various methodological variables, medium composition is one of the most influential factors on susceptibility testing outcomes (Bartizal and Odds 2003). Despite such limitation, CHX exhibited consistent antifungal efficacy, as demonstrated in **Chapter 5**, as MIC, MFC and MBEC values were consistent regardless of media conditions, indicating that media supplementation did not change *C. albicans* susceptibility to CHX.

6.7 Limitations and future work

Findings from this research highlight the central role of EPS in antimicrobial tolerance of biofilms, especially those of *Streptococcus mutans*. The demonstrated ability of dextranase to degrade EPS formation leading to enhanced susceptibility to chlorhexidine, presents an opportunity of application in oral healthcare.

While the findings presented in this research provide new insights into the structure, composition, and functional role of extracellular polymeric substances (EPS) in oral biofilms, several limitations should be acknowledged. The work relied on *in vitro* biofilm growth models, which enabled a controlled manipulation of growth conditions, reproducible EPS detection, and systematic assessment of enzymatic and antimicrobial interventions, they cannot fully replicate the complexity of oral environment. *In vivo*, biofilms are continuously exposed to salivary flow, mechanical shear, host immune factors, and fluctuating nutrient availability, all of which could influence biofilm architecture, EPS composition, and response to antimicrobial. Consequently, while *in vitro* findings presented here provide a proof of concept, their direct translation to clinical settings requires further investigation.

The work focused predominantly on *Streptococcus mutans* biofilms, alongside selected mixed species and saliva derived models. While these systems are highly relevant to cariogenic biofilms, natural environment of biofilms comprise a far greater diversity of microbial taxa, with complex interspecies interactions that may influence EPS production, structure, and function. Therefore, further assessment across biofilm related fields is necessary to explore the extent to which the EPS targeting strategies are applicable across diverse biofilm communities. Although a combination of techniques was employed to characterise EPS, including CLSM, biochemical quantification, and CRM, each approach has inherent

constraints. Fluorescent staining relies on probe specificity and accessibility within dense biofilm matrix, while Raman spectroscopy, although label-free, showed limited capacity for definitive EPS component identification in complex biofilms.

Dextranase can be proposed as a candidate for formulation and evaluation of EPS targeting agents and could be incorporated as a component in oral hygiene products. Inclusion of dextranase in toothpaste could be explored as an agent that degrades glucan. Another benefit is dextranase's ability to limit the accumulation of glucan, which if included in toothpaste would inhibit the formation of EPS within oral biofilms. Furthermore, if antimicrobial treatment was needed, dextranase could facilitate antimicrobial activity, improving management of dental plaque and caries. Another possible application is for dextranase to be incorporated into mouthrinses as they are distributed all over the oral cavity covering areas that cannot be reached by toothpaste. Importantly, as dextranase alone is not biocidal, it should be coupled with antimicrobial agents or ingredients, in cases where eradication is required. In addition, DNase could be explored as an agent targeting EPS of *N. gonorrhoea* since eDNA is considered to be the major constituent of the matrix.

Such applications should extend to *in vivo* models, to evaluate the efficacy, safety and impact on microbiome of EPS targeting interventions under clinically relevant conditions. Additionally, using combined enzymatic treatments, such as mutanase and DNase, could be explored, as targeting multiple EPS components may enhance biofilm disruption when complete removal is desired. Also, tests on the stability and safety of adding dextranase to oral hygiene products must be established.

Finally, literature and work presented here highlight the need for future research focused on EPS mediated antimicrobial tolerance in biofilms. By integrating advanced biofilm models,

targeted EPS strategies, and analyses to establish how selective disruption of the biofilm matrix influences antimicrobial susceptibility under clinically relevant conditions. This is particularly relevant given the increasing burden of cariogenic disease reported in both low- and middle-income countries and around the world, where changing dietary patterns, sugar consumption, and access to preventive oral healthcare have contributed to rising carious lesion incidence. Therefore, systematic optimisation of EPS targeting interventions alongside conventional antimicrobials, could provide a rational adjunctive strategy for biofilm management. In parallel, translational assessment in more complex biological systems would be essential to evaluate safety, efficacy, and impacts under clinically relevant conditions.

6.8 Conclusion

This study employed various techniques that demonstrated the importance of EPS in development, structure and antimicrobial tolerance of biofilms. Biofilms showed increased tolerance compared to planktonic counterparts. Sucrose enhanced EPS production in oral biofilms containing *S. mutans* and biofilms of whole saliva inoculum. Using *S. mutans* as model microorganism, it was shown that EPS presence contributes to increased tolerance against CHX treatment. Enzymatic degradation of glucan using dextranase, particularly when applied during biofilm formation, degraded the EPS matrix and rendered the biofilm more susceptible to antimicrobial treatment.

CLSM was valuable for visualising biofilm and coupled with COMSTAT image analysis, enabled quantitative assessment of various parameters such as biomass, thickness and viability. In parallel, quantification assays proved useful in establishing the content of specific components within biofilms, such as carbohydrates and proteins. Lightsheet confocal Raman microscopy offered a complementary, label-free method for characterising the EPS disruption,

highlighting that it could be an important technique in case of limitations associated with fluorescent labelling in CLSM. Although identifying components was challenging, development and expansion of Raman spectral libraries by adding a wide range of EPS and biofilms components could aid in future attempts in identification of EPS components.

References

Abdelhamid, A. G. and Yousef, A. E. 2023. Combating bacterial biofilms: current and emerging antibiofilm strategies for treating persistent infections. *Antibiotics* 12(6), p. 1005.

Abdulrahman, H., Misba, L., Ahmad, S. and Khan, A. U. 2020. Curcumin induced photodynamic therapy mediated suppression of quorum sensing pathway of Pseudomonas aeruginosa: An approach to inhibit biofilm in vitro. *Photodiagnosis and Photodynamic Therapy* 30, p. 101645.

Abebe, G. M. 2020. The role of bacterial biofilm in antibiotic resistance and food contamination. *International journal of microbiology* 2020(1), p. 1705814.

Abranches, J. et al. 2018. Biology of oral streptococci. *Microbiology spectrum* 6(5), pp. 10.1128/microbiolspec. gpp1123-0042-2018.

Abuhajar, E., Ali, K., Zulfiqar, G., Al Ansari, K., Raja, H. Z., Bishti, S. and Anweigi, L. 2023. Management of chronic atrophic candidiasis (denture stomatitis)—a narrative review. *International journal of environmental research and public health* 20(4), p. 3029.

Abusleme, L. et al. 2013. The subgingival microbiome in health and periodontitis and its relationship with community biomass and inflammation. *The ISME journal* 7(5), pp. 1016-1025.

Achinas, S., Yska, S. K., Charalampogiannis, N., Krooneman, J. and Euverink, G. J. W. 2020. A technological understanding of biofilm detection techniques: a review. *Materials* 13(14), p. 3147.

Ahmad, A., Khan, A., Manzoor, N. and Khan, L. A. 2010. Evolution of ergosterol biosynthesis inhibitors as fungicidal against Candida. *Microbial pathogenesis* 48(1), pp. 35-41.

Al-kafaween, M. A., Mohd Hilmi, A. B., Jaffar, N., Al-Jamal, H. A. N. and Zahri, M. K. 2019. Determination of optimum incubation time for formation of Pseudomonas aeruginosa and Streptococcus pyogenes biofilms in microtiter plate. *Bulletin of the National Research Centre* 43, pp. 1-5.

Alcott, A. M., Werner, L. M., Baiocco, C. M., Belcher Dufrisne, M., Columbus, L. and Criss, A. K. 2022. Variable expression of opa proteins by Neisseria gonorrhoeae influences bacterial association and phagocytic killing by human neutrophils. *Journal of Bacteriology* 204(4), pp. e00035-00022.

Alhoshy, M. A., Samhan, F. A., El-Gendy, A. S. and Razek, T. M. 2025. Impact of Biofilm in Distribution Water Systems on Water Characteristics and Attempts for Treatment. *Water, Air, & Soil Pollution* 236(7), p. 463.

Ali, T., Basit, A., Karim, A. M., Lee, J.-H., Jeon, J.-H., Rehman, S. u. and Lee, S.-H. 2021. Mutation-based antibiotic resistance mechanism in methicillin-resistant Staphylococcus aureus clinical isolates. *Pharmaceuticals* 14(5), p. 420.

Allkja, J. et al. 2021. Interlaboratory study for the evaluation of three microtiter plate-based biofilm quantification methods. *Scientific reports* 11(1), p. 13779.

Alovisi, M. et al. 2022. Confocal laser scanner evaluation of bactericidal effect of chitosan nanodroplets loaded with benzalkonium chloride. *Journal of clinical medicine* 11(6), p. 1650.

Alves, C. T., Wei, X.-Q., Silva, S., Azeredo, J., Henriques, M. and Williams, D. W. 2014. Candida albicans promotes invasion and colonisation of Candida glabrata in a reconstituted human vaginal epithelium. *Journal of Infection* 69(4), pp. 396-407.

Amaechi, B. and Higham, S. 2001. In vitro remineralisation of eroded enamel lesions by saliva. *Journal of dentistry* 29(5), pp. 371-376.

Ammann, T., Bostanci, N., Belibasakis, G. and Thurnheer, T. 2013. Validation of a quantitative real-time PCR assay and comparison with fluorescence microscopy and selective agar plate counting for species-specific quantification of an in vitro subgingival biofilm model. *Journal of periodontal research* 48(4), pp. 517-526.

An, S. Q., Hull, R., Metris, A., Barrett, P., Webb, J. and Stoodley, P. 2022. An in vitro biofilm model system to facilitate study of microbial communities of the human oral cavity. *Letters in Applied Microbiology* 74(3), pp. 302-310.

Anderson, A. C. et al. 2018. In-vivo shift of the microbiota in oral biofilm in response to frequent sucrose consumption. *Scientific reports* 8(1), p. 14202.

Anderson, M. T., Byerly, L., Apicella, M. A. and Seifert, H. S. 2016. Seminal plasma promotes Neisseria gonorrhoeae aggregation and biofilm formation. *Journal of Bacteriology* 198(16), pp. 2228-2235.

Anju, V. et al. 2022. Polymicrobial infections and biofilms: clinical significance and eradication strategies. *Antibiotics* 11(12), p. 1731.

Appleton, S. S. 2000. Candidiasis: pathogenesis, clinical characteristics, and treatment. *Journal of the California Dental Association* 28(12), pp. 942-947.

Armbruster, C. R. and Parsek, M. R. 2018. New insight into the early stages of biofilm formation. *Proceedings of the National Academy of Sciences* 115(17), pp. 4317-4319.

Aruni, A. W., Dou, Y., Mishra, A. and Fletcher, H. M. 2015. The biofilm community: rebels with a cause. *Current oral health reports* 2(1), pp. 48-56.

Asare, E. O., Mun, E. A., Marsili, E. and Paunov, V. N. 2022. Nanotechnologies for control of pathogenic microbial biofilms. *Journal of Materials Chemistry B* 10(27), pp. 5129-5153.

Ashley, P. 2001. Toothbrushing: why, when and how? *Dental update* 28(1), pp. 36-40.

Asker, D. et al. 2021. Preventing Pseudomonas aeruginosa biofilms on indwelling catheters by surface-bound enzymes. *ACS applied bio materials* 4(12), pp. 8248-8258.

Assadian, O., Harbarth, S., Vos, M., Knobloch, J. K., Asensio, A. and Widmer, A. F. 2021. Practical recommendations for routine cleaning and disinfection procedures in healthcare institutions: a narrative review. *Journal of Hospital Infection* 113, pp. 104-114.

Atriwal, T., Azeem, K., Husain, F. M., Hussain, A., Khan, M. N., Alajmi, M. F. and Abid, M. 2021. Mechanistic understanding of Candida albicans biofilm formation and approaches for its inhibition. *Frontiers in microbiology* 12, p. 638609.

Ayala, J. C., Balthazar, J. T. and Shafer, W. M. 2024. Transcriptional responses of Neisseria gonorrhoeae to glucose and lactate: implications for resistance to oxidative damage and biofilm formation. *Mbio* 15(8), pp. e01761-01724.

Ayoub, H. M., Gregory, R. L., Tang, Q. and Lippert, F. 2020. Influence of salivary conditioning and sucrose concentration on biofilm-mediated enamel demineralization. *Journal of Applied Oral Science* 28, p. e20190501.

Azeredo, J. et al. 2017. Critical review on biofilm methods. *Critical reviews in microbiology* 43(3), pp. 313-351.

Balducci, E., Papi, F., Capialbi, D. E. and Del Bino, L. 2023. Polysaccharides' structures and functions in biofilm architecture of antimicrobial-resistant (AMR) pathogens. *International Journal of Molecular Sciences* 24(4), p. 4030.

Bales, P. M., Renke, E. M., May, S. L., Shen, Y. and Nelson, D. C. 2013. Purification and characterization of biofilm-associated EPS exopolysaccharides from ESKAPE organisms and other pathogens. *PloS one* 8(6), p. e67950.

Ballén, V., Cepas, V., Ratia, C., Gabasa, Y. and Soto, S. M. 2022. Clinical Escherichia coli: from biofilm formation to new antibiofilm strategies. *Microorganisms* 10(6), p. 1103.

Bamford, C. V., d'Mello, A., Nobbs, A. H., Dutton, L. C., Vickerman, M. M. and Jenkinson, H. F. 2009. Streptococcus gordonii modulates Candida albicans biofilm formation through intergeneric communication. *Infection and immunity* 77(9), pp. 3696-3704.

Barantsevich, N. and Barantsevich, E. 2022. Diagnosis and treatment of invasive candidiasis. *Antibiotics* 11(6), p. 718.

Barraud, N., Kjelleberg, S. and Rice, S. A. 2015. Dispersal from microbial biofilms. *Microbial Biofilms*, pp. 343-362.

Bartizal, C. and Odds, F. C. 2003. Influences of methodological variables on susceptibility testing of caspofungin against Candida species and Aspergillus fumigatus. *Antimicrobial Agents and Chemotherapy* 47(7), pp. 2100-2107.

Barzkar, N., Babich, O., Das, R., Sukhikh, S., Tamadoni Jahromi, S. and Sohail, M. 2022. Marine Bacterial dextranases: fundamentals and Applications. *Molecules* 27(17), p. 5533.

Baschong, W., Suetterlin, R. and Laeng, R. H. 2001. Control of autofluorescence of archival formaldehyde-fixed, paraffin-embedded tissue in confocal laser scanning microscopy (CLSM). *Journal of Histochemistry & Cytochemistry* 49(12), pp. 1565-1571.

Baty, J. J., Stoner, S. N. and Scoffield, J. A. 2022. Oral commensal streptococci: gatekeepers of the oral cavity. *Journal of Bacteriology* 204(11), pp. e00257-00222.

Bayani, M., Raisolvaezin, K., Almasi-Hashiani, A. and Mirhoseini, S. H. 2023. Bacterial biofilm prevalence in dental unit waterlines: a systematic review and meta-analysis. *BMC Oral Health* 23(1), p. 158.

Bedoya-Correa, C. M., Rincón-Rodríguez, R. J. and Parada-Sanchez, M. T. 2021. Acidogenic and aciduric properties of Streptococcus mutans serotype c according to its genomic variability. *European Journal of Oral Sciences* 129(6), p. e12824.

Behbahani, S. B., Kiridena, S. D., Wijayaratna, U. N., Taylor, C., Anker, J. N. and Tzeng, T.-R. J. 2022. pH variation in medical implant biofilms: Causes, measurements, and its implications for antibiotic resistance. *Frontiers in microbiology* 13, p. 1028560.

Belcher, T., Rollier, C. S., Dold, C., Ross, J. D. and MacLennan, C. A. 2023. Immune responses to Neisseria gonorrhoeae and implications for vaccine development. *Frontiers in immunology* 14, p. 1248613.

Bellou, N., Papathanassiou, E., Dobretsov, S., Lykousis, V. and Colijn, F. 2012. The effect of substratum type, orientation and depth on the development of bacterial deep-sea biofilm communities grown on artificial substrata deployed in the Eastern Mediterranean. *Biofouling* 28(2), pp. 199-213.

Benoit, M. R., Conant, C. G., Ionescu-Zanetti, C., Schwartz, M. and Matin, A. 2010. New device for high-throughput viability screening of flow biofilms. *Applied and Environmental Microbiology* 76(13), pp. 4136-4142.

Berlanga-Clavero, M. V. et al. 2022. Bacillus subtilis biofilm matrix components target seed oil bodies to promote growth and anti-fungal resistance in melon. *Nature microbiology* 7(7), pp. 1001-1015.

Besingi, R. N., Wenderska, I. B., Senadheera, D. B., Cvitkovitch, D. G., Long, J. R., Wen, Z. T. and Brady, L. J. 2017. Functional amyloids in Streptococcus mutans, their use as targets of biofilm inhibition and initial characterization of SMU_63c. *Microbiology* 163(4), pp. 488-501.

Bevilacqua, L., Milan, A., Del Lupo, V., Maglione, M. and Dolzani, L. 2018. Biofilms developed on dental implant titanium surfaces with different roughness: comparison between in vitro and in vivo studies. *Current microbiology* 75, pp. 766-772.

Bhattacharya, M. and Horswill, A. R. 2024. The role of human extracellular matrix proteins in defining Staphylococcus aureus biofilm infections. *FEMS microbiology reviews* 48(1), p. fuae002.

Bie, S. et al. 2025. Antibiofilm activity of Plumbagin against Staphylococcus aureus. *Scientific reports* 15(1), p. 7948.

Bijle, M. N. and Abdalla, M. M. 2024. The effect of arginine on the growth of probiotics. *Journal of dentistry* 149, p. 105272.

Billings, N., Ramirez Millan, M., Caldara, M., Rusconi, R., Tarasova, Y., Stocker, R. and Ribbeck, K. 2013. The extracellular matrix component Psl provides fast-acting antibiotic defense in Pseudomonas aeruginosa biofilms. *PLoS pathogens* 9(8), p. e1003526.

Bilotti, K., Potapov, V., Pryor, J. M., Duckworth, A. T., Keck, J. L. and Lohman, G. J. 2022. Mismatch discrimination and sequence bias during end-joining by DNA ligases. *Nucleic Acids Research* 50(8), pp. 4647-4658.

Board-Davies, E., Rhys-Williams, W., Hynes, D., Love, W. and Williams, D. 2023. Antimicrobial effects of XF drugs against Candida albicans and its biofilms. *Frontiers in Fungal Biology* 4, p. 1225647.

Bodey, G. P., Bolivar, R., Fainstein, V. and Jadeja, L. 1983. Infections caused by Pseudomonas aeruginosa. *Reviews of infectious diseases* 5(2), pp. 279-313.

Bollen, C. M., Papaioanno, W., Van Eldere, J., Schepers, E., Quirynen, M. and Van Steenberghe, D. 1996. The influence of abutment surface roughness on plaque accumulation and peri-implant mucositis. *Clinical oral implants research* 7(3), pp. 201-211.

Boulos, L., Prevost, M., Barbeau, B., Coallier, J. and Desjardins, R. 1999. LIVE/DEAD® BacLight™: application of a new rapid staining method for direct enumeration of viable and total bacteria in drinking water. *Journal of Microbiological Methods* 37(1), pp. 77-86.

Bourdichon, F. et al. 2012. Food fermentations: microorganisms with technological beneficial use. *International journal of food microbiology* 154(3), pp. 87-97.

Bowden, L. C., Finlinson, J., Jones, B. and Berges, B. K. 2024. Beyond the double helix: the multifaceted landscape of extracellular DNA in Staphylococcus aureus biofilms. *Frontiers in Cellular and Infection Microbiology* 14, p. 1400648.

Bowen, W. and Koo, H. 2011. Biology of Streptococcus mutans-derived glucosyltransferases: role in extracellular matrix formation of cariogenic biofilms. *Caries research* 45(1), pp. 69-86.

Bowen, W. H., Burne, R. A., Wu, H. and Koo, H. 2018. Oral biofilms: pathogens, matrix, and polymicrobial interactions in microenvironments. *Trends in microbiology* 26(3), pp. 229-242.

Bras, G. et al. 2024. Secreted aspartic proteinases: key factors in Candida infections and host-pathogen interactions. *International Journal of Molecular Sciences* 25(9), p. 4775.

Bridier, A., Briandet, R., Thomas, V. and Dubois-Brissonnet, F. 2011. Resistance of bacterial biofilms to disinfectants: a review. *Biofouling* 27(9), pp. 1017-1032.

Brookes, Z. L., Belfield, L. A., Ashworth, A., Casas-Agustench, P., Raja, M., Pollard, A. J. and Bescos, R. 2021. Effects of chlorhexidine mouthwash on the oral microbiome. *Journal of dentistry* 113, p. 103768.

Burne, R., Chen, Y.-Y., Wexler, D., Kuramitsu, H. and Bowen, W. 1996. Cariogenicity of Streptococcus mutans strains with defects in fructan metabolism assessed in a program-fed specific-pathogen-free rat model. *Journal of dental research* 75(8), pp. 1572-1577.

Buzzo, J. R. et al. 2021. Z-form extracellular DNA is a structural component of the bacterial biofilm matrix. *Cell* 184(23), pp. 5740-5758. e5717.

Cai, C., Chen, X., Li, Y. and Jiang, Q. 2023. Advances in the role of sodium hypochlorite irrigant in chemical preparation of root canal treatment. *BioMed research international* 2023(1), p. 8858283.

Cai, J.-N., Jung, J.-E., Dang, M.-H., Kim, M.-A., Yi, H.-K. and Jeon, J.-G. 2016. Functional relationship between sucrose and a cariogenic biofilm formation. *PloS one* 11(6), p. e0157184.

Calderone, R. A. and Fonzi, W. A. 2001. Virulence factors of Candida albicans. *Trends in microbiology* 9(7), pp. 327-335.

Cámara, M. et al. 2022. Economic significance of biofilms: a multidisciplinary and cross-sectoral challenge. *NPJ biofilms and microbiomes* 8(1), p. 42.

Carolus, H., Pierson, S., Lagrou, K. and Van Dijck, P. 2020. Amphotericin B and other polyenes—Discovery, clinical use, mode of action and drug resistance. *Journal of Fungi* 6(4), p. 321.

Catherwood, A. C. et al. 2020. Substrate and stereochemical control of peptidoglycan cross-linking by transpeptidation by Escherichia coli PBP1B. *Journal of the American Chemical Society* 142(11), pp. 5034-5048.

Cavalcanti, Y. W. et al. 2015. Virulence and pathogenicity of Candida albicans is enhanced in biofilms containing oral bacteria. *Biofouling* 31(1), pp. 27-38.

Ceri, H., Olson, M. E., Stremick, C., Read, R., Morck, D. and Buret, A. 1999. The Calgary Biofilm Device: new technology for rapid determination of antibiotic susceptibilities of bacterial biofilms. *Journal of clinical microbiology* 37(6), pp. 1771-1776.

Chang, C.-Y. 2018. Surface sensing for biofilm formation in Pseudomonas aeruginosa. *Frontiers in microbiology* 8, p. 2671.

Chang, H. and Rittmann, B. 1986. Biofilm loss during sample preparation for scanning electron microscopy. *Water research* 20(11), pp. 1451-1456.

Chawhuaveang, D. D., Yu, O. Y., Yin, I. X., Lam, W. Y.-H., Mei, M. L. and Chu, C.-H. 2021. Acquired salivary pellicle and oral diseases: A literature review. *Journal of Dental Sciences* 16(1), pp. 523-529.

Chen, W., Liang, J., He, Z. and Jiang, W. 2016. Preliminary study on total protein extraction methods from Enterococcus faecalis biofilm. *Genet Mol Res* 15(10.4238),

Chen, X., Daliri, E. B.-M., Kim, N., Kim, J.-R., Yoo, D. and Oh, D.-H. 2020. Microbial etiology and prevention of dental caries: exploiting natural products to inhibit cariogenic biofilms. *Pathogens* 9(7), p. 569.

Chen, Y. et al. 2024. The mechanical, wear, antibacterial properties and biocompatibility of injectable restorative materials under wet challenge. *Journal of dentistry* 146, p. 105025.

Chen, Y. et al. 2022. More than just a periodontal pathogen–the research progress on Fusobacterium nucleatum. *Frontiers in Cellular and Infection Microbiology* 12, p. 64.

Chen, Z., Ni, D., Zhang, W., Stressler, T. and Mu, W. 2021. Lactic acid bacteria-derived α-glucans: From enzymatic synthesis to miscellaneous applications. *Biotechnology Advances* 47, p. 107708.

Cheung, H.-Y., Wong, M. M.-K., Cheung, S.-H., Liang, L. Y., Lam, Y.-W. and Chiu, S.-K. 2012. Differential actions of chlorhexidine on the cell wall of Bacillus subtilis and Escherichia coli. *PloS one* 7(5), p. e36659.

Chiou, L.-L., Panariello, B. H., Hamada, Y., Gregory, R. L., Blanchard, S. and Duarte, S. 2023. Comparison of in vitro biofilm formation on titanium and zirconia implants. *BioMed research international* 2023(1), p. 8728499.

Cho, I. and Blaser, M. J. 2012. The human microbiome: at the interface of health and disease. *Nature Reviews Genetics* 13(4), pp. 260-270.

Choi, J. et al. 2020. Dynamics of the context-specific translation arrest by chloramphenicol and linezolid. *Nature chemical biology* 16(3), pp. 310-317.

Choudhari, S., Krithikadatta, J., Vejendla, I. and Doble, M. 2023. Microbial interactions in oral biofilm: evaluating therapeutic interventions and the emergence of resistance: a narrative review. *Cureus* 15(10),

Chow, E. W. L., Pang, L. M. and Wang, Y. 2021. From Jekyll to Hyde: the yeast–hyphal transition of Candida albicans. *Pathogens* 10(7), p. 859.

Chua, S. L. et al. 2014. Dispersed cells represent a distinct stage in the transition from bacterial biofilm to planktonic lifestyles. *Nature communications* 5(1), p. 4462.

Cialla-May, D. et al. 2021. Raman spectroscopy and imaging in bioanalytics. *Analytical Chemistry* 94(1), pp. 86-119.

Cieplik, F., Jakubovics, N. S., Buchalla, W., Maisch, T., Hellwig, E. and Al-Ahmad, A. 2019. Resistance toward chlorhexidine in oral bacteria–is there cause for concern? *Frontiers in microbiology* 10, p. 587.

Cifuente, J. O., Colleoni, C., Kalscheuer, R. and Guerin, M. E. 2024. Architecture, function, regulation, and evolution of α-glucans metabolic enzymes in prokaryotes. *Chemical reviews* 124(8), pp. 4863-4934.

Ciofu, O., Moser, C., Jensen, P. Ø. and Høiby, N. 2022. Tolerance and resistance of microbial biofilms. *Nature reviews microbiology* 20(10), pp. 621-635.

Ciofu, O., Rojo-Molinero, E., Macià, M. D. and Oliver, A. 2017. Antibiotic treatment of biofilm infections. *Apmis* 125(4), pp. 304-319.

Cleaver, L. and Garnett, J. A. 2023. How to study biofilms: technological advancements in clinical biofilm research. *Frontiers in Cellular and Infection Microbiology* 13, p. 1335389.

CLSI, C. 2018. Methods for dilution antimicrobial susceptibility tests for bacteria that grow aerobically. Clinical and Laboratory Standards Institute Wayne, PA.

Coenye, T. 2023. Biofilm antimicrobial susceptibility testing: where are we and where could we be going? *Clinical microbiology reviews* 36(4), pp. e00024-00023.

Coenye, T. and Nelis, H. J. 2010. In vitro and in vivo model systems to study microbial biofilm formation. *Journal of Microbiological Methods* 83(2), pp. 89-105.

Colvin, K. M., Gordon, V. D., Murakami, K., Borlee, B. R., Wozniak, D. J., Wong, G. C. and Parsek, M. R. 2011. The pel polysaccharide can serve a structural and protective role in the biofilm matrix of Pseudomonas aeruginosa. *PLoS pathogens* 7(1), p. e1001264.

Compant, S., Samad, A., Faist, H. and Sessitsch, A. 2019. A review on the plant microbiome: ecology, functions, and emerging trends in microbial application. *Journal of advanced research* 19, pp. 29-37.

Contaldo, M. et al. 2023. Oral candidiasis and novel therapeutic strategies: Antifungals, phytotherapy, probiotics, and photodynamic therapy. *Current Drug Delivery* 20(5), pp. 441-456.

Coppola, F., Fratianni, F., Bianco, V., Wang, Z., Pellegrini, M., Coppola, R. and Nazzaro, F. 2025. New Methodologies as Opportunities in the Study of Bacterial Biofilms, Including Food-Related Applications. *Microorganisms* 13(5), p. 1062.

Corbin, K. D. et al. 2023. Host-diet-gut microbiome interactions influence human energy balance: a randomized clinical trial. *Nature communications* 14(1), p. 3161.

Corcoll, N., Österlund, T., Sinclair, L., Eiler, A., Kristiansson, E., Backhaus, T. and Eriksson, K. M. 2017. Comparison of four DNA extraction methods for comprehensive assessment of 16S rRNA bacterial diversity in marine biofilms using high-throughput sequencing. *FEMS microbiology letters* 364(14), p. fnx139.

Cortez, A. A. et al. 2023. Recombinant Prevotella melaninogenica α-1, 3 glucanase and Capnocytophaga ochracea α-1, 6 glucanase as enzymatic tools for in vitro degradation of S. mutans biofilms. *World Journal of Microbiology and Biotechnology* 39(12), p. 357.

Costa-Barbosa, A. et al. 2025. Pre-clinical evaluation of a divalent liposomal vaccine to control invasive candidiasis. *npj Vaccines* 10(1), p. 124.

Costa Oliveira, B. E., Ricomini Filho, A. P., Burne, R. A. and Zeng, L. 2021. The route of sucrose utilization by Streptococcus mutans affects intracellular polysaccharide metabolism. *Frontiers in microbiology* 12, p. 636684.

Costa, O. Y., Raaijmakers, J. M. and Kuramae, E. E. 2018. Microbial extracellular polymeric substances: ecological function and impact on soil aggregation. *Frontiers in microbiology* 9, p. 1636.

Costa, R. C. et al. 2023. Polymicrobial biofilms related to dental implant diseases: unravelling the critical role of extracellular biofilm matrix. *Critical reviews in microbiology* 49(3), pp. 370-390.

Costa, R. C., Souza, J. G. S., Bertolini, M., Retamal-Valdes, B., Feres, M. and Barão, V. A. 2020. Extracellular biofilm matrix leads to microbial dysbiosis and reduces biofilm susceptibility to antimicrobials on titanium biomaterial: an in vitro and in situ study. *Clinical oral implants research* 31(12), pp. 1173-1186.

Crivello, G., Fracchia, L., Ciardelli, G., Boffito, M. and Mattu, C. 2023. In vitro models of bacterial biofilms: innovative tools to improve understanding and treatment of infections. *Nanomaterials* 13(5), p. 904.

Cugini, C., Ramasubbu, N., Tsiagbe, V. K. and Fine, D. H. 2021. Dysbiosis from a microbial and host perspective relative to oral health and disease. *Frontiers in microbiology* 12, p. 617485.

Cugini, C., Shanmugam, M., Landge, N. and Ramasubbu, N. 2019. The role of exopolysaccharides in oral biofilms. *Journal of dental research* 98(7), pp. 739-745.

D'Abramo, F. and Neumeyer, S. 2020. A historical and political epistemology of microbes. *Centaurus* 62(2), pp. 321-330.

da Silva, N. D. G. et al. 2022. Effect of experimental and commercial artificial saliva formulations on the activity and viability of microcosm biofilm and on enamel demineralization for irradiated patients with head and neck cancer (HNC). *Biofouling* 38(7), pp. 674-686.

Daily, J. P. 2017. Malaria 2017: update on the clinical literature and management. *Current infectious disease reports* 19(8), p. 28.

Danchik, C. and Casadevall, A. 2021. Role of cell surface hydrophobicity in the pathogenesis of medically-significant fungi. *Frontiers in Cellular and Infection Microbiology* 10, p. 594973.

Darville, T. 2021. Pelvic inflammatory disease due to Neisseria gonorrhoeae and Chlamydia trachomatis: immune evasion mechanisms and pathogenic disease pathways. *The Journal of infectious diseases* 224(Supplement_2), pp. S39-S46.

Dassanayake, R. P., Falkenberg, S. M., Stasko, J. A., Shircliff, A. L., Lippolis, J. D. and Briggs, R. E. 2020. Identification of a reliable fixative solution to preserve the complex architecture of bacterial biofilms for scanning electron microscopy evaluation. *PloS one* 15(5), p. e0233973.

Davey, M. E. 2008. Tracking dynamic interactions during plaque formation. *Journal of Bacteriology* 190(24), p. 7869.

Davey, M. E., Caiazza, N. C. and O'Toole, G. A. 2003. Rhamnolipid surfactant production affects biofilm architecture in Pseudomonas aeruginosa PAO1. *Journal of Bacteriology* 185(3), pp. 1027-1036.

Davies, D. 2003. Understanding biofilm resistance to antibacterial agents. *Nature reviews Drug discovery* 2(2), pp. 114-122.

Daw, A. E. et al. 2013. Differential cellular and microbial responses to nano-/micron-scale titanium surface roughness induced by hydrogen peroxide treatment. *Journal of biomaterials applications* 28(1), pp. 144-160.

Decker, E.-M., Klein, C., Schwindt, D. and Von Ohle, C. 2014. Metabolic activity of Streptococcus mutans biofilms and gene expression during exposure to xylitol and sucrose. *International Journal of Oral Science* 6(4), pp. 195-204.

Del Rey, Y. C., Parize, H., Assar, S., Göstemeyer, G. and Schlafer, S. 2024. Effect of mutanase and dextranase on biofilms of cariogenic bacteria: a systematic review of in vitro studies. *Biofilm* 7, p. 100202.

Deng, Y. et al. 2021. The vicK gene of Streptococcus mutans mediates its cariogenicity via exopolysaccharides metabolism. *International Journal of Oral Science* 13(1), p. 45.

Desai, J. V. 2018. Candida albicans hyphae: from growth initiation to invasion. *Journal of Fungi* 4(1), p. 10.

Deus, F. P. and Ouanounou, A. 2022. Chlorhexidine in dentistry: pharmacology, uses, and adverse effects. *International dental journal* 72(3), pp. 269-277.

Dhiman, S. et al. 2024. Bacterial biofilms: Pathogenesis, monitoring, treatment approaches and associated challenges. *Biologia* 79(10), pp. 3161-3181.

Di Bonaventura, G. and Pompilio, A. 2021. In vitro antimicrobial susceptibility testing of biofilm-growing bacteria: current and emerging methods. *Advances in Microbiology, Infectious Diseases and Public Health: Volume 16*, pp. 33-51.

Di Martino, P. 2018. Extracellular polymeric substances, a key element in understanding biofilm phenotype. *AIMS microbiology* 4(2), p. 274.

Di Martino, P. 2022. Antimicrobial agents and microbial ecology. *AIMS microbiology* 8(1), p. 1.

Díaz-Garrido, N., Lozano, C. P., Kreth, J. and Giacaman, R. A. 2022. Extended biofilm formation time by Streptococcus sanguinis modifies its non-cariogenic behavior, in vitro. *Brazilian oral research* 36, p. e107.

Dige, I., Paqué, P. N., Del Rey, Y. C., Lund, M. B., Schramm, A. and Schlafer, S. 2022. Fluorescence lectin binding analysis of carbohydrate components in dental biofilms grown in situ in the presence or absence of sucrose. *Molecular Oral Microbiology* 37(5), pp. 196-205.

Dillard, J. P. 2011. Genetic manipulation of Neisseria gonorrhoeae. *Current protocols in microbiology* 23(1), pp. 4A. 2.1-4A. 2.24.

Ding, X. et al. 2022. Challenges and innovations in treating chronic and acute wound infections: From basic science to clinical practice. *Burns & Trauma* 10, p. tkac014.

Dinu, S. et al. 2024. Insights into the Cytotoxicity and Irritant Potential of Chlorhexidine Digluconate: An In Vitro and In Ovo Safety Screening. *Dentistry Journal* 12(7), p. 221.

Djeribi, R., Bouchloukh, W., Jouenne, T. and Menaa, B. 2012. Characterization of bacterial biofilms formed on urinary catheters. *American journal of infection control* 40(9), pp. 854-859.

Dominguez, E. et al. 2018. Conservation and divergence in the Candida species biofilm matrix mannan-glucan complex structure, function, and genetic control. *Mbio* 9(2), pp. 10.1128/mbio. 00451-00418.

Donlan, R. M. 2002. Biofilms: microbial life on surfaces. *Emerging infectious diseases* 8(9), p. 881.

Donlan, R. M. and Costerton, J. W. 2002. Biofilms: survival mechanisms of clinically relevant microorganisms. *Clinical microbiology reviews* 15(2), pp. 167-193.

Drago, L. 2019. Chloramphenicol resurrected: A journey from antibiotic resistance in eye infections to biofilm and ocular microbiota. *Microorganisms* 7(9), p. 278.

Drew, R. H. 2010. Aminoglycosides.

Dsouza, F. P., Dinesh, S. and Sharma, S. 2024. Understanding the intricacies of microbial biofilm formation and its endurance in chronic infections: a key to advancing biofilm-targeted therapeutic strategies. *Archives of Microbiology* 206(2), p. 85.

Du, Q. et al. 2020. Sucrose promotes caries progression by disrupting the microecological balance in oral biofilms: an in vitro study. *Scientific reports* 10(1), p. 2961.

Duarte, S., Klein, M., Aires, C., Cury, J., Bowen, W. and Koo, H. 2008. Influences of starch and sucrose on Streptococcus mutans biofilms. *Oral microbiology and immunology* 23(3), pp. 206-212.

DuBois, M., Gilles, K. A., Hamilton, J. K., Rebers, P. A. and Smith, F. 1956. Colorimetric method for determination of sugars and related substances. *Analytical Chemistry* 28(3), pp. 350-356.

Dukanovic Rikvold, P., Skov Hansen, L. B., Meyer, R. L., Jørgensen, M. R., Tiwari, M. K. and Schlafer, S. 2024. The effect of enzymatic treatment with mutanase, beta-glucanase, and DNase on a saliva-derived biofilm model. *Caries research* 58(2), pp. 68-76.

Duque, C. et al. 2011. Downregulation of GbpB, a component of the VicRK regulon, affects biofilm formation and cell surface characteristics of Streptococcus mutans. *Infection and immunity* 79(2), pp. 786-796.

Durand, G. A., Raoult, D. and Dubourg, G. 2019. Antibiotic discovery: history, methods and perspectives. *International journal of antimicrobial agents* 53(4), pp. 371-382.

Dygico, L. K., Gahan, C. G., Grogan, H. and Burgess, C. M. 2020. The ability of Listeria monocytogenes to form biofilm on surfaces relevant to the mushroom production environment. *International journal of food microbiology* 317, p. 108385.

Ebaya, M. M. A., El-Mowafy, M., Adel El-Sokkary, M. M. and Hassan, R. 2020. Purification, characterization, and biocatalytic and antibiofilm activity of a novel dextranase from Talaromyces sp. *International journal of microbiology* 2020(1), p. 9198048.

Eggleston, G. and Monge, A. 2005. Optimization of sugarcane factory application of commercial dextranases. *Process Biochemistry* 40(5), pp. 1881-1894.

Elashiry, M. M., Bergeron, B. E. and Tay, F. R. 2023. Enterococcus faecalis in secondary apical periodontitis: Mechanisms of bacterial survival and disease persistence. *Microbial pathogenesis* 183, p. 106337.

Elias, S. and Banin, E. 2012. Multi-species biofilms: living with friendly neighbors. *FEMS microbiology reviews* 36(5), pp. 990-1004.

Elliott, A. D. 2020. Confocal microscopy: principles and modern practices. *Current protocols in cytometry* 92(1), p. e68.

Elshikh, M., Ahmed, S., Funston, S., Dunlop, P., McGaw, M., Marchant, R. and Banat, I. M. 2016. Resazurin-based 96-well plate microdilution method for the determination of minimum inhibitory concentration of biosurfactants. *Biotechnology letters* 38, pp. 1015-1019.

Enax, J., Ganss, B., Amaechi, B. T., Schulze zur Wiesche, E. and Meyer, F. 2023. The composition of the dental pellicle: an updated literature review. *Frontiers in Oral Health* 4, p. 1260442.

Ermer, M. A., Kottmann, S. C., Otten, J.-E., Wittmer, A., Poxleitner, P. and Pelz, K. 2018. In vitro investigation of the antimicrobial effect of three bisphosphonates against different bacterial strains. *Journal of Oral and Maxillofacial Surgery* 76(3), pp. 553-560.

Ernst, L., Schulz, C., Petzold, A., Thurn-Albrecht, T., Saalwächter, K. and Wefers, D. 2024. Detailed structural characterization of five water-insoluble α-glucans produced by glucansucrases from Streptococcus spp. *Carbohydrate Polymers* 337, p. 122164.

Evans, D. C., Mitkin, A. A., Rohde, H. and Meyer, R. L. 2025. Extracellular DNA and polysaccharide intercellular adhesin protect Staphylococcus epidermidis biofilms from phagocytosis by polymorphonuclear neutrophils. *Microbiological Research* 297, p. 128176.

Falsetta, M. L. et al. 2014. Symbiotic relationship between Streptococcus mutans and Candida albicans synergizes virulence of plaque biofilms in vivo. *Infection and immunity* 82(5), pp. 1968-1981.

Falsetta, M. L. et al. 2011. The composition and metabolic phenotype of Neisseria gonorrhoeae biofilms. *Frontiers in microbiology* 2, p. 75.

Fanaei Pirlar, R., Emaneini, M., Beigverdi, R., Banar, M., B. van Leeuwen, W. and Jabalameli, F. 2020. Combinatorial effects of antibiotics and enzymes against dual-species Staphylococcus aureus and Pseudomonas aeruginosa biofilms in the wound-like medium. *PloS one* 15(6), p. e0235093.

Fandilolu, P., Kumar, C., Palia, D. and Idicula-Thomas, S. 2024. Investigating role of positively selected genes and mutation sites of ERG11 in drug resistance of Candida albicans. *Archives of Microbiology* 206(11), p. 437.

Fang, J., Wang, C., Li, Y., Zhao, Z. and Mei, L. 2016. Comparison of bacterial adhesion to dental materials of polyethylene terephthalate (PET) and polymethyl methacrylate (PMMA) using atomic force microscopy and scanning electron microscopy. *Scanning* 38(6), pp. 665-670.

Fang, Y., Chen, X., Chu, C. H., Yu, O. Y., He, J. and Li, M. 2024. Roles of Streptococcus mutans in human health: beyond dental caries. *Frontiers in microbiology* 15, p. 1503657.

Félix-Rivera, H. and Hernández-Rivera, S. P. 2012. Raman spectroscopy techniques for the detection of biological samples in suspensions and as aerosol particles: a review. *Sensing and Imaging: An International Journal* 13(1), pp. 1-25.

Felz, S., Vermeulen, P., van Loosdrecht, M. C. and Lin, Y. M. 2019. Chemical characterization methods for the analysis of structural extracellular polymeric substances (EPS). *Water research* 157, pp. 201-208.

Ferguson, D. L., Gloag, E. S., Parsek, M. R. and Wozniak, D. J. 2023. Extracellular DNA enhances biofilm integrity and mechanical properties of mucoid Pseudomonas aeruginosa. *Journal of Bacteriology* 205(10), pp. e00238-00223.

Fleming, D., Chahin, L. and Rumbaugh, K. 2017. Glycoside hydrolases degrade polymicrobial bacterial biofilms in wounds. *Antimicrobial Agents and Chemotherapy* 61(2), pp. 10.1128/aac. 01998-01916.

Fleming, D. and Rumbaugh, K. 2018. The consequences of biofilm dispersal on the host. *Scientific reports* 8(1), p. 10738.

Flemming, H.-C. et al. 2025. Microbial extracellular polymeric substances in the environment, technology and medicine. *Nature reviews microbiology* 23(2), pp. 87-105.

Flemming, H.-C. et al. 2023. The biofilm matrix: multitasking in a shared space. *Nature reviews microbiology* 21(2), pp. 70-86.

Flemming, H.-C. and Wingender, J. 2010. The biofilm matrix. *Nature reviews microbiology* 8(9), pp. 623-633.

Flores-Mireles, A. L., Walker, J. N., Caparon, M. and Hultgren, S. J. 2015. Urinary tract infections: epidemiology, mechanisms of infection and treatment options. *Nature reviews microbiology* 13(5), pp. 269-284.

Folliero, V. et al. 2022. Rhein: A novel antibacterial compound against Streptococcus mutans infection. *Microbiological Research* 261, p. 127062.

Funari, R. and Shen, A. Q. 2022. Detection and characterization of bacterial biofilms and biofilm-based sensors. *ACS sensors* 7(2), pp. 347-357.

Galazzo, G. et al. 2020. How to count our microbes? The effect of different quantitative microbiome profiling approaches. *Frontiers in Cellular and Infection Microbiology* 10, p. 403.

Galdiero, E., Salvatore, M. M., Maione, A., de Alteriis, E., Andolfi, A., Salvatore, F. and Guida, M. 2021. GC-MS-based metabolomics study of single-and dual-species biofilms of Candida albicans and Klebsiella pneumoniae. *International Journal of Molecular Sciences* 22(7), p. 3496.

Galdino, R. V., Benevides, C. A. and Tenório, R. P. 2020. Diffusion maps of Bacillus subtilis biofilms via magnetic resonance imaging highlight a complex network of channels. *Colloids and surfaces B: Biointerfaces* 190, p. 110905.

Gan, W., Zhang, H., Zhang, Y. and Hu, X. 2014. Biosynthesis of oligodextrans with different Mw by synergistic catalysis of dextransucrase and dextranase. *Carbohydrate Polymers* 112, pp. 387-395.

Gao, L. et al. 2016. Nanocatalysts promote Streptococcus mutans biofilm matrix degradation and enhance bacterial killing to suppress dental caries in vivo. *Biomaterials* 101, pp. 272-284.

Gao, Z. et al. 2024. New strategies and mechanisms for targeting Streptococcus mutans biofilm formation to prevent dental caries: a review. *Microbiological Research* 278, p. 127526.

Garcia, B., Acosta, N., Tomar, S., Roesch, L., Lemos, J., Mugayar, L. and Abranches, J. 2021. Association of Candida albicans and Cbp+ Streptococcus mutans with early childhood caries recurrence. *Scientific reports* 11(1), p. 10802.

Gaur, S. and Bal, A. M. 2022. Tetracyclines.

Gayani, B., Dilhari, A., Kottegoda, N., Ratnaweera, D. R. and Weerasekera, M. M. 2021. Reduced crystalline biofilm formation on superhydrophobic silicone urinary catheter materials. *ACS omega* 6(17), pp. 11488-11496.

Georgiades, E. et al. 2021. The role of vessel biofouling in the translocation of marine pathogens: management considerations and challenges. *Frontiers in Marine Science*, p. 435.

Gerardi, D., Bernardi, S., Bruni, A., Falisi, G. and Botticelli, G. 2024. Characterization and morphological methods for oral biofilm visualization: where are we nowadays? *AIMS microbiology* 10(2), p. 391.

Gest, H. 2004. The discovery of microorganisms by Robert Hooke and Antoni Van Leeuwenhoek, fellows of the Royal Society. *Notes and records of the Royal Society of London* 58(2), pp. 187-201.

Gieroba, B., Krysa, M., Wojtowicz, K., Wiater, A., Pleszczyńska, M., Tomczyk, M. and Sroka-Bartnicka, A. 2020. The FT-IR and Raman spectroscopies as tools for biofilm characterization created by cariogenic streptococci. *International Journal of Molecular Sciences* 21(11), p. 3811.

Glasby, T. 2000. Surface composition and orientation interact to affect subtidal epibiota. *Journal of Experimental Marine Biology and Ecology* 248(2), pp. 177-190.

Goel, N., Fatima, S. W., Kumar, S., Sinha, R. and Khare, S. K. 2021. Antimicrobial resistance in biofilms: Exploring marine actinobacteria as a potential source of antibiotics and biofilm inhibitors. *Biotechnology Reports* 30, p. e00613.

Goeres, D. M., Loetterle, L. R., Hamilton, M. A., Murga, R., Kirby, D. W. and Donlan, R. M. 2005. Statistical assessment of a laboratory method for growing biofilms. *Microbiology* 151(3), pp. 757-762.

Gonçalves, L. S., Rodrigues, R. C. V., Junior, C. V. A., Soares, R. G. and Vettore, M. V. 2016. The effect of sodium hypochlorite and chlorhexidine as irrigant solutions for root canal disinfection: a systematic review of clinical trials. *Journal of endodontics* 42(4), pp. 527-532.

Gong, F. et al. 2024. Multiple biological characteristics and functions of intestinal biofilm extracellular polymers: friend or foe? *Frontiers in microbiology* 15, p. 1445630.

Gonzalez-Henao, S. and Schrenk, M. O. 2025. An astrobiological perspective on microbial biofilms: their importance for habitability and production of detectable and lasting biosignatures. *Applied and Environmental Microbiology* 91(3), pp. e01778-01724.

Goulart, T. S. et al. 2024. Assessment of multispecies biofilm growth on root canal dentin under different radiation therapy regimens. *Clinical oral investigations* 28(6), p. 324.

Gow, N. A. et al. 2022. The importance of antimicrobial resistance in medical mycology. *Nature communications* 13(1), p. 5352.

Gränicher, K. A., Karygianni, L., Attin, T. and Thurnheer, T. 2021. Low concentrations of chlorhexidine inhibit the formation and structural integrity of enzyme-treated multispecies oral biofilms. *Frontiers in microbiology* 12, p. 741863.

Grari, O. et al. 2025. A comprehensive review on biofilm-associated infections: Mechanisms, diagnostic challenges, and innovative therapeutic strategies. *The Microbe* 8, p. 100436.

Greenhalgh, R., Dempsey-Hibbert, N. C. and Whitehead, K. A. 2019. Antimicrobial strategies to reduce polymer biomaterial infections and their economic implications and considerations. *International Biodeterioration & Biodegradation* 136, pp. 1-14.

Greiner, L., Edwards, J., Shao, J., Rabinak, C., Entz, D. and Apicella, M. A. 2005. Biofilm formation by Neisseria gonorrhoeae. *Infection and immunity* 73(4), pp. 1964-1970.

Greule, A. and Cryle, M. J. 2020. The Glycopeptide Antibiotics.

Grooters, K. E. et al. 2024. Strategies for combating antibiotic resistance in bacterial biofilms. *Frontiers in Cellular and Infection Microbiology* 14, p. 1352273.

Grossman, A. B., Burgin, D. J. and Rice, K. C. 2021. Quantification of Staphylococcus aureus biofilm formation by crystal violet and confocal microscopy. *Staphylococcus aureus: methods and protocols*. Springer, pp. 69-78.

Guerra, M. E. S. et al. 2022. Klebsiella pneumoniae biofilms and their role in disease pathogenesis. *Frontiers in Cellular and Infection Microbiology* 12, p. 877995.

Guilhen, C., Forestier, C. and Balestrino, D. 2017. Biofilm dispersal: multiple elaborate strategies for dissemination of bacteria with unique properties. *Molecular microbiology* 105(2), pp. 188-210.

Guo, L., Hu, W., He, X., Lux, R., McLean, J. and Shi, W. 2013. Investigating acid production by Streptococcus mutans with a surface-displayed pH-sensitive green fluorescent protein. *PloS one* 8(2), p. e57182.

Guo, L., McLean, J. S., Lux, R., He, X. and Shi, W. 2015. The well-coordinated linkage between acidogenicity and aciduricity via insoluble glucans on the surface of Streptococcus mutans. *Scientific reports* 5(1), p. 18015.

Guzman-Soto, I. et al. 2021. Mimicking biofilm formation and development: Recent progress in in vitro and in vivo biofilm models. *Iscience* 24(5),

Guzmán-Soto, I. et al. 2021. Mimicking biofilm formation and development: Recent progress in in vitro and in vivo biofilm models. *Iscience* 24(5),

Hall-Stoodley, L., Costerton, J. W. and Stoodley, P. 2004. Bacterial biofilms: from the natural environment to infectious diseases. *Nature reviews microbiology* 2(2), pp. 95-108.

Harpf, V., Rambach, G., Würzner, R., Lass-Flörl, C. and Speth, C. 2020. Candida and complement: new aspects in an old battle. *Frontiers in immunology* 11, p. 1471.

Harrington, N. E., Sweeney, E. and Harrison, F. 2020. Building a better biofilm-formation of in vivo-like biofilm structures by Pseudomonas aeruginosa in a porcine model of cystic fibrosis lung infection. *Biofilm* 2, p. 100024.

Hasan, H. A. et al. 2024. A Review on the Roles of Extracellular Polymeric Substances (EPSs) in Wastewater Treatment: Source, Mechanism Study, Bioproducts, Limitations, and Future Challenges. *Water* 16(19), p. 2812.

Hasan, M. I. and Aggarwal, S. 2025. Matrix matters: how extracellular substances shape biofilm structure and mechanical properties. *Colloids and surfaces B: Biointerfaces* 246, p. 114341.

Hayacibara, M. F., Koo, H., Smith, A. M. V., Kopec, L. K., Scott-Anne, K., Cury, J. A. and Bowen, W. H. 2004. The influence of mutanase and dextranase on the production and structure of glucans synthesized by streptococcal glucosyltransferases. *Carbohydrate research* 339(12), pp. 2127-2137.

He, W., Liu, H., Wang, Z., Tay, F. R. and Shen, Y. 2024. The dynamics of bacterial proliferation, viability, and extracellular polymeric substances in oral biofilm development. *Journal of dentistry* 143, p. 104882.

Heijenoort, J. v. 2001. Formation of the glycan chains in the synthesis of bacterial peptidoglycan. *Glycobiology* 11(3), pp. 25R-36R.

Hellstein, J. W. and Marek, C. L. 2019. Candidiasis: red and white manifestations in the oral cavity. *Head and neck Pathology* 13, pp. 25-32.

Hengzhuang, W., Ciofu, O., Yang, L., Wu, H., Song, Z., Oliver, A. and Høiby, N. 2013. High β-lactamase levels change the pharmacodynamics of β-lactam antibiotics in Pseudomonas aeruginosa biofilms. *Antimicrobial Agents and Chemotherapy* 57(1), pp. 196-204.

Heydorn, A., Nielsen, A. T., Hentzer, M., Sternberg, C., Givskov, M., Ersbøll, B. K. and Molin, S. 2000. Quantification of biofilm structures by the novel computer program COMSTAT. *Microbiology* 146(10), pp. 2395-2407.

Highmore, C. et al. 2022. Translational challenges and opportunities in biofilm science: a BRIEF for the future. *NPJ biofilms and microbiomes* 8(1), p. 68.

Ho, J. et al. 2019. Candidalysin activates innate epithelial immune responses via epidermal growth factor receptor. *Nature communications* 10(1), p. 2297.

Hobley, L., Harkins, C., MacPhee, C. E. and Stanley-Wall, N. R. 2015. Giving structure to the biofilm matrix: an overview of individual strategies and emerging common themes. *FEMS microbiology reviews* 39(5), pp. 649-669.

Hof, H. 2006. A new, broad-spectrum azole antifungal: posaconazole–mechanisms of action and resistance, spectrum of activity. *Mycoses* 49, pp. 2-6.

Hong, Q., Sun, H., Chen, M., Zhang, S. and Yu, Q. 2022. Plasma treatment effects on destruction and recovery of Porphyromonas gingivalis biofilms. *PloS one* 17(9), p. e0274523.

Hoshino, T. and Fujiwara, T. 2022. The findings of glucosyltransferase enzymes derived from oral streptococci. *Japanese Dental Science Review* 58, pp. 328-335.

Hossain, T. J. 2024. Methods for screening and evaluation of antimicrobial activity: A review of protocols, advantages, and limitations. *European Journal of Microbiology and Immunology* 14(2), pp. 97-115.

Hou, K. et al. 2022. Microbiota in health and diseases. *Signal transduction and targeted therapy* 7(1), pp. 1-28.

Houchmandzadeh, B. and Ballet, P. 2023. A novel procedure for CFU plating and counting. *Journal of Microbiological Methods* 206, p. 106693.

Hrubanova, K., Nebesarova, J., Ruzicka, F. and Krzyzanek, V. 2018. The innovation of cryo-SEM freeze-fracturing methodology demonstrated on high pressure frozen biofilm. *Micron* 110, pp. 28-35.

Huang, L., Jin, Y., Zhou, D., Liu, L., Huang, S., Zhao, Y. and Chen, Y. 2022a. A review of the role of extracellular polymeric substances (EPS) in wastewater treatment systems. *International journal of environmental research and public health* 19(19), p. 12191.

Huang, L. et al. 2022b. Bacterial multidrug efflux pumps at the frontline of antimicrobial resistance: an overview. *Antibiotics* 11(4), p. 520.

Huang, X. et al. 2023. The oral microbiome in autoimmune diseases: friend or foe? *Journal of Translational Medicine* 21(1), pp. 1-24.

Huang, Y., Chakraborty, S. and Liang, H. 2020. Methods to probe the formation of biofilms: applications in foods and related surfaces. *Analytical methods* 12(4), pp. 416-432.

Hubbard, A., Coates, A. R. and Harvey, R. D. 2017. Comparing the action of HT61 and chlorhexidine on natural and model Staphylococcus aureus membranes. *The Journal of Antibiotics* 70(10), pp. 1020-1025.

Hwang, G. et al. 2016. Simultaneous spatiotemporal mapping of in situ pH and bacterial activity within an intact 3D microcolony structure. *Scientific reports* 6(1), p. 32841.

Ibáñez de Aldecoa, A. L., Zafra, O. and González-Pastor, J. E. 2017. Mechanisms and regulation of extracellular DNA release and its biological roles in microbial communities. *Frontiers in microbiology* 8, p. 1390.

International, A. 2007. *Standard Test Method for Quantification of Pseudomonas Aeruginosa Biofilm Grown with High Shear and Continuous Flow Using CDC Biofilm Reactor*. ASTM International.

Iorgulescu, G. 2009. Saliva between normal and pathological. Important factors in determining systemic and oral health. *Journal of medicine and life* 2(3), p. 303.

Jacobs, H. M., O'Neal, L., Lopatto, E., Wozniak, D. J., Bjarnsholt, T. and Parsek, M. R. 2022. Mucoid Pseudomonas aeruginosa can produce calcium-gelled biofilms independent of the matrix components Psl and CdrA. *Journal of Bacteriology* 204(5), pp. e00568-00521.

Jakubovics, N. S. and Burgess, J. G. 2015. Extracellular DNA in oral microbial biofilms. *Microbes and infection* 17(7), pp. 531-537.

Jakubovics, N. S., Goodman, S. D., Mashburn-Warren, L., Stafford, G. P. and Cieplik, F. 2021. The dental plaque biofilm matrix. *Periodontology 2000* 86(1), pp. 32-56.

Jamal, M. et al. 2018. Bacterial biofilm and associated infections. *Journal of the chinese medical association* 81(1), pp. 7-11.

James, P. et al. 2017. Chlorhexidine mouthrinse as an adjunctive treatment for gingival health. *Cochrane Database of Systematic Reviews* (3),

Järvinen, H., Pienihäkkinen, K., Huovinen, P. and Tenovuo, J. 1995. Susceptibility of Streptococcus mutans and Streptococcus sobrinus to antimicrobial agents after short-term oral chlorhexidine treatments. *European Journal of Oral Sciences* 103(1), pp. 32-35.

Järvinen, H., Tenovuo, J. and Huovinen, P. 1993. In vitro susceptibility of Streptococcus mutans to chlorhexidine and six other antimicrobial agents. *Antimicrobial Agents and Chemotherapy* 37(5), pp. 1158-1159.

Jeffries, J., Thongsomboon, W., Visser, J. A., Enriquez, K., Yager, D. and Cegelski, L. 2021. Variation in the ratio of curli and phosphoethanolamine cellulose associated with biofilm architecture and properties. *Biopolymers* 112(1), p. e23395.

Jennings, L. K. et al. 2015. Pel is a cationic exopolysaccharide that cross-links extracellular DNA in the Pseudomonas aeruginosa biofilm matrix. *Proceedings of the National Academy of Sciences* 112(36), pp. 11353-11358.

Jiménez, E. R. 2009. Dextranase in sugar industry: a review. *Sugar tech* 11, pp. 124-134.

Jo, J., Price-Whelan, A. and Dietrich, L. E. 2022. Gradients and consequences of heterogeneity in biofilms. *Nature reviews microbiology* 20(10), pp. 593-607.

Johnson, E., Petersen, T. and Goeres, D. M. 2021. Characterizing the shearing stresses within the CDC biofilm reactor using computational fluid dynamics. *Microorganisms* 9(8), p. 1709.

Joos, M. et al. 2025. EPS inhibitor treatment of Salmonella impacts evolution without selecting for resistance to biofilm inhibition. *NPJ biofilms and microbiomes* 11(1), p. 73.

Joshi, R. V., Gunawan, C. and Mann, R. 2021. We are one: multispecies metabolism of a biofilm consortium and their treatment strategies. *Frontiers in microbiology* 12, p. 635432.

Juntarachot, N., Kantachote, D., Peerajan, S., Sirilun, S. and Chaiyasut, C. 2020. Optimization of fungal dextranase production and its antibiofilm activity, encapsulation and stability in toothpaste. *Molecules* 25(20), p. 4784.

Jurakova, V. et al. 2023. Gene expression and metabolic activity of Streptococcus mutans during exposure to dietary carbohydrates glucose, sucrose, lactose, and xylitol. *Molecular Oral Microbiology* 38(5), pp. 424-441.

Kamali, M. and Sarvtin, M. T. 2023. Insights into candida albicans: a new perspective on pathogenic factors and regulatory mechanisms. *International Journal of Medical Laboratory*,

Kanampalliwar, A. and Singh, D. V. 2020. Extracellular DNA builds and interacts with vibrio polysaccharide in the biofilm matrix formed by Vibrio cholerae. *Environmental Microbiology Reports* 12(5), pp. 594-606.

Kaplan, J. B., Ragunath, C., Ramasubbu, N. and Fine, D. H. 2003. Detachment of Actinobacillus actinomycetemcomitans biofilm cells by an endogenous β-hexosaminidase activity. *Journal of Bacteriology* 185(16), pp. 4693-4698.

Kaplan, J. B., Sukhishvili, S. A., Sailer, M., Kridin, K. and Ramasubbu, N. 2024. Aggregatibacter actinomycetemcomitans dispersin B: The quintessential antibiofilm enzyme. *Pathogens* 13(8), p. 668.

Karygianni, L., Attin, T. and Thurnheer, T. 2020a. Combined DNase and proteinase treatment interferes with composition and structural integrity of multispecies oral biofilms. *Journal of clinical medicine* 9(4), p. 983.

Karygianni, L., Ren, Z., Koo, H. and Thurnheer, T. 2020b. Biofilm matrixome: extracellular components in structured microbial communities. *Trends in microbiology* 28(8), pp. 668-681.

Kasetty, S., Katharios-Lanwermeyer, S., O'Toole, G. A. and Nadell, C. D. 2021. Differential surface competition and biofilm invasion strategies of Pseudomonas aeruginosa PA14 and PAO1. *Journal of Bacteriology* 203(22), pp. 10.1128/jb. 00265-00221.

Keleştemur, S., Avci, E. and Çulha, M. 2018. Raman and surface-enhanced Raman scattering for biofilm characterization. *Chemosensors* 6(1), p. 5.

Kennedy, M. J. 1988. Adhesion and association mechanisms of Candida albicans. *Current topics in medical mycology*, pp. 73-169.

Khalikova, E., Susi, P. and Korpela, T. 2005. Microbial dextran-hydrolyzing enzymes: fundamentals and applications. *Microbiology and molecular biology reviews* 69(2), pp. 306-325.

Khan, R., Adil, M. and Khan, A. U. 2023. Molecular basis of cariogenic biofilm and infections. *Understanding Microbial Biofilms*, pp. 427-443.

Kilian, M. et al. 2016. The oral microbiome–an update for oral healthcare professionals. *British dental journal* 221(10), pp. 657-666.

Kim, D. et al. 2018. Bacterial-derived exopolysaccharides enhance antifungal drug tolerance in a cross-kingdom oral biofilm. *The ISME journal* 12(6), pp. 1427-1442.

Kim, H.-T., Çakmak, G., Jo, Y.-H., Jee, E.-B., Cho, J.-H., Yoon, H.-I. and Yilmaz, B. 2025. Surface properties and biofilm formation on resins for subtractively and additively manufactured fixed dental prostheses aged in artificial saliva: Effect of material type and surface finishing. *The Journal of Prosthetic Dentistry* 133(2), pp. 594. e591-594. e599.

Kim, W. J., Mai, A., Weyand, N. J., Rendón, M. A., Van Doorslaer, K. and So, M. 2019. Neisseria gonorrhoeae evades autophagic killing by downregulating CD46-cyt1 and remodeling lysosomes. *PLoS pathogens* 15(2), p. e1007495.

Kiran, M. A., Alghamdi, S., Ashgar, S., Alhindi, Z., Al-Abdullah, N. and Dablool, A. S. 2024. Systematic Review and Meta-analysis on Antimicrobial Resistance and Drug Resistance in Saudi Arabia. *Journal of global antimicrobial resistance*,

Kisley, L. and Landes, C. F. 2015. Molecular approaches to chromatography using single molecule spectroscopy. *Analytical Chemistry* 87(1), pp. 83-98.

Kives, J., Orgaz, B. and SanJosé, C. 2006. Polysaccharide differences between planktonic and biofilm-associated EPS from Pseudomonas fluorescens B52. *Colloids and surfaces B: Biointerfaces* 52(2), pp. 123-127.

Kiziltoprak, H., Ozkoyuncu, D., Tekin, K. and Koc, M. 2021. Confocal Scanning Laser Microscopy in Medicine.*Biomedical Signal and Image Processing*. IntechOpen.

Klahan, P. et al. 2018. Engineered dextranase from Streptococcus mutans enhances the production of longer isomaltooligosaccharides. *Bioscience, Biotechnology, and Biochemistry* 82(9), pp. 1480-1487.

Klein, M., Duarte, S., Xiao, J., Mitra, S., Foster, T. and Koo, H. 2009. Structural and molecular basis of the role of starch and sucrose in Streptococcus mutans biofilm development. *Applied and Environmental Microbiology* 75(3), pp. 837-841.

Klein, M. I., Xiao, J., Lu, B., Delahunty, C. M., Yates III, J. R. and Koo, H. 2012. Streptococcus mutans protein synthesis during mixed-species biofilm development by high-throughput quantitative proteomics.

Koehler, P. et al. 2019. Morbidity and mortality of candidaemia in Europe: an epidemiologic meta-analysis. *Clinical Microbiology and Infection* 25(10), pp. 1200-1212.

Kofla, G. and Ruhnke, M. 2011. Pharmacology and metabolism of anidulafungin, caspofungin and micafungin in the treatment of invasive candidosis-review of the literature. *European journal of medical research* 16(4), p. 159.

Kohno, T., Kitagawa, H., Tsuboi, R., Nishimura, Y. and Imazato, S. 2021. Establishment of novel in vitro culture system with the ability to reproduce oral biofilm formation on dental materials. *Scientific reports* 11(1), p. 21188.

Kong, E. F., Tsui, C., Kucharíková, S., Andes, D., Van Dijck, P. and Jabra-Rizk, M. A. 2016. Commensal protection of Staphylococcus aureus against antimicrobials by Candida albicans biofilm matrix. *Mbio* 7(5), pp. 10.1128/mbio. 01365-01316.

Koo, H., Allan, R. N., Howlin, R. P., Stoodley, P. and Hall-Stoodley, L. 2017. Targeting microbial biofilms: current and prospective therapeutic strategies. *Nature reviews microbiology* 15(12), pp. 740-755.

Koo, H., Falsetta, M. and Klein, M. 2013. The exopolysaccharide matrix: a virulence determinant of cariogenic biofilm. *Journal of dental research* 92(12), pp. 1065-1073.

Koo, H., Xiao, J., Klein, M. and Jeon, J. 2010. Exopolysaccharides produced by Streptococcus mutans glucosyltransferases modulate the establishment of microcolonies within multispecies biofilms. American Society for Microbiology.

Kotaskova, I. et al. 2019. Molecular techniques complement culture-based assessment of bacteria composition in mixed biofilms of urinary tract catheter-related samples. *Frontiers in microbiology* 10, p. 462.

Kozak, M. and Pawlik, A. 2023. The role of the oral microbiome in the development of diseases. *International Journal of Molecular Sciences* 24(6), p. 5231.

Kragh, K. N., Alhede, M., Kvich, L. and Bjarnsholt, T. 2019. Into the well—A close look at the complex structures of a microtiter biofilm and the crystal violet assay. *Biofilm* 1, p. 100006.

Krasowska, A. and Sigler, K. 2014. How microorganisms use hydrophobicity and what does this mean for human needs? *Frontiers in Cellular and Infection Microbiology* 4, p. 112.

Krause, K. M., Serio, A. W., Kane, T. R. and Connolly, L. E. 2016. Aminoglycosides: an overview. *Cold Spring Harbor perspectives in medicine* 6(6), p. a027029.

Krawczyk, S. J., Leśniczak-Staszak, M., Gowin, E. and Szaflarski, W. 2024. Mechanistic insights into clinically relevant ribosome-targeting antibiotics. *Biomolecules* 14(10), p. 1263.

Kreth, J., Zhu, L., Merritt, J., Shi, W. and Qi, F. 2008. Role of sucrose in the fitness of Streptococcus mutans. *Oral microbiology and immunology* 23(3), pp. 213-219.

Krzyściak, W., Pluskwa, K., Jurczak, A. and Kościelniak, D. 2013. The pathogenicity of the Streptococcus genus. *European Journal of Clinical Microbiology & Infectious Diseases* 32(11), pp. 1361-1376.

Kumar, D. and Kumar, A. 2023. High throughput bioanalytical techniques for elucidation of Candida albicans biofilm architecture and metabolome. *Rendiconti Lincei. Scienze Fisiche e Naturali* 34(1), pp. 117-129.

Kumar, R. and Srivastava, V. 2023. Application of anti-fungal vaccines as a tool against emerging anti-fungal resistance. *Frontiers in Fungal Biology* 4, p. 1241539.

Kurzyp, K. and Harrison, O. B. 2023. Bacterium of one thousand and one variants: genetic diversity of Neisseria gonorrhoeae pathogenicity. *Microbial Genomics* 9(6), p. 001040.

Kwasny, S. M. and Opperman, T. J. 2010. Static biofilm cultures of Gram-positive pathogens grown in a microtiter format used for anti-biofilm drug discovery. *Current protocols in pharmacology* 50(1), pp. 13A. 18.11-13A. 18.23.

Laudes, M., Geisler, C., Rohmann, N., Bouwman, J., Pischon, T. and Schlicht, K. 2021. Microbiota in Health and Disease—Potential Clinical Applications. *Nutrients* 13(11), p. 3866.

Le, P. H., Linklater, D. P., Medina, A. A., MacLaughlin, S., Crawford, R. J. and Ivanova, E. P. 2024. Impact of multiscale surface topography characteristics on Candida albicans biofilm formation: from cell repellence to fungicidal activity. *Acta Biomaterialia* 177, pp. 20-36.

Lebeaux, D., Chauhan, A., Rendueles, O. and Beloin, C. 2013. From in vitro to in vivo models of bacterial biofilm-related infections. *Pathogens* 2(2), pp. 288-356.

Leme, A. P., Koo, H., Bellato, C., Bedi, G. and Cury, J. 2006. The role of sucrose in cariogenic dental biofilm formation—new insight. *Journal of dental research* 85(10), pp. 878-887.

Lemos, J. et al. 2019. The biology of Streptococcus mutans. *Microbiology spectrum* 7(1), p. 7.1. 03.

Lertpimonchai, A., Rattanasiri, S., Vallibhakara, S. A.-O., Attia, J. and Thakkinstian, A. 2017. The association between oral hygiene and periodontitis: a systematic review and meta-analysis. *International dental journal* 67(6), pp. 332-343.

Lewenza, S. 2013. Extracellular DNA-induced antimicrobial peptide resistance mechanisms in Pseudomonas aeruginosa. *Frontiers in microbiology* 4, p. 21.

Lewis, M. and Williams, D. 2017. Diagnosis and management of oral candidosis. *British dental journal* 223(9), pp. 675-681.

LewisOscar, F., Nithya, C., Alharbi, S. A., Alharbi, N. S. and Thajuddin, N. 2018. Microfouling inhibition of human nosocomial pathogen Pseudomonas aeruginosa using marine cyanobacteria. *Microbial pathogenesis* 114, pp. 107-115.

Li, H., Liu, H., Zhang, L., Hieawy, A. and Shen, Y. 2023. Evaluation of extracellular polymeric substances matrix volume, surface roughness and bacterial adhesion property of oral biofilm. *Journal of Dental Sciences* 18(4), pp. 1723-1730.

Li, L. et al. 2024. Relationship between biofilm formation and antibiotic resistance of Klebsiella pneumoniae and updates on antibiofilm therapeutic strategies. *Frontiers in Cellular and Infection Microbiology* 14, p. 1324895.

Li, X. et al. 2025. The intricate interplay among microbiota, mucosal immunity, and viral infection in the respiratory tract. *Journal of Translational Medicine* 23(1), p. 488.

Li, Y., Xiao, P., Wang, Y. and Hao, Y. 2020. Mechanisms and control measures of mature biofilm resistance to antimicrobial agents in the clinical context. *ACS omega* 5(36), pp. 22684-22690.

Liang, S., He, Y., Chen, X., Wu, M. and Li, K. 2024. Effect of Different Concentrations of Chlorhexidine on Anti-Plaque in Oral Care Practice: A Systematic Review and Network Meta-Analysis. *International Journal of Dental Hygiene*,

Liao, S. et al. 2014. Streptococcus mutans extracellular DNA is upregulated during growth in biofilms, actively released via membrane vesicles, and influenced by components of the protein secretion machinery. *Journal of Bacteriology* 196(13), pp. 2355-2366.

Lim, K.-S. and Kam, P. 2008. Chlorhexidine-pharmacology and clinical applications. *Anaesthesia and intensive care* 36(4), pp. 502-512.

Limoli, D. H., Jones, C. J. and Wozniak, D. J. 2015. Bacterial extracellular polysaccharides in biofilm formation and function. *Microbial Biofilms*, pp. 223-247.

Lindsay, D., Killington, A., Fouhy, K., Loh, M. and Malakar, P. 2022. The CDC biofilm bioreactor is a suitable method to grow biofilms, and test their sanitiser susceptibilities, in the dairy context. *International Dairy Journal* 126, p. 105264.

Lionakis, M. S., Drummond, R. A. and Hohl, T. M. 2023. Immune responses to human fungal pathogens and therapeutic prospects. *Nature Reviews Immunology* 23(7), pp. 433-452.

LiPuma, J. J. 2010. The changing microbial epidemiology in cystic fibrosis. *Clinical microbiology reviews* 23(2), pp. 299-323.

Litvinjenko, S., Magwood, O., Wu, S. and Wei, X. 2023. Burden of tuberculosis among vulnerable populations worldwide: an overview of systematic reviews. *The Lancet Infectious Diseases* 23(12), pp. 1395-1407.

Liu, C. et al. 2013. Hyperosmotic response of streptococcus mutans: from microscopic physiology to transcriptomic profile. *BMC microbiology* 13, pp. 1-9.

Liu, H. Y., Prentice, E. L. and Webber, M. A. 2024. Mechanisms of antimicrobial resistance in biofilms. *npj Antimicrobials and Resistance* 2(1), p. 27.

Liu, R. et al. 2025. Imbalance of oral microbiome homeostasis: the relationship between microbiota and the occurrence of dental caries. *BMC microbiology* 25(1), p. 46.

Liu, X.-Y., Guo, S., Bocklitz, T., Rösch, P., Popp, J. and Yu, H.-Q. 2022. Nondestructive 3D imaging and quantification of hydrated biofilm matrix by confocal Raman microscopy coupled with non-negative matrix factorization. *Water research* 210, p. 117973.

Liu, Z., Wang, F., Ren, J. and Qu, X. 2019. A series of MOF/Ce-based nanozymes with dual enzyme-like activity disrupting biofilms and hindering recolonization of bacteria. *Biomaterials* 208, pp. 21-31.

Lobo, C. I. V., Rinaldi, T. B., Christiano, C. M. S., De Sales Leite, L., Barbugli, P. A. and Klein, M. I. 2019. Dual-species biofilms of Streptococcus mutans and Candida albicans exhibit more biomass and are mutually beneficial compared with single-species biofilms. *Journal of oral microbiology* 11(1), p. 1581520.

Lopes, L. Q. S., de Almeida Vaucher, R., Giongo, J. L., Gündel, A. and Santos, R. C. V. 2019. Characterisation and anti-biofilm activity of glycerol monolaurate nanocapsules against Pseudomonas aeruginosa. *Microbial pathogenesis* 130, pp. 178-185.

Lorenzo-Pouso, A. I. et al. 2022. Oral chronic hyperplastic candidiasis and its potential risk of malignant transformation: a systematic review and prevalence meta-analysis. *Journal of Fungi* 8(10), p. 1093.

Lorusso, A. B., Carrara, J. A., Barroso, C. D. N., Tuon, F. F. and Faoro, H. 2022. Role of efflux pumps on antimicrobial resistance in Pseudomonas aeruginosa. *International Journal of Molecular Sciences* 23(24), p. 15779.

Lu, H., Shrivastava, M., Whiteway, M. and Jiang, Y. 2021. Candida albicans targets that potentially synergize with fluconazole. *Critical reviews in microbiology* 47(3), pp. 323-337.

Lu, L., Zhao, Y., Li, M., Wang, X., Zhu, J., Liao, L. and Wang, J. 2024. Contemporary strategies and approaches for characterizing composition and enhancing biofilm penetration targeting bacterial extracellular polymeric substances. *Journal of Pharmaceutical Analysis* 14(4), p. 100906.

Lu, Y., Lin, Y., Li, M. and He, J. 2023. Roles of Streptococcus mutans-Candida albicans interaction in early childhood caries: a literature review. *Frontiers in Cellular and Infection Microbiology* 13, p. 1151532.

Luppens, S. B., Reij, M. W., van der Heijden, R. W., Rombouts, F. M. and Abee, T. 2002. Development of a standard test to assess the resistance of Staphylococcus aureus biofilm cells to disinfectants. *Applied and Environmental Microbiology* 68(9), pp. 4194-4200.

Lynch, D. J., Fountain, T. L., Mazurkiewicz, J. E. and Banas, J. A. 2007. Glucan-binding proteins are essential for shaping Streptococcus mutans biofilm architecture. *FEMS microbiology letters* 268(2), pp. 158-165.

Ma, J., Piao, X., Mahfuz, S., Long, S. and Wang, J. 2022. The interaction among gut microbes, the intestinal barrier and short chain fatty acids. *Animal Nutrition* 9, pp. 159-174.

Madsen, J. S., Burmølle, M., Hansen, L. H. and Sørensen, S. J. 2012. The interconnection between biofilm formation and horizontal gene transfer. *FEMS Immunology & Medical Microbiology* 65(2), pp. 183-195.

Magana, M. et al. 2018. Options and limitations in clinical investigation of bacterial biofilms. *Clinical microbiology reviews* 31(3), pp. 10.1128/cmr. 00084-00016.

Malard, F., Dore, J., Gaugler, B. and Mohty, M. 2021. Introduction to host microbiome symbiosis in health and disease. *Mucosal Immunology* 14(3), pp. 547-554.

Malea, E., Petala, M., Kostoglou, M. and Karapantsios, T. 2025. Contribution of the Gravity Component and Surface Type During the Initial Stages of Biofilm Formation at Solid–Liquid Interfaces. *Water* 17(15), p. 2277.

Manavathu, E. K. and Vazquez, J. A. 2017. The functional resistance of biofilms. *Antimicrobial Drug Resistance: Mechanisms of Drug Resistance, Volume 1*. Springer, pp. 149-162.

Manoharan-Basil, S. S., Laumen, J. G. E., Van Dijck, C., De Block, T., De Baetselier, I. and Kenyon, C. 2021. Evidence of horizontal gene transfer of 50S ribosomal genes rplB, rplD, and rplY in Neisseria gonorrhoeae. *Frontiers in microbiology* 12, p. 683901.

Marin, L. M., Xiao, Y., Seo, J., Queiroz, D. and Siqueira, W. L. 2025. Dietary Carbohydrates Modulate Streptococcus mutans Adherence and Bacterial Proteome. *Caries research* 59(2), pp. 128-138.

Markowska, K., Szymanek-Majchrzak, K., Pituch, H. and Majewska, A. 2024. Understanding quorum-sensing and biofilm forming in anaerobic bacterial communities. *International Journal of Molecular Sciences* 25(23), p. 12808.

Marsh, P. and Zaura, E. 2017. Dental biofilm: ecological interactions in health and disease. *Journal of clinical periodontology* 44, pp. S12-S22.

Marsh, P. D. ed. 2006. *Dental plaque as a biofilm and a microbial community–implications for health and disease*. *BMC Oral Health.* BioMed Central.

Martin, M. V. 1999. The use of fluconazole and itraconazole in the treatment of Candida albicans infections: a review. *Journal of Antimicrobial Chemotherapy* 44(4), pp. 429-437.

Martínez-Hernández, M., Reyes-Grajeda, J. P., Hannig, M. and Almaguer-Flores, A. 2023. Salivary pellicle modulates biofilm formation on titanium surfaces. *Clinical oral investigations* 27(10), pp. 6135-6145.

Martínez, D. et al. 2021. Removal of bacterial dextran in sugarcane juice by Talaromyces minioluteus dextranase expressed constitutively in Pichia pastoris. *Journal of Biotechnology* 333, pp. 10-20.

Martins, K. B., Ferreira, A. M., Pereira, V. C., Pinheiro, L., Oliveira, A. d. and Cunha, M. d. L. R. d. S. d. 2019. In vitro effects of antimicrobial agents on planktonic and biofilm forms of Staphylococcus saprophyticus isolated from patients with urinary tract infections. *Frontiers in microbiology* 10, p. 40.

Martins, M., Uppuluri, P., Thomas, D. P., Cleary, I. A., Henriques, M., Lopez-Ribot, J. L. and Oliveira, R. 2010. Presence of extracellular DNA in the Candida albicans biofilm matrix and its contribution to biofilms. *Mycopathologia* 169(5), pp. 323-331.

Marzucco, A. et al. 2024. Evaluation of biofilm production and antifungal susceptibility to fluconazole in clinical isolates of Candida spp. in both planktonic and biofilm form. *Microorganisms* 12(1), p. 153.

Maseda, H., Sawada, I., Saito, K., Uchiyama, H., Nakae, T. and Nomura, N. 2004. Enhancement of the mexAB-oprM efflux pump expression by a quorum-sensing autoinducer and its cancellation by a regulator, MexT, of the mexEF-oprN efflux pump operon in Pseudomonas aeruginosa. *Antimicrobial Agents and Chemotherapy* 48(4), pp. 1320-1328.

Masia, F., Glen, A., Stephens, P., Borri, P. and Langbein, W. 2013. Quantitative chemical imaging and unsupervised analysis using hyperspectral coherent anti-Stokes Raman scattering microscopy. *Analytical Chemistry* 85(22), pp. 10820-10828.

Masuda, N., Sakagawa, E., Ohya, S., Gotoh, N., Tsujimoto, H. and Nishino, T. 2000. Substrate specificities of MexAB-OprM, MexCD-OprJ, and MexXY-oprM efflux pumps in Pseudomonas aeruginosa. *Antimicrobial Agents and Chemotherapy* 44(12), pp. 3322-3327.

Mattern, R., Ernst, S., Böcher, S., Braun, A., Wenzler, J.-S. and Conrads, G. 2024. CLSM-guided imaging for quantifying endodontic disinfection. *Antibiotics* 13(1), p. 54.

Mayer, F. L., Wilson, D. and Hube, B. 2013. Candida albicans pathogenicity mechanisms. *Virulence* 4(2), pp. 119-128.

McDougald, D., Rice, S. A., Barraud, N., Steinberg, P. D. and Kjelleberg, S. 2012. Should we stay or should we go: mechanisms and ecological consequences for biofilm dispersal. *Nature reviews microbiology* 10(1), pp. 39-50.

McReynolds, D. E., Moorthy, A., Moneley, J. O. C., Jabra-Rizk, M. A. and Sultan, A. S. 2023. Denture stomatitis—An interdisciplinary clinical review. *Journal of Prosthodontics* 32(7), pp. 560-570.

Meisen, S., Wingender, J. and Telgheder, U. 2008. Analysis of microbial extracellular polysaccharides in biofilms by HPLC. Part I: development of the analytical method using two complementary stationary phases. *Analytical and bioanalytical chemistry* 391, pp. 993-1002.

Mendez, E., Walker, D. K., Vipham, J. and Trinetta, V. 2020. The use of a CDC biofilm reactor to grow multi-strain Listeria monocytogenes biofilm. *Food Microbiology* 92, p. 103592.

Mendhe, S., Badge, A., Ugemuge, S. and Chandi, D. 2023. Impact of biofilms on chronic infections and medical challenges. *Cureus* 15(11),

Metwalli, K. H., Khan, S. A., Krom, B. P. and Jabra-Rizk, M. A. 2013. Streptococcus mutans, Candida albicans, and the human mouth: a sticky situation. *PLoS pathogens* 9(10), p. e1003616.

Meyer, F., Enax, J., Epple, M., Amaechi, B. T. and Simader, B. 2021. Cariogenic biofilms: Development, properties, and biomimetic preventive agents. *Dentistry Journal* 9(8), p. 88.

Mhade, S. and Kaushik, K. S. 2023. Tools of the Trade: Image Analysis Programs for Confocal Laser-Scanning Microscopy Studies of Biofilms and Considerations for Their Use by Experimental Researchers. *ACS omega*,

Michaelis, C. and Grohmann, E. 2023. Horizontal gene transfer of antibiotic resistance genes in biofilms. *Antibiotics* 12(2), p. 328.

Mirghani, R. et al. 2022. Biofilms: Formation, drug resistance and alternatives to conventional approaches. *AIMS microbiology* 8(3), p. 239.

Mirzaei, R. et al. 2020. The biofilm-associated bacterial infections unrelated to indwelling devices. *IUBMB life* 72(7), pp. 1271-1285.

Mitchell, K. F., Zarnowski, R. and Andes, D. R. 2016. Fungal super glue: the biofilm matrix and its composition, assembly, and functions. *PLoS pathogens* 12(9), p. e1005828.

Mogavero, S. et al. 2021. Candidalysin delivery to the invasion pocket is critical for host epithelial damage induced by Candida albicans. *Cellular microbiology* 23(10), p. e13378.

Mohammed, A. and Abdullah, A. eds. 2018. *Scanning electron microscopy (SEM): A review*. *Proceedings of the 2018 international conference on hydraulics and pneumatics—HERVEX, Băile Govora, Romania.*

Montoya, C., Kurylec, J., Ossa, A. and Orrego, S. 2023. Cyclic strain of Poly (methyl methacrylate) surfaces triggered the pathogenicity of Candida albicans. *Acta Biomaterialia* 170, pp. 415-426.

Moon, J., Seo, K. and Kwon, J.-S. 2025. Novel two-stage expansion of Streptococcus mutans biofilm supports EPS-targeted prevention strategies for early childhood caries. *NPJ biofilms and microbiomes* 11(1), p. 65.

Moore-Ott, J. A., Chiu, S., Amchin, D. B., Bhattacharjee, T. and Datta, S. S. 2022. A biophysical threshold for biofilm formation. *Elife* 11, p. e76380.

Mora-Flores, L. P., Moreno-Terrazas Casildo, R., Fuentes-Cabrera, J., Pérez-Vicente, H. A., de Anda-Jáuregui, G. and Neri-Torres, E. E. 2023. The role of carbohydrate intake on the gut microbiome: a weight of evidence systematic review. *Microorganisms* 11(7), p. 1728.

Moreno-Gámez, S., Hochberg, M. E. and Van Doorn, G. 2023. Quorum sensing as a mechanism to harness the wisdom of the crowds. *Nature communications* 14(1), p. 3415.

Morse, D. J., Wilson, M. J., Wei, X., Bradshaw, D. J., Lewis, M. A. and Williams, D. W. 2019. Modulation of Candida albicans virulence in in vitro biofilms by oral bacteria. *Letters in Applied Microbiology* 68(4), pp. 337-343.

Moshynets, O. V., Pokholenko, I., Iungin, O., Potters, G. and Spiers, A. J. 2022. eDNA, amyloid fibers and membrane vesicles identified in Pseudomonas fluorescens SBW25 biofilms. *International Journal of Molecular Sciences* 23(23), p. 15096.

Mostowy, S. 2022. Louis Pasteur continues to shape the future of microbiology. The Company of Biologists Ltd.

Mountcastle, S. E. et al. 2021. Biofilm viability checker: An open-source tool for automated biofilm viability analysis from confocal microscopy images. *NPJ biofilms and microbiomes* 7(1), p. 44.

Moyes, D. L. et al. 2016. Candidalysin is a fungal peptide toxin critical for mucosal infection. *Nature* 532(7597), pp. 64-68.

Mrigwani, A., Pitaliya, M., Kaur, H., Kasilingam, B., Thakur, B. and Guptasarma, P. 2023. Rational mutagenesis of Thermobifida fusca cutinase to modulate the enzymatic degradation of polyethylene terephthalate. *Biotechnology and Bioengineering* 120(3), pp. 674-686.

Mu, M. et al. 2023. Influence of surface roughness, nanostructure, and wetting on bacterial adhesion. *Langmuir* 39(15), pp. 5426-5439.

Mugita, N., Nambu, T., Takahashi, K., Wang, P.-L. and Komasa, Y. 2017. Proteases, actinidin, papain and trypsin reduce oral biofilm on the tongue in elderly subjects and in vitro. *Archives of oral biology* 82, pp. 233-240.

Mukaremera, L., Lee, K. K., Mora-Montes, H. M. and Gow, N. A. 2017. Candida albicans yeast, pseudohyphal, and hyphal morphogenesis differentially affects immune recognition. *Frontiers in immunology* 8, p. 629.

Muller, C. 2022. Antibiotics and antimicrobials resistance: mechanisms and new strategies to fight resistant bacteria. MDPI.

Mutahar, M., Carpenter, G., Bartlett, D., German, M. and Moazzez, R. 2017. The presence of acquired enamel pellicle changes acid-induced erosion from dissolution to a softening process. *Scientific reports* 7(1), p. 10920.

Naghavi, M. et al. 2024. Global burden of bacterial antimicrobial resistance 1990–2021: a systematic analysis with forecasts to 2050. *The Lancet* 404(10459), pp. 1199-1226.

Naglik, J. R., Gaffen, S. L. and Hube, B. 2019. Candidalysin: discovery and function in Candida albicans infections. *Current opinion in microbiology* 52, pp. 100-109.

Naglik, J. R. et al. 2008. Quantitative expression of the Candida albicans secreted aspartyl proteinase gene family in human oral and vaginal candidiasis. *Microbiology* 154(11), pp. 3266-3280.

Nahum, Y., Gross, N., Cerrone, A., Matouš, K. and Nerenberg, R. 2024. Effect of biofilm physical characteristics on their susceptibility to antibiotics: impacts of low-frequency ultrasound. *NPJ biofilms and microbiomes* 10(1), p. 70.

Nairn, B. L., Lima, B. P., Chen, R., Yang, J. Q., Wei, G., Chumber, A. K. and Herzberg, M. C. 2024. Effects of fluid shear stress on oral biofilm formation and composition and the transcriptional response of Streptococcus gordonii. *Molecular Oral Microbiology*,

Nakamura, T. et al. 2024. Diverse antifungal potency of terbinafine as a therapeutic agent against Exophiala dermatitidis in vitro. *Scientific reports* 14(1), p. 27500.

Nakano, M. 2018. 16S rRNA gene primer validation for bacterial diversity analysis of vegetable products. *Journal of food protection* 81(5), pp. 848-859.

Narciso, A. R., Dookie, R., Nannapaneni, P., Normark, S. and Henriques-Normark, B. 2025. Streptococcus pneumoniae epidemiology, pathogenesis and control. *Nature reviews microbiology* 23(4), pp. 256-271.

Navazesh, M. 1993. Methods for collecting saliva. *Annals of the New York Academy of Sciences* 694(1), pp. 72-77.

Naylor, N. R. et al. 2025. The global economic burden of antibiotic-resistant infections and the potential impact of bacterial vaccines: a modelling study. *BMJ Global Health* 10(6),

Netrusov, A. I., Liyaskina, E. V., Kurgaeva, I. V., Liyaskina, A. U., Yang, G. and Revin, V. V. 2023. Exopolysaccharides producing Bacteria: a review. *Microorganisms* 11(6), p. 1541.

Nett, J. E. et al. 2015. Host contributions to construction of three device-associated Candida albicans biofilms. *Infection and immunity* 83(12), pp. 4630-4638.

Neu, T. R. and Kuhlicke, U. 2022. Matrix glycoconjugate characterization in multispecies biofilms and bioaggregates from the environment by means of fluorescently-labeled lectins. *Frontiers in microbiology* 13, p. 940280.

Neu, T. R., Swerhone, G. D. and Lawrence, J. R. 2001. Assessment of lectin-binding analysis for in situ detection of glycoconjugates in biofilm systems. *Microbiology* 147(2), pp. 299-313.

Nguyen, H. T., Nguyen, T. H. and Otto, M. 2020. The staphylococcal exopolysaccharide PIA–Biosynthesis and role in biofilm formation, colonization, and infection. *Computational and Structural Biotechnology Journal* 18, pp. 3324-3334.

Nguyen, J., Lara-Gutiérrez, J. and Stocker, R. 2021. Environmental fluctuations and their effects on microbial communities, populations and individuals. *FEMS microbiology reviews* 45(4), p. fuaa068.

Nickerson, K. P. et al. 2017. Analysis of Shigella flexneri resistance, biofilm formation, and transcriptional profile in response to bile salts. *Infection and immunity* 85(6), pp. 10.1128/iai. 01067-01016.

Nielsen, S. M. et al. 2024. Large-scale screening identifies enzyme combinations that remove in situ grown oral biofilm. *Biofilm* 8, p. 100229.

Niu, H., Gu, J. and Zhang, Y. 2024. Bacterial persisters: molecular mechanisms and therapeutic development. *Signal transduction and targeted therapy* 9(1), p. 174.

Nobre, C. M., König, B., Pütz, N. and Hannig, M. 2021. Hydroxyapatite-based solution as adjunct treatment for biofilm management: an in situ study. *Nanomaterials* 11(9), p. 2452.

Noh, E. S. et al. 2021. Discrimination of raw material species in mixed seafood products (surimi) using the next generation sequencing method. *Food Bioscience* 41, p. 100786.

O'Toole, G., Kaplan, H. B. and Kolter, R. 2000. Biofilm formation as microbial development. *Annual Reviews in Microbiology* 54(1), pp. 49-79.

Oba, P. M. et al. 2021. Microbiota populations in supragingival plaque, subgingival plaque, and saliva habitats of adult dogs. *Animal microbiome* 3(1), p. 38.

Okshevsky, M. and Meyer, R. L. 2014. Evaluation of fluorescent stains for visualizing extracellular DNA in biofilms. *Journal of Microbiological Methods* 105, pp. 102-104.

Olaimat, A. N. et al. 2024. A Review of Bacterial Biofilm Components and Formation, Detection Methods, and Their Prevention and Control on Food Contact Surfaces. *Microbiology Research* 15(4), pp. 1973-1992.

Oliva, R. L., Khadka, U. B., Camenzind, T., Dyckmans, J. and Joergensen, R. G. 2025. Constituent of extracellular polymeric substances (EPS) produced by a range of soil bacteria and fungi. *BMC microbiology* 25(1), p. 298.

Olsen, I. 2015. Biofilm-specific antibiotic tolerance and resistance. *European Journal of Clinical Microbiology & Infectious Diseases* 34, pp. 877-886.

Opal, S. M. 2010. A brief history of microbiology and immunology. *Vaccines: a biography*. Springer, pp. 31-56.

Or, D., Smets, B. F., Wraith, J., Dechesne, A. and Friedman, S. 2007. Physical constraints affecting bacterial habitats and activity in unsaturated porous media–a review. *Advances in Water Resources* 30(6-7), pp. 1505-1527.

Oshiki, M., Saito, T., Nakaya, Y., Satoh, H. and Okabe, S. 2023. Growth of the Nitrosomonas europaea cells in the biofilm and planktonic growth mode: Responses of extracellular polymeric substances production and transcriptome. *Journal of bioscience and bioengineering* 136(6), pp. 430-437.

Ozmeric, N. et al. 2025. Evaluating the effects of chlorhexidine and vitamin c mouthwash on oral health in non-surgical periodontal therapy: a randomized controlled clinical trial. *Scientific reports* 15(1), p. 3703.

Palanisamy, V., Bosilevac, J. M., Barkhouse, D. A., Velez, S. E. and Chitlapilly Dass, S. 2023. Shotgun-metagenomics reveals a highly diverse and communal microbial network present in the drains of three beef-processing plants. *Frontiers in Cellular and Infection Microbiology* 13, p. 1240138.

Pan, J., Albarrak, A., Hicks, J., Williams, D. and Williamson, A. 2025a. Influence of the ATP-dependent DNA ligase, Lig E, on Neisseria gonorrhoeae microcolony and biofilm formation. *Biofilm*, p. 100292.

Pan, J., Singh, A., Hanning, K., Hicks, J. and Williamson, A. 2024. A role for the ATP-dependent DNA ligase lig E of Neisseria gonorrhoeae in biofilm formation. *BMC microbiology* 24(1), p. 29.

Pan, M. et al. 2022. Effects of hydrodynamic conditions on the composition, spatiotemporal distribution of different extracellular polymeric substances and the architecture of biofilms. *Chemosphere* 307, p. 135965.

Pan, T. et al. 2025b. Development of a cost-effective confocal Raman microscopy with high sensitivity. *Talanta* 281, p. 126754.

Park, S.-H., Kim, K., Cho, S., Chung, D.-H. and Ahn, S.-J. 2022. Variation in adhesion of Streptococcus mutans and Porphyromonas gingivalis in saliva-derived biofilms on raw materials of orthodontic brackets. *Korean Journal of Orthodontics* 52(4), pp. 278-286.

Pattnaik, S., Syed, A. and Siddhardha, B. 2020. Pathogenesis, Virulence Factors, and Antibiotic Resistance of Group B Streptococcus. *Model Organisms for Microbial Pathogenesis, Biofilm Formation and Antimicrobial Drug Discovery*, pp. 117-130.

Paula, A. J., Hwang, G. and Koo, H. 2020. Dynamics of bacterial population growth in biofilms resemble spatial and structural aspects of urbanization. *Nature communications* 11(1), p. 1354.

Pearson, J. C., Gillett, E., Gadri, N. D. and Dionne, B. 2025. Tetracyclines, the old and the new: A narrative review. *CMI Communications*, p. 105059.

Pedersen, A. M. L. and Belstrøm, D. 2019. The role of natural salivary defences in maintaining a healthy oral microbiota. *Journal of dentistry* 80, pp. S3-S12.

Penesyan, A., Paulsen, I. T., Kjelleberg, S. and Gillings, M. R. 2021. Three faces of biofilms: a microbial lifestyle, a nascent multicellular organism, and an incubator for diversity. *NPJ biofilms and microbiomes* 7(1), p. 80.

Pereira, L. C., Correia, A. F., da Silva, Z. D. L., de Resende, C. N., Brandão, F., Almeida, R. M. and de Medeiros Nóbrega, Y. K. 2021a. Vulvovaginal candidiasis and current perspectives: new risk factors and laboratory diagnosis by using MALDI TOF for identifying species in primary infection and recurrence. *European Journal of Clinical Microbiology & Infectious Diseases* 40, pp. 1681-1693.

Pereira, R., dos Santos Fontenelle, R. O., De Brito, E. and De Morais, S. 2021b. Biofilm of Candida albicans: formation, regulation and resistance. *Journal of applied microbiology* 131(1), pp. 11-22.

Pérez-Cobas, A. E., Gomez-Valero, L. and Buchrieser, C. 2020. Metagenomic approaches in microbial ecology: an update on whole-genome and marker gene sequencing analyses. *Microbial Genomics* 6(8), p. e000409.

Pergolizzi, G., Wagner, G. K. and Bowater, R. P. 2016. Biochemical and structural characterization of DNA ligases from bacteria and archaea. *Bioscience Reports* 36(5), p. e00391.

Perić, M., Miličić, B., Kuzmanović Pfićer, J., Živković, R. and Arsić Arsenijević, V. 2024. A systematic review of denture stomatitis: Predisposing factors, clinical features, etiology, and global Candida spp. distribution. *Journal of Fungi* 10(5), p. 328.

Pestrak, M. J. et al. 2019. Treatment with the Pseudomonas aeruginosa glycoside hydrolase PslG combats wound infection by improving antibiotic efficacy and host innate immune activity. *Antimicrobial Agents and Chemotherapy* 63(6), pp. 10.1128/aac. 00234-00219.

Petrovic, M. et al. 2022. Surface modification of poly (methyl-methacrylate) with farnesol to prevent Candida biofilm formation. *Letters in Applied Microbiology* 75(4), pp. 982-990.

Pezzotti, G. et al. 2023. In situ Raman analysis of biofilm exopolysaccharides formed in Streptococcus mutans and Streptococcus sanguinis commensal cultures. *International Journal of Molecular Sciences* 24(7), p. 6694.

Piñol, J., Senar, M. A. and Symondson, W. O. 2019. The choice of universal primers and the characteristics of the species mixture determine when DNA metabarcoding can be quantitative. *Molecular ecology* 28(2), pp. 407-419.

Pinto, R. M., Soares, F. A., Reis, S., Nunes, C. and Van Dijck, P. 2020. Innovative strategies toward the disassembly of the EPS matrix in bacterial biofilms. *Frontiers in microbiology* 11, p. 952.

Pleszczyńska, M., Wiater, A., Janczarek, M. and Szczodrak, J. 2015. (1→ 3)-α-d-Glucan hydrolases in dental biofilm prevention and control: a review. *International Journal of Biological Macromolecules* 79, pp. 761-778.

Pohl, C. H. 2022. Recent advances and opportunities in the study of Candida albicans polymicrobial biofilms. *Frontiers in Cellular and Infection Microbiology* 12, p. 836379.

Powell, L. C. et al. 2018. Targeted disruption of the extracellular polymeric network of Pseudomonas aeruginosa biofilms by alginate oligosaccharides. *NPJ biofilms and microbiomes* 4(1), p. 13.

Prakobphol, A., Burdsal, C. and Fisher, S. 1995. Quantifying the strength of bacterial adhesive interactions with salivary glycoproteins. *Journal of dental research* 74(5), pp. 1212-1218.

Prasad, P. and Tippana, M. 2023. Morphogenic plasticity: the pathogenic attribute of Candida albicans. *Current Genetics* 69(2), pp. 77-89.

Pratten, J., Wilson, M. and Spratt, D. 2003. Characterization of in vitro oral bacterial biofilms by traditional and molecular methods. *Oral microbiology and immunology* 18(1), pp. 45-49.

Prestinaci, F., Pezzotti, P. and Pantosti, A. 2015. Antimicrobial resistance: a global multifaceted phenomenon. *Pathogens and global health* 109(7), pp. 309-318.

Priya, A., Kumar, C. B. M., Valliammai, A., Selvaraj, A. and Pandian, S. K. 2021. Usnic acid deteriorates acidogenicity, acidurance and glucose metabolism of Streptococcus mutans through downregulation of two-component signal transduction systems. *Scientific reports* 11(1), p. 1374.

Priyadarshanee, M. and Das, S. 2023. Bacterial extracellular polymeric substances: biosynthesis and interaction with environmental pollutants. *Chemosphere* 332, p. 138876.

Pytko-Polonczyk, J., Jakubik, A., Przeklasa-Bierowiec, A. and Muszynska, B. 2017. Artificial saliva and its use in biological experiments. *J. Physiol. Pharmacol* 68(6), pp. 807-813.

Quan, K. et al. 2022. Water in bacterial biofilms: pores and channels, storage and transport functions. *Critical reviews in microbiology* 48(3), pp. 283-302.

Radaic, A. and Kapila, Y. L. 2021. The oralome and its dysbiosis: New insights into oral microbiome-host interactions. *Computational and Structural Biotechnology Journal* 19, pp. 1335-1360.

Ragupathi, H., Pushparaj, M. M., Gopi, S. M., Govindarajan, D. K. and Kandaswamy, K. 2024. Biofilm matrix: a multifaceted layer of biomolecules and a defensive barrier against antimicrobials. *Archives of Microbiology* 206(11), p. 432.

Rainey, K., Michalek, S. M., Wen, Z. T. and Wu, H. 2019. Glycosyltransferase-mediated biofilm matrix dynamics and virulence of Streptococcus mutans. *Applied and Environmental Microbiology* 85(5), pp. e02247-02218.

Reda, B., Dudek, J., Martínez-Hernández, M. and Hannig, M. 2021. Effects of octenidine on the formation and disruption of dental biofilms: an exploratory in situ study in healthy subjects. *Journal of dental research* 100(9), pp. 950-959.

Reekie, J. et al. 2019. Risk of ectopic pregnancy and tubal infertility following gonorrhea and Chlamydia infections. *Clinical Infectious Diseases* 69(9), pp. 1621-1623.

Reichhardt, C. and Parsek, M. R. 2019. Confocal laser scanning microscopy for analysis of Pseudomonas aeruginosa biofilm architecture and matrix localization. *Frontiers in microbiology* 10, p. 677.

Ren, S., Cheng, Y., Deng, Y., Xia, M., Yang, Y., Lei, L. and Hu, T. 2023. Pudilan Keyanning mouthwash inhibits dextran-dependent aggregation and biofilm organization of Streptococcus mutans. *Journal of applied microbiology* 134(12), p. lxad298.

Rezaei, T. et al. 2023. Factors associated with Streptococcus mutans pathogenicity in the oral cavity. *Biointerface Res Appl Chem* 13(4), p. 368.

Ribeiro, A. B. et al. 2022. Effect of a Hygiene Protocol on Denture-Related Stomatitis Remission, Local Inflammatory Factors, and Hemodynamic Responses by Arterial Pressure. *Antibiotics* 11(10), p. 1320.

Ribeiro, S. M., de Castro, A. P. and Franco, O. L. 2017. Metagenomic approach to study biofilm in medical context. *Medical Research Archives* 5(5),

Richards, C., O'Connor, N., Jose, D., Barrett, A. and Regan, F. 2020. Selection and optimization of protein and carbohydrate assays for the characterization of marine biofouling. *Analytical methods* 12(17), pp. 2228-2236.

Richardson, J. P. et al. 2022. Candidalysins are a new family of cytolytic fungal peptide toxins. *Mbio* 13(1), pp. e03510-03521.

Rikvold, P. D., Skov, L. B. H., Meyer, R. L., Jorgensen, M. R., Tiwari, M. K. and Schlafer, S. 2023. The effect of enzymatic treatment with mutanase, beta-glucanase and DNase on a saliva-derived biofilm model. *Caries research*,

Roberts, A. E., Kragh, K. N., Bjarnsholt, T. and Diggle, S. P. 2015. The limitations of in vitro experimentation in understanding biofilms and chronic infection. *Journal of molecular biology* 427(23), pp. 3646-3661.

Robertson, J., McGoverin, C., Vanholsbeeck, F. and Swift, S. 2019. Optimisation of the protocol for the LIVE/DEAD® BacLightTM bacterial viability kit for rapid determination of bacterial load. *Frontiers in microbiology* 10, p. 801.

Rooney, L. M., Amos, W. B., Hoskisson, P. A. and McConnell, G. 2020. Intra-colony channels in E. coli function as a nutrient uptake system. *The ISME journal* 14(10), pp. 2461-2473.

Rosan, B. and Lamont, R. J. 2000. Dental plaque formation. *Microbes and infection* 2(13), pp. 1599-1607.

Rosário, W. et al. 2022. Evaluation of the Presence of Biofilms in Corrosive Points in Surgical Instruments after Reprocessing. *Hygiene* 2(4), pp. 243-250.

Rosiana, S. et al. 2021. Comprehensive genetic analysis of adhesin proteins and their role in virulence of Candida albicans. *Genetics* 217(2), p. iyab003.

Rowe III, W. J., Lebman, D. A. and Ohman, D. E. 2023. Mechanism of resistance to phagocytosis and pulmonary persistence in mucoid Pseudomonas aeruginosa. *Frontiers in Cellular and Infection Microbiology* 13, p. 1125901.

Rubio-Canalejas, A., Baelo, A., Herbera, S., Blanco-Cabra, N., Vukomanovic, M. and Torrents, E. 2022. 3D spatial organization and improved antibiotic treatment of a Pseudomonas aeruginosa–Staphylococcus aureus wound biofilm by nanoparticle enzyme delivery. *Frontiers in microbiology* 13, p. 959156.

Rudi, K., Moen, B., Drømtorp, S. M. and Holck, A. L. 2005. Use of ethidium monoazide and PCR in combination for quantification of viable and dead cells in complex samples. *Applied and Environmental Microbiology* 71(2), pp. 1018-1024.

Rudney, J. et al. 2012. A reproducible oral microcosm biofilm model for testing dental materials. *Journal of applied microbiology* 113(6), pp. 1540-1553.

Rued, B. E., Covington, B. C., Bushin, L. B., Szewczyk, G., Laczkovich, I., Seyedsayamdost, M. R. and Federle, M. J. 2021. Quorum sensing in streptococcus mutans regulates production of tryglysin, a novel ras-ripp antimicrobial compound. *Mbio* 12(2), pp. 10.1128/mbio. 02688-02620.

Rusu, D. et al. 2020. A qualitative and semiquantitative SEM study of the morphology of the biofilm on root surfaces of human teeth with endodontic-periodontal lesions. *Experimental and Therapeutic Medicine* 20(6), pp. 1-1.

Sae-Tun, O. et al. 2020. Comparison of commonly used extraction methods for ergosterol in soil samples. *International Agrophysics* 34(4),

Saharan, B. S., Beniwal, N. and Duhan, J. S. 2024. From formulation to function: A detailed review of microbial biofilms and their polymer-based extracellular substances. *The Microbe* 5, p. 100194.

Sánchez, M. et al. 2014. An in vitro biofilm model associated to dental implants: Structural and quantitative analysis of in vitro biofilm formation on different dental implant surfaces. *Dental Materials* 30(10), pp. 1161-1171.

Sanders, C. C. and Sanders Jr, W. E. 1992. β-Lactam resistance in gram-negative bacteria: global trends and clinical impact. *Clinical Infectious Diseases* 15(5), pp. 824-839.

Sangha, J. S., Gogulancea, V., Curtis, T. P., Jakubovics, N. S., Barrett, P., Metris, A. and Ofiţeru, I. D. 2024. Advancing dental biofilm models: the integral role of pH in predicting S. mutans colonization. *mSphere*, pp. e00743-00724.

Sasidharan Pillai, S., Gagnon, C. A., Foster, C. and Ashraf, A. P. 2024. Exploring the gut microbiota: key insights into its role in obesity, metabolic syndrome, and type 2 diabetes. *The Journal of Clinical Endocrinology & Metabolism* 109(11), pp. 2709-2719.

Sauer, K., Stoodley, P., Goeres, D. M., Hall-Stoodley, L., Burmølle, M., Stewart, P. S. and Bjarnsholt, T. 2022. The biofilm life cycle: expanding the conceptual model of biofilm formation. *Nature reviews microbiology* 20(10), pp. 608-620.

Scaffa, P. M. C. et al. 2023. The potential use of glycosyl-transferase inhibitors for targeted reduction of S. mutans biofilms in dental materials. *Scientific reports* 13(1), p. 11889.

Scheld, W. M. 2012. Introduction to microbial disease: host-pathogen interactions. *Goldman's Cecil Medicine*, p. 1761.

Schilling, K. M. and Bowen, W. H. 1992. Glucans synthesized in situ in experimental salivary pellicle function as specific binding sites for Streptococcus mutans. *Infection and immunity* 60(1), pp. 284-295.

Schindelin, J. et al. 2012. Fiji: an open-source platform for biological-image analysis. *Nature methods* 9(7), pp. 676-682.

Schlafer, S. and Meyer, R. L. 2017. Confocal microscopy imaging of the biofilm matrix. *Journal of Microbiological Methods* 138, pp. 50-59.

Schlafer, S., Meyer, R. L., Dige, I. and Regina, V. R. 2017. Extracellular DNA contributes to dental biofilm stability. *Caries research* 51(4), pp. 436-442.

Schneider-Rayman, M., Steinberg, D., Sionov, R. V., Friedman, M. and Shalish, M. 2021. Effect of epigallocatechin gallate on dental biofilm of Streptococcus mutans: An in vitro study. *BMC Oral Health* 21(1), p. 447.

Schönbächler, N., Thurnheer, T., Paqué, P. N., Attin, T. and Karygianni, L. 2023. In vitro versus in situ biofilms for evaluating the antimicrobial effectiveness of herbal mouthrinses. *Frontiers in Cellular and Infection Microbiology* 13, p. 1130255.

Schrader, S. M., Botella, H. and Vaubourgeix, J. 2023. Reframing antimicrobial resistance as a continuous spectrum of manifestations. *Current opinion in microbiology* 72, p. 102259.

Scribner, M. R., Santos-Lopez, A., Marshall, C. W., Deitrick, C. and Cooper, V. S. 2020. Parallel evolution of tobramycin resistance across species and environments. *Mbio* 11(3), pp. 10.1128/mbio. 00932-00920.

Seguya, A., Mowafy, M., Gaballah, A. and Zaher, A. 2022. Chlorhexidine versus organoselenium for inhibition of S. mutans biofilm, an in vitro study. *BMC Oral Health* 22(1), p. 14.

Şenel, S. 2021. An overview of physical, microbiological and immune barriers of oral mucosa. *International Journal of Molecular Sciences* 22(15), p. 7821.

Senpuku, H., Yonezawa, H., Yoneda, S., Suzuki, I., Nagasawa, R. and Narisawa, N. 2018. SMU. 940 regulates dextran-dependent aggregation and biofilm formation in Streptococcus mutans. *Molecular Oral Microbiology* 33(1), pp. 47-58.

Seper, A. et al. 2011. Extracellular nucleases and extracellular DNA play important roles in Vibrio cholerae biofilm formation. *Molecular microbiology* 82(4), pp. 1015-1037.

Serrage, H. J., Jepson, M. A., Rostami, N., Jakubovics, N. S. and Nobbs, A. H. 2021. Understanding the matrix: the role of extracellular DNA in oral biofilms. *Frontiers in Oral Health* 2, p. 640129.

Shailaja, A., Bruce, T. F., Gerard, P., Powell, R. R., Pettigrew, C. A. and Kerrigan, J. L. 2022. Comparison of cell viability assessment and visualization of Aspergillus niger biofilm with two fluorescent probe staining methods. *Biofilm* 4, p. 100090.

Shakeel, M. et al. 2022. Surface-enhanced Raman spectroscopy for the characterization of pellets of biofilm forming bacterial strains of Staphylococcus epidermidis. *Photodiagnosis and Photodynamic Therapy* 40, p. 103145.

Shao, T.-Y., Haslam, D. B., Bennett, R. J. and Way, S. S. 2022. Friendly fungi: symbiosis with commensal Candida albicans. *Trends in immunology* 43(9), pp. 706-717.

Sharif, N., Khoshnoudi-Nia, S. and Jafari, S. M. 2020. Confocal laser scanning microscopy (CLSM) of nanoencapsulated food ingredients. *Characterization of nanoencapsulated food ingredients*. Elsevier, pp. 131-158.

Sharma, A., Solis, N. V., Huang, M. Y., Lanni, F., Filler, S. G. and Mitchell, A. P. 2023a. Hgc1 Independence of Biofilm Hyphae in Candida albicans. *Mbio* 14(2), pp. e03498-03422.

Sharma, S., Mohler, J., Mahajan, S. D., Schwartz, S. A., Bruggemann, L. and Aalinkeel, R. 2023b. Microbial biofilm: a review on formation, infection, antibiotic resistance, control measures, and innovative treatment. *Microorganisms* 11(6), p. 1614.

Shen, H., Rösch, P., Pletz, M. W. and Popp, J. r. 2022. In vitro fiber-probe-based identification of pathogens in biofilms by Raman spectroscopy. *Analytical Chemistry* 94(13), pp. 5375-5381.

Sheng, C. et al. 2009. Three-dimensional model of lanosterol 14α-demethylase from Cryptococcus neoformans: Active-site characterization and insights into azole binding. *Antimicrobial Agents and Chemotherapy* 53(8), pp. 3487-3495.

Shi, D., Mi, G., Wang, M. and Webster, T. J. 2019. In vitro and ex vivo systems at the forefront of infection modeling and drug discovery. *Biomaterials* 198, pp. 228-249.

Shi, K. et al. 2018. T4 DNA ligase structure reveals a prototypical ATP-dependent ligase with a unique mode of sliding clamp interaction. *Nucleic Acids Research* 46(19), pp. 10474-10488.

Shineh, G., Mobaraki, M., Perves Bappy, M. J. and Mills, D. K. 2023. Biofilm formation, and related impacts on healthcare, food processing and packaging, industrial manufacturing, marine industries, and sanitation–A review. *Applied Microbiology* 3(3), pp. 629-665.

Shree, P., Singh, C. K., Sodhi, K. K., Surya, J. N. and Singh, D. K. 2023. Biofilms: Understanding the structure and contribution towards bacterial resistance in antibiotics. *Medicine in Microecology* 16, p. 100084.

Silva, S., Negri, M., Henriques, M., Oliveira, R., Williams, D. W. and Azeredo, J. 2012. Candida glabrata, Candida parapsilosis and Candida tropicalis: biology, epidemiology, pathogenicity and antifungal resistance. *FEMS microbiology reviews* 36(2), pp. 288-305.

Simões, L. C., Simões, M. and Vieira, M. J. 2008. Acinetobacter calcoaceticus plays a bridging function in drinking water biofilms.

Simon-Soro, A. et al. 2022. Polymicrobial aggregates in human saliva build the oral biofilm. *Mbio* 13(1), pp. e00131-00122.

Simon-Soro, A., Tomás, I., Cabrera-Rubio, R., Catalan, M., Nyvad, B. and Mira, A. 2013. Microbial geography of the oral cavity. *Journal of dental research* 92(7), pp. 616-621.

Singh, A., Singh, K., Sharma, A., Kaur, K., Chadha, R. and Bedi, P. M. S. 2023. Recent advances in antifungal drug development targeting lanosterol 14α-demethylase (CYP51): A comprehensive review with structural and molecular insights. *Chemical Biology & Drug Design*,

Singh, S., Datta, S., Narayanan, K. B. and Rajnish, K. N. 2021a. Bacterial exo-polysaccharides in biofilms: role in antimicrobial resistance and treatments. *Journal of Genetic Engineering and Biotechnology* 19(1), pp. 1-19.

Singh, S., Datta, S., Narayanan, K. B. and Rajnish, K. N. 2021b. Bacterial exo-polysaccharides in biofilms: role in antimicrobial resistance and treatments. *Journal of Genetic Engineering and Biotechnology* 19, pp. 1-19.

Singh, S., Datta, S., Narayanan, K. B. and Rajnish, K. N. 2021c. Bacterial exo-polysaccharides in biofilms: role in antimicrobial resistance and treatments. *Journal of Genetic Engineering and Biotechnology* 19(1), p. 140.

Singh, S., Singh, S. K., Chowdhury, I. and Singh, R. 2017. Understanding the mechanism of bacterial biofilms resistance to antimicrobial agents. *The open microbiology journal* 11, p. 53.

Singh, V., Proctor, S. D. and Willing, B. P. 2016. Koch's postulates, microbial dysbiosis and inflammatory bowel disease. *Clinical Microbiology and Infection* 22(7), pp. 594-599.

Singleton, D. R., Masuoka, J. and Hazen, K. C. 2005. Surface hydrophobicity changes of two Candida albicans serotype B mnn4 Δ mutants. *Eukaryotic cell* 4(4), pp. 639-648.

Smith, P. e. et al. 1985. Measurement of protein using bicinchoninic acid. *Analytical biochemistry* 150(1), pp. 76-85.

Solderer, A., Kaufmann, M., Hofer, D., Wiedemeier, D., Attin, T. and Schmidlin, P. R. 2019. Efficacy of chlorhexidine rinses after periodontal or implant surgery: a systematic review. *Clinical oral investigations* 23, pp. 21-32.

Soleimani, M., Szafranski, S. P., Qu, T., Mukherjee, R., Stiesch, M., Wriggers, P. and Junker, P. 2023. Numerical and experimental investigation of multi-species bacterial co-aggregation. *Scientific reports* 13(1), p. 11839.

Song, J. L., Harry, J. B., Eastman, R. T., Oliver, B. G. and White, T. C. 2004. The Candida albicans lanosterol 14-α-demethylase (ERG11) gene promoter is maximally induced after prolonged growth with antifungal drugs. *Antimicrobial Agents and Chemotherapy* 48(4), pp. 1136-1144.

Song, L., Wang, S., Zou, H., Yi, X., Jia, S., Li, R. and Song, J. 2025. Regulation of Ergosterol Biosynthesis in Pathogenic Fungi: Opportunities for Therapeutic Development. *Microorganisms* 13(4), p. 862.

Song, Y., Ma, F., Sun, M., Mu, G. and Tuo, Y. 2022. The Chemical Structure Properties and Promoting Biofilm Activity of Exopolysaccharide Produced by Shigella Flexneri. *Frontiers in microbiology* 12, p. 807397.

Southward, C. M. and Surette, M. G. 2002. The dynamic microbe: green fluorescent protein brings bacteria to light. *Molecular microbiology* 45(5), pp. 1191-1196.

Souza, J. G. S., Bertolini, M. M., Costa, R. C., Nagay, B. E., Dongari-Bagtzoglou, A. and Barão, V. A. R. 2021. Targeting implant-associated infections: titanium surface loaded with antimicrobial. *Iscience* 24(1),

Spatafora, G., Li, Y., He, X., Cowan, A. and Tanner, A. C. 2024. The evolving microbiome of dental caries. *Microorganisms* 12(1), p. 121.

Sreekantan, A. P., Rajan, P. P., Mini, M. and Kumar, P. 2022. Multidrug Efflux Pumps in Bacteria and Efflux Pump Inhibitors. *Postępy Mikrobiologii-Advancements of Microbiology* 61(3), pp. 105-114.

Sridhar, S., Suprabha, B. S., Shenoy, R., Suman, E. and Rao, A. 2020. Association of Streptococcus mutans, Candida albicans and oral health practices with activity status of caries lesions among 5-year-old children with early childhood caries. *Oral health & preventive dentistry* 18(4), p. a45411.

Steichen, C. T., Cho, C., Shao, J. Q. and Apicella, M. A. 2011. The Neisseria gonorrhoeae biofilm matrix contains DNA, and an endogenous nuclease controls its incorporation. *Infection and immunity* 79(4), pp. 1504-1511.

Stewart, P. S. et al. 2022. Search for a shared genetic or biochemical basis for biofilm tolerance to antibiotics across bacterial species. *Antimicrobial Agents and Chemotherapy* 66(4), pp. e00021-00022.

Stiefel, P., Schmidt-Emrich, S., Maniura-Weber, K. and Ren, Q. 2015. Critical aspects of using bacterial cell viability assays with the fluorophores SYTO9 and propidium iodide. *BMC microbiology* 15, pp. 1-9.

Stocks, S. 2004. Mechanism and use of the commercially available viability stain, BacLight. *Cytometry Part A: The Journal of the International Society for Analytical Cytology* 61(2), pp. 189-195.

Stogios, P. J. and Savchenko, A. 2020. Molecular mechanisms of vancomycin resistance. *Protein Science* 29(3), pp. 654-669.

Stojicic, S., Zivkovic, S., Qian, W., Zhang, H. and Haapasalo, M. 2010. Tissue dissolution by sodium hypochlorite: effect of concentration, temperature, agitation, and surfactant. *Journal of endodontics* 36(9), pp. 1558-1562.

Strushkevich, N., Usanov, S. A. and Park, H.-W. 2010. Structural basis of human CYP51 inhibition by antifungal azoles. *Journal of molecular biology* 397(4), pp. 1067-1078.

Subramanian, S., Huiszoon, R. C., Chu, S., Bentley, W. E. and Ghodssi, R. 2020. Microsystems for biofilm characterization and sensing–A review. *Biofilm* 2, p. 100015.

Sutherland, I. W. 2001. The biofilm matrix–an immobilized but dynamic microbial environment. *Trends in microbiology* 9(5), pp. 222-227.

Talapko, J., Juzbašić, M., Matijević, T., Pustijanac, E., Bekić, S., Kotris, I. and Škrlec, I. 2021. Candida albicans—the virulence factors and clinical manifestations of infection. *Journal of Fungi* 7(2), p. 79.

Talari, A. C. S., Movasaghi, Z., Rehman, S. and Rehman, I. U. 2015. Raman spectroscopy of biological tissues. *Applied spectroscopy reviews* 50(1), pp. 46-111.

Tamai, R. and Kiyoura, Y. 2025. Candida Infections: The Role of Saliva in Oral Health—A Narrative Review. *Microorganisms* 13(4), p. 717.

Tamashiro, R. et al. 2023. Smoking-induced subgingival dysbiosis precedes clinical signs of periodontal disease. *Scientific reports* 13(1), p. 3755.

Tan, Z. et al. 2024. A comprehensive synthetic library of poly-N-acetyl glucosamines enabled vaccine against lethal challenges of Staphylococcus aureus. *Nature communications* 15(1), p. 3420.

Teixeira, M. M., Carvalho, D. T., Sousa, E. and Pinto, E. 2022. New antifungal agents with azole moieties. *Pharmaceuticals* 15(11), p. 1427.

Teschler, J. K., Nadell, C. D., Drescher, K. and Yildiz, F. H. 2022. Mechanisms underlying Vibrio cholerae biofilm formation and dispersion. *Annual Review of Microbiology* 76(1), pp. 503-532.

Thangavelu, A., Kaspar, S. S., Kathirvelu, R. P., Srinivasan, B., Srinivasan, S. and Sundram, R. 2020. Chlorhexidine: An elixir for periodontics. *Journal of Pharmacy and Bioallied Sciences* 12(Suppl 1), pp. S57-S59.

Thieme, L., Hartung, A., Tramm, K., Graf, J., Spott, R., Makarewicz, O. and Pletz, M. W. 2021. Adaptation of the start-growth-time method for high-throughput biofilm quantification. *Frontiers in microbiology* 12, p. 631248.

Thöming, J. G. and Häussler, S. 2022. Pseudomonas aeruginosa is more tolerant under biofilm than under planktonic growth conditions: a multi-isolate survey. *Frontiers in Cellular and Infection Microbiology* 12, p. 851784.

Tomkinson, A. E., Vijayakumar, S., Pascal, J. M. and Ellenberger, T. 2006. DNA ligases: structure, reaction mechanism, and function. *Chemical reviews* 106(2), pp. 687-699.

Tonna, I. and Tonna, A. P. 2022. Glycopeptide and Lipoglycopeptide Antibiotics.

Tran, N. N., Morrisette, T., Jorgensen, S. C., Orench-Benvenutti, J. M. and Kebriaei, R. 2023. Current therapies and challenges for the treatment of Staphylococcus aureus biofilm-related infections. *Pharmacotherapy: The Journal of Human Pharmacology and Drug Therapy* 43(8), pp. 816-832.

Tsagkari, E., Connelly, S., Liu, Z., McBride, A. and Sloan, W. T. 2022. The role of shear dynamics in biofilm formation. *NPJ biofilms and microbiomes* 8(1), p. 33.

Tsui, C., Kong, E. F. and Jabra-Rizk, M. A. 2016. Pathogenesis of Candida albicans biofilm. *FEMS Pathogens and Disease* 74(4), p. ftw018.

Turner, J., Muraoka, A., Bedenbaugh, M., Childress, B., Pernot, L., Wiencek, M. and Peterson, Y. K. 2022. The chemical relationship among beta-lactam antibiotics and potential impacts on reactivity and decomposition. *Frontiers in microbiology* 13, p. 807955.

Turonova, H., Neu, T. R., Ulbrich, P., Pazlarova, J. and Tresse, O. 2016. The biofilm matrix of Campylobacter jejuni determined by fluorescence lectin-binding analysis. *Biofouling* 32(5), pp. 597-608.

Unemo, M., Seifert, H. S., Hook III, E. W., Hawkes, S., Ndowa, F. and Dillon, J.-A. R. 2019. Gonorrhoea. *Nature Reviews Disease Primers* 5(1), p. 79.

Upadhyay, A., Pal, D. and Kumar, A. 2023. Combinatorial enzyme therapy: A promising neoteric approach for bacterial biofilm disruption. *Process Biochemistry* 129, pp. 56-66.

Upadhyay, A., Pal, D. and Kumar, A. 2024. Combinatorial therapeutic enzymes to combat multidrug resistance in bacteria. *Life Sciences*, p. 122920.

Uppuluri, P., Acosta Zaldívar, M., Anderson, M. Z., Dunn, M. J., Berman, J., Lopez Ribot, J. L. and Köhler, J. R. 2018. Candida albicans dispersed cells are developmentally distinct from biofilm and planktonic cells. *Mbio* 9(4), pp. 10.1128/mbio. 01338-01318.

Uppuluri, P., Chaturvedi, A. K. and Lopez-Ribot, J. L. 2009. Design of a simple model of Candida albicans biofilms formed under conditions of flow: development, architecture, and drug resistance. *Mycopathologia* 168, pp. 101-109.

Uppuluri, P. et al. 2010. Dispersion as an important step in the Candida albicans biofilm developmental cycle. *PLoS pathogens* 6(3), p. e1000828.

Uruén, C., Chopo-Escuin, G., Tommassen, J., Mainar-Jaime, R. C. and Arenas, J. 2020. Biofilms as promoters of bacterial antibiotic resistance and tolerance. *Antibiotics* 10(1), p. 3.

Vacca-Smith, A. and Bowen, W. 1998. Binding properties of streptococcal glucosyltransferases for hydroxyapatite, saliva-coated hydroxyapatite, and bacterial surfaces. *Archives of oral biology* 43(2),pp. 103-110.

Valencia, S., Zuluaga, M., Florian Pérez, M. C., Montoya-Quintero, K. F., Candamil-Cortés, M. S. and Robledo, S. 2025. Human Gut Microbiome: A Connecting Organ Between Nutrition, Metabolism, and Health. *International Journal of Molecular Sciences* 26(9), p. 4112.

Valm, A. M. 2019. The structure of dental plaque microbial communities in the transition from health to dental caries and periodontal disease. *Journal of molecular biology* 431(16), pp. 2957-2969.

Van den Poel, B., Saegeman, V. and Schuermans, A. 2022. Increasing usage of chlorhexidine in health care settings: blessing or curse? A narrative review of the risk of chlorhexidine resistance and the implications for infection prevention and control. *European Journal of Clinical Microbiology & Infectious Diseases* 41(3), pp. 349-362.

Van Hoogstraten, S., Kuik, C., Arts, J. and Cillero-Pastor, B. 2024. Molecular imaging of bacterial biofilms—a systematic review. *Critical reviews in microbiology* 50(6), pp. 971-992.

Venkitaraman, A., Vacca-Smith, A., Kopec, L. and Bowen, W. 1995. Characterization of glucosyltransferaseB, GtfC, and GtfD in solution and on the surface of hydroxyapatite. *Journal of dental research* 74(10), pp. 1695-1701.

Verbanic, S., Shen, Y., Lee, J., Deacon, J. M. and Chen, I. A. 2020. Microbial predictors of healing and short-term effect of debridement on the microbiome of chronic wounds. *NPJ biofilms and microbiomes* 6(1), p. 21.

Vermes, A., Guchelaar, H.-J. and Dankert, J. 2000. Flucytosine: a review of its pharmacology, clinical indications, pharmacokinetics, toxicity and drug interactions. *Journal of Antimicrobial Chemotherapy* 46(2), pp. 171-179.

Vernon-Parry, K. D. 2000. Scanning electron microscopy: an introduction. *III-Vs review* 13(4), pp. 40-44.

Virgen-Ortíz, J., Ibarra-Junquera, V., Escalante-Minakata, P., Ornelas-Paz, J. d. J., Osuna-Castro, J. and González-Potes, A. 2015. Kinetics and thermodynamic of the purified dextranase from Chaetomium erraticum. *Journal of Molecular Catalysis B: Enzymatic* 122, pp. 80-86.

Vorregaard, M. 2008. *Comstat2-a modern 3D image analysis environment for biofilms.* Technical University of Denmark, DTU, DK-2800 Kgs. Lyngby, Denmark.

Vukosavljevic, D., Custodio, W., Buzalaf, M. A., Hara, A. T. and Siqueira, W. L. 2014. Acquired pellicle as a modulator for dental erosion. *Archives of oral biology* 59(6), pp. 631-638.

Vyas, N., Sammons, R., Addison, O., Dehghani, H. and Walmsley, A. 2016. A quantitative method to measure biofilm removal efficiency from complex biomaterial surfaces using SEM and image analysis. *Scientific reports* 6(1), p. 32694.

Wagner, M., Ivleva, N. P., Haisch, C., Niessner, R. and Horn, H. 2009. Combined use of confocal laser scanning microscopy (CLSM) and Raman microscopy (RM): investigations on EPS–matrix. *Water research* 43(1), pp. 63-76.

Wainwright, J., Hobbs, G. and Nakouti, I. 2021. Persister cells: formation, resuscitation and combative therapies. *Archives of Microbiology* 203(10), pp. 5899-5906.

Wall, G., Montelongo-Jauregui, D., Bonifacio, B. V., Lopez-Ribot, J. L. and Uppuluri, P. 2019. Candida albicans biofilm growth and dispersal: contributions to pathogenesis. *Current opinion in microbiology* 52, pp. 1-6.

Wang, B. et al. 2024. The Screening and Identification of a Dextranase-Secreting Marine Actinmycete Saccharomonospora sp. K1 and Study of Its Enzymatic Characteristics. *Marine Drugs* 22(2), p. 69.

Wang, X., Zhang, Y., Li, M., Qin, Q. and Xie, T. 2022. Purification and characterization of dextranase from Penicillium cyclopium CICC-4022 and its degradation of dextran. *International Journal of Biological Macromolecules* 204, pp. 627-634.

Wang, Y., Samaranayake, L. P. and Dykes, G. A. 2021. Tea extracts modulate oral biofilm development by altering bacterial hydrophobicity and aggregation. *Archives of oral biology* 122, p. 105032.

Warreth, A. 2023. Dental caries and its management. *International journal of dentistry* 2023(1), p. 9365845.

Weber, K., Delben, J., Bromage, T. G. and Duarte, S. 2014. Comparison of SEM and VPSEM imaging techniques with respect to Streptococcus mutans biofilm topography. *FEMS microbiology letters* 350(2), pp. 175-179.

Weller, G. R. and Doherty, A. J. 2001. A family of DNA repair ligases in bacteria? *FEBS letters* 505(2), pp. 340-342.

White, P. L., Williams, D. W., Kuriyama, T., Samad, S. A., Lewis, M. A. and Barnes, R. A. 2004. Detection of Candida in concentrated oral rinse cultures by real-time PCR. *Journal of clinical microbiology* 42(5), pp. 2101-2107.

White, T. C., Marr, K. A. and Bowden, R. A. 1998. Clinical, cellular, and molecular factors that contribute to antifungal drug resistance. *Clinical microbiology reviews* 11(2), pp. 382-402.

Whiteley, M., Brown, E. and McLean, R. J. 1997. An inexpensive chemostat apparatus for the study of microbial biofilms. *Journal of Microbiological Methods* 30(2), pp. 125-132.

Wickramasinghe, N. N., Hlaing, M. M., Ravensdale, J. T., Coorey, R., Chandry, P. S. and Dykes, G. A. 2020. Characterization of the biofilm matrix composition of psychrotrophic, meat spoilage pseudomonads. *Scientific reports* 10(1), p. 16457.

Wilkinson, A., Day, J. and Bowater, R. 2001. Bacterial DNA ligases. *Molecular microbiology* 40(6), pp. 1241-1248.

Willems, H. M., Xu, Z. and Peters, B. M. 2016. Polymicrobial biofilm studies: from basic science to biofilm control. *Current oral health reports* 3, pp. 36-44.

Williams, D. and Lewis, M. 2011. Pathogenesis and treatment of oral candidosis. *Journal of oral microbiology* 3(1), p. 5771.

Williams, D. L., Smith, S. R., Peterson, B. R., Allyn, G., Cadenas, L., Epperson, R. T. and Looper, R. E. 2019. Growth substrate may influence biofilm susceptibility to antibiotics. *PloS one* 14(3), p. e0206774.

Williams, M. 2023. *Modulation of Candida albicans-associated denture biofilms by environmental and microbial factors.* Cardiff University.

Wilson, C. et al. 2017. Quantitative and qualitative assessment methods for biofilm growth: a mini-review. *Research & reviews. Journal of engineering and technology* 6(4), pp. http://www. rroij.

com/open-access/quantitative-and-qualitative-assessment-methods-for-biofilm-growth-a-minireview-. pdf.

Wohlgemuth, I., Garofalo, R., Samatova, E., Günenç, A. N., Lenz, C., Urlaub, H. and Rodnina, M. V. 2021. Translation error clusters induced by aminoglycoside antibiotics. *Nature communications* 12(1), p. 1830.

Wong, H. S., Maker, G. L., Trengove, R. D. and O'Handley, R. M. 2015. Gas chromatography-mass spectrometry-based metabolite profiling of Salmonella enterica serovar Typhimurium differentiates between biofilm and planktonic phenotypes. *Applied and Environmental Microbiology* 81(8), pp. 2660-2666.

Wu, H. et al. 2024. Isobavachalcone Exhibits Potent Antifungal Efficacy by Inhibiting Enolase Activity and Glycolysis in Candida albicans. *ACS Infectious Diseases* 10(8), pp. 3059-3070.

Wu, L. and Luo, Y. 2021. Bacterial quorum-sensing systems and their role in intestinal bacteria-host crosstalk. *Frontiers in microbiology* 12, p. 611413.

Wu, M., Huang, S., Du, J., Li, Y., Jiang, S., Zhan, L. and Huang, X. 2022. D-alanylation of lipoteichoic acid contributes to biofilm formation and acidogenesis capacity of Streptococcus mutans. *Microbial pathogenesis* 169, p. 105666.

Xiao, H. and Kang, S. 2020. The role of the gut microbiome in energy balance with a focus on the gut-adipose tissue axis. *Frontiers in genetics* 11, p. 297.

Xiao, J. et al. 2012. The exopolysaccharide matrix modulates the interaction between 3D architecture and virulence of a mixed-species oral biofilm. *PLoS pathogens* 8(4), p. e1002623.

Xiao, J. and Koo, H. 2010. Structural organization and dynamics of exopolysaccharide matrix and microcolonies formation by Streptococcus mutans in biofilms. *Journal of applied microbiology* 108(6), pp. 2103-2113.

Xu, V. W., Yin, I. X., Niu, J. Y., Yu, O. Y., Nizami, M. Z. I. and Chu, C. H. 2024. The anti-caries effects of copper tetraamine fluoride on enamel: An in vitro study. *Journal of dentistry* 151, p. 105446.

Yang, L., Hu, Y., Liu, Y., Zhang, J., Ulstrup, J. and Molin, S. 2011. Distinct roles of extracellular polymeric substances in Pseudomonas aeruginosa biofilm development. *Environmental microbiology* 13(7), pp. 1705-1717.

Yano, A., Kikuchi, S., Yamashita, Y., Sakamoto, Y., Nakagawa, Y. and Yoshida, Y. 2010. The inhibitory effects of mushroom extracts on sucrose-dependent oral biofilm formation. *Applied microbiology and biotechnology* 86(2), pp. 615-623.

Yekani, M., Dastgir, M., Fattahi, S., Shahi, S., Maleki Dizaj, S. and Memar, M. Y. 2025. Microbiological and molecular aspects of periodontitis pathogenesis: an infection-induced inflammatory condition. *Frontiers in Cellular and Infection Microbiology* 15, p. 1533658.

Yeon, L. S. and Young, L. S. 2019. Susceptibility of oral streptococci to chlorhexidine and cetylpyridinium chloride. *Biocontrol science* 24(1), pp. 13-21.

Yoon, S. A., Park, S. Y., Cha, Y., Gopala, L. and Lee, M. H. 2021. Strategies of detecting bacteria using fluorescence-based dyes. *Frontiers in chemistry* 9, p. 743923.

Yu, M. and Chua, S. L. 2020. Demolishing the great wall of biofilms in Gram-negative bacteria: To disrupt or disperse? *Medicinal research reviews* 40(3), pp. 1103-1116.

Yuan, Y., Hays, M. P., Hardwidge, P. R. and Kim, J. 2017. Surface characteristics influencing bacterial adhesion to polymeric substrates. *RSC advances* 7(23), pp. 14254-14261.

Zanacchi, F. C., Bianchini, P. and Vicidomini, G. 2014. Fluorescence microscopy in the spotlight. Wiley Online Library.

Zarnowski, R. et al. 2014. Novel entries in a fungal biofilm matrix encyclopedia. *Mbio* 5(4), pp. 10.1128/mbio. 01333-01314.

Zhang, J. S., Chu, C.-H. and Yu, O. Y. 2022a. Oral microbiome and dental caries development. *Dentistry Journal* 10(10), p. 184.

Zhang, S., Zhao, J. and Yao, M. 2020. A comprehensive and comparative evaluation of primers for metabarcoding eDNA from fish. *Methods in Ecology and Evolution* 11(12), pp. 1609-1625.

Zhang, Y. et al. 2023. Targeting multidrug-recalcitrant pseudomonas aeruginosa biofilms: combined-enzyme treatment enhances antibiotic efficacy. *Antimicrobial Agents and Chemotherapy* 67(1), pp. e01358-01322.

Zhang, Z., Yang, Y., Sun, Q., Zeng, W. and Li, Y. 2022b. Inhibition of biofilm formation and virulence factors of cariogenic oral pathogen Streptococcus mutans by shikimic acid. *Microbiology spectrum* 10(4), pp. e01199-01122.

Zhao, A., Sun, J. and Liu, Y. 2023. Understanding bacterial biofilms: From definition to treatment strategies. *Frontiers in Cellular and Infection Microbiology* 13, p. 1137947.

Zheng, S., Bawazir, M., Dhall, A., Kim, H.-E., He, L., Heo, J. and Hwang, G. 2021. Implication of surface properties, bacterial motility, and hydrodynamic conditions on bacterial surface sensing and their initial adhesion. *Frontiers in Bioengineering and Biotechnology* 9, p. 643722.

Zheng, T. et al. 2023. Regulatory mechanisms of exopolysaccharide synthesis and biofilm formation in Streptococcus mutans. *Journal of oral microbiology* 15(1), p. 2225257.

Zuber, P. and Kreth, J. 2023. Aspects of oral streptococcal metabolic diversity: Imagining the landscape beneath the fog. *Molecular microbiology* 120(4), pp. 508-524.

Zweig, M. et al. 2014. Secreted single-stranded DNA is involved in the initial phase of biofilm formation by N eisseria gonorrhoeae. *Environmental microbiology* 16(4), pp. 1040-1052.

Appendix I

Peer-reviewed published manuscript incorporating work from Chapters 3 involving *Neisseria gonorrhoeae* was published as follows:

Pan, J., Albarrak, A., Hicks, J., Williams, D. and Williamson, A. 2025. Influence of the ATP-dependent DNA ligase, Lig E, on *Neisseria gonorrhoeae* microcolony and biofilm formation. Biofilm, p. 100292.

Biofilm 10 (2025) 100292

Contents lists available at ScienceDirect

Biofilm

journal homepage: www.sciencedirect.com/journal/biofilm

Influence of the ATP-dependent DNA ligase, Lig E, on *Neisseria gonorrhoeae* microcolony and biofilm formation

Jolyn Pan [a], Abdullah Albarrak [b], Joanna Hicks [c], David Williams [b], Adele Williamson [a,*]

[a] School of Science, University of Waikato, Private Bag 3105, Hamilton, 3240, New Zealand
[b] School of Dentistry, Health Park, Cardiff University, Wales, CF14 4XY, United Kingdom
[c] School of Health, University of Waikato, Private Bag 3105, Hamilton, 3240, New Zealand

ARTICLE INFO

Keywords:
Biofilm
DNA ligase
Extracellular DNA
Neisseria gonorrhoeae
Reconstituted epithelial tissue

ABSTRACT

Neisseria gonorrhoeae, the causative agent of the sexually transmitted infection, gonorrhoea, is known to form biofilms rich in extracellular DNA on human cervical cells. Biofilm formation is conducive to increased antimicrobial resistance and evasion of the host immune system, potentially causing asymptomatic infections. Using plate-based assays we have previously shown that disruption of a potential extracellular DNA ligase, Lig E, in *N. gonorrhoeae* impacts biofilm formation. In this research, we further explored this phenotype using confocal and scanning electron microscopy to directly visualise the morphology of microcolony and biofilm formation. Biofilm growth on artificial surfaces and on 3-dimensional human vaginal epithelial tissue was evaluated for strains where *lig E* was either disrupted or overexpressed. Results demonstrated that Lig E was important for the formation of robust, compact *N. gonorrhoeae* microcolonies, as well as extensive biofilms on artificial surfaces. The *lig E* deletion strain also had the highest tendency to be retained on the surface of epithelial tissues, with decreased invasion and damage to host cell layers. These findings support a role for Lig E to be secreted from *N. gonorrhoeae* cells for the purpose of inter-cell adhesion and biofilm formation. We suggest that Lig E strengthens the extracellular matrix and hence microcolony and biofilm formation of *N. gonorrhoeae* by ligation of extracellular DNA.

1. Introduction

Neisseria gonorrhoeae is a Gram-negative diplococcus bacterium responsible for the sexually transmitted infection (STI), gonorrhoea. With the World Health Organisation estimating 106 million new cases each year, gonorrhoea is the second most common STI in the world [1,2]. Infections occur in the mucosal epithelial cells of the urogenital tract, causing inflammation that presents as pain with urination in men (urethritis) and abnormal bleeding and pain in women (cervicitis) [3,4]. Additionally, infections in women may spread to the upper reproductive tract, causing pelvic inflammatory disease, as well as ectopic pregnancy or infertility [5]. If left untreated, infections in pregnant women may also lead to neonatal conjunctivitis and blindness in the newborn [5,6]. In females, a high proportion of *N. gonorrhoeae* infections are asymptomatic (≥50 %), allowing the bacterium to spread undetected in the community [1,5]. This trait is often attributed to the bacterium's ability to readily form biofilms, which aid in oxidative stress survival, attachment to surfaces and evasion from the host immune system [7,8].

Interestingly, *N. gonorrhoeae* lacks the genes necessary to produce the exopolysaccharides that contribute to biofilm architecture in other bacterial species [8]. Instead, *N. gonorrhoeae* utilises extracellular DNA (exDNA) as the major component which provides structural integrity to the biofilm [9]. This exDNA may originate from the frequent autolysis that occurs in *N. gonorrhoeae* cells, or from active secretion of DNA via the type IV secretion system (T4SS) [10–14]. In addition, the membranous extensions or blebs of the outer membrane that are extruded during gonococcal biofilm formation often harbour DNA [8,15,16]. The abundance of exDNA in the biofilm has the potential to act as a pool for gene exchange and acquisition of new antibiotic resistance genes [17]; however the extent of DNA diffusion through established gonococcal biofilm is modulated by its maturity and density, which may limit horizontal gene transfer by this mechanism [17,18].

The DNA component of gonococcal biofilms is enzymatically remodelled by a secreted thermonuclease, Nuc, that degrades exDNA in the biofilm matrix, as well neutrophil extracellular traps (NETs), the latter aiding in bacterial escape from NET killing [9,19]. However in

* Corresponding author.
E-mail address: Adele.williamson@waikato.ac.nz (A. Williamson).

https://doi.org/10.1016/j.biofilm.2025.100292
Received 18 February 2025; Received in revised form 2 May 2025; Accepted 27 May 2025
Available online 5 June 2025

addition to this nuclease, *N. gonorrhoeae* also encodes a minimal ATP-dependent DNA ligase, Lig E, which like Nuc, possesses an N-terminal signal peptide that is predicted to direct its extracellular secretion. Removal of this signal sequence has been shown to increase both stability and activity of recombinantly-expressed Lig E, which promotes the view that it is the cleaved isoform that represents the biologically-relevant mature protein. Lig E is encoded in the genomes of many Gram-negative bacteria without any synthetic organisation or consistent co-localisation with other genes [20,21]. This, together with the presence of the N-terminal signal sequence, suggests a function of Lig E other than chromosomal DNA repair and that it may act on exDNA [22,23]. Consistent with this is the fact that Lig E is found in many biofilm-forming and competent proteobacteria like *N. gonorrhoeae* [21]. Recently, we reported that deletion of *lig E* from *N. gonorrhoeae* (*lig E*) negatively impacted the extent of biofilm formation when measured via an indirect crystal violet assay, as well as impacting *N. gonorrhoeae* adhesion to host human cervical cells [24].

In the present study, we further explore this phenotype using microscopy to visualise biofilms formed by *lig E* deletion and overexpressing strains of *N. gonorrhoeae*. We provide the first reported use of the Centre for Disease Control (CDC) Biofilm Reactor® (BioSurface Technologies) to generate constant shear forces during growth of *N. gonorrhoeae* biofilms, in conjunction with subsequent assessment of biofilms using confocal laser scanning microscopy (CLSM). We also used commercially available 3-dimensional (3-D) reconstituted human vaginal epithelium (rHVE) (SkinEthic Laboratories) in lieu of traditional 2-dimensional (2-D) cell lines for host-cell assays. Such reconstituted epithelial models account for different cell morphologies, tissue architecture and differentiation that occur during normal microbial infection *in* vivo [25]. Use of these approaches demonstrated the potential importance of Lig E on *N. gonorrhoeae* microcolony and biofilm formation, as well as quantifying the damage to human tissue.

2. Methods

2.1. Neisseria gonorrhoeae manipulation

All *N. gonorrhoeae* used in this study were of the MS11 strain (GenBank: CP003909.1). Gonococci were grown at 37 °C with 5 % CO_2 either on gonococcal base (GCB) agar (Difco) or in gonococcal base liquid (GCBL) (15 g/L Bacto™ Protease Peptone No. 3, 4 g/L K_2HPO_4, 1 g/L KH_2PO_4, 1 g/L NaCl), both supplemented with 1 % Kellogg's supplement (22.22 mM glucose, 0.68 mM glutamine, 0.45 mM cocarboxylase, 1.23 mM $Fe(NO_3)_3$) [6]. Liquid growth was supplemented with sodium bicarbonate (0.042 %), while solid growth was maintained in a 5 % CO_2 atmosphere. Piliation status was determined by morphology under a dissecting microscope at the start of each experiment.

The *Δnuc*^{kan} mutant (Table 1) was generated in the same manner as the previously-described mutants used in this study via spot transformation [6,24]. Briefly, the transforming DNA constructs were ordered as gene fragments from Twist Biosciences with flanking sequences surrounding the *nuc* site to facilitate homologous recombination. Piliated, Opa negative (Opa-) colonies were streaked through 10 ng spots of the DNA construct. Mutants were selected on GCB agar with 50 μg/mL kanamycin before verification by PCR and sequencing.

The generation of other strains used in this study (Table 1) has been reported previously [24]. As described, the *Δlig E*^{kan} and *wt* genomes were previously re-sequenced to confirm that there were no significant differences between the two genomes apart from the disruption of *lig E* [24].

2.2. Biofilm formation in CDC Biofilm Reactors®

To facilitate imaging via confocal microscopy, *wt N. gonorrhoeae* and the *lig E* mutants (Table 1) were each transformed with the pEG2 cryptic plasmid [26], which was kindly gifted to us by the Radcliff laboratory

Table 1
List of N. gonorrhoeae MS11 mutants used in this study (GenBank: CP003909.1).

Mutant	Insertion	Purpose	Source
Δlig E^{kan}	Kanamycin resistance cassette disrupting the *lig E* gene (NGPG_RS11310)	*lig E* knock-out mutant	[24]
lig E-his^{kan}	6-His-tag and a kanamycin resistance cassette inserted at the C-terminus of *lig E*	Control for the insertion of the kanamycin resistance cassette in the *ΔLig E*^{kan} mutant, with the His-tag serving as an epitope tag	[24]
opaB-lig E-his^{kan}	Codon-optimised *lig E* gene under the constitutive *opaB* promoter inserted in a neutral site in the genome (NGPG_RS15145, annotated as a phage protein)	*Lig E* under a strong constitutive promoter in a neutral site in the genome to observe the effects of overexpression of Lig E	[24]
Δnuc^{kan}	Kanamycin resistance cassette interrupting the *nuc* (thermonuclease) gene, NGPG_RS05400 as outlined by [9]	Positive control for increased biofilm formation in *N. gonorrhoeae* for scanning electron microscopy	This work, based on [9]

(University of Auckland). The pEG2 plasmid contains an *sfGFP* gene under a *porA* promoter and was introduced to the MS11 variants via spot transformation with selection via erythromycin (10 μg/mL). Successful transformants were verified by fluorescence of the sfGFP under blue light, and the plasmids were continuously maintained in *N. gonorrhoeae* by addition of erythromycin to culture media.

The pEG2 transformants of the *N. gonorrhoeae* variants were streaked and cultured for 24 h on GCB plates with erythromycin. Piliated bacteria were then lawned and cultured for 16 h on chocolate agar before resuspension in GCBL. For each mutant, a 1 mL suspension of an OD_{600} of 0.05 was used to inoculate media for growth in the CBR 90 Standard CDC Biofilm Reactor® (Biosurface Technologies), which was assembled as per the manufacturer's protocol (Fig. 1). Briefly, polycarbonate coupons (diameter: 12.7 mm; thickness: 3.8 mm) were fitted into vertical polypropylene rods in the biofilm reactor. The 1 mL inoculum was introduced via the inlet port into the vessel containing GCBL with erythromycin and sodium bicarbonate (333 mL). Batch growth with stirring was performed for 6 h before continuous flow with sterile GCBL at 0.6 mL per min for 16–17 h. The coupons were then extracted from the rods and rinsed twice in water before CLSM.

2.3. Infection of reconstructed human vaginal epithelium (rHVE)

SkinEthic™ HVE tissue (0.5 cm^2, age day 5; HVE/S/5) was obtained from Episkin (Lyon, France). These are vulval epidermoid carcinoma A431 cells seeded on a polycarbonate filter in inserts and maintained at the air-liquid interface (Fig. 2). This model epithelium was selected as this cell line is histologically similar to vaginal mucosal cells which *N. gonorrhoeae* readily infects. Upon receipt, cells were equilibrated with the SkinEthic™ Maintenance Medium (Episkin) for 4 h in 12-well plates in a humidified chamber (37 °C, 5 % CO_2), before replacement with fresh medium (1 mL). *N. gonorrhoeae* pEG2 cultures prepared in the same medium (100 μL) were inoculated onto the cells at 1×10^8 CFU per cm^2 and left for 16–17 h in a humidified chamber (37 °C, 5 % CO_2). The supernatant under each tissue insert was recovered and used for lactate dehydrogenase (LDH) activity assays, while the cell inserts were washed twice with phosphate-buffered saline (PBS). The tissue and their membranes were then isolated from the inserts for microscopic imaging.

2.4. Histological techniques

The isolated cells and membranes were individually wrapped in Surgipath® Bio-Wraps™ (Leica Biosystems) and placed in cassettes before soaking in Reagecon Formal Buffered Saline for 3 h. Dehydration

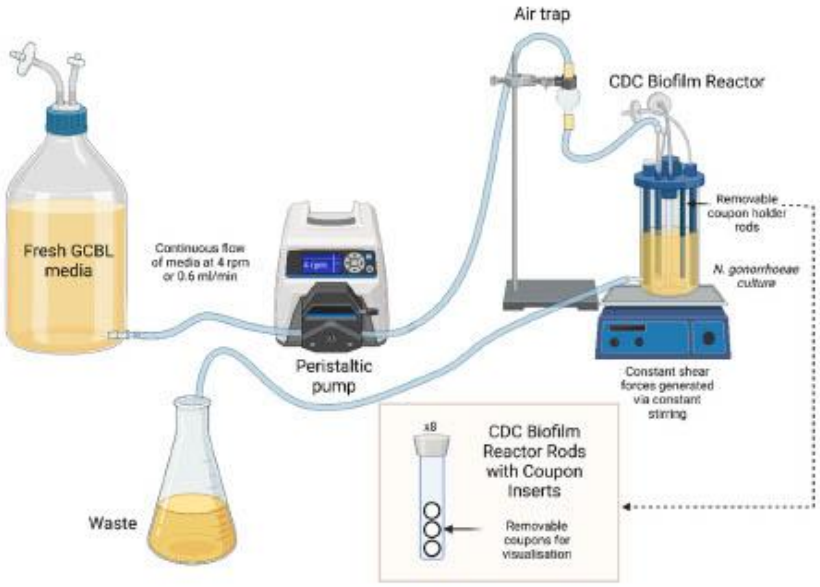

Fig. 1. Schematic of the set up used to generate N. gonorrhoeae biofilms using the CBR 90 Standard CDC Biofilm Reactor® (Biosurface Technologies). Created in https://BioRender.com.

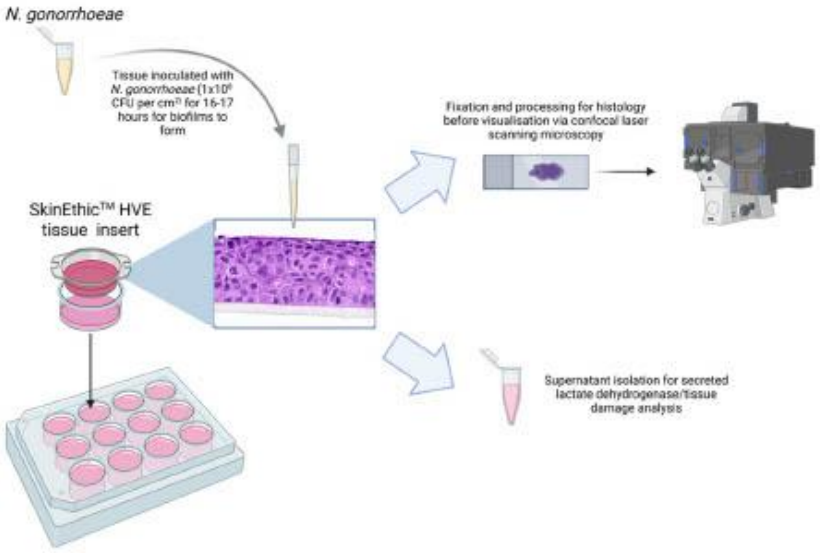

Fig. 2. Schematic of the infection work-flow with the SkinEthic™ HVE tissue model obtained from Episkin (Lyon, France). Created in https://BioRender.com. Image of HVE cells obtained from https://www.episkin.com/HVE-Vaginal-Epithelium.

was performed using the LeicaASP300S Fully Enclosed Tissue Processor (90 % v/v ethanol 1 h, 95 % v/v ethanol 1 h, 100 % v/v ethanol 4 × 1 h, xylene 3 × 1 h). The cassettes were embedded in Surgipath® Formula 'R' paraffin wax (Leica Biosystems) using the Leica EG1150 Modular Tissue Embedding Center. Transverse sectioning was performed at the Bio-imaging Technology Hub at the School of Biosciences at Cardiff University to obtain 20 μm sections on microscope slides. Paraffin wax was removed with xylene (5 min) before washes with 70 % v/v ethanol (5 min) and 100 % v/v ethanol (5 min), followed by rehydration in water (5 min). VECTASHIELD® Antifade Mounting Medium with DAPI (H-1200-10, Vector Laboratories) (20 μL) was placed on the sections before visualisation using CLSM.

2.5. Confocal laser scanning microscopy (CLSM)

CLSM was conducted at the Cardiff University Bioimaging Hub Core Facility (RRID:SCR_022556). Biofilms grown on polycarbonate coupons were visualised using the Zeiss Cell Discoverer 7 microscope at ×40 (objective) magnification using the suGFP channel (laser excitation (exc) wavelength: 480 nm, laser emission wavelength (em): 505 nm) to image the sfGFP-expressing gonococcal cells. Infected rHVE tissues were visualised using the Zeiss LSM 880 with Airyscan microscope at ×63 magnification. rHVE nuclei were visualised using the DAPI channel (exc: 405 nm, em: 449 nm) and sfGFP-expressing *N. gonorrhoeae* were visualised using the GFP channel (exc: 488 nm, em: 519 nm). Five

random fields-of-view (z-stacks) were obtained for each slide/coupon.

Images were analysed using COMSTAT 2.1 [27,28] in an OME-TIFF format (Otsu thresholding). Quantified parameters included biovolume/biomass (volume over area, $\mu m^3/\mu m^2$), average thickness (biomass) (height distribution of biomass-containing columns, μm), average thickness (entire area) (height distribution of the biofilm for the entire observed area including empty columns, μm), maximum thickness (highest point of the biofilm ignoring empty voxels, μm), surface to biovolume ratio of the biofilms (total surface facing the void over biovolume, $\mu m^2/\mu m^3$) and dimensionless roughness coefficient, R_a^* (variability in biofilm height; $R_a^* = \frac{1}{N}\sum_i^N \frac{|L_{fi} - \overline{L_f}|}{\overline{L_f}}$ where N = number of measurements, $L_{fi} = i$'th individual thickness measurement and $\overline{L_f}$ = average thickness) [27–30].

To ensure consistency in acquisition of parameters, all confocal images obtained using the Zeiss LSM 880 with Airyscan microscope were acquired at the same zoom setting (zoom setting 3), which in the infection experiments, focused on the biofilm layer at the surface of the rHVE tissue. As described below, differences in tissue thickness were observed after inoculation with different strains, meaning that the lower membrane was not visible in some fields-of-view. To account for this difference, the depth of *N. gonorrhoeae* invasion was normalised relative to the depth of remaining tissue in the same field-of view.

2.6. Scanning electron microscopy (SEM)

N. gonorrhoeae variants were lawned on GCB agar for 16 h before resuspension in GCBL. The bacteria were seeded into 12-well plates with a starting OD_{600} of 0.05 and on to 0.2 μm pore size filter papers. After 9 h (exponential phase, based on growth experiment from Ref. [24]) the medium was removed and the bacteria fixed overnight in 2.5 % V/v glutaraldehyde. The bacteria were washed (x4) in 0.1 M sodium cacodylate and distilled water before successive dehydration with 50 % ethanol (1 h), 75 % ethanol (1 h), 95 % ethanol and four rinses with 100 % ethanol. The critical point drying process and coating with platinum (5 nm) was performed by the Electron Microscope Facility at the University of Waikato. Images were obtained via the Hitachi SU8230 microscope (3 kV acceleration). Three fields-of-view were taken for each sample. The area of microcolonies formed (μm^2) was quantified via ImageJ [31].

2.7. Lactate dehydrogenase (LDH) activity assay

LDH quantification was performed on the isolated rHVE supernatant after *N. gonorrhoeae* infection using the CyQUANT™ LDH Cytotoxicity Assay kit as per the manufacturer's instructions. Absorbances at 490 and 680 nm were measured and the background absorbance at 680 nm was subtracted from that at 490 nm.

2.8. Immunoblotting against PilE

To determine if there were any differences in piliation status between strains, the level of PilE expression was quantified via immunoblotting. Briefly, cultures of *N. gonorrhoeae* were isolated and freeze-thawed five times to lyse the cells. Equal amounts of protein (5500 ng) were run on 12 % sodium dodecyl sulphate-polyacrylamide gel electrophoresis (SDS-PAGE) before transfer onto nitrocellulose membranes. After protein transfer, membranes were blocked for 1 h with 5 % milk in Tris buffered saline-Tween 20 (TBS-T) before overnight probing with a primary antibody against the EYLLN motif on the conserved N-terminus domain of T4P major pilin, PilE, (SM-1, 1:1000) [32] which was kindly gifted to us by the So Laboratory (University of Arizona, USA). This was used in combination with a goat anti-mouse polyclonal IgG antibody conjugated to horseradish peroxidase ab97023 (Abcam, 1:5000) for 1 h. The membranes were incubated with the SuperSignal™ West Femto Maximum Sensitivity Substrate for 5 min before imaging using the iBright Imaging System (Invitrogen).

2.9. Statistical methods

Statistical analyses were preformed using the GraphPad Prism 9.4.0 software (https://www.graphpad.com/). One-way analysis of variance (ANOVA) with Tukey's multiple comparisons test was used to compare the different measurements and p values < 0.05 were deemed statistically significant.

3. Results

3.1. Adhesion and biofilm formation of Neisseria gonorrhoeae on polycarbonate surfaces is dependent on lig E

To determine if Lig E impacted the ability of *N. gonorrhoeae* to adhere to, and form biofilms on abiotic surfaces, their growth on polycarbonate coupons after 16–17 h cultivation in CDC Biofilm Reactors® under constant shear forces was studied. Confocal images of the coupons (Fig. 3 and Fig. S1) indicated that *N. gonorrhoeae* had relatively low adherence to the polycarbonate surfaces compared with other organisms that we have studied using a similar set-up, such as *Candida albicans* and *Enterococcus faecalis* [33].

Despite this, CLSM images of the coupons after growth showed a clear decrease in the ability of the *Δlig E*^{kan} mutant to attach to surfaces and to form extensive or continuous biofilms compared to *wt* (Fig. 3 (a) and Fig. S1). Conversely, biofilms formed when *lig E* was overexpressed (*opaB-lig E-his*^{kan}) were more extensive across the surface, while *wt* and *lig E-his*^{kan} seemed to extend similarly to each other. Quantification via COMSTAT analysis showed no significant differences in the total biomass among the different gonococcal variants (volume per area, Fig. 3 (b)). However, there was a significant reduction in both the thickness of the entire area of growth (indicative of spatial size of the biofilm across the entire area (Fig. 3 (c)), and the thickness of the biomass (thickness distribution of only biomass-containing columns, Fig. 3 (d)) when *lig E* was disrupted compared to *wt* and *lig E-his*^{kan}. Although the overexpressing *opaB-lig E-his*^{kan} mutant had a significantly higher average biomass thickness compared to the other three variants (Fig. 3 (d)), its average thickness or spatial spread over the entire area was similar to that of *wt N. gonorrhoeae* (Fig. 3 (c)), while also displaying higher overall maximum biofilm thickness (highest point of the biofilm, Fig. 3 (e)) and lower surface:biovolume ratio (ratio of total surface facing the void over biovolume, Fig. 3 (f)) than the other variants. Furthermore, the dimensionless roughness coefficient indicated slightly higher roughness or variability in the height of the biofilms formed by the *opaB-lig E-his*^{kan} mutant compared to the other *N. gonorrhoeae* variants (Fig. 3 (g)).

3.2. Lig E increases the damage and migration of Neisseria gonorrhoeae into reconstructed human vaginal epithelium (rHVE) tissue

To further explore the impact of this sparse biofilm phenotype of the *N. gonorrhoeae lig E* deletion strain on pathogenicity and virulence, we investigated its ability to form biofilms on a 3-D SkinEthic™ rHVE tissue model. The intended experiments involved allowing the *N. gonorrhoeae* pEG2 cells to establish biofilms on the polycarbonate coupons in CDC Biofilm Reactors® before placing these in direct contact with the rHVE tissues. However, as extensive biofilms were not formed on the coupons, we inoculated cultures of the *N. gonorrhoeae* pEG2 strains directly on to the rHVE cells to allow them to form stable biofilms on a more biologically relevant surface. Confocal imaging (Fig. 4 (a) and Fig. S2) of these infections showed increased depths of invasion of *wt N. gonorrhoeae*, the his-tagged mutant (*lig E-his*^{kan}) and the overexpressor (*opaB-lig E-his*^{kan}) in the tissue model, while *Δlig E*^{kan} remained on the upper surface of the tissue. Furthermore, tissues infected with the *Δlig E*^{kan} mutant appeared more intact after inoculation, while those infected by the other

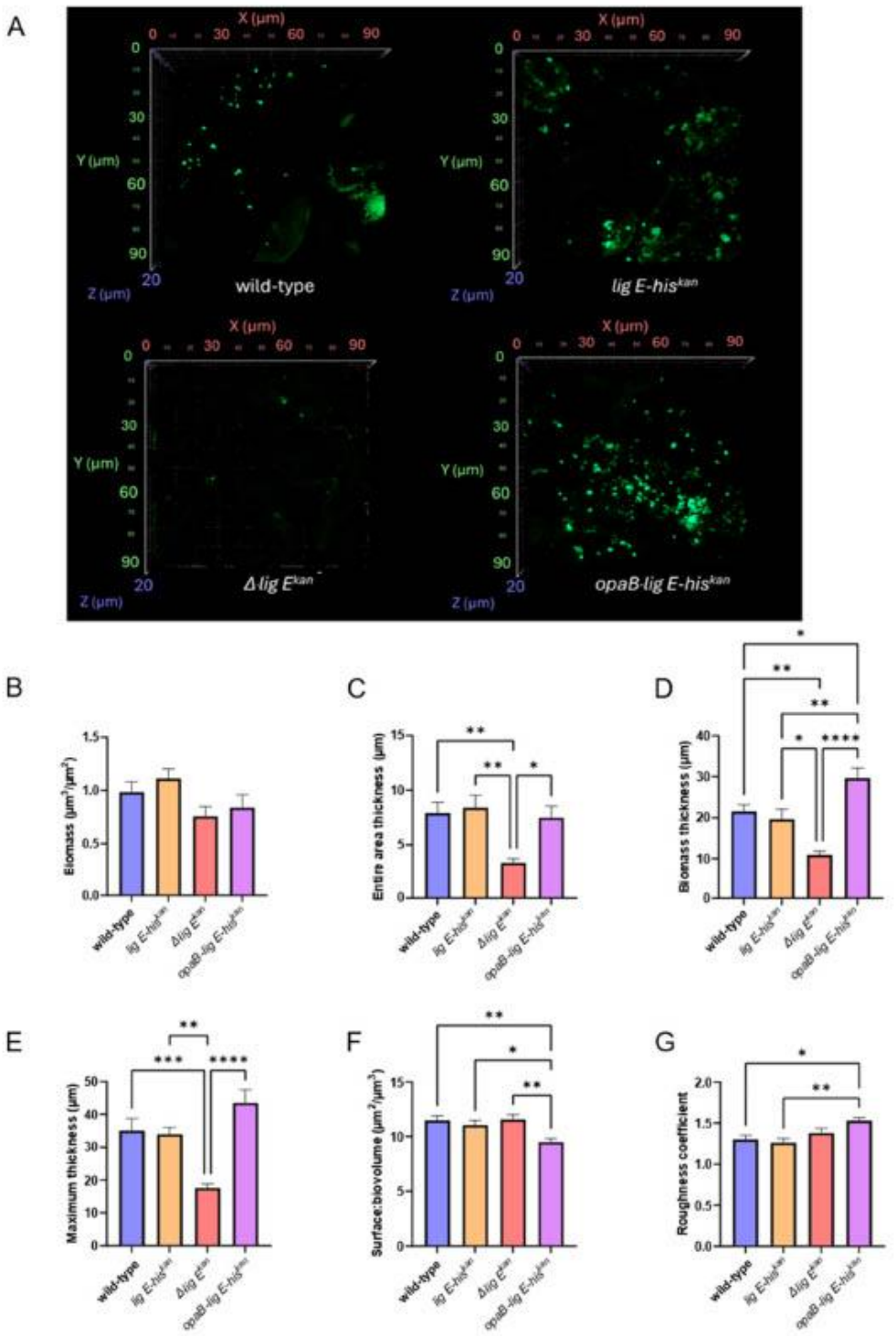

Fig. 8. Biofilm formation and adhesion of N. gonorrhoeae pEG2 (expressing sfGFP) on polycarbonate coupons in CDC Biofilm Reactors® (a) Representative CLSM z-stack images (x40 objective magnification, em:480 nm, exc:505 nm). Five fields-of-view were imaged for each of the three biological replicates. Additional supporting images can be found in Fig S1 (b) Biomass (c) Surface to biovolume ratio (d) Dimensionless roughness coefficient. (e) Average thickness (entire area) (f) Average thickness (biomass) (g) Maximum thickness. Parameters were calculated using the COMSTAT 2.1 software [27,28]. Points in the bar graphs are the mean of values from the five fields-of-view of three biological replicates and error bars represent the standard error of the mean. Significance values are given as * $p \leq 0.05$; **$p \leq 0.01$; ***$p \leq 0.001$; ** **$p \leq 0.0001$. Comparisons which showed no significant differences ($p > 0.05$) are not indicated.

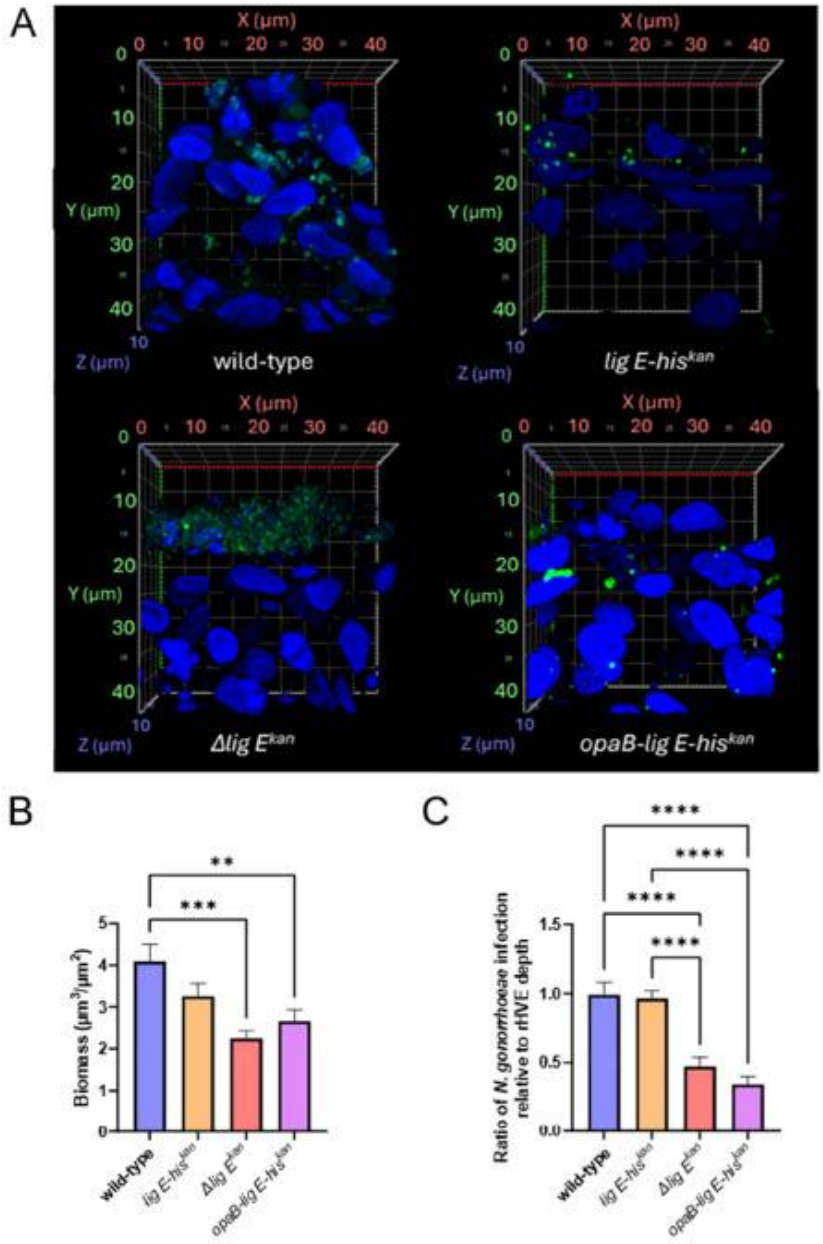

Fig. 4. Infection and invasion of SkinEthic™ HVE cells by N. gonorrhoeae (a) CLSM z-stack images (x63 objective magnification, zoom setting 3) of the N. gonorrhoeae-infected HVE cells (20 µm) with N. gonorrhoeae pEG2 (expressing sfGFP) shown in green (exc: 488 nm, em: 519 nm) and the nuclei of the rHVE cells in blue (exc: 405 nm, em: 449 nm). Additional supporting images can be found in Fig S2 (b) Biomass of N. gonorrhoeae growth (green channel) quantified using the COMSTAT 2.1 software [27,28]. (d) Quantification of the depth of N. gonorrhoeae infection on the y-axis (green channel, highest to lowest point observed) relative to the depth of remaining HVE cells on the y-axis (blue) in the same field-of-view (measurements in Table S1) as a measure of relative tissue invasion depth. Points in the bar graphs are the mean of values from the five fields-of-view of three biological replicates, with two 20 µm sections each (total 30 field-of-views). Error bars represent the standard error of the mean. Significance values are given as $^{**}p \leq 0.01$; $^{***}p \leq 0.001$; $^{****}p \leq 0.0001$. Comparisons which showed no significant differences ($p > 0.05$) are not indicated. (For interpretation of the references to colour in this figure legend, the reader is referred to the Web version of this article.)

N. gonorrhoeae variants appeared more damaged or were perforated. The final z-stack images obtained for quantification via COMSTAT were focused and zoomed (zoom setting 3) on to the surface of the rHVE cells where *N. gonorrhoeae* was predicted to form biofilms. This was an optimal setting for *wt N. gonorrhoeae*, the his-tagged mutant (*lig E-his*^{kan}) and the overexpressor (*opaB-lig E-his*^{kan}) as it showed the extent of the damage caused by the bacteria to the host cells which decreased tissue thickness and hence the bottom membrane was visible for most. However, as a majority of the *Δlig E*^{kan}-infected tissue were more intact, the membrane was only visible on a lower zoom setting (Fig. S3).

COMSTAT quantification of the biofilms formed by *N. gonorrhoeae* on the rHVE cells showed a slightly lower biomass for *Δlig E*^{kan} and the

overexpressor *opaB-lig E-his*^{kan} compared to *wt* on the host tissue cells (Fig. 4 (b)). However, this did not take into account the extent of tissue damage induced by the bacteria. To measure this, the range of *N. gonorrhoeae* infection (highest to lowest point on the y-axis), relative to the height of remaining HVE in that particular field-of-view (Fig. 4 (c)) was calculated. Results showed that both *Δlig E*^{kan} and *opaB-lig E-his*^{kan} had significantly lower invasion rates than *wt* and *lig E-his*^{kan}, the latter two strains having similar depth ratios.

To further quantify the extent of epithelial cell damage, the amount of LDH released in the supernatant after biofilm establishment was measured as a proxy for epithelial membrane disruption. LDH levels were significantly lower for *Δlig E*^{kan} on the rHVE cells relative to infection with the *wt* strain (Fig. 5), mirroring the trend observed when the invasion depth was calculated from the CLSM images (Fig. 4 (c)). Interestingly, although the amount of LDH released by cells infected with the overexpressor *opaB-lig E-his*^{kan} was also significantly lower than that of *wt*, this decrease was not as large as that caused by the *Δlig E*^{kan} mutant.

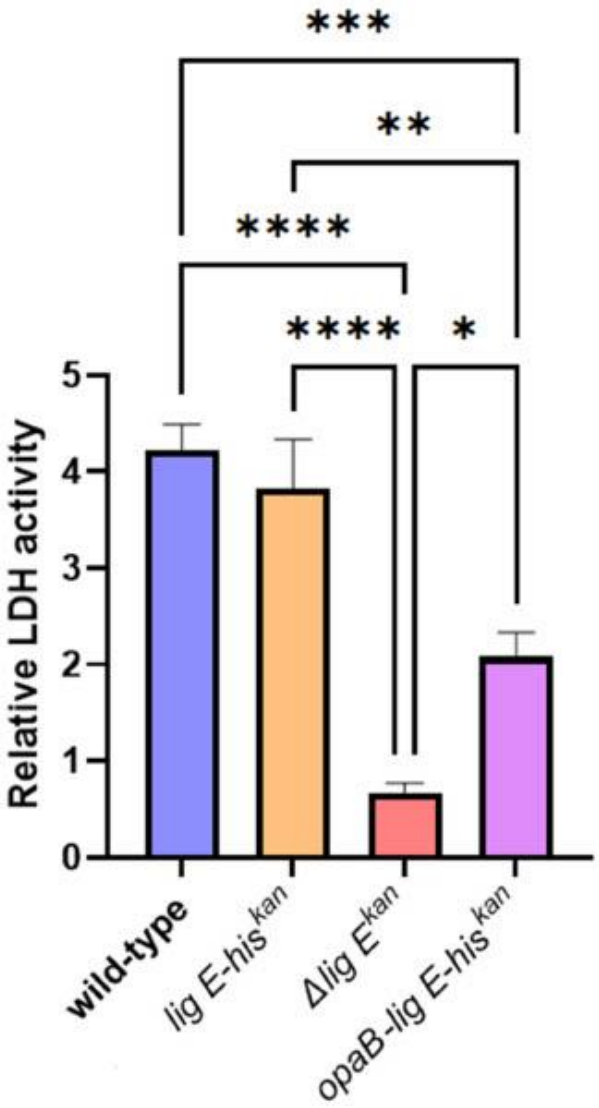

Fig. 5. Quantification of lactate dehydrogenase (LDH) release in the supernatant after N. gonorrhoeae infection of rHVE tissue. Relative LDH activity was obtained via absorbance at 490 nm relative to the absorbance of blank medium and corrected for by the background absorbance at 680 nm (raw data in Table S2). Points (data in Table S3) are the mean of values from three technical replicates of each biological replicate and error bars represent the standard error of the mean. Significance values are given as * $p \leq 0.05$; ** $p \leq 0.01$; *** $p \leq 0.001$; **** $p \leq 0.0001$ Comparisons which showed no significant differences ($p > 0.05$) are not indicated.

3.3. Lig E is important for microcolony formation in Neisseria gonorrhoeae

To determine if the observed differences in biofilm morphology were attributable to altered microcolony formation, SEM microscopy on the *N. gonorrhoeae* strains during exponential-phase growth was performed. These images showed that *Δlig E*^{kan} forms markedly fewer and smaller microcolonies compared to *wt N. gonorrhoeae* (Fig. 6(a) and Fig. S4), and that these covered significantly lower surface areas (Fig. 6(b)). Furthermore, the microcolonies formed by *lig E*^{kan} were slightly more dispersed and 'loose' compared to the cohesive microcolonies formed by the *wt* strain. Meanwhile the his-tagged control (*lig E-his*^{kan}) microcolonies covered a similar total surface area to the *wt* (Fig. 6(b)). To evaluate the impact of increased exDNA on microcolony formation, microcolonies formed by the *nuc* deletion strain (*Δnuc*^{kan}) were imaged. Deletion of *nuc* has been previously demonstrated to increase biofilm formation in *N. gonorrhoeae* [9], and here, we showed that the microcolonies formed by this mutant were similar in size to that formed by *wt*, albeit slightly denser and more compact (Fig. 6(a)). Furthermore, the *Δnuc*^{kan} cells also adhered to one another more closely in what appears to be a thicker extracellular matrix (ECM).

SEM images at higher magnification (x30,000) showed piliation filaments that seemed to tether individual bacteria to each other in the microcolonies for both *wt* and the his-tagged control, *lig E-his*^{kan} (Fig. 6 (a), indicated via orange arrows). Although also present in *Δlig E*^{kan}, these piliation filaments were not as extensive when *lig E* was disrupted, which is supported by Western blot analysis against the EYLLN motif of PilE which show a reduction in the levels of its PilE expression compared to the wild-type counterpart (Fig. S5). However, this reduction was also observed in the *lig E-his*^{kan} mutant as well and did not appear to impact the overall phenotype relative to wt. Interestingly, the extensions observed projecting between cells in the *Δnuc*^{kan} mutant were thicker than the pili filaments observed in the other variants (Fig. 6 (a), indicated by the green arrow), which could be due to a covering of ECM.

4. Discussion

In a previous study, we showed via an end-point crystal violet assay that the disruption of the DNA ligase Lig E negatively affected biofilm formation by *N. gonorrhoeae* [24]. Here, we have expanded on this finding by culturing the same mutants under constant shear forces and in continuous medium flow in CDC Biofilm Reactors®. The morphology of the resulting biofilms was assessed and demonstrated marked reduction in colonisation and biofilm formation on artificial surfaces when *lig E* was disrupted compared to the *wt* and the *lig E-his*^{kan} mutant. The latter strain served as a control for the insertion of the kanamycin resistance marker which was used to construct the deletion and overexpressing strains, and indicated that the resistance cassette and transformation procedure were not responsible for the observed phenotype. This control was included in lieu of complementation of the *Δngo-lig E*^{kan} strain as the location of the native Lig E promoter is unclear, precluding expression under native conditions. Specifically, the region upstream of Lig E lacks a Pribnow box and classical-35 sequence, and the surrounding genes do not form part of a common operon.

In contrast to its deletion, overexpression of *lig E* (*opa-lig E-his*^{kan}) formed denser and thicker biofilms which were more compact relative to *wt*. We previously demonstrated a 90-fold upregulation of *lig E* expression in this strain, indicating that Lig E activity contributed positively to

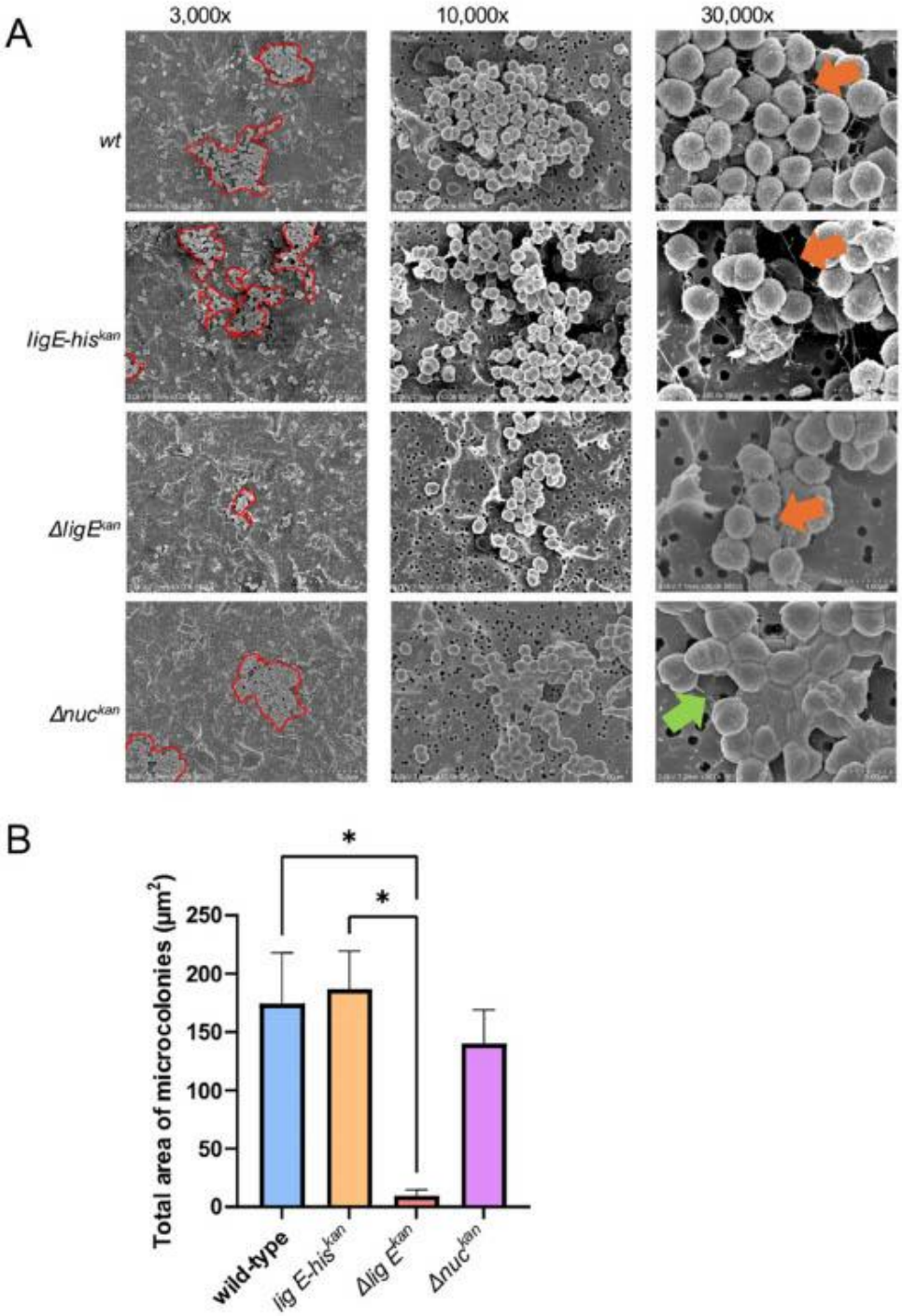

Fig. 6. N. gonorrhoeae microcolony formation (a) Representative SEM images of N. gonorrhoeae microcolonies formed on 0.2 μm pore size filter paper during the exponential phase of growth (9 h). The approximate outline of microcolonies in the field-of-view are shown in red and were annotated manually after image collection. Orange arrows indicate pili filaments, while the green arrow points at a similar extended filamentous structure. Additional supporting fields-of-view can be found in Fig. S4. (b) Quantification of the average total area covered by the microcolonies in each field-of-view via ImageJ [31]. Points are the mean of values of the total surface area covered in each field-of-view and error bars represent the standard error of the mean. Significance values are given as * $p \leq 0.05$. Comparisons which showed no significant differences ($p > 0.05$) are not indicated. (For interpretation of the references to colour in this figure legend, the reader is referred to the Web version of this article.)

biofilm formation [24]). Our previous work [24] also revealed no differences in growth rates between any of the *lig E* variants and *wt*, and since the inocula were normalised before each experiment, the observed differences in biofilm formation were not due to differences in initial cell density or growth rates. Although immunoblotting showed lower levels of PilE expression when Lig E was deleted, this was also observed in the *lig E-his*^{kan} mutant which showed similar biofilm and microcolony formation phenotype to that of the *wt*, indicating that the impaired microcolony and biofilm formation observed in *ΔligE*^{kan} is unlikely to be a result of different piliation levels, but rather due to the absence of Lig E.

Consistent with the phenotype on artificial surfaces, *lig E* deletion also causes defects in *N. gonorrhoeae* attachment to human cells and invasion into tissue. Previous results from our group showed decreased adhesion of the *Δlig E*^{kan} mutant on a monolayer of ME-180 human cervical cells [24]. Here, we also show the reduced capabilities of the same mutant to invade and migrate into reconstituted 3-D rHVE tissue, which in turn equates to less cellular damage by the deletion mutant relative to *wt N. gonorrhoeae*. Instead, *Δlig E*^{kan} accumulated on the upper surface of the tissue, which appeared healthier and less perforated than in the *wt*-infected sections. This has important implications on the extent of *N. gonorrhoeae* infection in the human host, as *N. gonorrhoeae* invasion and transcytosis into tissues may lead to disseminated infections after crossing the subepithelial space [3]. Although the overexpressor *opa-lig E-his*^{kan} appeared to follow this trend as well, we note that most of the bacteria were closer to the membrane, and we speculate that this could be indicative of deeper invasion past the membrane into the supernatant. We predict that due to the decreased ability of *Δlig E*^{kan} to attach to the surfaces of cells, the strain is less able to invade human cells and cause damage. However, as we were only able to obtain end-point images after 16–17 h of infection, we did not capture the step-by-step process of internalisation and transcytosis of the other mutants into the host cells as it occurred (*e.g.* via time-lapse microscopy).

Our observations of the consequences of *lig E* deletion on biofilm morphology are consistent with our hypothesis that this ligase acts on exDNA to form high molecular weight substrates that better contribute to initial biofilm formation by overcoming any repulsive forces between the ECM and the surface [34]. Unlike many other bacterial biofilms, exDNA is likely the primary structural biopolymer of gonococcal biofilms, with dsDNA being a critical component of mature *N. gonorrhoeae* biofilms [14,17]. Work by Bender et al. has demonstrated that for *N. gonorrhoeae* larger pieces of DNA (>3000 bp) are more likely to have a high concentration gradient outside the colony and integrate into the biofilm [18]. We hypothesise that extracellular Lig E is important for repairing breaks in free exDNA fragments, increasing their length and integrity and allowing them to be retained outside the colonies and therefore contribute to the pool of exDNA that stabilises the extracellular biofilm matrix of *N. gonorrhoeae*. This action would counteract the activity of the extracellular Nuc, which remodels gonococcal biofilms through its cleavage and degradation of exDNA [9] and suggests that some level of interplay or regulatory control between these two opposing activities is likely. Here, we show that the *nuc* deletion strain formed microcolonies of similar size to *wt N. gonorrhoeae*; however, these microcolonies appeared more globular, with filamentous extensions that seemed to indicate thicker ECM. It is possible that this observed morphology was due to the inability of the *nuc* deletion to regulate exDNA content, and suggests that in the *wt* strain, Nuc works in conjunction with Lig E to manipulate exDNA, and thus optimise and modulate the architecture of the biofilm. We also question if the increase in exDNA length and integrity performed by Lig E allows the exDNA to interact with other DNA binding proteins, which may assemble to create a more stable framework for the biofilm to build on.

Here, we have shown that Lig E affects biofilm formation, potentially via its activity on exDNA, which in turn affects the adhesion of *N. gonorrhoeae* to human cells, and their subsequent invasion and damage. Based on these observations, we consider extracellular Lig E to be important for the pathogenicity and virulence of *N. gonorrhoeae*, making it an appealing target for future drug design against this incredibly resistant bacterium. Despite this, many questions about Lig E remain, including its specific cellular location, its regulation and its direct consequences for the exDNA fraction. The presence of an N-terminal signal peptide indicates that Lig E is transported to the periplasmic space, however, it may be further transported to the extracellular milieu via membranous blebs that contribute to the ECM of *N. gonorrhoeae* biofilms [15,16,35]. Additionally, it remains unknown if Lig E is required for biofilm maintenance, or if it is more important during early biofilm formation when exDNA is most critical [14]. Answering this question would require quantifying the amount and arrangement of exDNA in the ECM when *lig E* is disrupted (i.e. via exDNA staining); this was attempted in the present study, however we encountered difficulties in its visualisation after growth in the Biofilm Reactors, potentially due to the constant stirring that may damage the exDNA.

A final area of interest is how Lig E activity, and especially a potential influence on DNA size may affect gene transfer, which is more frequent in early biofilms [17]. This would involve studying biofilm formation by the different gonococcal mutants at different timepoints.

4.1. New tools and methods for understanding Neisseria gonorrhoeae biofilm and pathogenicity

Previously, our group had used a crystal violet assay to demonstrate the importance of Lig E on biofilm formation, which although rapid and convenient, was an indirect method that assessed static biofilms [24]. Other more advanced techniques that have been used to study *N. gonorrhoeae* biofilms include the growth of the bacteria on glass or patterned silicone coverslips (the latter to study the effect of surface topography) in continuous flow chambers or cells, or even static growth on glass dishes [7–9,17,36–39]. While such methods have greatly increased our understanding of gonococcal biofilm formation, they often require bespoke laboratory equipment, and can be subject to technical complications such as bubble formation in the flow channels that disrupt cellular adhesion.

Here, we report the first use of a commercially-available CDC Biofilm Reactor® to study *N. gonorrhoeae* biofilms, involving the continuous flow of fresh medium controlled via a periplasmic pump into a growth chamber filled with retrievable coupons that the bacteria can adhere to, while maintaining a constant shear force across the surface [40]. Adhesion of *N. gonorrhoeae* to polycarbonate coupons was not as extensive as we had anticipated, however we attribute this to the polycarbonate material used. This was readily available in our laboratory, but has not been widely used for *N. gonorrhoeae* biofilm studies, with glass being the preferred substrate for *N. gonorrhoeae* surface adhesion for other reports [7–9,36,37,39]. In addition, the constant stirring of medium may have damaged exDNA, which since it is a major constituent of *N. gonorrhoeae* biofilms, would also affect the adhesion and biofilm formation in this setting. Despite this, we believe that with further optimisation, CDC Biofilm Reactors® offer great promise for further studies of biofilm formation in *N. gonorrhoeae*, especially if a glass surface and slower shear forces are used.

We also showed the importance of a 3-D model for studying bacterial-host interactions, which allowed us to examine the effects of Lig on *N. gonorrhoeae* migration into host tissues; a phenotype not observable in a cell monolayer. Common techniques employed by other groups involve the use of a primary cell line or biopsy samples which can be directly coated onto glass coverslips for easy microscopy [8,39]. The search for appropriate 3-D models for *N. gonorrhoeae* study is of increasing interest, with one particular group developing a model for this purpose using porcine small intestinal submucosa as a scaffold [41]. Until models like this are readily available however, the SkinEthic rHVE™ tissue model used here from Episkin provides a good substitute as it is easy to obtain, reproducible and provides a more biologically-relevant model with different tissue cell types and

morphologies.

5. Conclusion

The DNA ligase, Lig E, is present in many bacteria like *N. gonorrhoeae* that form exDNA-dependent biofilms. Here we show that Lig E from *N. gonorrhoeae* (Lig E) influences the formation of gonococcal biofilms and microcolonies on artificial surfaces, as well as the invasion into and damage of 3-D reconstituted HVE tissue. We propose that Lig E may be acting on fragmented exDNA in the extracellular space of *N. gonorrhoeae*, which is conducive for microcolony formation and proto-biofilm interactions to occur. Future directions include studying the role of Lig E at different stages of gonococcal biofilm formation, as well as investigation into the potential interplay between Lig E and Nuc on exDNA-mediated biofilm remodelling. Regardless, the results presented in this report highlight the importance of Lig E on the virulence and pathogenicity of *N. gonorrhoeae*. We predict that this may open up new avenues and pathways for targeting not only *N. gonorrhoeae*, but other human pathogens that express this minimal ligase, potentially finding a way to target extensive biofilm formation in many clinical settings.

CRediT authorship contribution statement

Jolyn Pan: Writing – review & editing, Writing – original draft, Methodology, Investigation, Formal analysis, Data curation, Conceptualization. **Abdullah Albarrak:** Methodology, Investigation. **Joanna Hicks:** Supervision, Conceptualization. **David Williams:** Methodology, Funding acquisition, Conceptualization. **Adele Williamson:** Writing – review & editing, Supervision, Resources, Project administration, Funding acquisition, Data curation, Conceptualization.

Funding

This work was supported by the Maurice Wilkins Centre Flexible Research Programme (Category 4) and the Cardiff University and the University of Waikato Strategic International Partnership Collaborative Seed Fund. AW is supported by a Rutherford Discovery Fellowship (grant number 20-UOW-004). JP is supported by a University of Waikato Doctoral Scholarship. AA is supported by the Saudi Ministry of Education.

Declaration of competing interest

The authors declare that they have no known competing financial interests or personal relationships that could have appeared to influence the work reported in this paper.

Acknowledgements

We would like to thank Fiona Clow and Fiona Radcliff from the Radcliff Laboratory (University of Auckland) for providing us with the pEG2 plasmid, as well as Adam Jones (School of Dentistry, Cardiff University) for guidance with histological processing of the tissue. We would also like to extend our thanks to Helen Turner (University of Waikato) for performing the critical point drying process for SEM microscopy and Marc Isaacs (Bioimaging Hub, Cardiff University) for help with wax microtomy and slide preparation.

Appendix A. Supplementary data

Supplementary data to this article can be found online at https://doi.org/10.1016/j.biofilm.2025.100292.

Data availability

Data will be made available on request.

References

[1] Unemo M, Shafer WM. Antimicrobial resistance in *Neisseria gonorrhoeae* in the 21st century: past, evolution, and future. Clin Microbiol Rev 2014;27(3):587–613. https://doi.org/10.1128/CMR.00010-14.
[2] World Health Organization. Global sexually transmitted infections programme: diagnostics for gonococcal antimicrobial resistance. https://www.who.int/teams/global-hiv-hepatitis-and-stis-programmes/stis/testing-diagnostics/diagnostics-for-gonococcal-antimicrobial-resistance; 2024.
[3] Edwards JL, Apicella MA. The molecular mechanisms used by *Neisseria gonorrhoeae* to initiate infection differ between men and women. Clin Microbiol Rev 2004;17(4):965–81. https://doi.org/10.1128/cmr.17.4.965-981.2004.
[4] Tapsall JW. Antibiotic resistance in *Neisseria gonorrhoeae*. Clin Infect Dis 2005;41(Supplement_4):S263–8. https://doi.org/10.1086/430787.
[5] McCormack WM. Clinical spectrum of infection with *Neisseria gonorrhoeae*. Sex Transm Dis 1981;8(4):305–7. http://www.jstor.org/stable/44963763.
[6] Dillard JP. Genetic manipulation of *Neisseria gonorrhoeae*. Current Protocols in Microbiology 2011;4:Unit4A.2. https://doi.org/10.1002/9780471729259.mc04a02s23. *Unit4A.2, Chapter*.
[7] Falsetta ML, Bair TB, Ku SC, Vanden Hoven RN, Steichen CT, McEwan AG, Jennings MP, Apicella MA. Transcriptional profiling identifies the metabolic phenotype of gonococcal biofilms. Infect Immun 2009;77(9):3522–32. https://doi.org/10.1128/iai.00036-09.
[8] Greiner LL, Edwards JL, Shao J, Rabinak C, Entz D, Apicella MA. Biofilm formation by *Neisseria gonorrhoeae*. Infect Immun 2005;73(4):1964–70. https://doi.org/10.1128/IAI.73.4.1964-1970.2005.
[9] Steichen CT, Cho C, Shao JQ, Apicella MA. The *Neisseria gonorrhoeae* biofilm matrix contains DNA, and an endogenous nuclease controls its incorporation. Infect Immun 2011;79(4):1504–11. https://doi.org/10.1128/iai.01162-10.
[10] Elmros T, Burman LG, Bloom GD. Autolysis of *Neisseria gonorrhoeae*. J Bacteriol 1976;126(2):969–76. https://doi.org/10.1128/jb.126.2.969-976.1976.
[11] Hebeler BH, Young FE. Autolysis of *Neisseria gonorrhoeae*. J Bacteriol 1975;122(2):385–92. https://doi.org/10.1128/jb.122.2.385-392.1975.
[12] Morse SA, Bartenstein L. Factors affecting autolysis of *Neisseria gonorrhoeae*. Experimental biology and medicine (Maywood, N.J.) 1974;145(4):1418–21. https://doi.org/10.3181/00379727-145-38025.
[13] Zola TA, Strange HR, Dominguez NM, Dillard JP, Cornelissen CN. Type IV secretion machinery promotes ton-independent intracellular survival of *Neisseria gonorrhoeae* within cervical epithelial cells. Infect Immun 2010;78(6):2429–37. https://doi.org/10.1128/iai.00228-10.
[14] Zweig M, Schork S, Koerdt A, Siewering K, Sternberg C, Thormann K, Albers SV, Molin S, van der Does C. Secreted single-stranded DNA is involved in the initial phase of biofilm formation by *Neisseria gonorrhoeae*. Environ Microbiol 2014;16(4):1040–52. https://doi.org/10.1111/1462-2920.12291.
[15] Dorward DW, Garon CF, Judd RC. Export and intercellular transfer of DNA via membrane blebs of *Neisseria gonorrhoeae*. J Bacteriol 1989;171(5):2499–505. https://doi.org/10.1128/jb.171.5.2499-2505.1989.
[16] Steichen CT, Shao JQ, Ketterer MR, Apicella MA. Gonococcal cervicitis: a role for biofilm in pathogenesis. J Infect Dis 2008;198(12):1856–61. https://doi.org/10.1086/593336.
[17] Kouzel N, Oldewurtel ER, Maier B. Gene transfer efficiency in gonococcal biofilms: role of biofilm age, architecture, and pilin antigenic variation. J Bacteriol 2015;197(14):2422–31. https://doi.org/10.1128/JB.00171-15.
[18] Bender N, Hennes M, Maier B. Mobility of extracellular DNA within gonococcal colonies. Biofilm 2022;4:100078. https://doi.org/10.1016/j.bioflm.2022.100078.
[19] Juneau RA, Stevens JS, Apicella MA, Criss AK. A thermonuclease of *Neisseria gonorrhoeae* enhances bacterial escape from killing by neutrophil extracellular traps. J Infect Dis 2015;212(2):316–24. https://doi.org/10.1093/infdis/jiv031.
[20] Pan J, Lian K, Sarre A, Leiros H-KS, Williamson A. Bacteriophage origin of some minimal ATP-dependent DNA ligases: a new structure from *Burkholderia pseudomallei* with striking similarity to Chlorella virus ligase. Sci Rep 2021;11(1):18693. https://doi.org/10.1038/s41598-021-98155-w.
[21] Williamson A, Hjerde E, Kahlke T. Analysis of the distribution and evolution of the ATP-dependent DNA ligases of bacteria delineates a distinct phylogenetic group 'Lig E'. Mol Microbiol 2016;99(2):274–90. https://doi.org/10.1111/mmi.13229.
[22] Magnet S, Blanchard JS. Mechanistic and kinetic study of the ATP-dependent DNA ligase of *Neisseria meningitidis*. Biochemistry 2004;43(3):710–7. https://doi.org/10.1021/bi0355387.
[23] Williamson A, Rothweiler U, Leiros HK. Enzyme-adenylate structure of a bacterial ATP-dependent DNA ligase with a minimized DNA-binding surface. Acta Crystallographica Section D: Biological Crystallography 2014;70(Pt 11):3043–56. https://doi.org/10.1107/s1399004714021099.
[24] Pan J, Singh A, Hanning K, Hicks J, Williamson A. A role for the ATP-dependent DNA ligase lig E of *Neisseria gonorrhoeae* in biofilm formation. BMC Microbiol 2024;24(1):29. https://doi.org/10.1186/s12866-024-03193-9.
[25] Malfa P, Brambilla L, Giardina S, Masciarelli M, Squarzanti DF, Carlomagno F, Meloni M. Evaluation of antimicrobial, antiadhesive and co-aggregation activity of a multi-strain probiotic composition against different urogenital pathogens. Int J Mol Sci 2023;24(2):1323. https://www.mdpi.com/1422-0067/24/2/1323.

[26] Christodoulides M, Everson JS, Liu BL, Lambden PR, Watt PJ, Thomas EJ, Heckels JE. Interaction of primary human endometrial cells with *Neisseria gonorrhoeae* expressing green fluorescent protein. Mol Microbiol 2000;35(1):32–43. https://doi.org/10.1046/j.1365-2958.2000.01694.x.
[27] Heydorn A, Nielsen AT, Hentzer M, Sternberg C, Givskov M, Ersbøll BK, Molin S. Quantification of biofilm structures by the novel computer program COMSTAT. Microbiology (Reading) 2000;146(Pt 10):2395–407. https://doi.org/10.1099/00221287-146-10-2395.
[35] Dorward DW, Garon CF. DNA-binding proteins in cells and membrane blebs of *Neisseria gonorrhoeae*. J Bacteriol 1989;171(8):4196–201. https://doi.org/10.1128/jb.171.8.4196-4201.1989.
[36] Falsetta ML, Steichen CT, McEwan AG, Cho C, Ketterer M, Shao J, Hunt J, Jennings MP, Apicella MA. The composition and metabolic phenotype of *Neisseria gonorrhoeae* biofilms. Front Microbiol 2011;2:75. https://doi.org/10.3389/fmicb.2011.00075. 75.
[37] Kwiatek A, Bacal P, Wasiluk A, Trybunko A, Adamczyk-Poplawska M. The dam

Appendix II

- Biomass of *Neisseria gonorrhoeae* biofilms.
- Carbohydrate content quantification of *S. mutans* biofilms.
- COMSTAT assessment values of percentage viability of *Streptococcus mutans* biofilms treated with chlorhexidine (CHX), with or without prior 0.25% dextranase post growth

Biomass of *Neisseria gonorrhoeae* biofilms formed on polycarbonate coupons in the CDC biofilm reactor, quantified by COMSTAT analysis of CLSM images. Biomass is expressed as $\mu m^3/\mu m^2$

Wild type	*ngo-Lig E-His*	*Δngo-Lig E*	*opaB-ngo-Lig E*
0.86253	0.84263	0.85968	0.98435
1.21502	0.65453	1.11986	0.86197
1.89102	1.23174	1.2735	0.5852
0.31082	0.83663	0.29884	0.22248
0.89143	1.43427	1.5469	1.81283
0.86314	1.47626	0.77144	0.49029
0.76984	0.46198	0.37268	1.0654
1.14815	1.57948	0.63806	1.81283
0.70029	1.57413	0.4211	1.01571
1.21926	1.0081	0.5197	0.41018
1.2823	0.99745	0.66808	0.94598
1.22925	1.31493	1.03816	0.37439
0.60661	0.83062	0.56708	0.59415
1.20971	1.30094	0.57026	0.85545
0.57241	1.1519	0.70419	0.54994
0.86253	0.84263	0.85968	0.98435
1.21502	0.65453	1.11986	0.86197
1.89102	1.23174	1.2735	0.5852
0.31082	0.83663	0.29884	0.22248
0.89143	1.43427	1.5469	1.81283
0.86314	1.47626	0.77144	0.49029
0.76984	0.46198	0.37268	1.0654
1.14815	1.57948	0.63806	1.81283
0.70029	1.57413	0.4211	1.01571
1.21926	1.0081	0.5197	0.41018
1.2823	0.99745	0.66808	0.94598
1.22925	1.31493	1.03816	0.37439
0.60661	0.83062	0.56708	0.59415
1.20971	1.30094	0.57026	0.85545
0.57241	1.1519	0.70419	0.54994
0.86253	0.84263	0.85968	0.98435
1.21502	0.65453	1.11986	0.86197
1.89102	1.23174	1.2735	0.5852
0.31082	0.83663	0.29884	0.22248

Biomass of biofilms formed by different *Neisseria gonorrhoeae* strains on infected human vaginal epithelial tissue, quantified by COMSTAT analysis of CLSM images. Biomass is expressed as $\mu m^3/\mu m^2$

Wild type	*ngo-Lig E-His*	*Δngo-Lig E*	*opaB-ngo-Lig E*
6.9522	1.12563	3.11629	3.02904
3.78074	3.78856	0.79401	2.12254
0.77445	2.82023	3.42531	3.35829
1.9452	3.40868	0.73227	0.44175
5.07322	6.17858	0.85023	4.11938
4.17843	5.40162	2.74863	3.39674
8.67486	1.09119	2.7147	2.85557
3.60722	1.43967	1.09752	2.13372
1.14963	1.88333	4.47573	1.64632
1.97361	1.85254	2.69592	1.10037
5.86722	5.56958	2.87925	3.19494
2.78548	5.1559	2.17149	4.01386
8.75537	0.95495	1.90104	2.55299
3.83954	4.60435	1.22785	6.77851
1.71368	1.21005	2.73534	0.55493
3.48078	5.32139	2.22664	3.80778
3.90891	6.7507	2.38466	2.07962
4.85052	3.49509	1.73906	1.57373
9.60784	2.45057	3.19961	1.4136
4.45532	4.38251	0.7813	2.80128
3.04191	1.38793	3.41499	0.4735
2.2547	3.24555	1.73467	4.27346
5.22162	4.80865	2.81242	1.54333
5.01314	3.89559	1.61554	3.61728
4.7087	2.94478	2.59977	4.07657
4.93786	3.34145	0.53521	1.10728
1.7265	1.81343	3.77839	0.50919
1.77336	1.55471	3.12583	4.54551
3.2267	2.71012	2.54027	3.3137
3.54287	3.22681	1.46405	3.4778
6.9522	1.12563	3.11629	3.02904
3.78074	3.78856	0.79401	2.12254
0.77445	2.82023	3.42531	3.35829
1.9452	3.40868	0.73227	0.44175

Carbohydrate content (normalised to µg/10^6 cells) of *S. mutans* biofilms treated with 0.25% dextranase compared to untreated controls

Untreated *S. mutans* biofilm	0.25% dextranase treated *S. mutans* biofilm
2.936	1.102
3.339	1.458
3.390	1.852
4.211	1.805
3.934	1.978
3.830	1.407
3.740	2.073
4.090	1.387
1.802	1.865
3.898	1.912
3.325	1.540
2.884	1.644
7.935	3.412
5.521	2.537
6.868	2.671
5.564	3.236
8.429	4.815
7.981	5.070
7.015	3.719
8.368	4.071
5.648	3.426
7.891	3.521
6.485	4.043
4.948	2.595

Values represent individual replicates for each condition, of 8 biological repeats and 3 technical repeats for each.

COMSTAT assessment values of percentage viability of *Streptococcus mutans* biofilms treated with chlorhexidine (CHX), with or without prior 0.25% dextranase post growth

	Percentage of live biofilm biomass		
Field of view	No dextranase	Dextranase post biofilm	Dextranase during biofilm
1	52.683	59.931	0
2	56.437	55.407	0
3	63.442	55.244	0
4	60.613	51.796	0
5	57.347	47.877	0
6	58.227	42.225	0
7	54.325	41.918	0
8	43.102	35.161	0
9	48.885	34.325	0
10	49.990	42.865	0
11	50.030	35.893	0
12	47.619	34.782	0
13	48.809	30.580	0
14	49.108	35.819	0
15	43.218	21.259	0
Mean	**52.256**	**41.672**	**0**

Values are percentage of live biofilm biomass, calculated as the ratio of live cells to total biomass (measured by live/dead staining of CLSM image stacks) by COMSTAT analysis.